Bio-Based FRP Floors:
A Comprehensive Feasibility Analysis

I.L. van der Toorn

Delft University of Technology

TUDelft abt

Bio-Based FRP Floors:
A Comprehensive Feasibility Analysis

Structural, environmental, and economic performance in modular buildings compared to conventional floors

by

Iona van der Toorn

Master of Science Thesis
Structural Engineering Track // Steel, Timber, and Composite Structures Specialisation
Delft University of Technology // Faculty of Civil Engineering (CiTG)

Student number:	4649613	
Project duration:	December 2022 – September 2023	
Thesis committee:	Dr. Ir. M. Pavlovic,	TU Delft, Chair
	Dr. Ir. G.J.C Ravenhorst,	TU Delft, Supervisor
	Dr. Ir. O. Karpenko,	TU Delft, Supervisor
	Ir. J.C. van der Ploeg,	ABT, Supervisor

An electronic version of this thesis is available at `http://repository.tudelft.nl/`.

Cover image: `https://www.ameriflax.com/`

TUDelft abt

Preface

This thesis was written for my Master of Civil Engineering graduation at the Faculty of Civil Engineering and Geosciences, Delft University of Technology. During the program, I enjoyed following the track Structural Engineering, with the specialization in Steel, Timber, and Composites Structures. I have always been curious about how theoretical knowledge can be applied in practice. This, together with my interest in buildings and sustainability, led me to choose the topic of this thesis.

I would like to thank my research committee. Throughout my research journey, I could always turn to you for guidance, and you gave me direction. I want to thank Marko Pavlovic for his insightful ideas and for showing me how to approach certain problems. Geert Ravenhorst, I want to thank you for your critical view on the research structure, which ensured the academic quality of my work. I want to thank Olena Karpenko for her assistance when I faced obstacles and for being a supportive listener. Chris van der Ploeg, thank you for your daily guidance and discussions that helped improve my problem-solving skills.

This thesis was made in collaboration with ABT, and I would like to express my gratitude to all colleagues at ABT. I always had the opportunity to ask questions and gain insights into real-world applications. I am also thankful for the positive working atmosphere I experienced at ABT. Taking a stroll with colleagues during lunch breaks was enjoyable and allowed me to return to work with a fresh perspective.

Lastly, I would like to thank my friends and family for their continuous support and care. You were always there to talk about my thesis and, most importantly, when I needed distractions. Special thanks go to my boyfriend, Krijn; you have been on my side during the whole thesis, which means a lot to me.

Iona van der Toorn
Delft, September 2023

Abstract

Climate change is one of the biggest unsolved problems in the world. In 2015, countries worldwide established the Paris Agreement, which states that global emissions must reach net zero by 2050. The building and construction industry contributes approximately 40% to the global CO_2 emissions, which means a high pressure exists to reduce its environmental impact. In buildings, floors contribute to a substantial part of the environmental impact, offering an opportunity to make a big impact.

To find sustainable construction alternatives, environmentally friendly materials and innovative design solutions are explored. Bio-based fiber-reinforced polymer (BFRP), a composite material, has gained interest because it utilizes locally produced natural fibers and has promising material properties. Furthermore, design solutions, such as modular buildings with standardized elements, offer a sustainable alternative because of their high quality, cost savings, low weight, and reduced waste.

This research investigates the **feasibility and potential of utilizing BFRP floors in modular buildings as a low environmental impact and cost-effective alternative to conventional floors**. A modular building is introduced as a case study, the Natural Pavilion in Almere, to bring focus to the research and set a baseline for the requirements of the BFRP floor. A second case study, the bio-composite bridge in Ritsumasyl, is introduced to utilize its comprehensive dataset of material properties representing the state-of-the-art BFRP. Using the two case studies, two design solutions, a one-way and two-way floor, are developed.

The purpose of this report is to describe the process of material selection, design, and verification of the BFRP floors and their performance compared to conventional floors. The report first focuses on using BFRP as a construction material and the structural topology utilized for BFRP floors. The timber and FRP Eurocodes are used to identify the failure modes in the ultimate limit state (ULS) and the serviceability limit state (SLS) requirements. Analytical calculations are used to find a geometry that meets these criteria and to validate the numerical models. Numerical models are used to understand the floors' load-bearing characteristics, vibration response, and deflection behavior. A detailed numerical model is utilized to evaluate a specific failure mode for delamination in the two-way floor.

Comparing the designed BFRP floor to conventional floors such as cross-laminated timber (CLT), concrete hollow core slab (HC), and concrete flat slab (FS), several conclusions can be drawn:

1. The construction height of BFRP floors is similar to that of the conventional floors. The weight of the floor is similar to a CLT floor, while a concrete floor is 6-8 times heavier. Design optimization is possible, and the amount of BFRP material utilized can be reduced by up to 21% for the one-way floor and 19% for the two-way floor. Additionally, the floor design proposed in this thesis is intended for buildings with a design life of 15 years and no specific fire resistance requirements. For structures with a design life of 50 years, it is imperative to increase the floor height to meet deflection criteria. Further research on fire resistance and additional measures is necessary to extend applicability beyond single-compartment buildings and terrace housing.

2. The environmental impact of a BFRP floor, assessed in terms of Global Warming Potential (GWP) through a Life Cycle Analysis (LCA) encompassing stages A1-A5, is found to be twice that of a concrete floor. Through optimization of the floor design and reduction of BFRP material usage, it is possible to achieve a reduction in CO_2 emissions of approximately 10%. Nevertheless, in the current state-of-the-art, BFRP floors exhibit a higher environmental impact than conventional flooring systems. The use of resin and the production process are the primary contributors to CO_2 emissions. The contribution from the production process requires nuance, as results heavily depend on the data source. Factors such as manufacturing techniques and production scale significantly affect this impact. By reducing the impact of the resin and production techniques while also exploring end-of-life possibilities for 100% bio-based BFRP, the environmental impact of BFRP floors holds potential for the future.

3. The floor cost is nearly twice as high as a comparable CLT floor. This can be attributed to introducing new design solutions with a sustainability focus, often resulting in increased costs due to lower demand, higher material and design expenses, and limited production scale. Even though current costs are much higher for BFRP floors than for conventional floors, there is potential for BFRP floors to become more cost-effective and competitive in the future, especially when the environmental impact is reduced. It is difficult to estimate how the price of BFRP floors would change over time, and therefore, it has not been taken into account in the results.

Based on this study, it is recommended to do further research on bio-based core materials and their material properties such that they can be effectively used in a BFRP floor design and contribute to the reduction in the BFRP material used. Furthermore, it is recommended to focus on environmentally friendly and 100% bio-based resins, as they account for a substantial portion of CO_2 emissions. Moreover, a resin derived from bio-based sources enhances the environmental impact at end-of-life. Finally, it is recommended to investigate the fire resistance of the floor to make the floor more widely applicable.

Contents

Nomenclature

Abbreviations

BFRP   Bio-Based Fiber Reinforced polymers

CLLT   Classical Laminate Theory

CLT   Cross-Laminated Timber

ECI   Environmental Cost Indicator

EPD   Environmental Product Declaration

FEA   Finite Element Analysis

FEM   Finite Element Modelling

FRP   Fiber Reinforced Polymers

GFRP   Glass Fiber Reinforced polymers

ILSS   Inter Laminar Shear Strength

LCA   Life Cycle Assessment

LCI   Life Cycle Inventory

LCIA   Life Cycle Impact Assessment

MPG   MilieuPrestatie Gebouwen

PLA   Poly Lactic Acid

QI   Quasi-isotropic

RTM   Resin Transfer Molding

SLS   Serviceability Limit State

UD   Uni-directional

ULS   Ultimate Limit State

VARTM Vacuum Assisted Resin Transfer Molding

Greek Symbols

ϵ Strain [mm/mm]

η Conversion factor [-]

η Factor for root mean square velocity [-]

η Viscosity factor [-]

γ Shear strain [mm/mm]

μ Resonant buildup factor [-]

ν Poisson ratio [-]

ϕ Creep coefficient [-]

ϕ Empirical Reduction Factor [-]

ρ Density [kg/m^3]

σ Stress [MPa]

τ Shear stress [MPa]

θ Angle [°]

ζ Modal damping ratio [-]

Latin Symbols

B Width [mm or m]

b Width [mm or m]

c Spacing [mm]

E Young's modulus [MPa or GPa]

F Concentrated point load [N or kN]

f Strength [MPa]

G Fracture energy [N/mm]

G Shear modulus [MPa or GPa]

h Height [mm]

I Impulse [Ns]

I Moment of inertia [mm^4]

K Rotational stiffness [kNm/rad]

K Stiffness [N/mm]

L Length [mm or m]

l Length [mm or m]

M^* Modal mass [kg]

N Normal force [N or kN]

T Temperature [C°]

t Thickness [mm]

V Volume [m^3]

v Velocity [m/s]

Subscripts

1   Fundamental

1	Local 1 direction	m	Material
2	Local 2 direction	m	Mean
c	Compression	mod	Modal
c	Conversion	n	Normal
c	Core	R	Resin
cm	Conversion for moisture effects	Rd	Resistance design value
conc	Concentrated	red	Reduction
ct	Conversion for temperature effects	res	Resonance
d	Design	rms	Root Mean Square
dyn	Dynamic	s	Service temperature
Ed	Design value	s	Shear
f	Facing	T	Transversal
f	Fiber	t	Tension
f	Flexural	tot	Total
g	Glass temperature	w	Web
imp	Higher modes in transient response	wr	Wrinkling
k	Characteristic	x	Direction x
L	Longitudinal	y	Direction y
M	Material		

List of Figures

List of Tables

1

Introduction

In this chapter, the introduction to this master thesis research is presented. The first section aims to familiarize the reader with the background knowledge of the project. Subsequently, the problem statement is defined, leading to the formulation of the objective and research questions. Lastly, the methodology is discussed, which is a guideline in this research and report.

1.1. Background
1.1.1. Environmental performance of buildings
One of this time's most significant environmental challenges is human-induced climate change [1]. The building and construction industry contributes to approximately 40% of global energy-related carbon emissions [2]. This pressing concern aligns with the objectives outlined in the Paris Agreement, an international accord aimed at mitigating climate change [3]. The agreement emphasizes the urgent need to limit global warming to well below $2°C$ above pre-industrial levels and strives to limit the temperature increase to $1.5°C$. To achieve this, greenhouse gas emissions must peak before 2025 at the latest and decline by 43% by 2030.

To achieve these goals, it is crucial for buildings to comply with sustainability standards. Governments are implementing "Paris-proof" criteria, which require buildings, among other things, to emit below a specific threshold of CO_2 emissions. In the Netherlands, a criterion concerning the environmental impact is the Environmental Performance of Buildings (MPG = MilieuPrestatie Gebouwen) [4]. The MPG is mandatory for every environmental permit and applies to buildings larger than 100 m² and newly constructed homes. Starting from January 1, 2018, the maximum limit for the MPG is set at 1.0. On July 1, 2021, the environmental performance requirement for new homes (excluding offices) was tightened from 1.0 to 0.8. The objective is to make the requirement stricter and reduce it by half by 2030. The rapid tightening of these criteria can lead to difficulties for projects that fail to meet them, potentially facing the threat of delays or even being halted [5].

To achieve these more strict regulations and reduce the environmental impact of buildings, innovative building solutions will have to be found. To explore alternative ways, this research will look into an innovative floor solution. Floors have the highest potential for carbon and energy savings, accounting for approximately 20% of a building's overall environmental impact, and are thus a good place to start [6]. Ways to reduce environmental impact are by, for example, using sustainable materials, increasing reusability, using local materials, or any other way. Sustainable materials contribute to lower emissions and reduced resource depletion while minimizing material usage and self-weight. Reusability is significant in waste reduction, and incorporating local materials helps reduce transportation emissions.

1.1.2. Fiber-reinforced polymer
FRP is a composite material that has gained significant popularity in the construction industry. It comprises a polymer matrix reinforced with fibers, typically made of glass and carbon (see Figure 1.1). This combination results in a lightweight yet robust material that offers exceptional strength, durability, and design freedom. The fibers can be orientated in a specific lay-up to achieve specific material properties.
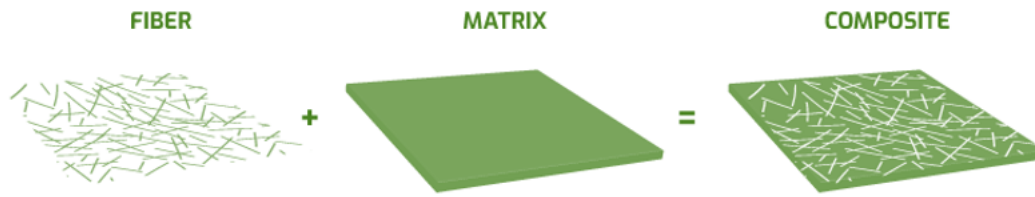
Figure 1.1: Composition of fiber reinforced polymer [7]

FRP finds widespread use in various construction applications, including pedestrian bridges, traffic bridges, building facades, and repairing existing structures [8]. A commonly used application is bridge decks currently commercially produced up till spanning 3 meters [9, 10]. However, using synthetic fibers and resins hinders the potential of achieving sustainable solutions [11]. The utilization of bio-based material in FRP poses the potential to improve the environmental impact of FRP. Natural fibers such as flax fibers with partial bio-based resins have been used in the construction industry for bridge designs and facades. But also in other industries, such as the automobile industry, bio-based FRP (BFRP) is utilized [12].

Aiming to encourage the integration of bio-based materials into construction practices, particularly those involving natural fibers, the Dutch government initiated a program. The primary goal is to motivate farmers to shift their focus toward fiber cultivation. Additional information regarding the specifics of this endeavor can be found in a letter addressed to the House of Representatives by the Dutch Government [13]. In addition to their bio-based nature, the fact that they are locally produced is a significant advantage for the environmental impact [14].

1.1.3. Modular buildings

Modular buildings have gained attention as a sustainable and efficient design solution in the construction industry [15, 16]. These structures are characterized by their prefabricated components, manufactured off-site and assembled on-site. These components can be elements of the structure or whole modules containing beams, columns, and a floor. This approach offers numerous benefits, not only in terms of sustainability but also during the construction phase. There are also limitations to modular construction. Both the advantages and limitations are briefly addressed. According to an extensive literature review by Subramanya et al., the benefits outperform the limitations [15].

Benefits
- **Project scheduling**: With modular construction, various activities can be performed simultaneously, leading to faster project completion. Additionally, weather conditions have minimal impact, as most work is done in a controlled off-site environment.

- **Cost savings**: Implementing modularization can result in a construction cost decrease of 10%-25%. Factors contributing to the lower cost include reduced material transportation and on-site labor requirements.

- **Labor safety**: Enhanced due to the tightly controlled and predominantly automated production of prefabricated components. Skilled workers repetitively perform the same procedures in a controlled environment, minimizing safety risks. Accidents in construction projects can be reduced by up to 80% when modular construction methods are employed.

- **Quality**: Standardization in the design procedure is facilitated by ensuring consistency and efficiency in the construction process. Additionally, the components are not exposed to adverse weather conditions that could affect material quality.

- **Environmental impact**: Traditional construction methods generate significant waste, posing environmental challenges. Modular construction has the potential to reduce waste by up to 83.2%, depending on the rate of prefabrication [16].

- **Staff shortage**: The construction industry is facing similar challenges to other fields of expertise, primarily the issue of staff shortage. However, the production of modular buildings off-site provides a promising solution by automation and reducing the need for manual labor.

Limitations

- **Project planning**: Accurate planning with explicit scope and design details is crucial. This requirement sets it apart from traditional building methods and poses a challenge due to the different planning approaches involved.

- **Transportation**: An adequate number of vehicles for delivery and special transportation considerations are necessary for oversized components. To avoid additional permits, modules must have a width below 3.5 meters. These factors can result in delays, increased costs, and heightened complexity in the overall construction process.

- **Public opinion**: The concept of modular construction is still viewed negatively by the public and even by some construction experts. Overcoming this perception and gaining acceptance will be vital for the wider adoption of modular construction. Raising awareness about its positive aspects is necessary for this change to occur.

- **Establishment costs**: Establishing a fabrication plant requires off-site construction, which adds to the establishment cost. Furthermore, modular construction relies on experienced suppliers, contractors, designers, and engineers knowledgeable in prefabricated construction.

- **Coordination and transitioning**: Coordination and transitioning between construction stages are crucial for project completion on schedule and within budget. However, the different procedure involved in modular construction presents a greater challenge in terms of coordination.

Modular building examples

Timber is frequently used as a primary material for a module in a modular building. These timber modules are typically constructed using cross-laminated timber (CLT) for the floor and roof, ensuring stability, while columns are utilized to maintain interior design flexibility and facilitate vertical load transfer. A great example of modular buildings is the temporary houses by Flexwoning [17]. They created houses with both CLT and a timber frame construction. Another example is The Natural Pavilion in Almere [18]. The objective of this project was to construct an innovative building that embodies modularity, demountability, circularity, and the utilization of bio-based materials. The building is built with modules and frames, and the stability is provided by steel bracing.

Figure 1.2: Left: Temporary housing [17]. Right: The Natural Pavilion Almere [18]

1.2. Problem Statement

The building industry faces substantial environmental challenges. Among other things, modular construction and utilization of bio-based materials can potentially contribute to a building industry with a lower environmental impact. BFRP is a bio-based material that is getting more attention because of its favorable material properties. Nonetheless, BFRP is currently not employed for constructing building floors. This means there is limited knowledge regarding BFRP floor design, its environmental implications, and costs. This thesis looks into the feasibility of applying BFRP floors in modular buildings. It addresses the problem of reducing the environmental impact of the building industry and answers the question of whether the use of BFRP can contribute to achieving this goal.

1.3. Research Question

The research objective will be accomplished by answering the main research question. The sub-research questions are formulated to provide a clear direction throughout the research process.

What is the feasibility and potential of a BFRP floor as a sustainable and cost-effective alternative to conventional floors in modular buildings?

1. Which BFRP can be used in floors, and what are its required physical and mechanical properties?

2. What specific design requirements must a BFRP floor satisfy concerning the ultimate and serviceability limit state?

3. How does the structural, environmental, and economic performance of a BFRP floor compare to that of a conventional floor?

1.4. Scope

To ensure a clear definition of the research focus, it is crucial to define the scope of the study. The following list outlines the key boundaries and limitations of this research:

- The focus of this research is on evaluating the feasibility of BFRP floors, in general, using representative BFRP material rather than providing a detailed comparison of the performance of different BFRP.

- Given the focus on modular building structures, the study concentrates on a design solution for both a one-way floor supported by beams and a two-way floor supported by columns. This research does not address two-way floors supported by beams; nonetheless, the methodology used in this study is applicable to such floor arrangements.

- Detailed design of the connection between the floor and the main structure is beyond the scope of this research. The supporting area of the support is taken into account for the design.

- The environmental comparison is restricted to CO_2 emissions and includes the scope from the sourcing of materials to the realization of construction.

1.5. Methodology

The general methodology is outlined in Figure 1.3 to address the research question and sub-questions. In essence, this entails several steps. First, conduct a literature review to gather information on material properties and design requirements. Next, introduce a case study and develop BFRP floors, both one- and two-way systems. Finally, the BFRP floors are compared to conventional floor systems. The conventional floors considered are CLT, concrete flat slab, and concrete hollow-core slab. The following paragraphs elaborate on these steps.

Step 1: Literature review

The literature review contains two main aspects. Firstly, it explores floors in general, examines their functions, and provides an overview of the design requirements. Additionally, the current state-of-the-art in BFRP is identified, considering applications utilizing BFRP and available literature on material properties' design values. The findings from this literature review, the design requirements, state-of-the-art, and material properties form the basis for developing BFRP floors.

Step 2: Case study
Instead of investigating numerous floor configurations with various boundary and loading conditions, a more focused approach is adopted to establish a baseline for the BFRP floor. This approach involves selecting a representative case study for which an alternative BFRP floor design is developed. The chosen case study should adequately represent modular building floors and offer the potential for the designed floor to be applicable in general cases.

Step 3: Floor design
This section represents a crucial and extensive part of the research, focusing on floor design and Finite Element Modelling (FEM). Figure 1.4 presents a visualization of the set-up of the design procedure. The key aspects can be summarized as follows:

- **Design:** The floor design is based on the structural systems employed in FRP bridge deck designs, specifically designed to span from one point to another, currently used for spans up to 3 meters for prefabricated bridges. Different solutions are found for a module floor of a modular building in the case study. These solutions can be divided into one- and two-way floors. Analytical calculations are used to verify specific failure modes and determine the initial geometry of the floor. Finally, the failure modes of the floors are identified for analysis in the modeling phase.

- **FEM:** The one- and the two-way floor is modeled. The design values of the material properties obtained from the literature and the design are combined. The numerical model of the one-way floor is used for validation using analytical equations for deflection and fundamental frequency. The numerical model of the two-way floor is used to understand the behavior of the floor. Furthermore, a mesh sensitivity analysis is done to get the most realistic results out of the models.

Step 4: Comparison
A comparative analysis is conducted between BFRP one-way and two-way floors and conventional floors. This comparison involves structural, environmental, and economic aspects. For the environmental analysis, a Life Cycle Assessment (LCA) in the scope from the sourcing of materials to the realization of construction is made for CO_2 emissions. Regarding the cost comparison, a basic evaluation of the material and assembly costs is conducted to provide a glimpse into the potential of BFRP floors.

Step 5: Research outcome
To answer the research question, a conclusion has to be drawn from the previously made from the floor design and performed comparison. To determine the structural feasibility of BFRP floor applications in modular buildings and assess their potential in terms of environmental impact and costs, the following hypotheses have been formulated:

1. The BFRP floor is feasible for use in modular buildings when thickness and weight are similar or less than the CLT and concrete floors for the same design criteria.

2. The BFRP floor has potential in modular buildings when the CO_2 emission and costs are the same or less than the CLT and concrete floors.
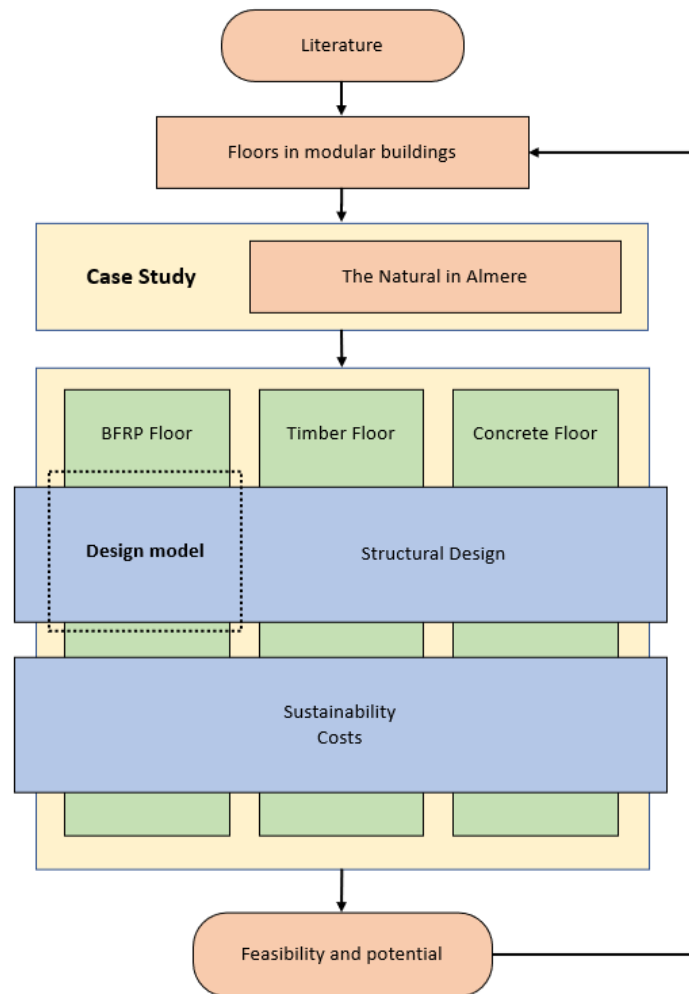
Figure 1.3: Methodology outline

Figure 1.4 represents the design and modeling part of this research. This framework represents the black dashed box 'design model' in Figure 1.3. The following enumeration presents a brief explanation of this framework:

1. The input for the model originates from the literature review and is based on whether a one- or two-way floor is designed.

2. The two-way floor requires additional analysis on special failure modes that do not occur for the one-way floor. These failure modes are addressed by a local model, resulting in threshold stress for the two-way floor design.

3. The global model is set up the same for one- and two-way floors. The validation is done with a mesh sensitivity study and analytical calculations for the one-way model. The analysis that is run to require the input to verify whether the floor fulfills the design requirements are linear analysis, modal analysis, and steady-state analysis.

4. The verification is done based on the second-generation Eurocodes for timber and FRP, together with the input from Abaqus.
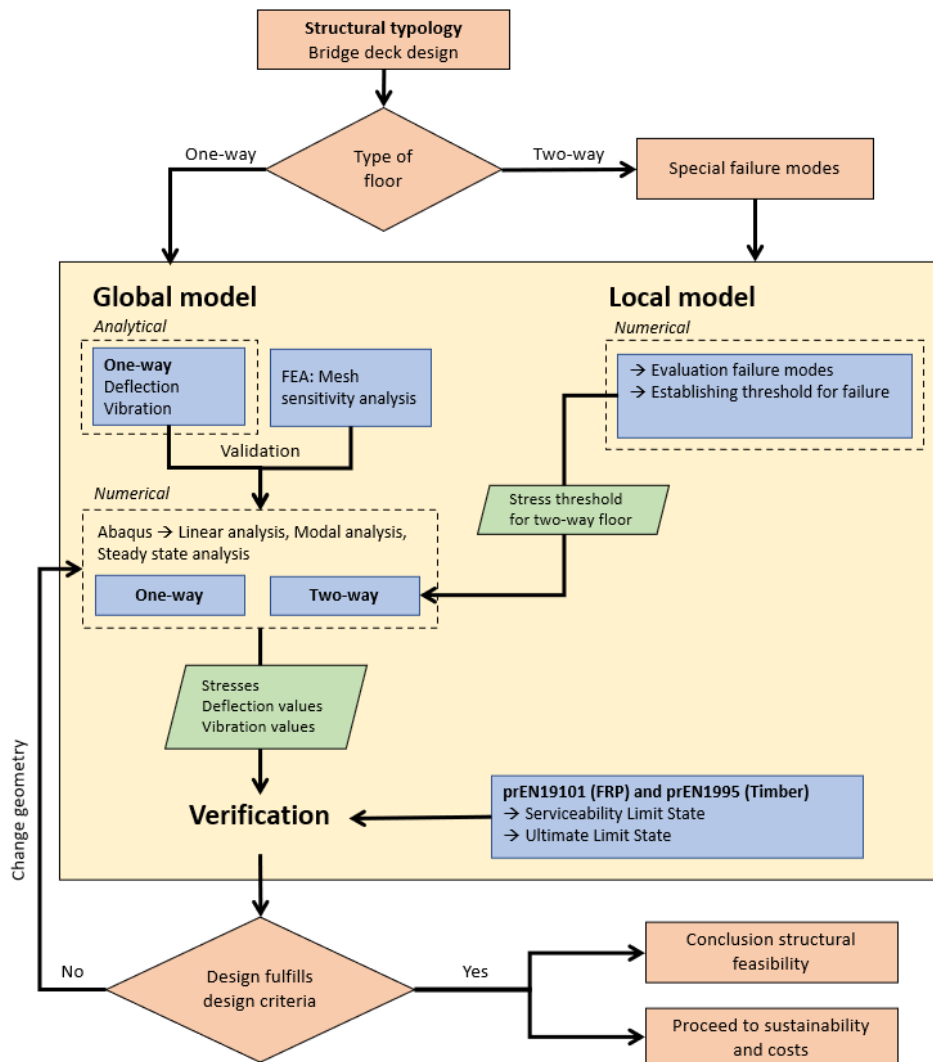
Figure 1.4: Methodology of design model

1.6. Structure of Report

This report is divided into three parts. The first part includes the literature review on floors, BFRP, and sustainable design, corresponding to **Step 1** of the methodology. In the second part, the case study and design of the BFRP floor are discussed, corresponding to **Step 2** and **Step 3** of the methodology. The final part includes comparing the floors, the discussion, the conclusion, and the recommendation, covering **Step 4** and **Step 5**.

Part I

Literature Review

<div align="right">

2

</div>

<div align="right">

Floors

</div>

2.1. Introduction

In this chapter, the various functions and applications of floors in buildings are discussed. The following questions will be addressed:

- What are the functions of a floor, and how are they addressed in regulations and existing floor structures?
- What are one- and two-way floor systems, and what are their advantages and disadvantages?
- What floor systems are currently utilized with conventional materials such as concrete and timber?

2.2. Functions

A floor structure serves multiple functions, both structural and comfort aspects. It is responsible for load transfer while providing stiffness, addressing acoustics, and mitigating vibrations for occupant comfort. This section briefly discusses these functions, highlighting their importance in floor design.

2.2.1. Strength and stability

Vertical loads

As a structural member, the primary function of a floor is to bear vertical loads. Vertical load transfer occurs as the floor transmits the loads to the beams, transferring them to the columns and, ultimately, to the foundation. Depending on the floor system employed, the floor may also directly transfer loads to the columns. In Figure 2.1, a simple example demonstrates how vertical loads of the structure are transferred through the floor to the (beams and) columns.
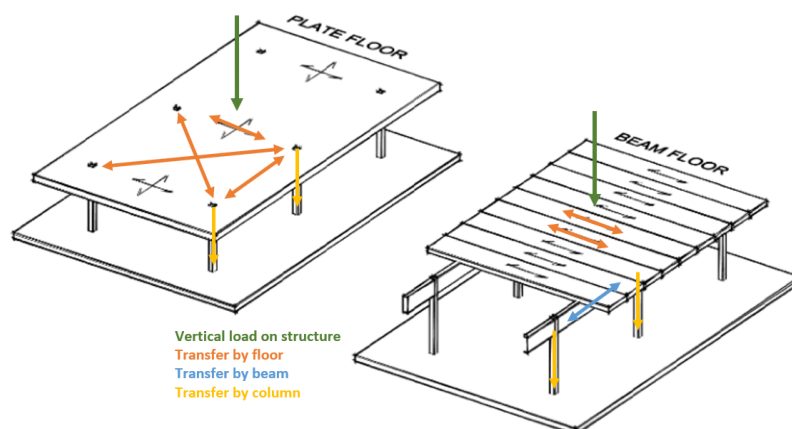
Figure 2.1: Principal of plate and beam floor [19]

Horizontal loads

To provide stability in a building, horizontal loads need to be transferred to the stabilizing elements of the building. Commonly used stabilizing systems are [20]:

- **Framework structures**: In these structures, columns and beams, as well as walls and floors, are interconnected in a moment-fixed manner, providing robust stability.
- **Flat concrete walls**: Flat concrete walls contribute to the building's overall stability by resisting lateral forces and providing stiffness.
- **Core structures**: Core structures consist of a central vertical core offering vertical load transfer and significant resistance against horizontal forces.
- **Outrigger structures**: Outrigger systems employ outrigger walls or braces at regular intervals to enhance the building's lateral stability.
- **Supporting facades**: Facades designed to withstand horizontal forces can also contribute to the overall stability of the building.

The allocation of horizontal load transfer can be attributed to either the floors or a bracing system. Bracing systems comprise diagonal or vertical elements strategically placed within the building structure. These bracing components redirect lateral loads. When the floors assume the role of horizontal load transfer elements, the rigidity of the floors in the horizontal plane is important. This phenomenon is recognized as the floor section effect or diaphragm action, where the floor operates as a horizontal plane, transferring horizontal loads efficiently throughout the entire structure. Figure 2.2 shows how the horizontal loads are transmitted to the stabilizing system of a structure.
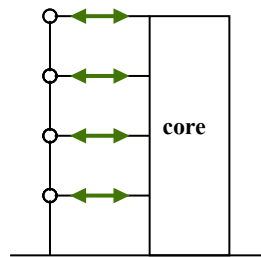
Figure 2.2: Structural system with stabilizing core

Load-bearing capacity

Careful analysis of internal forces resulting from vertical and horizontal load transfer is essential. This involves examining the load-bearing capacity of the floor and determining its ability to withstand loads before failure. This verification is vital for meeting safety standards.

Engineers rely on guidelines and regulations when designing buildings and floors. In Europe, the Eurocodes are extensively employed for this purpose. Eurocode 0 and Eurocode 1 are utilized to ensure structural safety, serviceability, and durability and consider actions on structures. Eurocode 2 to Eurocode 9 are used to facilitate design and detailing, with each code addressing specific materials. In 2012, the European Commission issued a detailed work program to revise the existing Eurocodes and expand the coverage of structural Eurocodes [21]. This second generation encompasses the development of a Eurocode for FRP, denoted as CEN/TS 19101 [22], alongside the expansion of the timber Eurocode through prEN1995.

By Eurocode 0, the consequence class of a floor needs to be determined. The consequences involve the risk of loss of human life and the effects on the environment and economic interests. The consequence classes are subdivided into three categories. The description of each class can be seen in Table 2.1. Besides the consequence classes, the design life of the structure should be set. The design life for a specific application can be seen in Table 2.2. The design life of residential, office, and conference buildings is all 50 years.

These Eurocodes offer valuable insights into potential failure modes in structures. However, an engineer should always be objective and assess and address possible failure modes to mitigate risks and ensure the structure's structural integrity.

Table 2.1: Consequence classes adapted from Eurocode 0 [21]

Concequence Class	Explanation
CC3	Large consequences regarding the loss of human lives or significant economic or social impacts or impacts on the environment.
CC2	Moderate consequences regarding the loss of human lives or significant economic or social impacts or impacts on the environment.
CC1b	Slight consequences regarding the loss of human lives and small or negligible economic or social impacts or impacts on the environment.
CC1a	Virtually no loss of human lives and very small or negligible economic or social impacts or impacts on the environment.

Table 2.2: Design life of a specific application adapted from Eurocode 0 [21]

Design Life	Application
5	Structures of non-building works for one-time use. Temporary buildings for a maximum duration of 5 years.
15	Structures for agriculture, horticulture, and similar applications solely for production purposes with limited occupancy. Temporary buildings with the destinations described in this class.
50	Buildings and other ordinary structures of buildings, including temporary ones, not classified in classes 2 and 4.
100	Monumental buildings. The decision to designate a building as monumental is at the discretion of the client.

2.2.2. Fire safety
General

The fire safety of a building is of utmost importance, with primary objectives focused on minimizing casualties and mitigating damage to the building and its contents. For the sake of completeness, it is mentioned, but a thorough investigation of the fire resistance of a BFRP floor is outside the scope of this research.

In addition to minimizing property damage, fire safety design aims to ensure the safety of building occupants during evacuation. Various measures can be implemented to achieve this objective effectively. These may include providing numerous escape routes, installing an early warning detection system to alert occupants promptly, implementing a ventilation system to remove smoke and extend evacuation time, or dividing the building into smaller fire compartments to restrict fire spread and prolong evacuation periods. In practice, combining these measures collectively serves the intended safety objectives.

Buildings are often divided into compartments. Floors play a crucial role in the fire spread between compartments. They act as barriers that help prevent the rapid spread of fire, smoke, and heat between compartments in the structure. By containing the fire within a specific area, the floors aid in buying valuable time for evacuation procedures and allow emergency responders to focus their efforts on controlling and extinguishing the flames. Moreover, the floor must maintain its structural integrity for a specific duration to ensure that evacuation routes remain viable and emergency response operations can be conducted safely. The floor's ability to withstand intense heat and structural stresses during a fire incident is imperative.

Requirements

Fire regulations are defined in the Building Degree 2012 (Bouwbesluit 2012) [23]. These regulations specify how long a fire compartment must maintain its integrity and prevent the spread of fire. For buildings, there is a basic requirement of either 30, 60, 90, or 120 minutes for fire resistance, with a potential reduction of 30 minutes if the permanent fire load is lower than 500 MJ/m^2. Table 2.3 illustrates the fire requirements for various building functions above ground level for new constructions (Article 2.10 in the Building Degree 2012). In the case of terrace housing, the neighboring fire compartment can fail after 60 minutes, as one house can be considered a single fire compartment.

When assessing structural failure, as described in Article 2.10, consideration is given to the loading combinations that occur during a fire, as outlined in EN1990. The fire resistance is different for each material and can be calculated using the guidelines provided in EN1992 through EN1996 and EN1999, specifically in Part 1.2.

Table 2.3: Fire resistance requirements according to Building Degree 2012 [23]

Residential buildings			
Highest floor [m]	h ≤ 7	7 < h ≤ 13	h > 13
Requirement [min]	60	90	120
Potential reduction [min]	30	-	-
Building with sleeping function (hotel, jail, etc.)			
Highest floor [m]	h ≤ 5	5 < h ≤ 13	h > 13
Requirement [min]	60	90	120
Potential reduction [min]	30	30	30
Other buildings (without sleeping function)			
Highest floor [m]	h ≤ 5		5 > h
Requirement [min]	no requirement		90
Potential reduction [min]	-		30

Fire resistance of timber

Timber undergoes a process called charring when exposed to fire. The outer layer of the wood gradually burns away, forming a protective char layer. This char layer acts as an insulating barrier, shielding the inner, unaffected wood from the direct heat of the flames. The charring process effectively delays the spread of fire through the timber and slows down the degradation of its structural integrity. However, it is important to note that the timber's load-bearing capacity gradually decreases as the charring occurs. The charring rates for timber, accounting for corner rounding and cracks, are 0.7 mm/min for laminated timber and 0.8 mm/min for solid timber [24].

2.2.3. Comfort

Floors should provide a comfortable living area. For example, they must be designed to limit deflections and vibrations. Furthermore, adequate insulation is essential to maintain a consistent indoor temperature while reducing energy usage. Finally, the acoustic requirements of a building floor are important to ensure adequate sound insulation and acoustic performance.

Deflections

Deflection limits are primarily established to ensure user comfort and prevent the perception of an imminent failure of the floor. Additionally, these limits are put in place to avoid any (significant) damage to the elements supported by the structure. The assessment of deformations occurs during the serviceability limit state (SLS). However, the client can adjust the criteria to be less or more strict as long as the structural integrity is not compromised. The requirements for vertical deformations for floors are included in Appendix B.

Vibrations

Preventing disruptive vibrations resulting from walking and jumping is important for the comfort of the user and, ultimately, structural integrity. To ensure a comfortable floor, it is necessary to conduct fundamental frequency, velocity, and acceleration checks.

Eurocode 5 (prEN1995) for timber structures provides guidelines for vibration criteria in timber floors, which can also serve as appropriate guidelines for a BFRP floor because of the lightweight nature of both [24]. This Eurocode offers some general considerations regarding vibration, as outlined below:

- For non-residential floors and floors with unobstructed walking distances below 10 meters, a walking frequency of 2 Hz should be considered.
- Resonant response is not expected to occur above four times the walking frequency.
- Floors with a fundamental frequency equal to or greater than four times the walking frequency exhibit a transient response, meaning that vibrations diminish between impulses.
- Acceleration requirements (resonance response) must only be assessed when the fundamental frequency is lower than four times the walking frequency.
- The mass to be considered includes self-weight, permanent loads, and 10% of the characteristic imposed loads.

The vibration criteria depend on the floor performance level, which is determined by the user category and the floor's quality/base/economy choice. The requirements and calculation methods according to Eurocode 5 can be found in Appendix B [24].

Acoustics

It is crucial to ensure a proper acoustic design to create a comfortable and functional building environment. Acoustic requirements can be categorized into airborne and contact sound requirements. Airborne sound insulation requirements primarily focus on controlling the transmission of sound waves through the floor assembly, while structure-borne sound transmission involves mitigating vibration and impact noise. The latter aspect is particularly significant, especially for residential buildings subjected to strict regulations.

Adequate mass is required to provide sufficient contact sound insulation. Top floors are used to meet these requirements. They can be directly applied to the structural floor or installed as a floating top floor with an insulation layer in between. For lightweight floors, such as timber floors, a single top floor is not always sufficient, and additional mass has to be applied to meet the requirements.

Figure 2.3 shows an example of a structural concrete floor with a floating screed layer on top. The layer between the structural floor and screed layer is a flexible spring layer, accommodating sound vibrations while maintaining sufficient rigidity and strength to withstand loads. To prevent the transfer of vibrations, the spring-loaded screed should be free from direct contact with walls and other elements connected to the structural slab. The quality of the execution of floating screeds is crucial, as even a few "contact bridges" can significantly undermine the acoustic function of the spring-loaded screed.

It is essential to note that while this research does not explicitly address the acoustic requirements of the floor, an additional permanent load for the top or finishing floor is considered.

2.2.4. Other

The floors of a building often serve as a platform for various building services, including ventilation, electricity, plumbing, and other systems. In the design of a floor, the load-bearing requirements of these services should be considered. These services can be integrated into the floor structure or attached using hangers, brackets, or other supports. An integrated system should provide adequate space and access for installation and maintenance.

In this research, no in-depth analysis is done on the required services of the floor. However, the load resulting from the services is integrated into the permanent load of the floor.
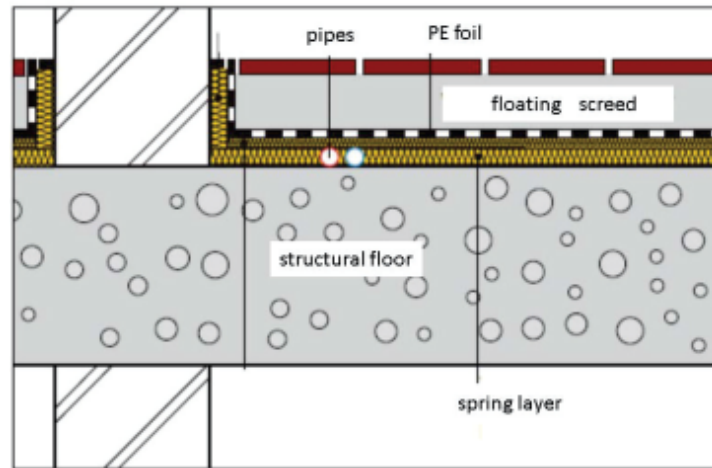
Figure 2.3: Side view of a structural floor with a floating screed layer [20]

2.3. One- and Two-Way Floor Systems

In subsection 2.2.1, the load path of vertical loads was briefly discussed. The type of floor used in a building depends on the chosen global structural system, defining the floor's functions and boundary conditions. A distinction in floors can be made between one- and two-way floors, also known as single and double-span floors. These types of floors can already be identified in Figure 2.1, where a beam floor behaves like a one-way floor, and a plate floor behaves like a two-way floor. In one-way floors, the load is primarily transferred in one principal direction, while for two-way floors, the load is transferred in two directions. It is important to consider the boundary conditions and size of the floor. For example, a floor supported by four columns may seem like a two-way system, but when $L_x/L_y > 2$, the floor is considered to be one-way [25].

The choice of a structural system and the required functions of a floor determine whether a one-way or two-way system is more suitable. One-way floors often have more straightforward design and construction processes. However, they perform less effectively in terms of diaphragm action and the transfer of lateral loads, often requiring a top layer to ensure sufficient load transfer between panels. On the other hand, two-way floors have more complex designs and are usually constructed under controlled conditions (with exceptions like concrete flat slabs). However, a two-way floor has a higher potential to provide lateral load transfer and stability, eliminating the need for an additional top floor or bracing system.

2.4. Existing Floor Systems

Two major design choices that need to be made for a floor are the selection of the material and the structural system. The most commonly used floor materials are concrete, steel, and timber. This section presents various structural systems utilizing these materials for floors, offering an overview of design solutions.

2.4.1. Concrete floors

Concrete floors are popular for structural floor systems due to their strength, durability, and versatility. Concrete floors are commonly used in industrial and commercial buildings because of their good structural resistance and limited deflection. In general, concrete has good vibration behavior due to its high stiffness and mass, which can help reduce the amplitude of vibrations and prevent them from propagating through the floor. Additionally, concrete's thermal mass can help maintain a stable internal temperature in buildings, which is important for energy efficiency. Concrete floors are also highly fire-resistant, which can help to prevent the spread in the event of a fire.

The application of concrete floors can have some critical considerations. One important factor to consider is the structure's design, as concrete floors can be heavy, and the building's foundation and structural frame must be able to support the weight. Installing an in-situ concrete floor can also be complex, requiring careful planning and coordination to ensure the concrete is poured and cured correctly. While concrete floors have many advantages, their production and use can have significant environmental impacts.

There is a wide range of concrete floor systems available for use in construction (see Figure 2.4). One of the simplest options is the flat slab, a popular choice for buildings with irregular shapes or layouts. The flat slab can be designed to span in multiple directions without the need for beams or columns, and its performance can be improved through post-tensioning techniques. This is the perfect example of a two-way floor and is cast in situ. Another option is the concrete hollow core slab, which minimizes material use while providing a robust and durable floor system. This floor is prefabricated and typically only spans in one direction. A third example of a concrete floor system is the suspended T-beam floor.

Figure 2.4: Concrete hollow floor, flat slab, T-beams [26, 27, 28]

2.4.2. Steel

Steel is a material commonly used in combination with concrete. Steel is normally used as reinforcement or tensioning with cables of a concrete slab. Steel can also be used in a composite steel deck floor. The steel deck provides support during construction and acts as a permanent formwork for the concrete slab. The concrete slab, in turn, provides compressive strength and stiffness to the composite system. A composite steel deck can efficiently transfer loads in longitudinal and transverse directions when properly designed.

Figure 2.5: Composite steel deck floor [29]

2.4.3. Timber

Timber is a popular material for floor systems due to its versatility, strength, and sustainability. Traditionally, timber is used in a joist system, where individual timber joists are spaced apart and supported by load-bearing walls or beams. Other systems used for timber floors are stressed skin panels. These can be open (joist timber floor), closed (sandwich), or with T-flanges. These systems are limited to span in only one direction but are still popular due to their simple design and ease of installation. They create a lightweight yet strong, stable floor system well-suited to various building types.

When a project requires a timber floor system to span in more than one direction, a popular choice is CLT. CLT is an engineered wood product that has become increasingly popular as a sustainable alternative to traditional concrete and steel floor systems in recent years. The process involves layering small timber in alternating directions, resulting in a panel with excellent structural integrity and load-bearing capacity. CLT offers many advantages, including a reduced carbon footprint compared to traditional floor systems, faster installation times, and the ability to prefabricate elements off-site. However, it is essential to note that CLT floors have some drawbacks. One of the main concerns is the potential for deflection and vibration due to its low weight compared to other materials.
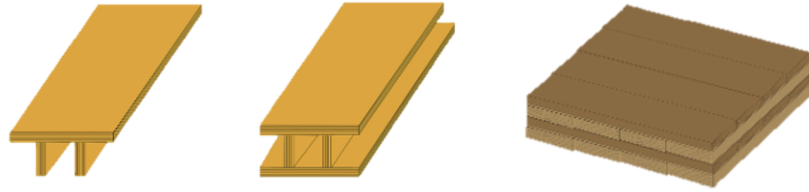
Figure 2.6: (a) Timber joist floor, (b) Stressed skin panel, (c) CLT

2.5. Conclusion

In conclusion, this chapter has provided a comprehensive overview of floors in buildings, addressing critical questions posed in the introduction.

Functions of a floor
- Floors serve critical functions in load transfer, stability, fire safety, comfort, and building services.
- They contribute to vertical and horizontal load transfer and ensure structural integrity and stability.
- Comfort aspects include managing deflections, vibrations, and acoustics, ensuring occupant well-being.

One- and two- systems
- Floors can be categorized as one- or two-way systems based on the primary load transfer direction.
- One-way systems primarily transfer loads in one direction, while two-way systems distribute loads in two directions.
- Selection between the two depends on design requirements, stability, and load distribution efficiency.
- One-way floors are easier to design and construct due to simpler load paths and reduced complexity.
- One-way floors may require additional measures for lateral load distribution, such as bracing systems.
- Two-way floors are well-suited for open-plan spaces and irregular layouts, providing structural efficiency.
- Two-way floors have more potential for diaphragm action, contributing to lateral load distribution and overall stability.

Existing Floor Systems
- Concrete floors are durable, offer fire resistance, and possess good vibration behavior.
- Concrete floor options include flat slabs, hollow core slabs, and suspended T-beam floors.
- Composite steel deck floors combine steel and concrete, providing efficient load transfer.
- Timber floors are versatile, sustainable, and common in joist systems or stressed skin panels.
- CLT floors are an innovative solution for multi-directional span floors, offering advantages in sustainability and prefabrication.

3

Bio-Based Fiber Reinforced Polymers

3.1. Introduction

This chapter focuses on BFRP. First, a general background and an overview of their current state-of-the-art applications are provided. Subsequently, the raw materials of BFRP and its material properties are discussed. Lastly, the chapter introduces the structural typology for the BFRP floors. The following questions are answered in this chapter:

- What is the current state-of-the-art in BFRP applications?
- Which raw materials, including natural fibers and resins, are commonly employed in BFRP?
- What are the key factors influencing the mechanical properties of BFRP?
- Which BFRP materials are suitable for the design of floors?
- What are the various production techniques available for BFRP?
- What structural typologies are suitable for BFRP floors?

3.2. General

FRP is a composite material. A composite is a material composed of at least two different materials and has different properties than the materials individually. FRP comprises reinforcing fibers embedded in a polymer matrix, also called resin. Figure 3.1 shows how the fibers and matrix form a fiber-reinforced polymer. FRP is mainly used because of its high specific strength and stiffness, low weight, freedom in shape, and tailor-able material properties [30]. These characteristics make FRP used in many fields ranging from household and office appliances to spacecraft and bridges.

FIBER + MATRIX = COMPOSITE
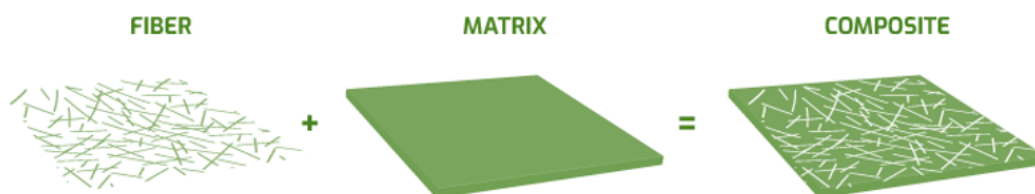
Figure 3.1: Composition of fiber reinforced polymer [7]

There are two different types of FRP: continuous FRP with long fibers and discontinuous FRP with short fibers. In discontinuous FRP, the fibers are randomly distributed throughout the resin (see Figure 3.1), whereas for continuous FRP, the fibers are aligned and placed in specific orientations (see Figure 3.2). Different fibers are used as reinforcement, including glass, carbon, and aramid fibers. However, the environmental considerations tied to synthetic materials have introduced a shift towards the increased utilization of natural fibers.
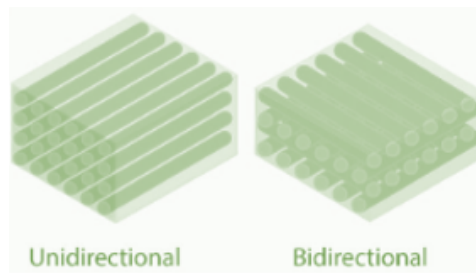
Figure 3.2: Continuous unidirectional and bi-directional lay-up [11]

However, using natural fibers is not the only factor in reducing the environmental impact. The resin, in fact, constitutes a significant proportion of FRP and thus holds considerable influence. Therefore, caution is required when employing the term "bio-based FRP". FRP can be categorized as bio-based if at least one of its constituent materials is bio-based [30]. This implies that the resulting material may not necessarily be 100% bio-based. The definitions utilized in this thesis for the different compositions of FRP are outlined in Table 3.1.

Table 3.1: Definitions of FRP materials and rate of natural materials used

Definition	Explanation
Fiber-reinforced polymer (FRP)	General; reinforced composites using fibers and polymers
Fiber-reinforced polymer with glass fibers (GFRP)	Glass fibers and petroleum-derived polymers
Bio-Based Fiber-Reinforced Polymer RP (BFRP)	At least one of the constituents is derived from natural resources
Green Fiber-Reinforced Polymer (green-FRP)	All constituents are derived from natural resources

3.3. Applications with BFRP

BFRP is being used in various industries. Table 3.2 gives an overview of natural fibers and their potential application in different sectors. Appendix A shows a more comprehensive overview. The following paragraphs delve deeper into the automobile and construction sectors.

Table 3.2: Potential applications of natural FRP adapted from [11]

Sector	Fibers	Applications
Civil construction	Banana	Compressed earth block
	Juce, sisal, ramie, pineapple	Cementitious materials
	Flax, jute, sisal, hemp, coir, palm	Masonry
	Jute	Deck panel
	Kenaf	Ceiling
	Wheat straw, corn husk	Thermal insulation materials
	Wood cellulose, cork	Thermal insulation materials
Furniture and architecture	Lignocellulose, straw	Lounge furniture
	Hemp	Chair furniture
	Hemp. flax	Ignot bio- and Polycal acoustic panel
	Lignocellulose	BioMat research pavilion
Aerospace	Hemp	Electronics racks for helicopter
	Ramie	Aircraft wing boxes
	Kenaf	Aircraft materials

3.3.1. Automotive

Attempts to use natural fibers in the automobile industry go back to 1941 when Henry Ford and George Washington Carver attempted to use hemp and flax fibers. Natural fibers are mainly used for interior parts, dashboards, trays, headliners, seat backs, and door panels because of their relatively low mechanical properties and moisture sensitivity [11]. Other applications where flax fibers are used for the exterior are, for example, parts of bodywork in the new BMW M4 GT4 and the Porsche Cayman 718 GT4 CS MR. For these applications, the ampliTex fibers from the company Bcomp are used [31]. The main reasons for using BFRP in the automobile industry are because they are lightweight, effective in reducing noise and vibration through damping, and have a low environmental impact.

3.3.2. Construction

In the construction industry, BFRP is utilized in several different applications. For example, it is used as roof tiles, floor matting, ceilings, doors, window frames, and bridges.

Facades

An example from practice is the BFRP facade tile of Nabasco; see Figure 3.3. This tile is composed of 33% reed, 33% lime, and 33% bio-resin.

Figure 3.3: Nabasco BFRP facade tiles [12]

Bridges

Movable pedestrian bridge Emmen

The first foldable Dutch bridge with BFRP can be found in Wildlands Adventure Zoo in Emmen. For the bridge deck, a composite sandwich design is used with BFRP facings of flax and cobalt-free bio-resin (Venylester of ATLAC) and a foam core created from recycled PET bottles. The bridge's width is 4 meters, and it spans 5 meters [32, 33]. Figure 3.4 shows the bridge built in Emmen.

Figure 3.4: Foldable BFRP bridge in Wildlands Adventure Zoo in Emmen [32, 34]

Figure 3.5 illustrates the cross-section of the sandwich configuration used for the bridge. This schematic presentation corresponds to the outer right picture in Figure 3.4. Unfortunately, detailed information about the bridge design is unavailable, necessitating an assumption regarding the panel thickness.
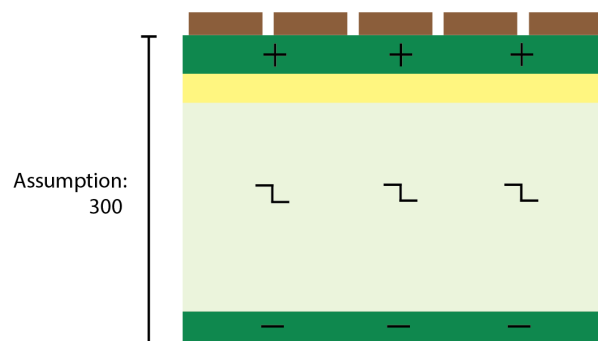
Figure 3.5: Cross-section of pedestrian bridge Emmen [mm]

The top surface primarily undergoes in-plane compressive loading, while the bottom surface experiences tensile loading, both induced by bending moments. Notably, the top surface has a larger thickness than the bottom surface. This distinction can be attributed to two potential factors: either additional compressive resistance was deemed necessary due to BFRP demonstrating higher tensile strength than compressive strength, or it offers enhanced resistance against concentrated loads. Moreover, it is presupposed that the presence of wooden planks and the supplementary yellow layer contributes to the ability to withstand concentrated loads. As for the foam core, its role involves withstanding shear loading, such as that arising from concentrated loads, and facilitating load transfer between the two surfaces.

Pedestrian bridge Eindhoven
A second pedestrian bridge made of BFRP can be found at the Eindhoven University campus, as shown in Figure 3.6. This bridge spans a length of 14 meters and is constructed with a single beam, which is accentuated by fan-shaped balustrades. The materials used in its construction include PLA (poly lactic acid) foam, cork, hemp, and flax fibers, combined with a bio-based epoxy resin (bio-content of 45%). Due to its low melting point, the cork is utilized as a layer around the core to protect the PLA foam during production.

Figure 3.6: BFRP bridge at University Eindhoven

Figure 3.7 illustrates the bridge's cross-section at mid-span. The cross-sections at the bridge sides are about a third of the height. The top flange deals primarily with compression at the bridge center, while the bottom flange handles tension. The cross-section's height peaks at mid-span, where the most significant bending moments and resulting stresses occur. The flanges are thicker (20 mm) to tackle these forces than the webs (10 mm). The bridge's bow shape also contributes to its ability to span 14 meters. The central core combines with the side flanges to resist shear forces, providing resistance against concentrated loads alongside the core.
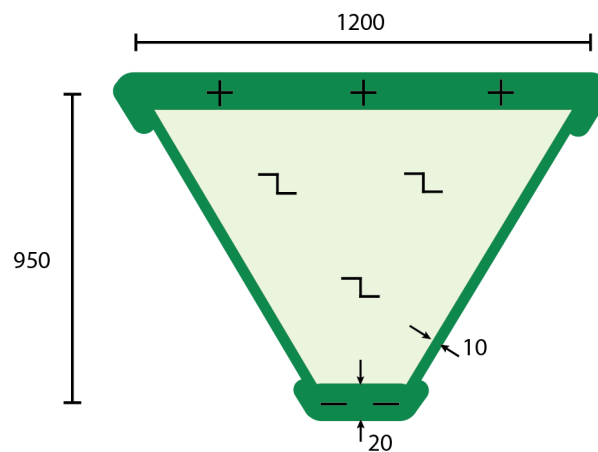
Figure 3.7: Cross-section of pedestrian bridge Eindhoven [mm]

Movable biking bridge Ritsumasyl
The largest BFRP bridge mentioned is the Ritsumasyl bridge. The bridge spans two times 22 meters. This bridge is located in Friesland, a province in The Netherlands. A BFRP with ampliTex flax fibers from Bcomp and a (33%) bio-based epoxy are used for this bridge. This is not a 100% bio-based bridge because of durability challenges and costs. Five main girders with a U-shape, a bottom flange, and a sandwich with balsa as the top deck form the boxed-girder cross-section of the bridge, see Figure 3.8. Compared to a concrete bridge variant at the same location of 400 tonnes, the BFRP bridge is lightweight at only 30 tonnes.

Figure 3.8: Movable bio-composite bridge spanning 22 m in Ritsumasyl and cross-section [35]

Figure 3.9 shows the cross-section of the Ritsumasyl bridge. The external dimensions of the cross-section are 3.65 m wide and 1.2 m high. The bridge consists of a sandwich deck with a balsa core and skins made of flax composite. The bottom is made of solid flax composite and locally reinforced with stiffeners to improve buckling strength. To enhance buckling resistance, the three middle girders are executed as thin sandwiches with a balsa core. Due to multiple girders and the absence of bearing stress, the cross-section has sufficient load-carrying capacity to prevent progressive failure. The sides are executed solidly to allow for the connection of railings and edge elements. All parts are laminated together, resulting in a liquid-tight deck. At the location of the pivot, bulkheads are positioned. Besides adequate load absorption of reaction forces, the bulkheads provide additional stability and robustness to the whole system.
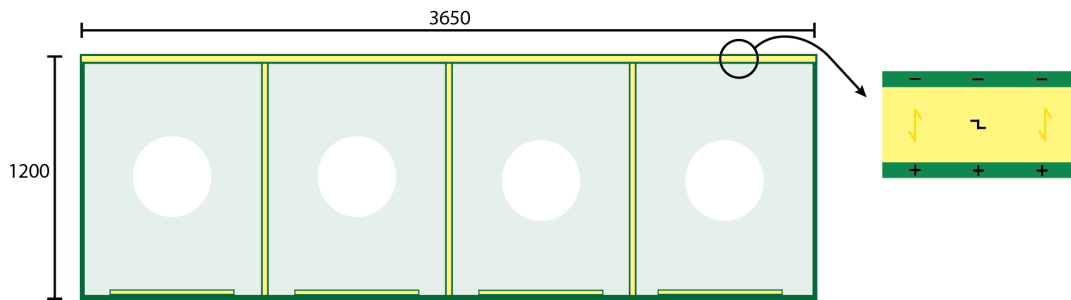
Figure 3.9: Cross-section of pedestrian bridge Ritsumasyl [mm]

Focusing on the sandwich panel used as the bridge deck, all elements perform similar functions to the Emmen pedestrian bridge. The 15 mm thick facings primarily provide tensile and compressive resistance from bending moments. The sandwich core, made of balsa wood, serves the primary function of providing sufficient shear stiffness and concentrated load resistance. The Baltek SB150 of 3A Composites Core Materials with a thickness of 45 mm was used for this bridge. The density of this balsa core is 288 kg/m², providing substantial characteristic shear resistance of 4.9 N/mm² [36]. The grain of the balsa core is oriented out-of-plane.

FiberCore Europe bridge

FiberCore Europe specializes in manufacturing infrastructure components, such as bridges, sluice gates, and bridge decks, using FRP. One notable achievement is the successful collaboration in constructing the Ritsumasyl Bridge. While FiberCore has an impressive portfolio of projects utilizing synthetic FRP materials, their experience with BFRP remains limited. As depicted in Figure 3.10, FiberCore has used bio-based materials for bridge construction. The pictured bridge, with a span of 9 meters and a width of 2 meters, features basalt fibers and a bio-based polyester resin with a partial bio-content. Unfortunately, specific data on the materials used remains undisclosed.

Figure 3.10: Bio-based bridge at Schiphol Logistics Park [37]

FiberCore employs a unique layup method for building FRP bridge decks, known as InfraCore technology, which is further explained in section 3.11. This technology is based on the load transfer principles of an I-shaped beam, as illustrated in Figure 3.11. The webs primarily handle shear forces, while the top and bottom facings bear bending forces. The webs also bear concentrated loads. Presently, they produce bridge decks with spans of up to 3 meters.
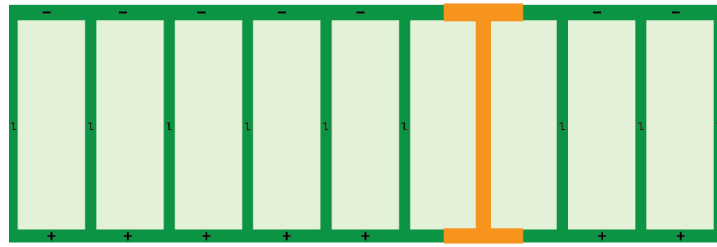
Figure 3.11: Cross-section of bridge deck of FiberCore

3.4. Factors Affecting Mechanical Properties

BFRP offers unique possibilities in building design, allowing for tailored shapes, good material properties, and greater design freedom. While there is already considerable experience with designing with GFRP, many important considerations must be taken into account when using natural fibers [11]. Table 3.3 gives an overview of the advantages and disadvantages of BFRP to GFRP. Factors that primarily influence the behavior of BFRP are listed below and are addressed one by one:

- The choice of fiber
- The choice of matrix
- The strength of the interface between fibers and matrix
- The dispersion and orientation of fibers
- The manufacturing process on the material level
- The production process of BFRP

Table 3.3: Advantages and disadvantages of BFRP compared to synthetic FRP [38]

Advantages	Disadvantages
Lower CO_2 emission and required production energy	Variability of properties which causes difficulties in standardization
Less abrasive to processing equipment than synthetic FRP	Degradation due to moisture absorption
Relatively high specific strength and stiffness to weight ratio	Low curing temperatures
Higher damping coefficient than synthetic FRP	Costly durability enhancement necessary

3.5. Fibers

The origin of the fiber is important to consider. Fibers are often classified according to their source: plant-based, animal-based, or mineral-based (see some examples in Figure 3.12). Plant-based fibers are used in the construction industry because they are derived from vegetable sources. Therefore, completely biodegradable and sustainable [11]. Additionally, plant-based fibers have desirable mechanical properties, such as sufficient tensile strength, flexibility, and durability, making them suitable for various construction applications. In contrast, animal-based fibers, such as wool, silk, and hair, are not commonly used in the construction industry due to their high cost and limited availability. Mineral-based fibers are made from naturally occurring materials but are often not considered bio-based because living organisms do not produce them. Well-known mineral fibers are basalt fibers; they have high tensile strength, excellent resistance to heat and fire, and good chemical stability [39]. Basalt is commonly used in the construction industry as a reinforcement material added to concrete. Additionally, basalt can be employed as a raw material for producing basalt rebar, providing corrosion-resistant reinforcement in concrete structures. Other mineral-based fibers, such as asbestos, have been banned due to health and safety concerns associated with their use and are banned in many countries [40]. In this research, plant fibers are investigated in-depth because of their bio-based nature and the initiative of the Dutch government to increase its local production in the Netherlands [13].

Figure 3.12: Natural fibers: (1) Plant-based flax fiber [41], (2) Animal-based silk fiber [42], and (3) Mineral-based basalt fiber [43]

3.5.1. Plant fibers and its constituents

Cellulosic fibers produced by plants can be categorized as bast, leaf, seed, wood, and grass fibers. Figure 3.13 shows an overview of some fibers within each category.
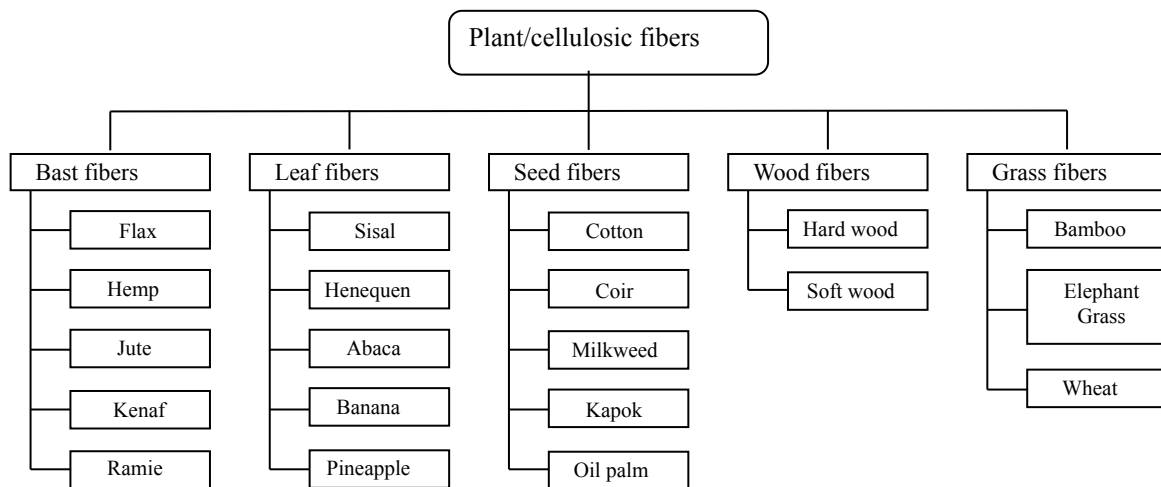
Figure 3.13: Categorization of plant/cellulosic fibers [11, 40, 44, 45]

The properties of natural fibers depend on a lot of factors. Among other things, the age of the plant, growing environment, harvesting, humidity, quality of soil, temperature, and processing steps influence the performance of the fiber. This results in a wide range of material properties. An overview of fibers and their properties, including those of commonly utilized synthetic fibers for reference, is presented in Table 3.4. A more comprehensive overview of fibers can be found in Appendix A.

Table 3.4: Properties of several natural fibers and commonly used synthetic fibers adapted from [30]

Fiber	Density [g/cm^3]	Elongation [%]	Tensile strength [MPa]	Young's modulus [GPa]
Banana	1.3-1.4	2.0-7.0	54-789	3.4-32.0
Cotton	1.5-1.6	3.0-10.0	287-597	5.5-12.6
Flax	1.4-1.5	1.2-3.2	345-1500	27.6-80.0
Hemp	1.4-1.5	1.6	550-900	70
Jute	1.3-1.5	1.5-1.8	393-800	10.0-30.0
Ramie	1.5	2.0-3.8	220-938	44.0-128.0
Carbon	1.4	1.4-1.8	1500-5500	230.0-240.0
E-glass	2.5	2.5-3.0	2000-3500	70.0
S-glass	2.5	2.8	4570	86.0

The chemical composition of a cellulosic fiber influences its mechanical properties. Plant fibers comprise complex polymers, primarily composed of cellulose, hemicellulose, lignin, and pectin [40, 44, 45]. Each component has its function in a plant fiber:

- **Cellulose**: Cellulose is a key component of plant and wood fibers and plays a major role in providing strength and stability to the cell wall. The cellulose chains together and forms microfibrils composed of amorphous and crystalline regions (see Figure 3.14). When the cellulose microfibrils align with the fiber direction, it enhances the mechanical performance. Amorphous regions have more hydroxyl groups exposed, which tend to interact with water molecules, making them relatively more hydrophilic than the crystalline regions. Crystalline regions are tightly packed and have fewer hydroxyl groups for bonding, making them relatively less hydrophilic. This difference in hydrophilicity between the amorphous and crystalline regions of cellulose microfibrils affects the mechanical properties of BFRP. The hydrophilicity of fibers is further discussed in section 3.7.

  The presence of crystalline regions is thus essential for structural performance, as these regions provide higher stiffness and strength to the fibers. Crystalline regions also contribute to the ability of fibers to resist deformation and maintain their shape under stress [46]. Figure 3.15 shows how the structural constituents of cellulose fiber are arranged.
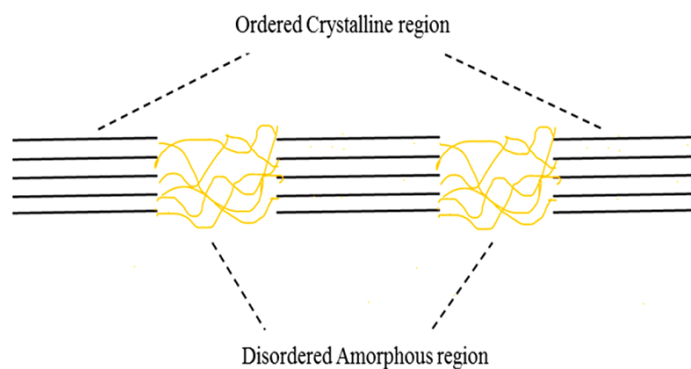
Figure 3.14: Regions in cellulose [47]

- **Hemicellulose**: Unlike cellulose, hemicellulose is not commonly found in a crystalline form. Hemicellulose is primarily responsible for the water absorption of fibers. In addition to its role in water absorption, hemicellulose also contributes to the flexibility and toughness of the fibers by acting as a "glue" between the lignin and cellulose.

- **Lignin**: Lignin is essential in providing strength and stability to plant and wood fibers. It acts as a binding agent with hemicellulose and helps hold cellulose microfibrils together. Lignin also increases fibers' resistance to microorganisms and UV radiation, making them more durable and long-lasting. In addition to these benefits, lignin can improve the interface bond between fibers and resin in BFRP. Fibers that have more accessible lignin may have a better ability to bond with the resin, resulting in a more robust and more stable BFRP.

- **Pectin**: Pectin is an essential component of plant and wood fibers that connects the fibers. It forms the interface where the fibers are connected and is the most hydrophilic substance in the fibers. Pectin also plays a role in the formation of the cell wall. Additionally, pectin can be used as a natural adhesive in the production of BFRP.

3.5.2. Geometry of a plant fiber
Lumen area fraction
Another important aspect to consider with plant fibers is the lumen area fraction. This is the ratio of the lumen's cross-sectional area to the fiber's total cross-sectional area. The hollow lumen is shown in Figure 3.15. The lumen area fraction varies depending on the type of fiber and growing conditions. In general, fibers with a higher lumen area fraction will have lower mechanical properties per cross-sectional area because the lumen reduces the amount of material available to transfer load.
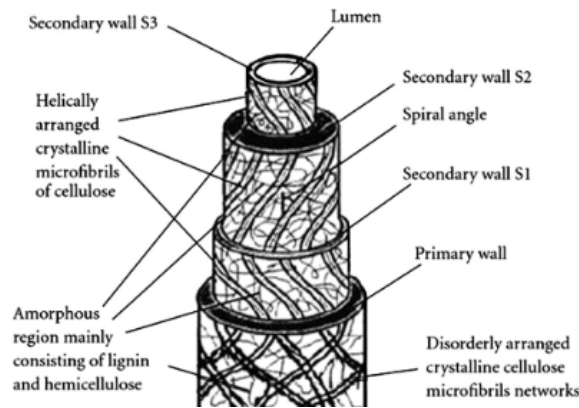
Figure 3.15: Structure constituents of plant fiber adapted from [46]

This leads to underestimating the tensile strength and Young's modulus of the fibers if the lumen area fraction is not considered. It can also affect the water absorption properties of the fibers; fibers with a high lumen area fraction tend to absorb more water. Overall, the lumen area fraction is an important parameter to consider when evaluating the mechanical properties of fibers, and its consideration in the measurements can improve the accuracy of the results [40]. Figure 3.16 shows the luminal area fraction of commonly used plant fibers. Considering the advantages of low luminal area fraction, the predominant usage of flax and hemp fibers in continuous BFRP can be explained.

	Fibre	Cellulose content [wt%]	Cellulose crystallinity [%]	Microfibril angle MFA [°]	Aspect ratio l_f/d_f [-]	Luminal porosity [%]
Bast	Flax	64-71	50-90	5-10	1750	2-11
	Hemp	70-74	50-90	2-6	900	2-11
	Jute	61-72	50-80	8	100	10-16
Leaf	Sisal	66-78	50-70	10-25	100	10-22
	Pineapple	70-82	44-60	10-15	450	10-22
	Banana	44-64	45-55	10-12	150	35-53
Seed	Cotton	85-93	50-90	46	1000	5
	Coir	32-43	27-33	30-49	35	30-50
	Oil palm	40-50	20-30	42-46	100	5-10
Other	Bamboo	26-60	40-60	8-11	100	-
	Wood fibre [a]	40-60	60-70	10-25	50	20-70

[a] Including softwoods and hardwoods.

Figure 3.16: Typical values of structural parameters for various plant fibers [44]

Aspect ratio

The size and shape of a fiber play a role in its effectiveness as a reinforcement [40]. To utilize the strength of a fiber, the fiber should have a sufficient length to transfer the loads effectively. A critical length can be defined as the minimal length to break under tensile loading of the BFRP rather than being pulled out of the matrix. The critical length can be estimated by measuring the interfacial shear strength of the fiber/matrix interface and using the Kelly-Tyson equation [48]. The higher the aspect ratio, the better the tensile load transfer between fibers. Figure 3.16 shows the aspect ratio of several plant fibers. Considering the advantages of a high aspect ratio, the predominant usage of flax fibers compared to hemp and jute in continuous BFRP can be explained.

3.6. Matrix

The matrix is the base material of FRP, and its main function is to protect the fibers from abrasion and environmental effects, transfer the stresses, and hold the fibers in the correct position and orientation. It also helps isolate the fibers, improving the crack propagation resistance. Two types of resins are used: thermosets and thermoplastics. A thermoset undergoes an irreversible chemical reaction that transforms the resin from liquid to solid. A

thermoset is more difficult to recycle because it does not melt but degrades when heated. A thermoplastic, on the other hand, is a melt-processable plastic. When heated, the thermoplastic softens, and when the heat source is removed, it solidifies again [30]. In construction, thermosets are used more frequently because of better resistance to creep, higher modulus, good stability to thermal variations, and higher chemical resistance than thermoplastic matrices [11].

Bio-derived matrices have been explored throughout the literature. Bio-based polymers are biodegradable as they undergo deterioration due to aerobic, anaerobic, or microbial processes. There are three common ways of producing bio-based polymers [11]:

1. Use of natural bio-based polymers with partial modifications, such as starch and cellulose

2. Using organic waste

3. Using microorganisms such as for direct synthesis and providing high thermal stability

PLA is found to have potential because it has been found to exhibit superior strength and stiffness properties when combined with natural fibers compared to the commonly used polypropylene (PP) matrix [40]. PLA is produced from agricultural raw materials, such as dextrose, which undergoes fermentation to produce lactic acid, followed by polymerization. Its versatility is demonstrated by its ability to be stress-crystallized, thermally crystallized, impact-modified, filled, copolymerized, and processed using various polymer processing equipment. Moreover, PLA is fully biodegradable via hydrolysis to lactic acid and eventually to water and carbon monoxide [49]. This makes PLA an ideal candidate for a wide range of applications. Another development is soy-based resins. However, they often have low strength and high moisture absorption. It is often mixed with other natural or biodegradable polymers to enhance its properties to create soy-based bioplastics.

Table 3.5 gives an overview of matrices that are commonly used as synthetic thermosets, thermoplastics, and bio-polymers. When choosing the matrix material, the softening point should be considered. This must be below the thermal degradation temperature of the natural fibers used. Natural fibers are mostly unstable above 200 degrees [40]. This limits the application of thermoplastics with a curing temperature above this temperature.

Table 3.5: Summary of some key properties of polymer matrices adapted from [11]. PE = Polyethylene; PP = Polypropylene; PVC = Polyvinyl chloride; PS = Polystyrene; UPE = Unsaturated polyester; EP = Epoxy; PH = Phenolic; VE = Vinyl ester; PLA = Polylactic acid; PBS = Polybutylene succinate; PHA = Polyhydroxy alkanoate

Matrices	Resin	Density [g/cc]	Tensile strength [MPa]	Elongation at break [%]	Young's modulus [GPa]	Compression strength [MPa]
Thermoplastic	PE	0.91-0.95	25-45	150	0.3-0.5	-
	PP	0.90-0.91	20-40	80	1.1-1.6	-
	PVC	1.3-1.5	52-90	50-80	3.0-4.0	-
	PS	1.04-1.05	35-60	1.6	2.5-3.5	-
Thermoset	UPE	1.2-1.5	40-90	2	2.0-4.5	90-250
	EP	1.1	28-100	1-6	3.0-6.0	100-200
	PH	1.3	35-62	1-2	2.8-4.8	210-360
	VE	1.2-1.4	69-86	4-7	3.1-3.8	86
Bio-polymer	PLA	1.2-1.3	7-185	2.1-30.7	5.1-19.5	-
	PBS	1.26	39-55	5-12	3.6-7.4	-
	PHA	1.2-1.3	10-39	2-1200	0.3-3.8	-

3.7. Interface Between Fiber and Matrix
3.7.1. Interfacial strength
The bond that forms between the matrix and fibers at the interface is critical for the mechanical properties of FRP. This bond can occur through various mechanisms, such as molecular inter-diffusion, electrostatic bonding, mechanical interlocking, and chemical bonding [11]. However, the hydrophilic nature of fibers and the hydrophobic nature of matrices can cause incompatibility issues; fibers naturally tend to cluster together, resulting in non-uniform dispersion. As a consequence, not all resins can encapsulate the fibers. This affects the mechanical properties and the moisture resistance. Additionally, the surface characteristics of the fiber play a significant role in determining the interfacial bond. A fiber with good wettability properties promotes the spreading of the matrix over the surface, resulting in improved adherence. Wettability is the ability of a solid surface to reduce surface tension such that the resin spreads more quickly over the surface.

3.7.2. Modifications
To improve the interfacial bond in BFRP, various modifications have been explored. One approach is the removal of hemicellulose and pectin from plant and wood fibers. The removal of pectin has created more void spaces between fibers, resulting in better impregnation of fibers with an epoxy matrix, leading to improved mechanical properties of the BFRP. Removing hemicellulose further enhances fiber separation and cleanliness of fiber surfaces, resulting in BFRP with low porosity. However, the removal of hemicellulose reduces the strength of BFRP, and therefore, the balance between stiffness and strength should be considered while removing hemicellulose and pectin from fibers. Additionally, the removal process should be environmentally friendly [50, 51, 52].

Other surface treatments, such as plasma, UV, heat, electron, alkali, and enzyme treatments, are also explored. For example, plasma treatment improves roughness and hydrophobicity without compromising interfacial strength, and alkali treatment is environmentally friendly and effective.

3.8. Natural Fiber and Matrix Composites
The previous sections underscore the possibility of a diverse range of fiber-matrix combinations, each with unique properties. Hence, conducting tests when implementing a new BFRP is always necessary. This section delves deeper into BFRP with flax fibers due to the frequent utilization of flax fibers in the industry. Flax fibers possess essential traits like a favorable aspect ratio for pull-out strength, production flexibility, and low lumen area fraction. A substantial amount of testing on BFRP with flax fibers is documented in the literature. However, although flax fibers are always utilized, different processing methods have been used. This influences the material properties of the BFRP.

- **Hackled fibers**: Hackled fibers are used in some research. Any impurities and short fibers are removed to get hackled fibers. Long, straight, and smooth fibers aligned in parallel are left behind. The resulting hackled flax fibers have a silky appearance. Eco-Technilin in France produces hackled fibers.

- **Yarn fibers**: Yarn fibers are fibers spun over their longitudinal axis, resulting in a continuous strand of interlocked fibers. The yarn fibers have a more uniform length and thickness than hackled fibers. A company producing flax yarn fibers is Bcomp in Switzerland. The ampliTex fiber of Bcomp has been used for a BFRP bridge in Ritsumasyl discussed in section 3.3 [36].

- **Sliver fibers**: Some research available uses sliver fibers. Getting sliver fibers aligns the fibers roughly parallelly but leaves some impurities and short fibers behind. The resulting sliver flax fibers have a more rough and uneven appearance and are commonly used in lower-end applications such as rope.

Besides the type of flax fiber, it is also important to consider the fiber orientation in the specimen that is tested in research. While most BFRP is tested for unidirectional plies with all fibers oriented in the direction of loading, some research also examines woven flax, where the fibers are oriented in both the loading direction and the transverse direction (0 and 90 degrees).

Table 3.6 shows an overview of the mechanical properties of BFRP with flax fibers available in the literature. An extensive overview can be found in Appendix A. It can be seen that there is variation in the type of flax, the production of the BFRP, the type of resin, the treatment of BFRP, and fiber volume fraction. Furthermore, not

all data is available, and there is a scattering in properties within fiber and matrix combinations. It can also be noted that primarily non-bio-based resins have been tested. Comparing these to a green-FRP with the PLA resin, a substantially lower tensile strength and stiffness is obtained. This indicates that a 100% bio-based FRP should still be improved significantly to make it feasible in the construction industry.

Table 3.6: Mechanical properties for BFRP with flax adopted from [40], Bi = bi-axial, Vf = fiber content, ϵ = failure strain, σ_t = tensile strength, E_y = Stiffness/Young's modulus, σ_f = flexural strength, E_f = Flexural modulus (GPa), RTM = resin transfer molding, MAA-PP = maleic acid anhydride modified PP, CM = compression molding

fiber	Matrix	Vf (m%)	ϵ (%)	σ_t (MPa)	E_y (GPa)	σ_f (MPa)	E_f (GPa)	Notes
UD (yarn)	Epoxy	45				311	25	Alkali treatment and pre-impreganation
UD (yarn)	Epoxy	∼31		160	15	190	15	Hand lay-up
UD (yarn)*	Bio-Epoxy	50		166	24			Ritsumasyl Bridge with bio-epoxy of 33% bio-content [35]
UD (sliver)	Epoxy	∼28				182	20	Pultruded
UD (yarn)	VE	∼24	1,5	248	24			RTM
UD (yarn)	UP	∼34	1,3	143	14	198	17	RTM
UD (yarn)	PP	30		89/70	7/6			Pultruded
UD (sliver)	PP	44				146	15	Wrap spun hybrid yarn
UD (hackled)	PLA	∼30	1	53	8,3			Pultruded
Bi (sliver)	Epoxy	∼46		200	17	194	13	Weft:warp strength 10:1
Bi (yarn)	Epoxy	∼50		104	10			Sized and dried prior to pre-preg

*This data is adapted from the design report of the Ritsumasyl bridge.

The properties are design values instead of test results.

Selected material

Given the considerable variability in BFRP material properties and the incomplete datasets, this study focuses on the material properties of the material employed in the Ritsumasyl bridge. Looking at Table 3.6, the tensile strength and Young's modulus of the Ritsumasyl bridge properties are in the range of the research for BFRP with flax in general. The material properties are already the design values extracted from test data [36]. The material properties are detailed in Table 7.12, which also accounts for the partial material factor. Conversion factors for moisture, temperature, and creep must be determined and applied to ensure a safe design. These factors are discussed in section 4.6.

The fiber volume fraction of the BFRP of the Ritsumasyl bridge is 50%, which is deemed achievable through vacuum infusion. Different ply lay-ups were utilized for the Ritsumasyl bridge. More background on what a laminated entails and what these different lay-ups mean is discussed in chapter 4. The laminate thicknesses employed for the bridge span a range of 5-24 mm, aligning with the anticipated laminated in the BFRP floor. The fibers used are AmpliTex fibers of Bcomp and a Bio-Epoxy 1804 of ResolTech with a bio-based content of 33%.

3.9. Core

FRP is often used for the fabrication of sandwich panels. A well-known application of sandwich panels is bridge decks. The FRP laminate is a top and bottom facing with a core in between. The core provides sufficient distance between facing laminates for adequate bending resistance. Furthermore, it provides stability to the laminates and improves shear resistance, given a structural material is utilized. The core also serves as insulation material.

Based on the purpose of the sandwich panel, an appropriate core is chosen. The most commonly used core materials are solid, flexible, and honeycomb cores, as shown in Figure 3.17. A solid core is defined as a rigid core and provides significant strength and stiffness to the panel. Balsa wood is often used because of its high strength-to-weight ratio. However, the application of the sandwich decides what solid core should be used best. Flexible

cores are often foam materials. Their primary function is to act as a mold during production and insulation. They also contribute to the load-bearing resistance, but substantially less than a solid and honeycomb core. Honeycomb cores are the most expensive option but offer superior compression and shear rigidity. These cores can be made from various materials, including carbon fabric, glass fabric, aramid paper, or aluminum [53].

Another addition to a sandwich panel with a rigid or flexible core would be to incorporate vertical webs of the same material as the sandwich facing within the core. An example of these webs can be seen in Figure 3.11. These webs provide additional stiffness and shear resistance to the panel. In these sandwich configurations, the core offers a form of work during production and extra stability to the web. The strength of the core material determines the rate of stability it provides to the webs and the additional shear resistance in relation to the webs.

(a) Solid   (b) Foam   (c) Honeycomb
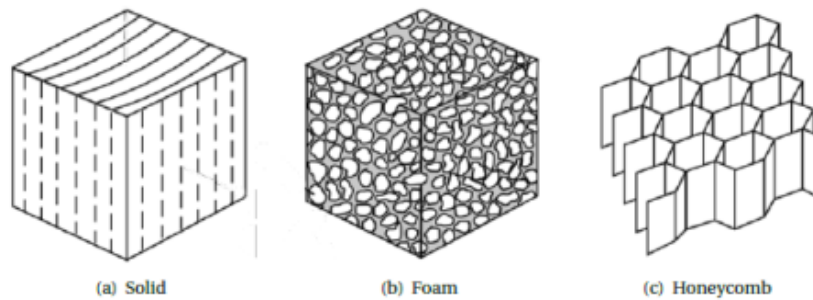
Figure 3.17: Typical cores of sandwich panels [54]

Research has been done into bio-based sandwich panels, both with bio-based facings and synthetic cores, synthetic facings and bio-based cores, or fully bio-based sandwich panels. Table 3.7 shows an overview of some bio-based sandwich panels adapted from [55]. Appendix A shows a more extensive overview. In this overview, it can be seen that all kinds of different bio-based cores can be used, both homogeneous and honeycomb. It also shows that there lacks a focus on a specific bio-based sandwich panel, and research is still broad.

Table 3.7: Bio-based sandwich panels with properties

	σ_{skin} [MPa]	τ_{core} [MPa]	$E_{flexural}$ [GPa]	ρ [kg/m^3]
Jute (15%)/PP skins + Balsa core (25mm)	12.9		0.8	
PP laminate skins + Balsa core (15mm)	15.9		0.6	
Flax fiber skins (∼0.8mm) + Plywood core (∼10mm)	46.8		26.3	488
Multiplex skin + Bamboo HC core	9.9			
Flax skins + Bamboo HC (Ø30mm) core	48.4	0.9	4.2	391
Wood /PLA gyroid panel (2.5mm skin/5mm core)	11.8		2.5	658
Flax fiber skins + PLLA /Balsa core	70.5	2.7		617

Solid/rigid core

All kinds of timber can be used as solid core material for bio-based sandwich panels. Timber is a versatile material used in various construction applications. While balsa is favored for its lightweight properties in FRP applications, other timber options like pine, spruce, and douglas are commonly utilized in the construction industry. Depending on the function, availability, and necessity for lightweight, a sufficient solid core should be chosen.

Flexible (foam) core

A commonly used flexible core is foam. Using foam polymers as conventional core materials has raised environmental concerns due to the high energy consumption and toxic emissions during production. As a result, extensive research has been conducted to explore bio-based alternatives. Among these alternatives are homogeneously structured cellular materials derived from bio-based sources, which include foams composed of bio-based polymers. Vegetable oil polymers, including starch, tannin, and PLA, form the basis of bio-based polymeric foams. Starch is particularly appealing due to its low density and biodegradability, while tannin-based foams are known

for their low flammability and insulating properties [55]. Derived from renewable sources like corn or sugarcane, PLA is a promising polymer. Initially, the high production costs of PLA hindered its widespread use, but with improvements in processing techniques and cost reduction, it has become a more competitive alternative to materials like PU foam [56]. Another drawback of PLA is its minimal resistance against high temperatures. This is also the reason why the BFRP bridge in Eindhoven has a cork layer around the PLA core.

Another bio-based material that is gaining interest is mycelium. However, extensive research on using mycelium as a core material is minimal. Mycelium finds applications in various products such as insulating panels, acoustic tiles, or bricks [57]. The production process involves inoculating agricultural residue fibers with fungal mycelium, which forms a three-dimensional filamentous network that binds the feedstock together, resulting in a lightweight material. Following the growth process, the mycelium-based material is heat-killed. In a study conducted by Elsacker et al., [57], different mycelium spawns combined with various fiber crops were tested to determine their compressive modulus and strength.

Figure 3.18: Bio-based materials mycelium panel [12]

This study does not thoroughly investigate the structural performance of the core materials used. It assumes that the core material merely functions as formwork. As a result, two core materials, PLA and mycelium, will be examined to understand the potential of BFRP floors. An overview of the PLA and mycelium material properties is presented in Table 3.8. The inclusion of PUR foam in this overview serves as reference material. The bio-based core materials need to possess comparable compressive strength to PUR in order to endure the pressure applied during production.

Table 3.8: Potential bio-based core materials for FRP sandwich panels

Material	ρ [kg/m^3]	E_{1c} [MPa]	f_{1c} [MPa]	Source
PUR*	50	6	0.3	[22] Characteristic value
	100	29	0.6	[22] Characteristic value
Mycelium composites	88.8-186.45	0.17-2.3	0.1-0.8	[58] Test value
Hemp loose	94.4	0.17	Graph from	[58] Test value
Hemp chopped	94	0.7	paper is	[58] Test value
Hemp pre-compressed	152.4	2.3	unclear	[58] Test value
Flax loose	99.3	0.2		[58] Test value
Flax chopped	159.3	1.5		[58] Test value
Flax pre-compressed	144.6	0.2		[58] Test value
PLA with bleached birch kraft pulp fibers	320±10	95.3±20	2.4±0.16	[56] Test value

*Non-bio-based core material as reference

One area of concern when utilizing bio-based core materials is their tendency to absorb resin. This absorption rate is contingent on both the density and openness of the grain structure. The significant absorption of core material not only adds to the total weight of the element but also increases the amount of material required.

Surface treatment such as resin painting or an additional laminate layer before vacuum infusion can be applied to limit the absorption rate [59]. For example, the absorption of balsa wood can be reduced with pre-sealing by approximately 10% [59].

3.10. Bio-Fiber Reinforced Polymer Floors

Floor systems made of concrete, timber, and steel are commonly employed in construction. However, utilizing a floor system composed of BFRP has not yet undergone extensive research. To gain insight into the possibilities offered by BFRP as a construction material for floors, floors with the same structural typology as bridge decks are investigated. The structural typology for the bridge decks is a sandwich structure with FRP facings and webs with a flexible core material between the webs, as can be seen in Figure 3.11.

The fundamental principles of floor systems, namely one-way and two-way systems, can be used to apply a suitable structural system for BFRP. In the case of one-way systems, the configuration employed for bridge decks can be easily adapted: a sandwich structure consisting of BFRP facings and BFRP webs. However, for two-way floors, the load transfer in two directions poses a greater challenge.

One straightforward solution involves constructing a solid slab using BFRP. Nevertheless, this approach does not make efficient use of the material. Alternatively, a solid core material with sufficient strength throughout the entire core could be utilized. However, this also deviates from efficient material use. Consequently, this research aims to investigate a sandwich panel configuration with webs oriented in two directions, longitudinally and transversely. This particular configuration offers the potential for both design flexibility and efficient utilization of materials. Figure 3.19 shows the structural system for both a one- and two-way floor with BFRP.
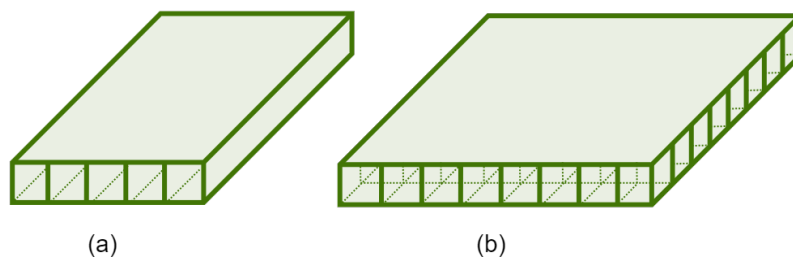
Figure 3.19: (a) One-way BFRP structural system, (b) Two-way BFRP structural system

3.11. Production of FRP

Different techniques are available for the production of FRP applications. The first step of every method involves arranging the fibers in the desired direction, which can be in the form of rovings or fabrics. This can be done manually or with advanced technology. The next step in the process is to impregnate the fibers with resin and finally cure the product. For every production technique, a mold is required to get the FRP in the required shape. A distinction can be made between an open and closed mold process [8].

3.11.1. Open mold

In an open mold process, the material is exposed to the environment, and additional pressure cannot be applied. This increases the risk of emitting unwanted substances into the environment, which is potentially harmful to manufacturers. Two well-known examples of open mold processes are spray-up and hand layup. In spray-up, a mixture of chopped fibers and resin is sprayed on a mold. For hand layup, plies are applied manually and wetted by a brush or roller. Both of these processes are labor-intensive, and the quality of the final product depends on the skill level of the worker. The product may also have areas with high resin content and voids. These methods are cost-effective for single-series production. An alternative, more automated process of open molding is filament winding. In this method, continuous rovings are wrapped around a rotating mandrel, resulting in a hollow shape that can be used for pipes. This process is more automated and more cost-effective when a series of products is required.

3.11.2. Closed mould

Closed mold processes offer better control over the final product as the mold is sealed. A production process that is used for structural applications is pultrusion. In pultrusion, continuous rovings are pulled through a resin bath, shaped through dies, cured at high temperatures, and cut to the desired length. This continuous process is cost-effective for large production runs, but the fiber orientation is limited. To improve this, fibers can be placed at 90 and 45-degree angles on the surface. Furthermore, for natural fibers, this production has limitations because of the minimum fiber strength for tearing [38].

Another closed mold process involves sealing the mold with a covering sheet or a vacuum bag. The core and face sheets are inserted into the mold, and everything is sealed. Once the set-up is airtight, a vacuum is applied at various locations, making the resin flow through the mold and impregnate the panel, see Figure 3.20. The process is called vacuum-assisted resin transfer molding (VARTM) and is suitable for larger structural applications.
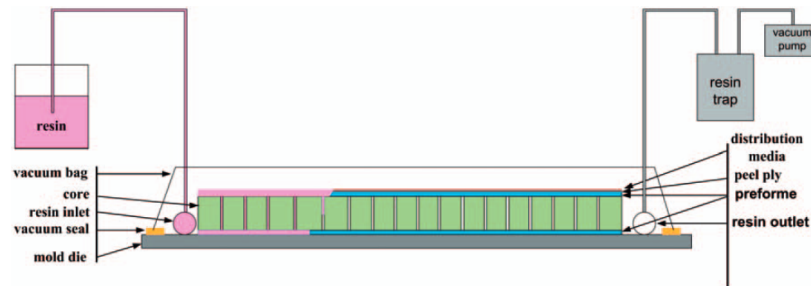
Figure 3.20: Schematic view of VARTM process (vacuum assisted resin transfer molding) [60]

The success of VARTM-produced products relies on properly managing resin flow, pressure, temperature, and surface treatment. Through this technique, a fiber volume fraction of 55% can be achieved. Although, it should be noted that the impregnation of the fibers with a bio-based thermoplastic resin (e.g. PLA) is more difficult because of the higher polymer viscosity [61]. The initial costs of the VARTM are high, but the process is cost-efficient when the mold is used multiple times. This production process is most likely to use for the BFRP floor discussed in this research and will be elaborated on for both the one- and two-way floor.

One-way

FiberCore Europe stands at the forefront of producing FRP bridges and bridge decks. They use their InfraCore technology, which is a specific approach for the fiber lay-up, as depicted in Figure 3.21. The key advantage lies in the strategic overlap of fibers, a factor that significantly enhances the structural integrity of the deck. This innovative process involves employing the VARTM method for deck construction. Notably, the molds employed in this procedure can be partially reused, reducing production costs.

Figure 3.21: Lay-up in sandwich structure using principal of InfraCore [62]

Two-way

Regarding sandwich panels featuring webs in two directions, a more labor-intensive process is required than for one-way panels. This involves individually wrapping core blocks, a task that demands considerable effort and currently lacks automation. As illustrated in Figure 3.22, the arrangement of fiber-wrapped blocks within a mold for vacuum infusion is shown. It is essential to observe that, unlike the production method used for one-way panels, there is no fiber overlap between the blocks in this process, raising concerns about the potential risk of delamination failure.
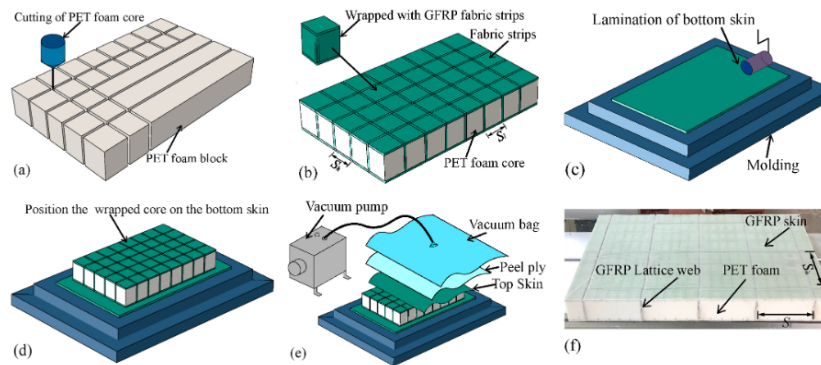
Figure 3.22: Fabrication process of sandwich panel with webs in two directions [63]

Some factors should be taken into account for sandwich structures with BFRP:

- The resin flow needs a certain pressure to be able to penetrate between all fibers. This requires a certain minimal strength of the core material. This means that a non-structural core used as formwork should not fall apart during production due to the pressure of the resin.

- For natural fibers, it is important to consider the maximum curing temperature. High temperatures cause the degradation of bio-based fibers.

3.12. Conclusion

State-of-the-art of BFRP
- BFRP are composite materials with reinforcing natural fibers embedded in a polymer matrix (resin).
- BFRP usage is driven by lightweight properties, high specific strength and stiffness, and environmental performance potential.
- BFRP is employed in various industries, including automotive (interior components), aerospace (lightweight components), and construction (roof tiles, bridges, facades).
- BFRP is used in the construction sector for roof tiles, floor matting, ceilings, doors, window frames, and bridges.
- Examples of BFRP bridges include the movable pedestrian bridge in Emmen, the pedestrian bridge at Eindhoven University, the movable biking bridge in Ritsumasyl, and the FiberCore Europe bridge.
- In bridges and bridge decks the technology of InfraCore for sandwich panels with BFRP facings and webs is utilized.

Raw materials for BFRP and influencing factors on mechanical properties
- BFRP can be considered "bio-based" if at least one of its constituents is derived from natural resources.
- Natural fibers like flax, hemp, jute, and kenaf are commonly used as reinforcements in BFRP.
- Fibers are categorized based on their origin: plant-based, animal-based, or mineral-based. Plant-based fibers are further investigated because of their origin, availability, promising material properties, and the local initiative of the government.
- Both the fiber composition and geometry influence the mechanical properties. A higher cellulose content means a stronger and stiffer fiber in general. With a smaller lumen area fraction, the fiber mechanical properties are favorable. The aspect ratio, the length-to-diameter ratio of a fiber, affects load transfer effectiveness. Flax fibers are widely used in BFRP composites, offering good mechanical properties and availability.
- Matrices protect fibers from abrasion and transfer stresses and hold fibers in place. The resin contributes the most to the environmental impact of BFRP.
- The interfacial bond between fiber and matrix is critical for mechanical properties.
- Considerations in BFRP design include addressing issues related to moisture absorption, fire resistance, mechanical properties, durability, quality variations, and manufacturing challenges.
- Every BFRP material should be tested when utilized in construction.

Selected material

- The Ritsumasyl bridge employs BFRP with yarn flax fibers, Bio-Epoxy matrix, and different lay-up configurations and is selected as the BFRP material used in this research.
- Material properties of the bridge are within the range of literature data.
- Material factors, moisture, temperature, and creep effects must be considered for safe design.
- The core material is not investigated thoroughly in this research. As structural core material, timber (balsa or solid timber) is utilized where necessary. As flexural/non-structural core, PLA with cork and mycelium are included for the sake of completeness.

Structural typologies for BFRP floors

- For one-way floors, the structural typology of bridge decks is utilized. This entails a sandwich structure with vertical webs.
- For two-way floors, the same typology is utilized, but it has webs in both transversal and vertical webs.
- For one-way BFRP floors, InfraCore technology utilizing VARTM with fiber overlap, providing structural integrity and cost efficiency, can be used.
- Two-way BFRP floors require more labor-intensive processes due to individually wrapping core blocks. The individual blocks raise concerns about fiber overlap and delamination risk.
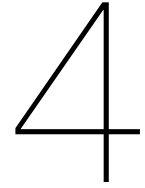
Mechanical Properties of BFRP

4.1. Introduction

The performance of FRP depends on the fibers and matrix but also the fiber volume and direction. The material is constructed using layers, also called plies or laminae, which form a laminate. The Classical Laminate Theory (CLLT) can be used to determine the properties of the laminate. This chapter aims to evaluate FRP's properties and behavior to understand its structural behavior and failure mechanisms better. This chapter will address the following topics:

- What is anisotropic behavior?
- How can the properties of FRP be determined, and what is the difference compared to BFRP?
- What are the failure mechanisms of FRP?

4.2. Anisotropic Properties

FRP can be analyzed at three levels: microscale, mesoscale, and macroscale [64]. The microscale analysis focuses on studying the properties of the fiber and resin. The mesoscale analysis investigates the behavior of the ply formed by the fibers and resin. Finally, the analysis is performed at the macroscale when plies are stacked on each other.

The fibers and resin in FRP have different properties, which make the material heterogeneous. This is a common characteristic of composite materials. A uni-directional (UD) ply is considered anisotropic, meaning its behavior varies in different directions. This is because the fibers are oriented in a specific direction. For a UD ply, the longitudinal direction, which is the direction of the fibers, is the stiffest. This property sets FRP apart from conventional materials, such as steel, which exhibit isotropic behavior. Furthermore, FRP can also be considered an orthotropic material, as it has three mutually perpendicular planes of symmetry that result in different mechanical properties in each direction.

Figure 4.1 shows what the coordinate system for an orthotropic material looks like. Numbers 1 and 2 indicate the directions of the fibers, and x and y are the global directions for a laminate of more plies. The material properties are different in every direction. There are three principal orthogonal axes, meaning nine independent elastic parameters can define the behavior. However, a UD ply can be assumed to be quasi-isotropic. Assuming that the thickness and width direction have the same elastic behavior. This reduces the number of elastic parameters: E_1, E_2, G_{12}, ν_{12}, and ν_{21} [65, 8]. These properties can be obtained by testing, or when they are not known, they can be adopted by the Halpin-Tsai equations, Equation 4.1 till 4.4 [22]. The empirical reduction factor plays a crucial role in capturing the impact of interfacial shear stress between the fiber and matrix in a composite material. As highlighted in chapter 3, this interface significantly influences the composite's overall properties. Empirically determined, this reduction factor is considerably lower for natural fibers than for synthetic fibers [35].

$$E_1 = [E_R + (E_{f1} - E_R) \cdot V_f] \cdot \varphi_{UD} \tag{4.1}$$
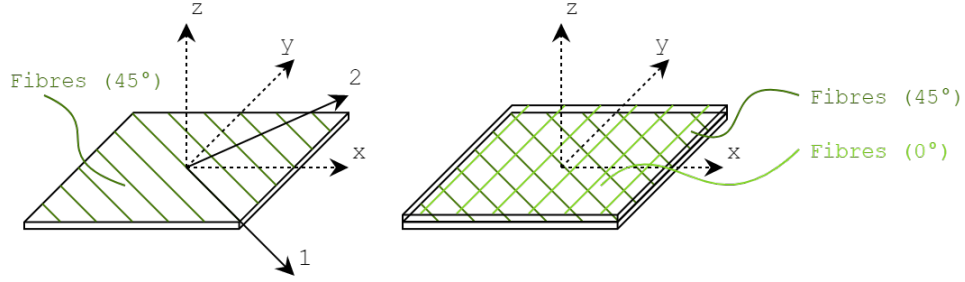
Figure 4.1: Single ply and laminate with two plies with coordinate system

$$E_2 = \left[\frac{(1 + \xi_2 \eta_2 V_f)}{(1 - \eta_2 V_f)} \cdot E_R \right] \cdot \varphi_{UD} \tag{4.2}$$

with

$$\eta_2 = \frac{\left(\frac{E_{f2}}{E_R} - 1 \right)}{\left(\frac{E_{f2}}{E_R} + \xi_2 \right)}, \xi_2 = 2$$

$$G_{12} = \left[\frac{(1 + \xi_G \eta_G V_f)}{(1 - \eta_G V_f)} \cdot G_R \right] \cdot \varphi_{UD} \tag{4.3}$$

with

$$\eta_G = \frac{\left(\frac{G_f}{G_R} - 1 \right)}{\left(\frac{G_f}{G_R} + \xi_G \right)}, \xi_G = 1$$

$$v_{12} = v_R - (v_R - v_f) \cdot v_f \tag{4.4}$$

In which:

E_1, E_2 in-plane Young's modulus of the ply;

G_{12} in ply shear modulus;

v_{12} Poisson's ratio;

v_R Poisson's ratio of the resin;

v_F Poisson's ratio of the fiber;

ϕ_{UD} empirical reduction factor;

E_R Young's modulus of the resin;

E_{F1}, E_{F2} Young's modulus of the fiber;

G_R shear modulus of the resin;

V_f fiber volume ratio of the ply.

Constitutive relation and transformation

In a UD ply, only one principal direction exists along which the material exhibits distinct behavior while it remains consistent in the plane normal to this direction. This characteristic, known as transverse isotropy, allows for a reduced stiffness matrix to represent the constitutive relation, as shown in Equation 4.5. The relationship between stress and strain and their reverse correlation can be expressed using Equation 4.6 [8].

$$\overline{\boldsymbol{\sigma}} = \overline{\boldsymbol{Q}}\overline{\boldsymbol{\varepsilon}} \quad \text{or} \quad \left\{ \begin{array}{c} \sigma_{11} \\ \sigma_{22} \\ \tau_{12} \end{array} \right\} = \begin{bmatrix} \frac{E_1}{(1 - v_{12}v_{21})} & \frac{v_{21}E_1}{(1 - v_{12}v_{21})} & 0 \\ \frac{v_{21}E_1}{(1 - v_{12}v_{21})} & \frac{E_2}{(1 - v_{12}v_{21})} & 0 \\ 0 & 0 & G_{12} \end{bmatrix} \left\{ \begin{array}{c} \varepsilon_{11} \\ \varepsilon_{22} \\ \gamma_{12} \end{array} \right\} \tag{4.5}$$

$$\overline{\varepsilon} = \overline{Q}^{-1}\overline{\sigma} \tag{4.6}$$

The stiffness matrix (Q) is employed to establish the stress-strain relationship in the local coordinate system. Transformation rules are then applied to establish the connection between the local and global coordinate systems, as depicted in Equation 4.7. Using Equation 4.9, the stiffness matrix in the local coordinate system can be transformed into the global plane stress stiffness matrix [8].

$$\boldsymbol{\sigma} = \mathbf{T}\overline{\boldsymbol{\sigma}} \quad \Leftrightarrow \quad \bar{\sigma} = \mathbf{T}^{-1}\boldsymbol{\sigma}$$
$$\varepsilon = \mathbf{T}^{-T}\bar{\varepsilon} \quad \Leftrightarrow \quad \bar{\varepsilon} = \mathbf{T}^{T}\varepsilon \tag{4.7}$$

with

$$\mathbf{T} = \begin{bmatrix} \cos^2\theta & \sin^2\theta & -2\sin\theta\cos\theta \\ \sin^2\theta & \cos^2\theta & 2\sin\theta\cos\theta \\ \sin\theta\cos\theta & -\sin\theta\cos\theta & \cos^2\theta - \sin^2\theta \end{bmatrix} \tag{4.8}$$

$$Q = \mathbf{T}\overline{Q}\mathbf{T}^{T} \tag{4.9}$$
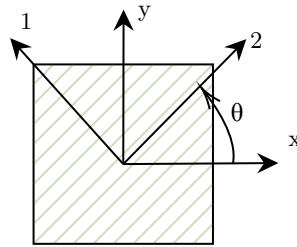
Figure 4.2: 2D planar local and global coordinate frames

4.3. Classical Laminate Theory

The CLLT is a powerful tool that can be utilized to determine the mechanical properties of multidirectional laminates. By determining the stresses and strains in each ply, CLLT calculates the stiffness of the entire laminate and estimates coupling effects. The underlying principle of CLLT is based on the assumption that the deformation of a laminate can be modeled as a thin plate, as suggested by the Kirchhoff hypothesis. The Kirchhoff hypothesis is based on the following assumptions [8, 65]:

- The perpendiculars to the middle surface in its original state remain straight and perpendicular to the middle surface after it has undergone deformation.
- The stress that is normal to the plate can be neglected, leading to $\epsilon_{zz} = \gamma_{xz} = \gamma_{yz} = 0$.
- The vertical deflection remains uniform throughout the thickness.
- Linear elasticity is applicable for this theory given the small magnitudes of the strains observed in the deformed plate.
- Perfectly bonded plies, meaning the theory cannot be used for delamination.

The stress resultants in a structure can be computed as distributed membrane forces and bending moments (represented by N and M). The relationship between these stress resultants and the corresponding deformations is given by Equation 4.10 [8]. The A matrix in this equation represents the relationship between the in-plane forces and in-plane strains, commonly called the extensional stiffness matrix. The B matrix, on the other hand, represents the relationship between the in-plane forces and the curvature and moments with in-plane strain and is known as the bending-extension coupling stiffness matrix. Finally, the D matrix describes the relationship between the bending moments, curvature, and strains and is referred to as the flexural stiffness matrix.

$$\begin{pmatrix} N \\ M \end{pmatrix} = \begin{bmatrix} A & B \\ B & D \end{bmatrix} \begin{pmatrix} \varepsilon \\ \kappa \end{pmatrix} \tag{4.10}$$

with extended matrix

$$\begin{pmatrix} N_x \\ N_y \\ N_{xy} \\ M_x \\ M_y \\ M_{xy} \end{pmatrix} = \begin{bmatrix} A_{11} & A_{12} & A_{16} & B_{11} & B_{12} & B_{16} \\ A_{12} & A_{22} & A_{26} & B_{12} & B_{22} & B_{26} \\ A_{16} & A_{26} & A_{66} & B_{16} & B_{26} & B_{66} \\ B_{11} & B_{12} & B_{16} & D_{11} & D_{12} & D_{16} \\ B_{12} & B_{22} & B_{26} & D_{12} & D_{22} & D_{26} \\ B_{16} & B_{26} & B_{66} & D_{16} & D_{26} & D_{66} \end{bmatrix} \begin{pmatrix} \varepsilon_x^0 \\ \varepsilon_y^0 \\ \gamma_{xy}^0 \\ \kappa_x \\ \kappa_y \\ \kappa_{xy} \end{pmatrix}$$

Due to the transformation from local to global coordinate frames, the stiffness matrices are not identical for a layered laminate compared to a UD laminate. As a result, the A and D matrices are no longer valid, and B may not be equal to zero. In the case of a layered material, the integrals used to calculate the stiffness matrices can be expressed as the sum of sub-integrals over the thickness of each layer, as shown in Equation 4.11. The notation for stacking the laminate is shown in Figure 4.3.

$$A = \sum_{j=1}^{n} (z_j - z_{j-1}) Q_j$$

$$B = \sum_{j=1}^{n} \frac{1}{2} \left(z_j^2 - z_{j-1}^2 \right) Q_j \tag{4.11}$$

$$D = \sum_{j=1}^{n} \frac{1}{3} \left(z_j^3 - z_{j-1}^3 \right) Q_j$$
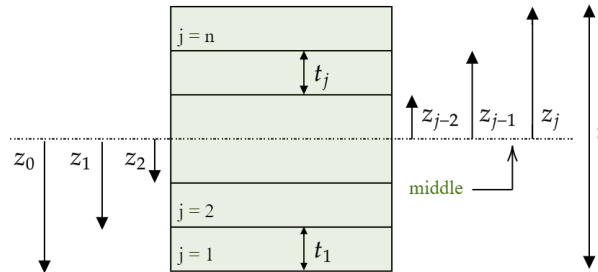
Figure 4.3: Notation of a layered laminate

4.4. Laminate Lay-Up

An advantage of FRP is that the lay-up can be changed, improving the strength and stiffness in a specific direction. The use of a particular lay-up depends on its applications. In this section, commonly used lay-up configurations and their notation are discussed.

UD laminates

All fibers are oriented in one direction for a UD laminate, leading to a high axial stiffness. An example of a zero-degree UD laminate with four plies is [0º/0º/0º/0º].

Cross-ply laminates

In a cross-ply laminate, the layers alternate between 0º and 90º orientations. For example, a cross-ply with four layers can be denoted as [0º/90º/0º/90º], which can be more concisely written as [0º/90º]₂, where the subscript 2 indicates that the layer sequence is repeated twice.

Angle-ply laminates

An angle-ply laminate comprises layers between $-\theta^o$ and $+\theta^o$ orientations. For instance, a laminate with four layers can be represented as $[+45^o/-45^o]_n$, where n indicates the number of times the sequence is repeated. This notation can be simplified to $[\pm 45^o]_n$. An angle ply with alternating $\pm 45^o$ directions is suitable for shear.

Symmetric laminates

In a symmetric laminate, the lay-up is a mirror image of itself with equal distances from the centerline. For instance, an eight-layer laminate can be symmetric with a lay-up of $[0^o/+45^o/90^o/-45^o]_s$, where the subscript 's' indicate a symmetric configuration. One benefit of using symmetric laminates is that they exhibit no bending/membrane coupling effects, which results in a B matrix equal to zero.

Balanced laminates

In a balanced laminate, for every ply oriented at θ degrees, there is a corresponding ply oriented at $-\theta$ degrees somewhere in the lay-up, such as $[+\theta_1^o/-\theta_1^o/+\theta_2^o/-\theta_2^o]$. As seen in the previous example of symmetric laminates, this configuration is also a balanced laminate. One of the main benefits of using a balanced laminate is that it exhibits no shear/normal coupling, resulting in A16 and A_{26} equal to zero.

Quasi-isotropic laminates

A quasi-isotropic ply is a composite material layer with fiber orientations arranged in a specific manner to achieve nearly isotropic properties. It is typically composed of layers of fibers oriented at $\pm 45^o$, 0°, and 90° angles, creating a symmetric lay-up. The quasi-isotropic ply has the advantage of providing similar strength and stiffness in all directions, making it a popular choice for structural applications where balanced properties are required.

Hybrid laminates

A hybrid laminate has layers with different types of fibers. The type of fibers used can be indicated with a superscript in each layer.

In general, the difference between two adjacent plies should not exceed 60°, or the adhesive layer should be placed at an angle of no more than 45° from the main direction [8].

4.5. Failure in FRP

The orthotropic behavior of FRP has significant consequences, as no single parameter can define the material's failure criteria. In contrast, isotropic materials like steel rely on a single criterion f_y to define their yield criteria. Additionally, the material's directionality must be considered, further complicating defining failure criteria. Unlike isotropic materials, the failure criterion for orthotropic materials like FRP cannot be expressed in three principal stress values but requires six values.

4.5.1. Failure processes

- Matrix cracking: first to observe and happens between fibers; they can occur at low-stress levels. Individually, matrix cracks do not immediately endanger the structural integrity of the laminate. Because fibers carry the load, and those are still intact. Matrix cracks can be tolerated, except where leakage is critical. However, they do pose a risk for initiating delamination. The crack in the matrix can grow substantially when the interface is not crossed by fibers anywhere. Delamination requires extra attention and is addressed in subsection 4.5.2.

- Fiber failure: Under tension, fiber failure is accompanied by fiber/matrix debonding and pullout; under compression, the local instability causes the fiber to kink, which leads to failure. It needs to be avoided because it quickly leads to global failure.

4.5.2. Delamination

Delamination is the crack formation between two plies in an FRP composite, posing a significant risk to structural integrity. It demands extra attention and is addressed in subsection 3.5.2. Delamination can grow large due to the absence of overlapping fiber reinforcement between layers, making it critical for overall performance.

Delamination can occur in three primary modes: Mode I, Mode II, and Mode III, see Figure 4.4. Mode I delamination, or tensile mode, occurs when external forces separate layers, causing cracks perpendicular to the fiber direction. Mode II delamination (sliding mode or shear mode) happens when layers separate along the applied shear force. It is common in sandwich structures or under-bending loads, with limited fiber bridging across the interface. Mode III delamination also called tearing shear mode, involves separating layers with crack growth perpendicular to the applied shear load. Although less common than Modes I and II, Mode III delamination can occur under specific loading conditions. It typically occurs in structures subjected to complex loading conditions where shear forces play a significant role, such as in rotating machinery or components experiencing twisting or torsional loads.

Delamination occurs in areas where fibers do not overlap, weakening the interface between layers. This reduces load-carrying capacity and compromises structural strength, especially under compressive loading, reducing buckling resistance. Delamination can also occur beyond layer interfaces due to inadequate fiber lay-up and overlap or curing during FRP production and manufacturing, resulting in voids or resin-rich regions.

In this thesis, the floor design takes delamination into account. Specifically, the failure of the floor is considered to occur as soon as delamination occurs, similar to "first ply failure." This concept is discussed in subsection 4.5.3. Furthermore, delamination risks can be reduced by avoiding clustering of plies with the same direction and minimizing mismatch angles.
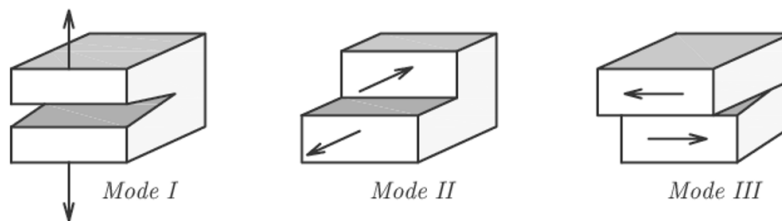
Figure 4.4: Delamination modes

4.5.3. Failure criteria

Commonly used methods for analyzing laminate failure are the maximum stress criterion, the maximum strain criterion, the Tsai-Wu criterion, and the Hashin criterion [65]. These failure criteria are determined based on specific strength parameters for in-plane loading, including tensile strength, compressive strength, and in-plane shear. Once a failure criteria method has been selected, the following steps should be taken to analyze laminate failure:

- Determine stresses or strains in each ply and critical areas for delamination.
- Transform the stresses/strains into the principal loading directions.
- Apply the failure criteria to determine if the ply has failed.
- Assume failure due to first-ply failure indicates the onset of failure. This approach is conservative as it does not account for stress redistribution situations that may potentially safeguard the structure. Progressive failure analysis can be performed to explore the behavior after the first ply failure. A simple approach is the ply discount method, where the stiffness of the failed plies is reduced. However, this method lacks mathematical objectivity. To analyze the progressive failure, the resistance against the growth of cracks should be addressed and is outside the scope of this research.

4.5.4. Maximum stress criterion

According to the maximum stress method, failure occurs when any stress in the principal directions reaches or exceeds the allowable strength in that direction [65].

$$
\begin{aligned}
-f_{1t} &< \sigma_{11} < f_{1c} \\
-f_{2t} &< \sigma_{22} < f_{2c} \\
-f_{12v} &< \tau_{12} < f_{12v}
\end{aligned}
\tag{4.12}
$$

where f indicates the strength of the laminate and σ and τ the acting load. Numbers 1 and 2 refer to the longitudinal and transverse direction, respectively, while the t and c refer to the tensile and compressive strength, which are generally unequal.

4.5.5. Maximum strain criterion

The maximum strain criterion is similar to the maximum stress criterion, but the maximum strain is used instead of stresses. Failure is predicted to occur when any strain in the principal direction exceeds the allowable strain limit [65].

$$
\begin{aligned}
\frac{-f_{1t}}{E_1} &< \epsilon_{11} < \frac{f_{1c}}{E_1} \\
\frac{-f_{2t}}{E_2} &< \epsilon_{22} < \frac{f_{2c}}{E_2} \\
\frac{-f_{12v}}{G_{12}} &< \gamma_{12} < \frac{f_{12v}}{G_{12}}
\end{aligned}
\tag{4.13}
$$

where the strains are:

$$
\begin{aligned}
\varepsilon_1 &= \frac{1}{E_1}\left(\sigma_1 - v_{12} \cdot \sigma_2\right) \\
\varepsilon_2 &= \frac{1}{E_2}\left(\sigma_2 - v_{12} \cdot \sigma_1\right) \\
\gamma_{12} &= \frac{\tau_{12}}{G_{12}}
\end{aligned}
\tag{4.14}
$$

4.5.6. Tsai-Wu criteria

According to [65], the Tsai-Wu criterion is generally considered the most effective failure criterion. This criterion is interactive as it considers the interactions between different stress components, making it more accurate in predicting material failure [8]. As it can not be supposed that the principal stresses are aligned with the material frame, shear stresses must be accounted for separately. The equation for the Tsai-Wu criterion can be found in Equation 4.15.

$$
\sigma_{11}\left(\frac{1}{f_{1t}} - \frac{1}{f_{1c}}\right) + \sigma_{22}\left(\frac{1}{f_{2t}} - \frac{1}{f_{2c}}\right) + \frac{\sigma_{11}^2}{f_{1t}f_{1c}} - \frac{\sigma_{11}\sigma_{22}}{\sqrt{f_{1t}f_{1c}f_{2t}f_{2c}}} + \frac{\sigma_{22}^2}{f_{2t}f_{2c}} + \frac{\sigma_{12}^2}{f_{12}^2} = 1
\tag{4.15}
$$

4.5.7. Hashin

In 1980, Hashin introduced a failure theory that gives separate expressions for different failure modes. The reason behind this is the fact that no single expression can cover all possible failure processes. Four different failure mechanisms are distinguished in the Hashin criteria [8]:

- **Tensile fiber failure mode**: The assumption is that longitudinal tension and longitudinal shear interact.

$$
\left(\frac{\sigma_{11}}{f_{1t}}\right)^2 + \left(\frac{\sigma_{31}^2 + \sigma_{12}^2}{f_{12}^2}\right) = 1
\tag{4.16}
$$

- **Compressive fiber failure mode**: The assumption is that the interaction with transverse compression is negligible, as failure occurs due to shear mode buckling. However, there is some uncertainty regarding the impact of longitudinal shear stress on the strength of the material, which has led to the decision to neglect any potential effects.

$$
\frac{\sigma_{11}}{f_{1c}} = 1
\tag{4.17}
$$

- **Tensile matrix failure mode**: $\sigma_{22} + \sigma_{33} > 0$.

$$
\frac{(\sigma_{22} + \sigma_{33})^2}{f_{2t}^2} + \frac{\sigma_{23}^2 - \sigma_{22}\sigma_{33}}{f_{23}^2} + \frac{\sigma_{31}^2 + \sigma_{12}^2}{f_{12}^2} = 1
\tag{4.18}
$$

- **Compressive matrix failure mode**: $\sigma_{22} + \sigma_{33} < 00$, the assumption is that the transversely isotropic pressure at which failure occurs is significantly greater than the stress required for uniaxial compressive failure.

$$\left[\left(\frac{f_{2c}}{2f_{23}}\right)^2 - 1\right]\frac{\sigma_{22} + \sigma_{33}}{f_{2c}} + \frac{(\sigma_{22} + \sigma_{33})^2}{4f_{23}^2} + \frac{\sigma_{23}^2 - \sigma_{22}\sigma_{33}}{f_{23}^2} + \frac{\sigma_{31}^2 + \sigma_{12}^2}{f_{12}^2} = 1 \qquad (4.19)$$

To determine which equation, Equation 4.18 or 4.19, to use, it is essential to identify the sign of the normal stress on the fracture plane. Because of the unknown angle of the fracture plane, tensile matrix and compression matrix are considered if $\sigma_{22} + \sigma_{33} > 0$ or $\sigma_{22} + \sigma_{33} < 0$ respectively. Although Hashin's criteria have limitations, particularly for matrix compression and fiber compression, several enhancements have been suggested. Although more sophisticated versions are available, they necessitate more complex equations. Nevertheless, Hashin's criteria remain dependable and widely used failure criteria in the industry.

4.5.8. Discussion

The main difference between the maximum stress/strain criteria and Hashin and the Tsai-Wu criterion is that only one criterion needs to be satisfied for Tsai-Wu. In contrast, five and four sub-criteria must be analyzed for maximum stress/strain and Hashin. The maximum stress criteria also do not account for interactions between different stresses. In contrast, the Tsai-Wu criterion considers these interactions, considering the combined effects of multiple stress components on material failure. The maximum strain criterion partially accounts for these interactions by considering Poisson's ratio, but the Tsai-Wu criterion provides a more complete picture. However, there is a minor drawback to the Tsai-Wu criterion in that it may produce unconservative values in the third quadrant [66]. Figure 4.5 visualizes comparing the different failure criteria methods. The failure of FRP can be modeled with finite element analyses (FEA). A commonly used FEA software is Abaqus. In Abaqus, the failure criteria used is Hashin [67].
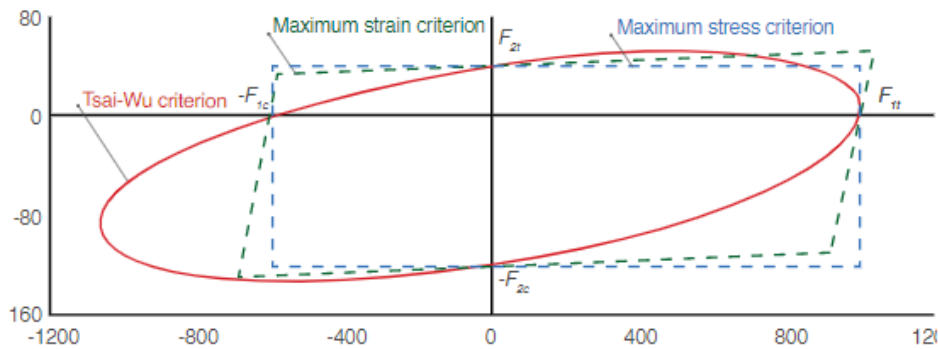
Figure 4.5: Comparison of Tsai-Wu, maximum stress criteria, and maximum strain criteria [64]

4.6. Property Reduction Composite

The Halpin Tsai equation, a semi-empirical formula (see Equation 4.1), can be utilized to estimate the stiffness properties of UD laminates—more on this in section 4.2. However, experimental results indicate that the stiffness values derived from this equation for BFRP are significantly higher than the actual stiffness. This discrepancy could be attributed to a lack of consistency in fiber properties or other factors, such as the fiber and resin interface interaction. For instance, when analyzing a flax fiber with epoxy resin composite, the Halpin Tsai equation yields a modulus of elasticity of approximately 30 GPa. However, experimental testing for the Ritsumasyl bridge demonstrates a modulus of elasticity of only 24 GPa, representing a reduction of 20%. This indicates that an appropriate empirical reduction factor should be used for bio-based composites, and sufficient testing is required since this reduction is different for different fiber-matrix combinations.

To consider the strength reduction due to the environmental effects of FRP, a conversion factor is used. This conversion factor includes the thermal and moisture effects and can be determined by Equation 4.20 according to CEN/TS 19101 for FRP [22].

$$\eta_{\text{c}} = \eta_{\text{ct}} \cdot \eta_{\text{cm}} \tag{4.20}$$

Where:
- η_{ct} is the conversion factor for temperature effects;
- η_{cm} is the conversion factor for moisture effects.

4.6.1. Temperature conversion factor

The thermal effects factor varies depending on the dominant property that leads to failure - the fiber, matrix, or core. It primarily depends on the service temperature (T_s) and the glass transition temperature (T_g) of the resin. At the glass transition point, the material's mechanical properties change. It represents the temperature range as FRP matrix material transitions from a rigid, glassy state to a more flexible, rubbery state. The temperature conversion factors can be calculated using the following equations adapted from [22]:

Fiber

$$\eta_{\text{ct}} = \min \left\{ 1.0 - 0.25 \cdot \frac{T_{\text{s}} - 20}{T_{\text{g}} - 20} ; 1.0 \right\} \tag{4.21}$$

Matrix

$$\eta_{\text{ct}} = \min \left\{ 1.0 - 0.8 \cdot \frac{T_{\text{s}} - 20}{T_{\text{g}} - 20} ; 1.0 \right\} \tag{4.22}$$

Core (polymeric foam)

$$\eta_{\text{ct}} = \min \left\{ 1.0 - 0.46 \cdot \frac{T_{\text{s}} - 20}{T_{\text{g}} - 20} ; 1.0 \right\} \tag{4.23}$$

Core (balsa wood)

$$\eta_{\text{ct}} = \min \left\{ 1.0 - \left(\frac{0.2}{\rho} + 0.004 \right) \cdot (T_{\text{s}} - 20) ; 1.0 \right\} \tag{4.24}$$

Epoxy adhesive

$$\eta_{\text{ct}} = \min \left\{ 1.0 - 0.85 \cdot \frac{T_{\text{s}} - 20}{T_{\text{g}} - 20} ; 1.0 \right\} \tag{4.25}$$

In this research, the service temperature of the floor is determined based on the building physics requirements outlined by NEN-EN15251 [68]. $20°$ Celsius is used as a baseline for T_s. However, to account for situations when cooling or heating systems are not functioning, a temperature range of 15-30 degrees Celsius is considered. This results in a T_s of $30°$ degrees since the material temperature in service conditions has to be considered.

The glass transition temperature depends on the matrix used. As discussed in chapter 3, the BFRP material from the Ritsumasyl bridge with a 33% bio-epoxy resin from resoltech is utilized. It has a T_g of $81°$ for 16 hours curing at $60°$ [69].

The temperature conversion factors used in this research are calculated, with $T_s = 30°$ and $T_g = 81°$, and are listed in the overview in Table 4.1. The solid core with strength class C24, the conversion factor equation for balsa wood is used.

Table 4.1: Temperature conversion factors

Type	η_{ct}
Fiber dominated properties	0.96
Matrix dominated properties	0.87
Core (polymeric foam)	0.92
Core (C24, with $\rho_{\text{mean}} = 420 \, \text{kg/m}^3$)	0.96
Epoxy adhesive	0.86

4.6.2. Moisture conversion factor

Moisture is a key factor that can potentially affect both the stiffness and strength of BFRP. The water absorption of natural fiber composites can compromise the interfacial strength due to the porous structure of flax fibers and the incompatibility between hydrophilic fibers and hydrophobic matrices. The degradation process is illustrated in Figure 4.6. When natural fibers absorb water, they can swell and cause micro-cracking in the polymer. As the composite cracks further, capillarity enables water molecules to flow through the fiber-matrix interface, leading to debonding and degradation of the composite structure [38].

In a study by Thuault et al., it was observed that the tensile strength of scutched flax fiber decreases significantly when the relative humidity exceeds 68% at 70°C [70]. High relative humidity can infiltrate the fibers, disrupting the microfibril network and reducing fiber strength. Berges et al. reported that the tensile modulus of flax-epoxy laminates was severely reduced at a relative humidity of 85%, while the strength remained relatively unaffected. These findings highlight the impact of moisture on BFRP and emphasize the necessity of incorporating a conversion factor for its mechanical properties [71].
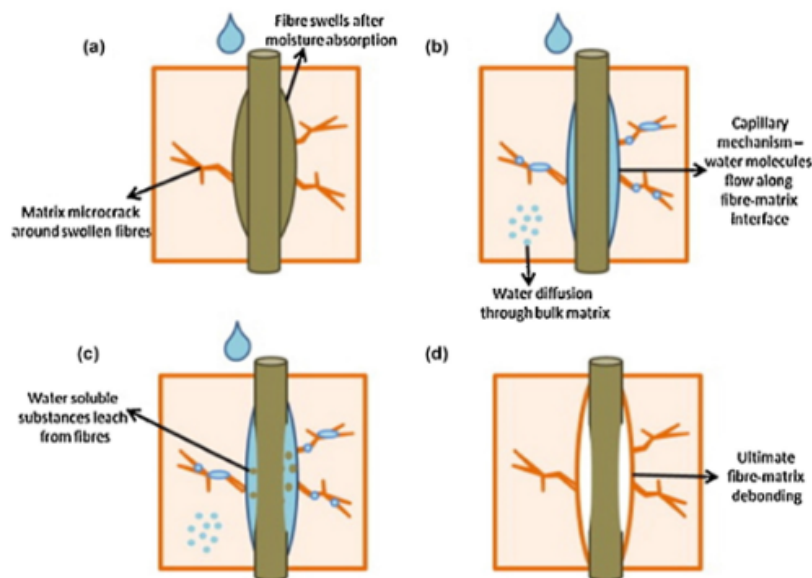
Figure 4.6: Degradation mechanism due to water absorption by fibers [38]

The floors investigated in this study are intended for indoor use, which corresponds to exposure class I and a moisture conversion factor (η_{cm}) of 1, according to FRP Eurocode standards [68]. This indicates that the relative humidity is below 80%. Although this aligns with the observations of Berges et al., it does not fully account for the moisture sensitivity of BFRP, mainly when a partial bio-based resin is utilized compared to the epoxy resin in the research of Berges et al. A suitable moisture conversion factor is estimated using plywood as a representative material to address this. Plywood is a layered wood product composed of thin veneer sheets bonded together. It is manufactured by subjecting multiple layers to high pressure and temperature, with the grain direction of each layer oriented perpendicular to one another. Considering that both BFRP and plywood are layered materials and share a natural fiber composition, it is assumed that the moisture effects are similar between these two materials.

Table 4.2 provides the k$_{mod}$ values for plywood, considering different load durations and service classes. The selection of the appropriate service class depends on the relative humidity of the surrounding air. By the Eurocode guidelines for indoor environmental parameters, a relative humidity range of 40-60% is considered comfortable for individuals in regular buildings, excluding museums and churches [68]. Based on this information, it can be concluded that service class 1 is suitable.

Considering the load duration of action, a k$_{mod}$ value of 0.6 should be tconsideredfor permanent loads. Referring to the book "Timber Engineering: Principles for Design" [72], specifically table C1-4, the load-duration class 'Medium-term' corresponds to imposed floor loads. Therefore, the imposed variable loads should consider k$_{mod}$ value of 0.8

Table 4.2: k$_{mod}$ values for plywood adapted from prEN1995-1-1 [24]

Material	Service class	Load-duration of action				
		Permanent	Long-term	Medium-term	Short-term	Instantaneous
Plywood	1	0.60	0.70	0.80	0.90	1.10
	2	0.60	0.70	0.80	0.90	1.10

Table 4.3: Moisture conversion factors

Type	η_{cm}
Permanent load	0.6
Variable load	0.8

4.6.3. Creep effects

Considering creep in the design and analysis of BFRP composites is crucial. Creep, the time-dependent deformation under sustained load, affects the long-term behavior of structures. Ignoring creep can lead to overestimating strength and deflection, potentially compromising structural integrity. The creep effects are taken into account by a creep factor. The reduced material properties can be calculated with Equation 4.26 [22].

$$X_{\mathrm{m}}(t) = \frac{X_{\mathrm{m}}(0)}{1 + \phi(t)} \tag{4.26}$$

where t is time, $X_m(t)$ the mean elastic or shear modulus, $X_m(t)$ the initial mean value of elastic or shear modulus and $\phi(t)$ is the creep coefficient.

The prEN of FRP and timber provide creep factors [22, 24]. The FRP Eurocode provides creep factors for laminates with a fiber volume fraction of at least 35%, material temperature of up to 25 degrees, and relative humidity of a maximum of 65% for 50 years. However, this is not representative of BFRP because of the use of synthetic fibers.

As stated in chapter 3, the material and properties utilized in this research pertain to the Ritsumasyl bridge. During the bridge's design process, creep relaxation tests were conducted. The determined creep factors for this specific material are outlined in Table 4.4. Note that the factors are different depending on the lay-up used. Two types of lay-ups are used: a quasi-isotropic lay-up and a quasi-isotropic lay-up with unidirectional plies. Additionally, this overview includes the creep factors for design lifespans of 50 and 15 years, obtained by downscaling the 100-year design life using a logarithmic scale.

Table 4.4: Creep factors used for Ritsumasyl bridge

	$\phi_{\mathbf{cr}}$					
	QI lay-up			QI-UD lay-up		
Type	100 yr	50 yr	15 yr	100 yr	50 yr	15 yr
Deflection	3.69	3.13	2.16	3.29	2.79	1.93
Strength	4.5	3.82	2.64	4.16	3.53	2.07

4.7. Conclusion

- FRP can be analyzed at three levels: microscale, mesoscale, and macroscale, respectively focusing on studying the properties of the fiber and resin, investigating the behavior of the ply formed by the fibers and resin, and examining the behavior of the laminate.
- FRP is a heterogeneous and orthotropic material, meaning that its components have different properties, and the properties in the three principal directions differ.
- The properties of a UD ply can be obtained by testing or using the Halphin-Tsai equation. For the Halphin-Tsai equations, an appropriate empirical reduction factor should be used. The empirical factor is unknown for BFRP, where the interface between fiber and resin is more critical.
- Using the constitutive relations and transformation rules, the stiffness matrix can be determined in the local and global coordinate systems.
- CLLT is used to determine the properties of a laminate using the distributed membrane forces to obtain the A matrix, the B matrix, and the D matrix.
- The stacking sequence influences the properties of the laminate, with quasi-isotropic being most often used. Symmetric and balanced sequences simplify the stiffness matrices.
- Moisture, temperature, and creep effects should be considered for BFRP.
- The temperature conversion factor depends on the dominant property that leads to failure. The moisture conversion factor is assumed to be similar to plywood according to EN1995 because of their similar nature and the limited research available on BFRP.
- The creep effects are taken into account by a creep factor. The creep factors are taken from the case study Ritsumasyl bridge.

5

Sustainable Design

5.1. Introduction

Given the challenges currently facing humanity, it is essential to prioritize sustainable design. According to the definition of sustainable design put forth by the World Commission of Environmental and Development (Brundtland Commission) [73], it involves "meeting the needs of the present without compromising the ability of future generations to meet their own needs." In this chapter, three aspects that are important to consider for a sustainable design are discussed [74]:

- Environmental
- Economical
- Social

5.2. Environmental Sustainability

Environmental sustainability is a crucial pillar of sustainable design. It concerns protecting the natural environment from the building project and, conversely, protecting humans from their environment. Considering protecting the environment from the construction project, two critical factors for achieving environmental sustainability are energy consumption and using building materials [1].

5.2.1. Energy

The supply of energy is a significant challenge that humanity is currently facing. To address this challenge, buildings that are energy-efficient throughout their life cycle should be built. During the production and erection phase, energy can be saved by automating and making the process more efficient. During the utilization phase, heating and cooling significantly contribute to energy consumption. One way to reduce this demand is to improve the building envelope by using better insulation and other methods that decrease energy losses. Additionally, energy-efficient building services, such as proper insulation, can help optimize energy use during the utilization phase. Finally, renewable energy sources should be used whenever possible [75].

5.2.2. Building materials

The materials used in building construction are also important to consider. Processing these materials and their characteristics can result in significant energy consumption and environmental impacts. Embodied energy includes the energy required to extract, process, and install the materials. Moreover, polluting substances are emitted during the production of the materials and construction elements, further harming the environment [75].

The choice of building material also impacts required maintenance, service life, and the recyclability of the structure. These factors, in turn, influence its sustainability. A durable material or structure can be utilized for an extended period without needing replacement. Recyclability enables materials, elements, parts of a structure, or the entire structure to have a second life, reducing the demand for new materials. However, the recyclability of the raw materials of composite materials is challenging in terms of separating the fibers and resin, making it more difficult to reclaim raw materials [1].

48

5.2.3. Life cycle assessment

The environmental impact of a structure can be evaluated using a life cycle assessment (LCA). This method considers the raw materials and energy consumption associated with the entire life cycle of a product and produces data on waste and emissions as output. Below, the procedure of an LCA is discussed.

Procedure LCA

The procedure for conducting an LCA varies based on the product being analyzed, resulting in a large variation in the LCA procedure. The International Organization for Standardization (ISO) has developed a general protocol to follow to complete an LCA. An environmental product declaration (EPD) can be used to compare the LCA between products. An EPD is a standardized document that informs about the potential impact of a product on the environment and human health. The EPD is produced based on calculations from an LCA and provides a quantitative basis for comparing products and services. EPDs are provided by companies about their products.

During the LCA process, a product's life cycle is broken into steps. The steps involved in the LCA process are: (1) identifying the goal and scope of the analysis, (2) compiling a life cycle inventory (LCI), (3) completing a life cycle impact assessment (LCIA), and (4) interpreting the results (see Figure 5.1). The following paragraphs elaborate on each of the steps.
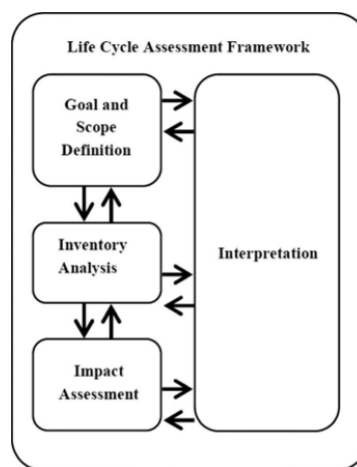
Figure 5.1: LCA framework (add reference)

Goal and scope

In the first step, the goal and scope of the LCA are specified. The system boundary is defined along with the stages of the product's life cycle that are analyzed. Four phases can be distinguished: product stage, construction stage, use stage, end-of-life stage, and final stage. The final stage defines aspects after the building life cycle stage, such as reuse and recycling, see Figure 5.2. In this step of the LCA, a functional unit must be set, a set amount of product, or another quantity that describes what is being studied.

Inventory

In the second step, the LCI is made. It is the most time-consuming and extensive phase and requires identifying and quantifying the resource flows for the system to create an inventory of the functional unit. To help with data accuracy and consistency, databases have been created for common areas of study such as energy, waste treatment, and chemical production. Environmental databases gather LCI data on commonly used raw materials, elements, and processes from the construction sector. However, not all data is included, and sometimes the analysis must be done manually, which is time-consuming and prone to errors.
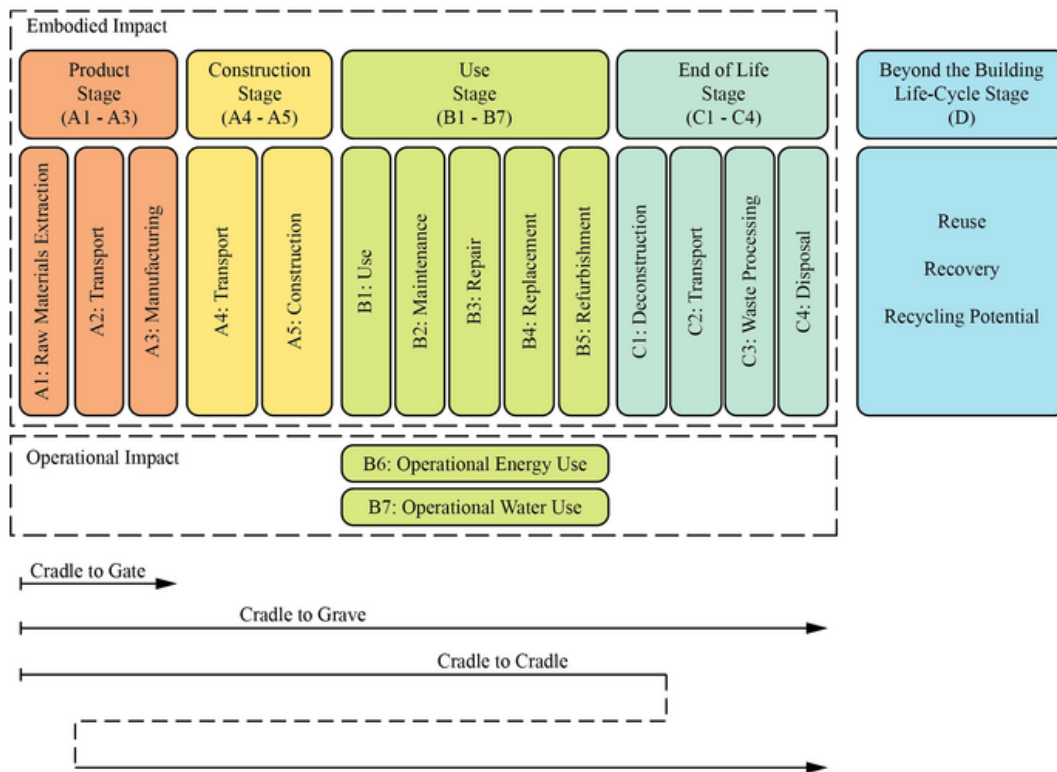
Figure 5.2: LCA stages [76]

Impact Assessment

The third step in the LCA process involves the LCIA, where the system's environmental impact is assessed and evaluated. LCIA converts the results obtained from the inventory analysis into common units across the impact categories. These impact categories collectively determine the overall environmental impact. Alternatively, an analysis can focus on a specific set of impact categories, thereby narrowing down the assessment to a particular area of environmental concern. In such cases, the impact categories must be carefully selected, and the indicators within each category are grouped based on resource flows and common environmental factors that contribute to a shared impact. The most commonly used environmental impact categories are:

- GWP: GHG emissions contribute to global warming; in kg CO_2 equivalent.
- ODP: Halogenated compounds harm the ozone layer; in kg CFC-11 equivalent.
- AP: Acidic compounds from fuel combustion cause acid rain; in kg SO_2 equivalent.
- EP: Excess nutrients cause disproportional growth in ecosystems; in kg PO_4 3- equivalent.
- POCP: Airborne pollutants react with sunlight to form harmful compounds in kg ethylene equivalent.
- ADP: Depletion of non-living finite resources; ADPe for non-fossil resources (kg Sb equivalent), ADPf for fossil resources (kg Sb/MJ).
- HTP: Toxic compounds affect human health; in kg 1,4 dichlorobenzene equivalent.
- FAETP: Toxic compounds affect freshwater organisms; in kg 1,4 dichlorobenzene equivalent.
- MAETP: Toxic compounds affect marine organisms; in kg 1,4 dichlorobenzene equivalent.
- TETP: Toxic compounds affect terrestrial organisms; in kg 1,4 dichlorobenzene equivalent.

ISO 14040 provides guidelines for normalizing, weighing, and aggregating the scores obtained for impact categories. It also allows for thematic grouping of categories. Furthermore, unit equivalents can be converted into monetary values or shadow costs to derive the Environmental Cost Indicator (ECI), as described in the Dutch 'Bouwbesluit 2012 - Bepalingsmethode'. To obtain each product's final environmental impact score, specific scores are calculated for each category and combined into a single value. The overall environmental footprint of a building is determined by summing the scores of all individual building products. Additionally, the environmental profile of the building can be assessed by summing the scores of the individual environmental impact categories.

In summary, LCIA involves seven steps: (1) selection of impact categories, (2) selection of impact category indicators, (3) classification of inventory results into categories, (4) characterization, (5) normalization, (6) grouping, and (7) weighting. While the first four steps are mandatory, the remaining three are optional.

Interpretation
The last step of LCA involves the interpretation of the results obtained from both the LCI and the LCIA. The main objective of this step is to answer the initial study goal by evaluating and analyzing the results, which enables drawing conclusions and providing recommendations. The data and procedures are assessed for consistency and reliability during this stage, and the study's limitations are discussed.

5.2.4. Biogenic carbon

Replacing fossil-based building materials with bio-based products is a key strategy for reducing the construction sector's impact on climate change. Bio-based materials can store or capture carbon, also called biogenic carbon, and effectively remove it from the atmosphere. However, when bio-based materials end their life cycle, the stored carbon is released through combustion or decomposition. Including biogenic carbon in LCAs is often a topic of debate, presenting a challenge in accurately accounting for its environmental impact.

Since wood, for instance, is a product of photosynthesis, it naturally sequesters carbon during the growth of trees and retains it until the wood is burned or decomposed. Utilizing harvested timber for construction extends the period of carbon storage within the material, delaying its re-release into the atmosphere. This entire process underscores the importance of tree planting initiatives and maximizing the lifespan of timber products to fully leverage their capacity for biogenic carbon storage. It is worth noting that the amount of biogenic carbon stored in timber gradually decreases over time due to various manufacturing processes involved. This process is illustrated in Figure 5.3 [77].
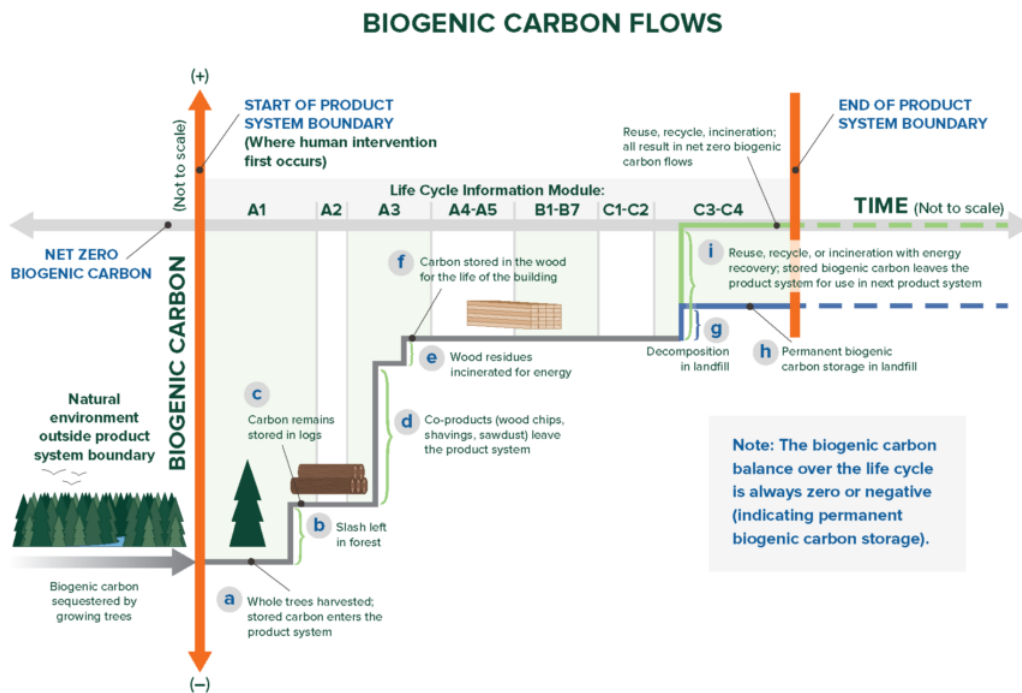
Figure 5.3: Biogenic carbon flow adapted from [77]

Assessing carbon storage in bio-based materials presents a significant challenge, primarily due to the transparency of underlying assumptions. Two main methods are used for accounting for biogenic carbon storage: the 0/0 approach and the -1/+1 approach [78]. Both static approaches operate under the assumption that timber is carbon neutral over the building's service life. However, they differ in handling biogenic carbon throughout the life cycle.

The 0/0 approach assumes complete carbon neutrality of bio-based products over the entire building system life cycle. This means the carbon release at the end of a bio-based product's life is assumed to be balanced by the carbon uptake during biomass growth. As a result, biogenic CO_2 is not considered in any module of the LCA.

On the other hand, the -1/+1 approach tracks all biogenic carbon flows across the building's life cycle. During biomass growth, the biogenic carbon uptake is reported as a "negative" emission in module A, reflecting the transfer of biogenic carbon from the forest system to the building. Similarly, when the building reaches its end-of-life, the stored carbon is modeled as a transfer from module C to module D, accounting for different end-of-life scenarios. This transfer results in a positive emission reported in module C.

When considering circularity, approach -1/+1 can be more suitable. For circularity, carbon storage is no longer assumed to be temporary but can be considered permanent. Consequently, the negative results in the production stage from the -1/+1 approach would translate to long-term carbon storage in bio-based materials, with a high certainty of being reused at their end-of-life. This highlights the importance of circularity in preventing carbon from reentering the atmosphere and underscores the potential for bio-based materials to contribute to sustainable carbon management strategies.

5.2.5. Paris agreement

The Netherlands' LCA system evaluates buildings' environmental impact throughout their designated lifespan. This assessment encompasses factors like recycling and reuse, extending beyond the building's intended life cycle. However, the LCA system faces limitations when determining compliance with greenhouse gas emission targets in line with the Paris Agreement. It considers future effects beyond the target timeframe and treats potential savings from bio-based materials as negative emissions, which does not align with a budget-oriented approach.

The Dutch Green Building Council commissioned NIBE to research the CO_2 impact of the building process and material usage in new construction and renovation projects [79]. The research aimed to address how the Dutch construction sector's impact aligns with the goals of the Paris Agreement. In terms of the scope of the Paris Agreement, it is confined to evaluating emissions from the sourcing of materials to the realization of construction, focusing specifically on LCA modules A1 through A5.

One concern is related to the new set of environmental impact assessments, which may result in negative values for bio-based products in module A1. NIBE advises refraining from treating biogenic CO_2 as a negative emission until further study is conducted. This recommendation aligns with EN 15804:A2 guidelines, which emphasize the need to consider the uptake and the release of biogenic CO_2 at the end of a product's life, ensuring a balanced assessment over its lifespan.

5.2.6. Ritsumasyl bridge

The Ritsumasyl bridge was used as a case study to select BFRP materials. An LCA study was conducted for this bridge. This section provides a brief overview of the environmental impact of the BFRP bridge compared to other bridges to gain insight into the environmental impact of an application using BFRP.

Variants

In this LCA study, five different bridge types were compared: concrete, steel, timber, GFRP, and BFRP bridges. The concrete bridge used standard pre-stressed prefabricated box girders with reinforced concrete elements at the abutment edges. The steel bridge featured a deck composed of two main girders made from HEB700 profiles, supplemented by transverse beams, stability bracing, and a rib-stiffened deck. The timber bridge's primary load-bearing structure consisted of two laminated beams measuring 1200 mm x 500 mm, transverse beams, stability bracing, and CLT deck panels. The GFRP bridge had a structure similar to the BFRP bridge discussed in section 3.3, but it did not incorporate a balsa core in the webs due to GFRP's superior strength over BFRP.

Scope

The main assumptions and scope of the Ritsumasyl LCA are listed below:

- Bridge components, such as the movable deck and foundation, have not been included. Also, the railing and edge elements are excluded from consideration, assuming they are the same for the five variants.
- The ECI and CO_2 calculations are based on the principles of LCA with a project lifespan of 100 years.

This means that replacements of materials with a shorter lifespan than 100 years have also been included. All phases have been considered, including production, transportation, construction, use, maintenance, and end-of-life.

- The LCI was created using the national environmental database and literature for the BFRP bridge. For specific data, please refer to [80].
- For the end-of-life, the recycling rate for concrete and steel is considered to be 99% and 94 %, respectively, and 0% for timber, GFRP, and BFRP. For timber, GFRP, and BFRP, a burning rate of approximately 80% is considered. Burning is more valuable for timber compared to GFRP and BFRP.

Results

Figure 5.4 and 5.5 show the results of the LCA analysis performed by Sweco and Witteveen+Bos. A more elaborate overview can be found in their report [80]. As for both the ECI and CO_2 emission, the GFRP variant performs the worst. For the ECI, the steel and concrete variants are lower than the timber and BFRP variants. This mainly concerns the high recyclability rate for both concrete and steel.

For the ECI, the timber variant is substantially lower than the BFRP variant, whereas it is the other way around for the CO_2 emission. The main difference between the BFRP and timber variants is that for BFRP, the end-of-life is significant, and for the timber variant, the maintenance variant is substantial.
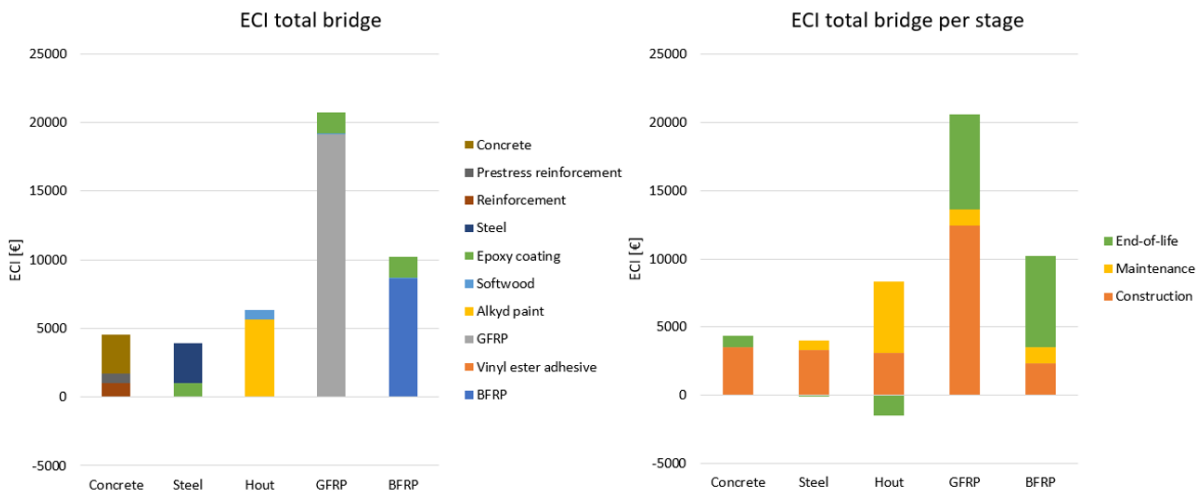
Figure 5.4: ECI results for total bridge and stages adapted from [80]
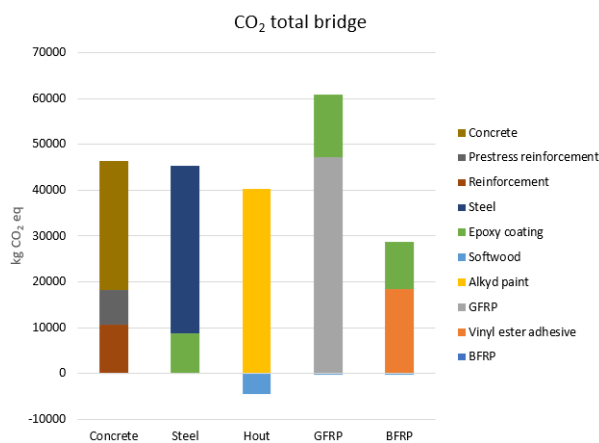
Figure 5.5: CO_2 emission results for total bridge adapted from [80]

Discussion

Several discussion points are discussed in the LCA report [80]. The most important points are elaborated on below.

- Opportunities for higher-end-of-life applications emerge if 100% bio-based BFRP manufacturing can be achieved. In the case of a 100% bio-based BFRP, the material can be used to recover or utilize energy or residual value through incineration or composting.
- The high ECI score in timber is primarily due to alkyd paint, as timber has a relatively low ECI score. Sustainable timber coatings are available but not yet included in the National Environmental Database. CO_2 emissions in the timber variant are entirely attributed to alkyd paint, while timber has negative CO_2 emissions. Not conserving the timber would be environmentally better regarding CO_2 and ECI scores but less cost-effective in the long run.
- Concrete performs well in most parameters except materialization. It has favorable CO_2 emissions and ECI scores due to the 99% concrete reuse. However, concrete reuse is relatively low-value, limited to foundations or gravel replacement, where cement, the highest-emission component, is no longer functionally utilized. Considering these factors would have a significant sustainability impact.

5.3. Social Sustainability

One well-known aspect of sustainability is the lifespan of a building. For a building to last, it must not only be structurally sound but also be used effectively. To ensure that users continue using a building, it should provide comfort and high-quality features, allowing people to feel safe and secure. Only then can the building's service life be extended. Moreover, a building should not only be functional and aesthetically pleasing, but it should also be accepted within its community. Collaboration with local businesses can strengthen the relationship between the project and its environment. Additionally, the building's architecture should be compatible with the surrounding area to create a harmonious visual effect [81].

Measuring the social sustainability of a building is challenging as the social impact can vary from individual to individual, city to city, and community to community. However, social sustainability provides numerous opportunities to improve the quality of life for those who use and live in the building [75].

5.3.1. Comfort

Comfort is a significant factor in building design as it focuses on the building occupants' well-being. It comprises thermal comfort, visual comfort, and sound protection. The building envelope plays a vital role in ensuring occupants' comfort. Thermal comfort is mainly concerned with room temperature and building materials. Proper insulation, ventilation, and heating/cooling systems are necessary to maintain a comfortable temperature. Visual comfort primarily depends on the building's architecture, including daylight and sun exposure. Sound insulation is also essential as it ensures that building occupants are not disturbed by external noise or each other. A well-designed building should provide adequate sound protection to minimize noise levels and provide a conducive environment for the occupants to work or relax. For sound insulation, both airborne and impact noise should be considered.

5.3.2. Flexibility

Improving the functionality of a building can significantly enhance its service life. Buildings should be adaptable and capable of meeting changing requirements over time. One way to achieve this is by using a structure with a skeleton system, which offers greater flexibility compared to a shear wall system [82]. Punctual supports are preferred in such structures, allowing components to be changed constantly and meeting the evolving needs of the building.

5.3.3. Local architecture

Integrating a building into its environment is crucial for sustainability as it relates to the urban and cultural context. To ensure that the local population accepts a building and contributes to the area's development, it should always be planned in the context of its surroundings [75, 83]. When considering the optimal use of FRP, it is essential to consider the building's environment. While FRP's shape freedom allows for creating domes, this may not be suitable for every area. For example, using cubes and high-rise buildings may be more appropriate in urban areas with limited space.

5.3.4. Local materials and services

Traditionally, architecture and construction techniques were closely tied to locally available building materials and services. However, with the advent of industrialization, this relationship changed. The use of local materials and services can significantly impact the development of a region and, therefore, the project's sustainability. In addition to macroeconomic considerations, local procurement also has implications for the carbon footprint [83]. Furthermore, shorter transport distances have a direct positive effect on environmental sustainability.

In line with this, Hugo de Jonge has launched an initiative to promote the use of bio-based materials in the building industry [13]. This initiative aims to encourage agriculture to transition towards cultivating natural fibers.

5.4. Economic Sustainability

The economic criteria of sustainability consider the cost of a building's life cycle, including construction, operation, and end-of-life. To ensure financial sustainability, optimized planning is crucial, with careful consideration of factors such as the building's predicted lifetime, renewal cycles, and future cost trends. By considering the total cost of a building's life cycle, stakeholders can make informed decisions that benefit the environment and society and provide financial benefits in the long term. It is important to note that economic sustainability should not come at the expense of environmental or social sustainability but should be integrated with these other aspects to achieve a truly sustainable outcome [75].

5.5. Conclusion

- Energy consumption and choice of building materials are important for environmental sustainability.
- LCA is a method to assess a product's or building's environmental impact. It involves defining goals, outlining scope, inventorying resources, assessing impacts, and interpreting results.
- Bio-based materials have the unique ability to store biogenic carbon. This feature is critical for effective carbon management strategies, as it helps offset emissions.
- In the Ritsumasyl Bridge LCA variant study, the BFRP bridge outperformed the timber bridge regarding CO_2 emissions. This difference is primarily due to the maintenance demands during the user phase of the timber bridge. Conversely, regarding ECI, the timber bridge exhibited superior performance to the BFRP bridge. Generally, the primary factor contributing to the BFRP bridge's relatively worse performance is its end-of-life stage.
- Social sustainability addresses equality, justice, and well-being within buildings and communities.
- Building flexibility ensures that structures adapt to changing needs over time. This feature enhances the lifetime and relevance of a building.
- Integrating buildings with their local surroundings using local materials and services benefits social acceptance and drives local development.
- Initiatives like Hugo de Jonge's drive to encourage bio-based materials align with social and environmental sustainability goals. His initiative aims to encourage agriculture to transition towards the cultivation of fibers.
- Economic sustainability encompasses the full life cycle cost of a building, from construction to operation and eventual decommissioning. It is important to note that economic sustainability should not come at the expense of environmental or social sustainability but should be integrated with these other aspects to achieve a sustainable outcome.

Part II

Floor Design

<div style="text-align: right; font-size: 4em;">6</div>

Case Study: The Natural Pavilion

6.1. Introduction

This chapter discusses the case study used to demonstrate the feasibility of BFRP floors. The modular building picked as the case study is the Natural Pavilion in Almere, the Netherlands (see Figure 6.1). Using this case study sets the design requirements for the BFRP floor and allows for a fair comparison between BFRP floors and conventional floors. It should be noted that a CLT floor is used in the case study; to compare to a concrete floor, a simple design is made and described in chapter 9.

This chapter provides a general description of the design considerations and important aspects of the Natural Pavilion project. This is a solid foundation for the subsequent analysis and design of the BFRP floor. The green boxes summarize the design assumptions and decisions for the BFRP floor.

Figure 6.1: The Natural Pavilion [6]

6.2. Project Description

This project aimed to build an innovative building that embodies modularity, demountability, circularity, and the utilization of bio-based materials. As part of the Oosterhof consortium, ABT participated in designing this sustainable structure in collaboration with the Noordereng Group and architect DP6. The building was successfully constructed at the Floriade in Almere. Initially, the plan was to relocate (a part of) the building and utilize its modularity and demountability. However, the building is currently used for various purposes, such as an office building, meeting place, or conference location.

As part of the Floriade Expo, the project allowed for exploring innovative solutions. Among the innovative solutions employed in the Natural Pavilion is the Houtkern method, which translates to the "timber core method." This method involves a demountable steel connection between columns and beams initially developed for the Energiehotel in Ede. [84, 85]. The Houtkern method enables the stacking of modules in various configurations, allowing stacking to heights up to 80 meters. In the case of the Natural Pavilion, a simplified version of the connection was utilized because requirements were less strict, and only three modules were stacked on top of each other. The connection configuration is depicted in Figure 6.2.
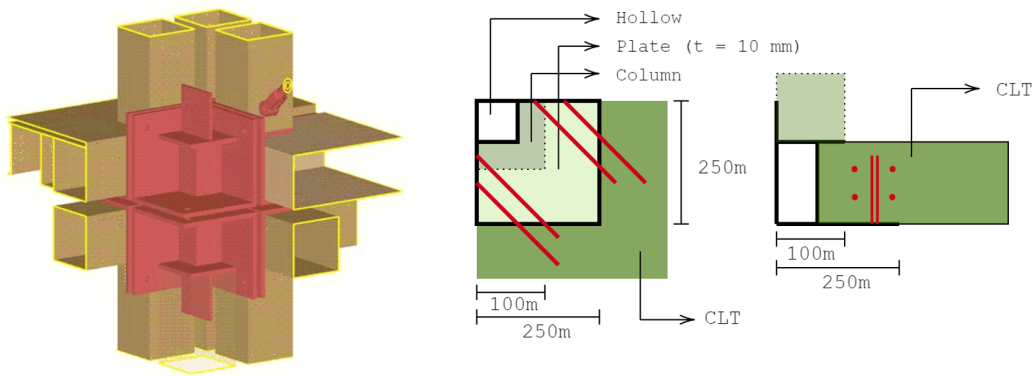
Figure 6.2: HoutKern building method connection adapted from ABT's Natural Pavilion report [85]

6.3. Structure

The main structure of the Natural Pavilion consists of frames, modules, and a roof, as illustrated in Figure 6.3. This research focuses on the floors used in the design of the modules. Therefore, the modules will be discussed in more detail.
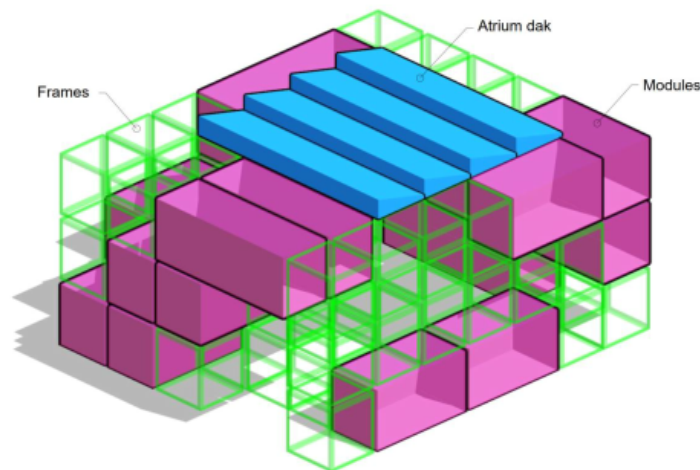
Figure 6.3: Components of the main structure of the Natural Pavilion adapted from ABT's Natural Pavilion Report

The modules come in two sizes: 3.5 meters wide and 3.25 meters high, with lengths of either 7 or 10.5 meters. Each module comprises a CLT floor, solid timber columns, and beams at the top. The CLT floor is supported by columns at intervals of 3.5 meters, as shown in Figure 6.4. The maximum width of 3.5 meters is determined based on the RDW (Netherlands Vehicle Authority) regulations, which state that the maximum width transportable with a regular waiver is 3.5 meters [86]. The CLT used is produced by Derix, with a total thickness of 180mm and a layering of 40/30/40/30/40mm. The outermost lamellae are oriented in the transverse direction of the module.
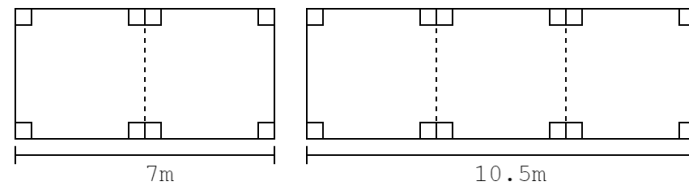
Figure 6.4: Two modules of Natural Pavilion with continuous CLT plates and column supports (Report of Natural Pavilion of ABT)

The modules are connected using steel connections from the Houtkern method. This connection acts as a shoe, with the CLT plate resting on a 250x250mm steel plate support area and secured with bolts. A section of the CLT plate is cut out in the corner to accommodate a hollow steel section that connects the columns. This configuration allows for direct transfer of forces through the columns without relying on the CLT plate for force transfer. The same principle applies to the timber beam at the top connection. Figure 6.2 illustrates the connection used.

6.3.1. Frame

The frame of the Natural Pavilion follows the same principles as the modules and consists of columns and beams. In contrast to the modules, where the CLT plate forms the bottom structure, the frame utilizes the timber beams at the bottom. The same steel connection system is used for the frame. The frames are transported as separate elements and assembled on-site to form the structure.

6.3.2. Stability

Although the CLT floors can transfer lateral loads, additional steel bracing is required for overall stability. These bracings can be connected to steel connections. Figure 6.5 illustrates the application of steel bracings between the steel connections to enhance stability. It is essential to highlight that utilizing 'thin' rods as bracing would not be suitable for using the Houtkern method for structures up to 80 meters in height. For example, in the case of the Energiehotel in Ede, a concrete core is utilized, and the connections are more rigid.
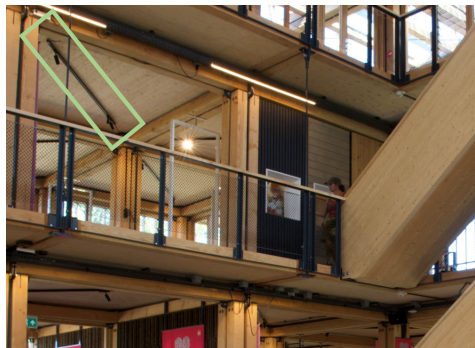
Figure 6.5: Steel bracing between steel connections

BFRP Floor design

- Only the floor plan configuration of 3.5x7 meters is considered for the BFRP floor. Designing for the larger size of 3.5x10.5 meters would involve the same design process but would not provide additional insights to address the main research question and increase the computational time.

- For the connection to the column, the same detail is assumed. Detailed connection analysis is not done, and a supporting area of 250x250mm is assumed.

- The study does not include a comprehensive analysis of the diaphragm action of the floor and connections.

6.4. Design Requirements and Boundaries

This section offers an overview of the support and loading conditions, as well as the specific design requirements for the CLT floor of the case study. This is set as design requirements for the BFRP floor.

6.4.1. Support conditions

The CLT floor is column-supported; depending on the module size (7 or 10.5 meters), either 8 or 12 columns support it. There are single columns in the corners, but at every 3.5 meters, two columns are located close to each other. Each of them is part of a frame. The columns are attached to the connection that provides a support surface of 250x250mm to the CLT plate.

The columns allow for rotational movement at the connection. This rotational flexibility needs to be considered in the support conditions for the design of the floor. Especially because selecting a lower rotational stiffness (or hinged) than in practice would yield conservative deflection results, and a higher rotational stiffness (or rigid) would be conservative for maximum stresses in the material at the support location. To determine the actual rotational stiffness of the support, it is necessary to assume a deformation of the columns, as shown in Figure 6.6. The rotational stiffness of the floor supports can then be calculated using a fundamental mechanical formula, as presented in Equation 6.1.

$$\theta = \frac{TL}{EI} \longrightarrow T = \theta \cdot K_r \longrightarrow K_r = \frac{3EI}{L} \qquad (6.1)$$

with K_r begin the rotational stiffness.
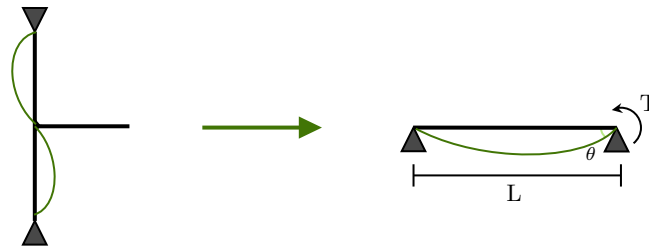
Figure 6.6: Column deformation assumption for rotational stiffness support

> **BFRP Floor design**
> The dimensions of the columns for the BFRP floor design are assumed to be the same as those used in the Natural Pavilion. Therefore, the rotational stiffness of the columns will also be the same, which is 727 kNm/rad.

6.4.2. Loading conditions

In the design of the Natural Pavilion, two loading cases have been considered: one for a regular floor and another for a floor with planting. Each loading case comprises a permanent load and a variable load component.

For the regular floor (load case one), the permanent load includes the structure's self-weight and the top floor's weight, which is necessary for acoustic requirements. Considering the building's classification, the variable load should be determined based on Eurocode 1: Actions on Structures [21]. The Natural Pavilion falls into class C assembly buildings, with a loading requirement of 5 kN/m^2. However, due to the unique assignment of the Natural Pavilion, a lower variable load of 3 kN/m^2 has been agreed upon with the client. This load is a more realistic load based on research conducted at Cambridge. The 3 kN/m^2 permanent load is also in line with the loading that has to be taken for residential buildings, which makes it possible to reflect on residential buildings as well. The permanent and variable loads for the floor with planting are lower than those for the regular floor and will not be discussed in further detail. For the floor design, different load combinations must be considered. The load combinations and factors that must be considered are summarized in Appendix B.

> **BFRP Floor design**
> Only the critical load case is considered in the analysis for the BFRP floor. The favorable and unfavorable load combinations are not considered to decrease computational time. The permanent and variable loads for a regular floor are:
>
> - g_{self} = case dependent
>
> - $g_{topfloor}$ = 0.8 kN/m^2
>
> - q_v = 3 kN/m^2
>
> - Q_v = 3 kN (over 100x100mm)

6.4.3. General requirements

The design requirements for the CLT floor encompass verifying internal forces in the ULS. Additionally, the floor must satisfy deflection and vibration criteria in the SLS. The specific criteria associated with the SLS are provided in Appendix B.

It is essential to account for the influence of creep on the floor deflections. To address this, the design life of the buildings is essential. This is necessary to determine the additional deflection resulting from creep over time. In the case of the Natural Pavilion, the design life is set at 15 years. However, this duration may seem relatively short compared to most buildings, typically 50 years.

> **BFRP Floor design**
> To ensure a fair comparison between the CLT floor in the case study and the BFRP floor, a design life of 15 years is adopted. The discussion presents the prospects for a design life of 50 years.

6.4.4. Fire safety

Regarding fire resistance, the Natural Pavilion, as per the Building Decree 2012, falls under existing building requirements. There is a requirement of 30 minutes of fire resistance for the structural construction based on the highest floor height (>5m). However, this requirement does not impact fire resistance since the pavilion has one single fire compartment. Collapsing of the compartment never results in the collapse of another compartment.

The stairwell is designed as a separate sub-fire compartment, requiring 20 minutes. This requirement is comfortably met with the applied wood dimensions. Combined with fast detection and alarms, the evacuation safety of pavilion occupants is assured.

> **BFRP Floor design**
> Aligned with the case study, the BFRP floor is designed for a building with one single compartment, not considering additional fire resistance requirements.

6.4.5. Acoustic requirements

There are no mass requirements imposed on the construction for sound insulation. If they were to be considered, it would involve incorporating a floating top floor and providing wall insulation to meet airborne sound requirements. Additionally, for the requirements related to contact-borne sound, the mass in the steel connection would need to be increased to minimize vibrations.

> **BFRP Floor design**
> In line with the case study, no mass requirements are imposed on the BFRP floor for sound insulation.

6.5. BFRP Floor

The case study is used as a framework for the design of a BFRP floor. This means a floor is designed that is supported by six columns. As explained in chapter 2, a one-way or two-way floor system is used.

One-way

The case study initially used a two-way floor system, a CLT floor, which raises the question of why a one-way system should be considered. One-way floor systems are the most commonly used floor types in the building industry due to their simplicity in design. Also, the production process for BFRP one-way floors is easier. Therefore, a one-way and a two-way floor are both considered.

When utilizing a one-way floor, additional beams are required to support the floor. The beams result in an increased construction height. The one-way floor will span over the shorter dimension, resulting in a length of 3.5 meters.

Two-way floor

A two-way BFRP floor would more easily fit into the existing design of the Natural Pavilion. The floor would be supported straight unto the columns, and no additional beams are required. Furthermore, a two-way floor can withstand horizontal loads and act as a diaphragm to ensure stability. However, the two-way floor is more complicated than a one-way floor because it should be able to transfer loads in two directions.

7

Global Numerical Model

7.1. Introduction

This chapter explains the design process for the one- and two-way BFRP floors. The most efficient and simplest approach involves using analytical calculations. Nonetheless, particularly in the case of two-way floors where stress distribution is complex and analytical methods have limitations, the utilization of FEA proves advantageous. Therefore, a global numerical model of the one- and two-way floor is made in Abaqus.

First, the relevant geometry and boundary conditions are described, whereafter, a comprehensive examination of the floor's ULS and SLS is conducted. They lead to guidelines and constraints governing feasible geometries. All checks of the whole verification procedure are integrated into the post-processing of the numerical model.

Subsequently, the model setup is discussed, and the meshing, model interactions, and analysis procedure are outlined. Additionally, an overview of material properties and safety factors is provided. Finally, a validation involving checking the numerical model with analytical methods is included to ensure the model represents the real-world floor.

7.2. Geometry Parameters

7.2.1. One-way floor

Geometry parameters of the one-way floor are the thickness of the facings (t_f), the web thickness (t_w), the core (or web) height (h_c), the total height (h_t) and the web spacing (c_w). Figure 7.1, shows a cross-section with the geometry parameters. The floor spans 3.5m and has a repetitive design over the width. The one-way floor is supported by beams spanning between the columns of the Natural pavilion. The steel connection is designed for beams with a width of 180mm; the same beam width is considered for the design of the one-way floor.
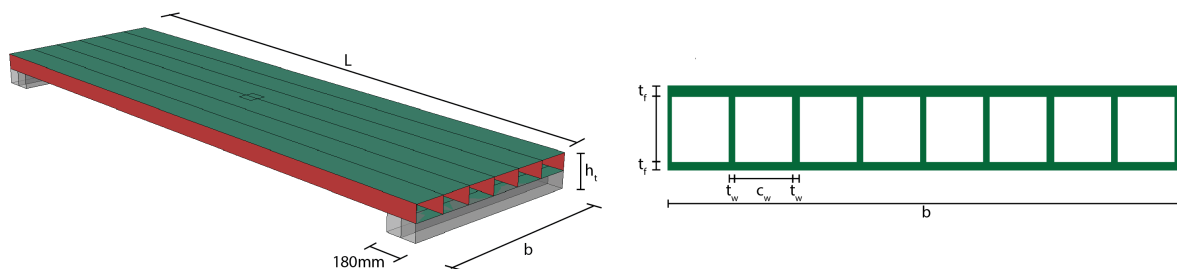
Figure 7.1: Geometry of one-way floor

7.2.2. Two-way floor

The geometry parameters for the two-way floor are the same as for the one-way floor. The transversal and longitudinal web spacing are the same. The floor plan is identical to the CLT floor in the Natural Pavilion. The floor has a length of 7 meters and a width of 3.5 meters. It is supported by eight columns, with the middle two closely together. Only a quarter of the floor is modeled to reduce computational time, as seen in Figure 7.2.
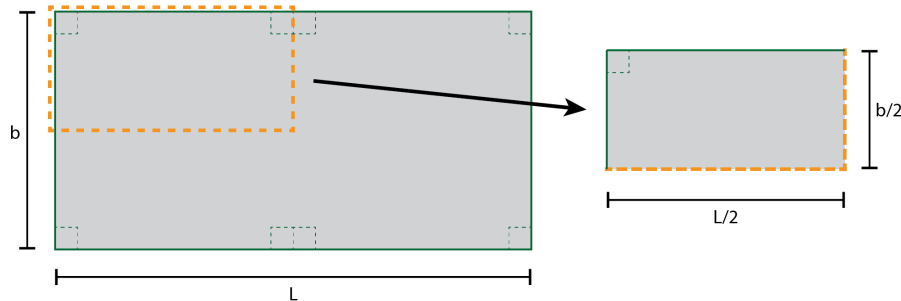
Figure 7.2: Decreased model size for the two-way floor to a quarter of total floor

Figure 7.3 shows the two-way floor and how it is modeled in Abaqus. At the supports, a solid core is added for practical reasons. It provides a robust core that can connect the floor to the steel connection with screws, similar to the Natural pavilion. Detailed analysis of how the connection behaves is outside the scope of this research.
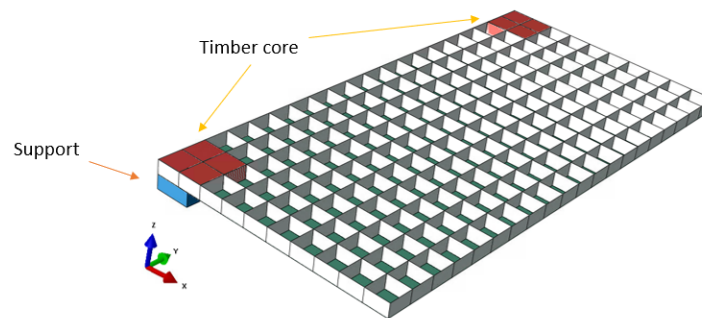
Figure 7.3: Timber core for two-way floor model

7.3. Boundaries

One-way

Two models with different boundary conditions are made. In the first model, the floor is simply supported at the ends. In this case, the deflections and critical stresses at mid-span are more significant than for the actual floor. The floor element is constrained in the z-direction on both sides. In the x-direction, the floor is free to move on both sides, but in the y-direction, it is constrained on one side. All rotations are free. This is done to prevent the floor from sagging during the analysis. For the second model, the boundary conditions are fixed, resulting in more conservative stress concentrations in the support area.

Two-way

The model must accurately reflect the behavior of the real floor. As the support significantly influences both the global behavior of the floor and stress concentration at the support, attention is required when modeling the boundary conditions. Ideally, a comprehensive representation would involve modeling the entire connection. However, creating a numerical model with such details demands substantial effort. Consequently, various solutions have been compared for a more simplified alternative to approximate reality.

The left illustration in Figure 7.4 shows a drawing of the actual connection and its deformed stage. As discussed in chapter 6, the floor is encased by a steel shoe, fastened using screws to secure its position. The steel enclosure surrounding the floor induces stress concentrations, particularly at the corners of the floor. It is important to note that the column and the steel connector are not infinitely rigid and can undergo deformation. Consequently, the connection allows for a degree of rotation, substantially reducing stress concentrations. Nonetheless, this connection still offers rotational stiffness. In summary, the behavior of the connection lies somewhere between hinged and rigid support.
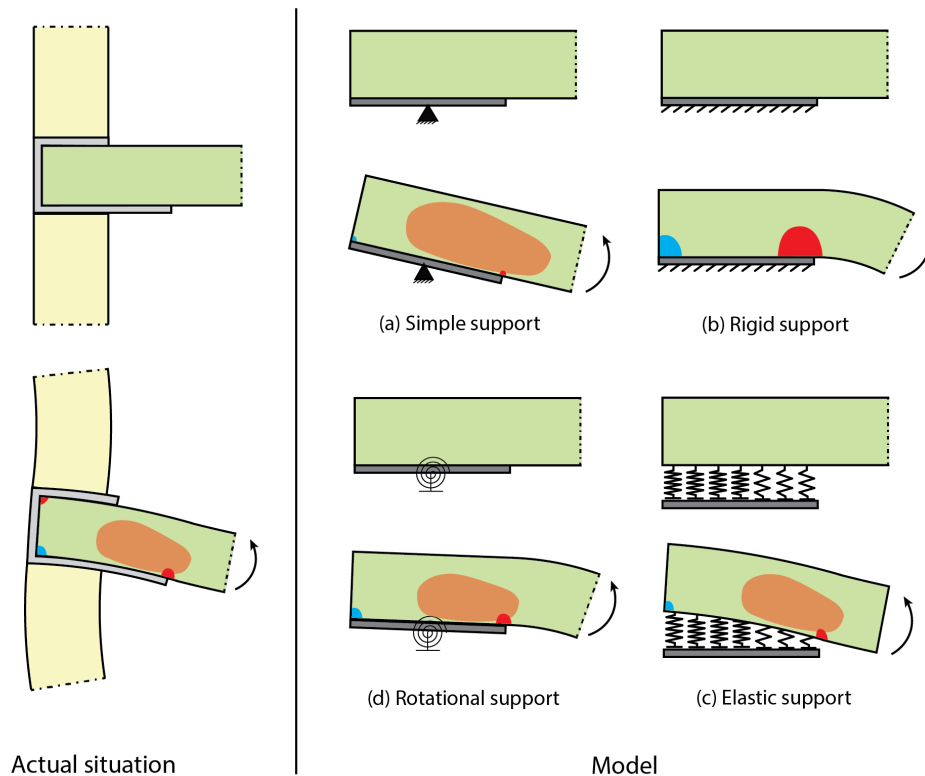
Figure 7.4: Actual connection situation and connection models with deformation-induced stress concentrations
(tension = blue, compression = red)

The right illustrations in Figure 7.4 show the simplified scenarios that offer a more straightforward approach to modeling the connection. In all of these models, the steel plate (250x250mm) is represented solely at the base of the connection, assuming a rigid plate configuration that is easy to model. Each simplification and its corresponding consequences for the model are addressed below.

(a) **Simple support**: The base plate is simply supported, allowing free rotation around the midpoint of the connection. This free rotation reduces stress concentrations that could occur at the edge of the base plate. However, the bending moment at mid-span increases, resulting in higher stresses in the facings at mid-span compared to the actual floor. Also, the deflection is higher compared to the actual floor.

(b) **Rigid support**: The rigid plate is rigidly connected, restraining both translations and rotations. This significantly affects stress concentrations at the base plate. On the other hand, the bending moments and deflection at mid-span are lower than in the actual situation.

(c) **Rotational support**: The rigid plate is supported by a rotational spring representing the stiffness of the timber column and connection. Half a timber column is modeled to represent the rotational support. This approach yields stress concentrations, critical stresses at mid-span, and deflection values closer to the actual situation than the simple and rigid support configurations.

(d) **Elastic support**: Spring support connects the floor to the base plate. This situation best simulates the actual stiffness of the column, connection, and steel connection. Stress concentrations and critical stresses at mid-span are the closest to the real situation among all the proposed models. This support type is not included in this research, as the simple, rigid, and rotational support configurations already encompass the limits of the floor. Therefore, further investigation into this support type is unnecessary for the objectives of this thesis.

To conclude, three models with three different boundary conditions, simple, rigid, and rotational, are modeled. Figure 7.5 shows the geometry of the three models and the boundary conditions and symmetry axis. The symmetry axis constrains the floor in the x- and y-direction.
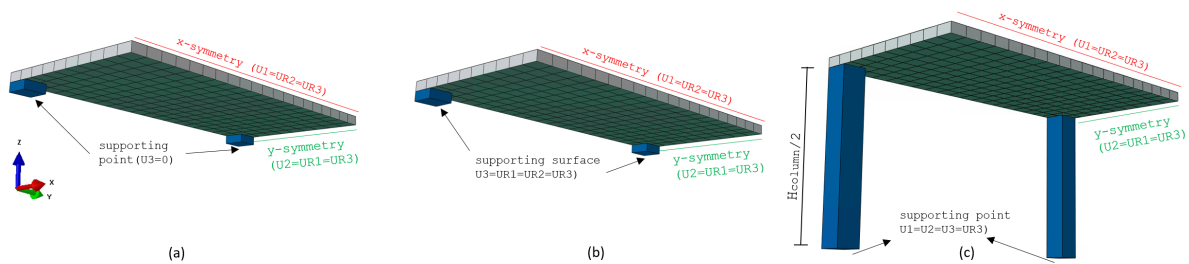
Figure 7.5: Boundary conditions for two-way floor model

Stiffness timber column
The column's cross-sectional area is assumed to be the same as the support area (250x250mm). The column height is half the module height, resulting in 1.75 meters, representing 3.5 meters. The rotational stiffness of the column matches that of the Natural Pavilion, which is 727 kNm/rad. The representative stiffness of the column can be determined using the mechanical formulas provided in chapter 6.

$$I = bh^3 = \frac{1}{12} \cdot 250 \cdot 250^3 = 3.26 \cdot 10^8$$

$$K_r = \frac{3EI}{L} \Rightarrow E = \frac{K_r L}{3I} = \frac{726.7 \cdot 10^6 \cdot 3500}{3 \cdot 3.26 \cdot 10^8} = 2605 \text{ N/mm}^2 \tag{7.1}$$

Since only half of the column is modeled, the stiffness is multiplied by a factor of 2, resulting in a stiffness of 5210 N/mm^2 in the grain direction. The stiffness perpendicular to the grain direction is determined based on the ratio of E$_0$ to E$_{90}$ of the timber strength classes, which is 0.03. This yields a stiffness perpendicular to the grain of 156 N/mm^2.

7.4. Verification

This section offers a thorough overview of the verification process utilized for the BFRP floor designs. The primary objectives of this section are twofold: firstly, to elaborate on the methodology employed in determining the floor's geometry; secondly, to explain all the checks that are automated using Python code, thereby enabling the swift verification of the floor through the numerical model in Abaqus.

For the first objective, several small geometry comparisons are made for some of the failure modes. This is done for a core height ranging from 120-140 mm, facing thickness from 10-18 mm, web thickness of 8 mm, and web spacing of 120-240 mm.

Ultimate limit state
The ultimate limit state contains all potential failure scenarios for the floor. In Table 7.1, an overview of possible failure modes and a summary of the methods used to verify each is presented. The criteria of the ULS requirements are all adapted from the FRP Eurocode (prCEN/TS 19101) [22]. This code can be used for BFRP since FRP's identical failure modes. However, reduction factors specifically for BFRP are used as discussed in section 4.6.

Table 7.1: Method of verification for ultimate limit state

Verification	Method
Compressive resistance of facings, webs and core	prCEN/TS 19101 + Abaqus
Tensile resistance of facings, webs and core	prCEN/TS 19101 + Abaqus
Shear resistance of facings, webs, and core	Analytical + Abaqus
Wrinkling of web and facing at support	prCEN/TS 19101 + Abaqus
Global bending failure	prCEN/TS 19101
Local bending failure due to concentrated load	Analytical + Abaqus
Local buckling due to concentrated load	prCEN/TS 19101 + Abaqus
Resistance at support	prCEN/TS 19101 + Abaqus
Delamination	Abaqus

Serviceability limit state

In Table 7.2, an outline of the necessary verifications for SLS is presented, accompanied by a summary of the methods used. The criteria for SLS requirements are all derived from the prEN1995, the Eurocode for timber [24]. This Eurocode outlines comfort-related specifications for lightweight floors, which applies to lightweight BFRP floors.

Table 7.2: Method of verification for serviceability limit state

Verification	Method
Global deflection	Abaqus
Local deflection	Abaqus + Analytical
Fundamental frequency	Abaqus + Analytical
Acceleration	Abaqus
Velocity	prEN 1995 + Abaqus

7.4.1. ULS: Compressive failure

The webs, facings, and core must meet the compressive resistance criteria specified in Equation 7.2. It is essential to check the laminates of the webs and facings in both primary directions: x and y. For the structural core at the support, the compressive resistance must be checked in all directions: x, y, and z. The numerical model determines the critical stresses in each element anywhere in the model.

$$(\sigma_{i,c,Ed})_j \leq f_{i,c,d})_j = \frac{\eta_c}{\gamma_m \cdot \gamma_{Rd}} \cdot (f_{i,c,k})_j \tag{7.2}$$

where c represents compresssive stresses, i is the direction in which compression is checked and j the element that is checked (w, f, or c).

7.4.2. ULS: Tensile failure

All elements must also meet the tensile resistance requirements specified in Equation 7.3. Again, the checks on the webs' and facings' laminates are performed in both primary directions: x and y. For the structural core at the support, the tensile resistance must be checked in all directions: x, y, and z. The numerical model determines the critical stresses in each element anywhere in the model.

$$(\sigma_{i,t,Ed})_j \leq f_{i,t,d})_j = \frac{\eta_c}{\gamma_m \cdot \gamma_{Rd}} \cdot (f_{i,t,k})_j \tag{7.3}$$

where t represents tensile stresses, i is the direction in which tension is checked, and j is the element that is checked (w, f, or c).

7.4.3. ULS: Shear failure

All elements must also meet the shear resistance requirements specified in Equation 7.3. The checks have to be done for each shear plane in the element. For the webs and facings, shear resistance in-plane needs to be met. For the core material, shear resistance in three different planes must be checked (see Figure 7.6). The numerical model determines the critical stresses in each element anywhere in the model.

$$(\tau_{\mathrm{i,Ed}})_{\mathrm{j}} \le f_{\mathrm{i,d}})_{\mathrm{j}} = \frac{\eta_c}{\gamma_{\mathrm{m}} \cdot \gamma_{\mathrm{Rd}}} \cdot (f_{\mathrm{i,k}})_{\mathrm{j}} \tag{7.4}$$

where i is the direction in which shear is checked, and j is the element that is checked (w, f, or c).
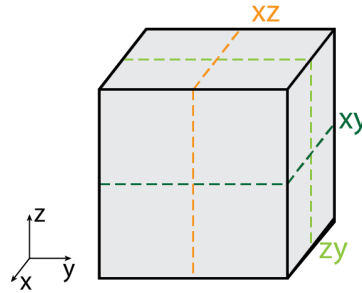
Figure 7.6: Coordinate system with the shear plane for structural core element

7.4.4. ULS: Global buckling failure

The webs and facings need to be verified for global buckling. FRP Eurocode provides a method for long plates with various boundary conditions. The support of the facing by the webs can be assumed to be simply supported because of the significantly lower thickness of the webs compared to the facings. The webs need to be checked for global buckling due to bending. The boundary conditions of the web can assumed to be clamped because the facings are significantly thicker than the web. Figure 7.7 shows the two checked cases.

It should be noted that this approach is utilized for both the one- and two-way floor. However, the facings and webs in the two-way floor are supported on all four edges because of the webs running in both transversal and longitudinal directions. This leads to a conservative approach and should be analyzed in case global buckling becomes critical using this approach.
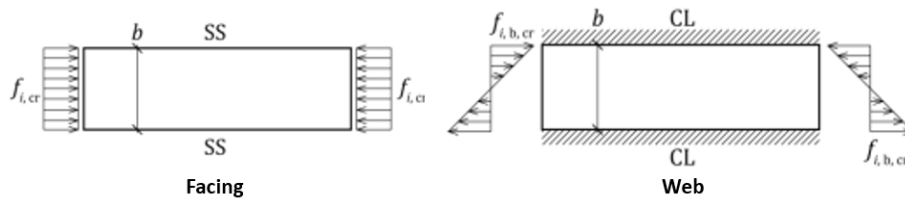
Figure 7.7: Global buckling cases for facing and web

Equation 7.5 should be satisfied to prevent global buckling. The flexural stiffnesses (D_{11}, D_{22}, D_{12}, and D_{66}) are obtained using Equation 7.6.

$$(\sigma_{\mathrm{Ed}})_{\mathrm{w,f}} \le (f_{\mathrm{cr,d}})_{\mathrm{w,f}} = \frac{1}{\gamma_{\mathrm{m}} \cdot \gamma_{\mathrm{Rd}}} \cdot \chi \cdot (f_{\mathrm{cr,k}})_{\mathrm{w,f}} \tag{7.5}$$

with χ as the buckling reduction factor, which may be taken as 1.0 for flat laminates, and f_{cr} as the critical buckling stress [22].

$$D_{11} = \frac{\eta_{\mathrm{c}} \cdot E_{\mathrm{x,c,k}} \cdot t^3}{12 \left(1 - v_{\mathrm{xy,k}} \cdot v_{\mathrm{yx,k}}\right)}$$

$$D_{12} = v_{\mathrm{yx,k}} \cdot D_{11}$$

$$D_{22} = \frac{\eta_{\mathrm{c}} \cdot E_{\mathrm{y,c,k}} \cdot t^3}{12 \left(1 - v_{\mathrm{xy,k}} \cdot v_{\mathrm{yx,k}}\right)} \tag{7.6}$$

$$D_{66} = \frac{\eta_{\mathrm{c}} \cdot G_{\mathrm{xy,k}} \cdot t^3}{12}$$

The critical buckling stress for global buckling due to compression in the facing can be determined using Equation 7.7. The critical buckling stress for in-plane buckling in the web can be determined using Equation 7.8.

$$f_{i,\mathrm{cr,k}} = \frac{\pi^2}{t \cdot b^2} \cdot \left[2\sqrt{D_{11} \cdot D_{22}} + 2 \left(D_{12} + 2 \cdot D_{66} \right) \right] \tag{7.7}$$

$$f_{i,\mathrm{b,cr,k}} = \frac{\pi^2}{t \cdot b^2} \cdot \left[26.8 \cdot \sqrt{D_{11} \cdot D_{22}} + 12.9 \left(D_{12} + 2 \cdot D_{66} \right) \right], \text{ if } K \le 3$$

$$f_{i,\mathrm{b,cr,k}} = \frac{\pi^2}{t \cdot b^2} \cdot \left[30.1 \cdot \sqrt{D_{11} \cdot D_{22}} + 11.5 \left(D_{12} + 2 \cdot D_{66} \right) \right], \text{ if } K > 3 \tag{7.8}$$

with K is

$$K = \frac{2D_{66} + D_{12}}{\sqrt{D_{11} - D_{22}}} \tag{7.9}$$

7.4.5. ULS: Wrinkling failure

The interaction between the core and the facing layers makes FRP in sandwich panels susceptible to wrinkling. Wrinkling is the formation of small, often regular, folds or creases on a surface. A localized deformation occurs when a material is subjected to compressive, shear, or bending forces that exceed its capacity to maintain its original shape. The mechanical properties of the core material affect the occurrence of wrinkling. The core can support the facing layers and distribute loads, but it can lead to localized deformations and wrinkling if it is not sufficiently rigid.

The wrinkling resistance needs to be checked for compression, bending, and shear. The conditions in Equation 7.10, 7.11, and 7.12.

$$(\tau_{\mathrm{Ed}})_{\mathrm{j}} \le f_{\mathrm{wr,v,d}})_{\mathrm{j}} = \frac{\eta_c}{\gamma_{\mathrm{m}} \cdot \gamma_{\mathrm{Rd}}} \cdot (f_{\mathrm{wr,v,k}})_{\mathrm{j}} \tag{7.10}$$

$$|(\sigma_{\mathrm{x,M,Ed}})_{\mathrm{j}}| \le f_{\mathrm{wr,x,d}})_{\mathrm{j}} = \frac{\eta_c}{\gamma_{\mathrm{m}} \cdot \gamma_{\mathrm{Rd}}} \cdot (f_{\mathrm{wr,x,k}})_{\mathrm{j}} \tag{7.11}$$

$$|(\sigma_{\mathrm{i,c,Ed}})_{\mathrm{j}}| \le f_{\mathrm{wr,i,d}})_{\mathrm{j}} = \frac{\eta_c}{\gamma_{\mathrm{m}} \cdot \gamma_{\mathrm{Rd}}} \cdot (f_{\mathrm{wr,i,k}})_{\mathrm{j}} \tag{7.12}$$

where j is the element that is checked (w or f).

Equation 7.13 is a semi-empirical formula from FRP Eurocode that can determine the wrinkling design stress, which considers common imperfections. This formula can be utilized for both the wrinkling compressive and bending check. The wrinkling shear stress may be assumed to equal the compression wrinkling stress in the principal stress direction ($\pm 45°$).

$$(f_{wr,i,k})_{\mathrm{f}} = 0.65 \cdot \sqrt[3]{\left[(\eta_{\mathrm{c}})_{\mathrm{f}} \cdot (E_{i,c,k})_{\mathrm{f}} \right] \cdot \left[(\eta_{\mathrm{c}})_{\mathrm{c}} \cdot (E_{\perp,k})_{\mathrm{c}} \right] \cdot \left[(\eta_{\mathrm{c}})_{\mathrm{c}} \cdot (G_{i\perp,k})_{\mathrm{c}} \right]} \tag{7.13}$$

Two types of core materials are utilized in the BFRP floors of this thesis. In the case of the one-way floor design, only the non-structural core is employed. However, the two-way floor design utilizes the non-structural and structural solid core. When it comes to the solid core, evaluating the wrinkling resistance of the facings and webs is a straightforward task. On the other hand, the available material properties in the literature exhibit significant variations for the non-structural core, and shear modulus properties are lacking.

7.4.6. ULS: Concentrated load

Concentrated loads induce localized failure modes. Therefore, these failure modes have been analyzed in more detail to set geometry guidelines and limits for the floor. The concentrated load of 3 kN is applied over an area of 100x100mm according to the regulations provided in the Eurocode.

Concentrated loads can cause localized stress concentrations and lead to 'punch-through' failure when positioned between webs and local buckling of the webs when positioned on top. Both cases are visualized for the one-way floor with webs spanning in a single direction in Figure 7.8. The green area is the area over which the concentrated load is applied.
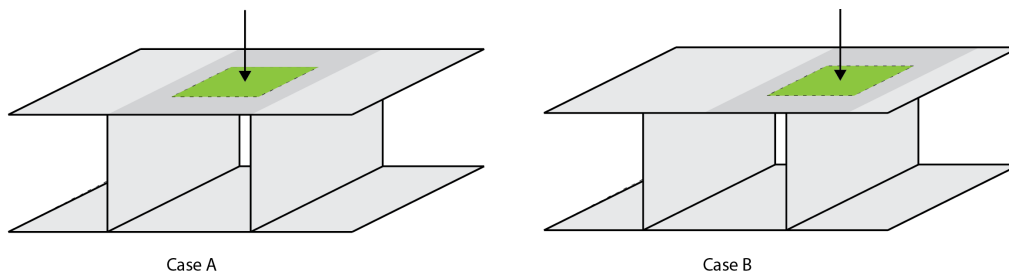
Figure 7.8: Critical cases for concentrated loads for one-way floor; (a) between webs, (b) on top of web

Between webs

In Case A, when the concentrated load is applied between the webs, the facing plays a crucial role. Due to its fibrous nature, BFRP is susceptible to local bending failure, which may result in localized punching through the material. The core material between the webs is considered non-structural, meaning that the facing must resist the concentrated load on its own. To analyze the behavior of the facing between the webs, a schematization is made, treating it as a simply supported beam element for the one-way floor and a simply supported plate for the two-way floor, as depicted in Figure 7.9.
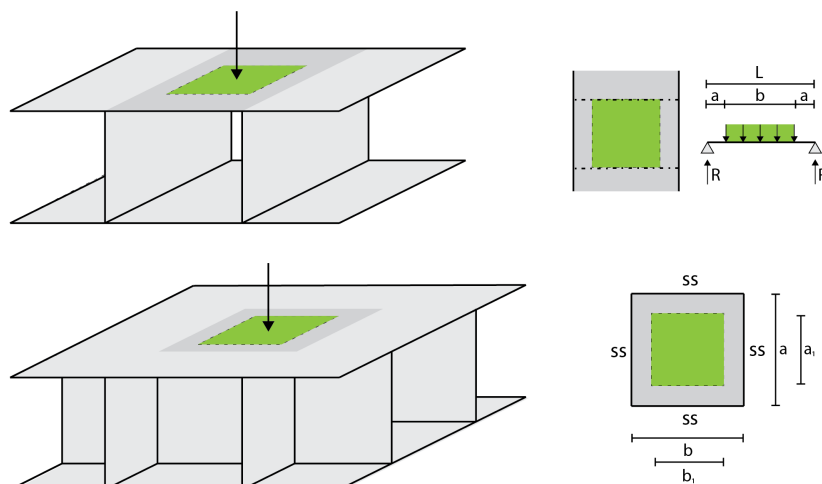
Figure 7.9: Top: schematization of the one-way floor. Bottom: schematization of two-way floor

One-way

The schematization for the one-way floor results in a statically determined beam, allowing us to derive the maximum bending moment using Equation 7.14 and 7.15. To determine the maximum bending stress in the cross-section where the concentrated load is applied, Equation 7.16 is used.

$$R = \frac{qb}{2L}(2a + b) \tag{7.14}$$

$$M_{\text{mid}} = R(a + \frac{R}{2q}) \tag{7.15}$$

$$\sigma_{\text{max}} = \frac{M}{W} \tag{7.16}$$

$$\sigma_{\text{max}} > \min(f_{Ed,1c}; f_{Ed,1t}) \tag{7.17}$$

The maximum stress resulting from the concentrated load on the facing primarily depends on the web spacing and facing thickness. It increases with larger spacing and decreases with thicker facings. The bending stress for a given web spacing and facing thickness is depicted in the right plot of Figure 7.10. This plot also displays the tensile and compressive design strength of the BFRP in the direction spanning between the webs, corresponding to the material strength properties perpendicular to the spanning direction of the floor. For the floor to be resistant against locally concentrated loads, the bending stress should be below the compressive design strength of the facing.
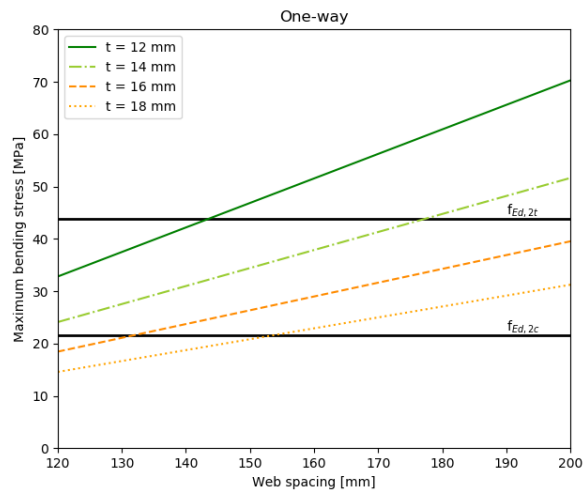
Figure 7.10: Critical bending stresses for one-way floor due to concentrated load between webs
for different facing thicknesses and web spacings

Local bending failure occurs for any facing thinner than 18 mm with a web spacing larger than 150 mm. This limitation significantly impacts the material optimization for the top facing. Consequently, a thicker facing is required than strictly necessary to comply with the other ultimate and serviceability design criteria. However, it is essential to consider the simplifications employed in the analysis. The current approach assumes a simply supported beam, which leads to overestimating the bending moment compared to the real-world scenario. The presence of adjacent webs, combined with the facings, provides additional stiffness and influences load distribution. Furthermore, the width of the schematized beam is set to match the load width, disregarding the contribution of adjacent material to the load distribution. This assumption further affects the accuracy of the results.

To put this into perspective, an FEA analysis of the floor was conducted for a web spacing of 140 mm and facing thicknesses of 12 and 16 mm for a concentrated load between webs. The web spacing of 140 mm was investigated because it would fail based on the analytical calculations and compressive strength of the ply. Since BFRP is a layered material, the composite lay-up options of Abaqus were used to examine the stresses in the top and bottom plies, as visualized in Figure 7.11, respectively.
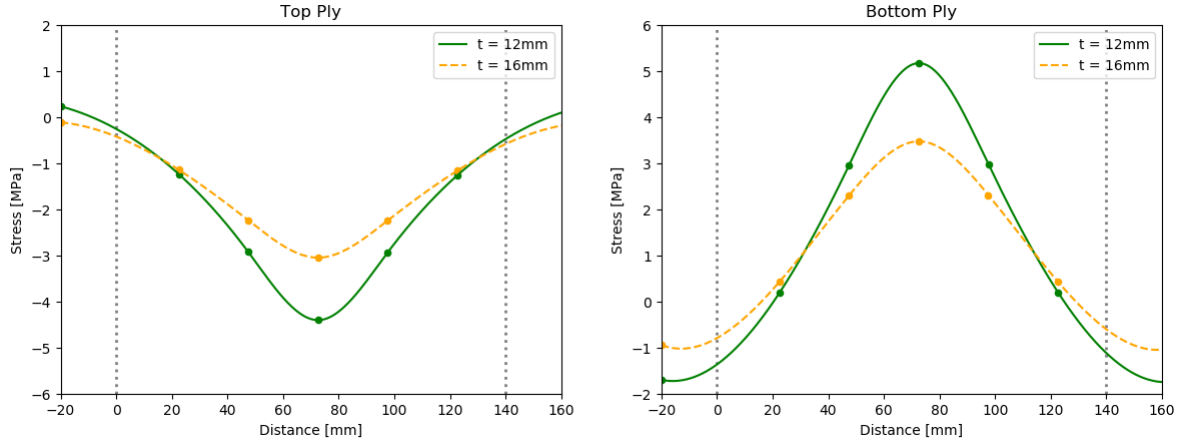
Figure 7.11: Tensile and compression stresses in facing subjected to concentrated load between webs (grey lines) in top and bottom ply

Verification is performed on ply level. For the top ply, where the main fiber direction is at a 0° angle with the floor span direction, the compressive stress must be verified against the compressive design strength perpendicular to the main fiber direction, as for the bottom ply, where the main fiber direction is at -45°, the tensile strength is to be verified with the corresponding tensile design strength of this ply. However, since the specific tensile design strength for the fiber direction is unknown, it is verified against the tensile design strength of a UD-ply perpendicular to the fiber direction. This approach provides a more conservative outcome because the fibers are in a less favorable position.

It can be observed that the stresses for both web thicknesses of 12 and 16 mm are well below the compressive and tensile design strengths perpendicular to the grain of a UD ply ($f_{\mathrm{Ed},2t/2c} = f_{2t/2c} \cdot \eta_c/\gamma_{\mathrm{lam}} = 22 \cdot 0.8/1.4 = 12.1$ MPa). This indicates a satisfactory safety margin in the design, ensuring the floor can withstand the applied concentrated loads between webs without experiencing local bending failure.

Two-way
The schematization of the webs in the two-way floor resembles that of a simple edge-supported plate, with a concentrated load acting as a distributed load in the middle. To estimate the maximum bending stresses, we apply Roark's formulas for homogeneous plates [87]. Despite the QI lay-up of the facing not exhibiting uniform properties and composition throughout its volume, it can be approximated to behave homogeneously due to the symmetrical arrangement of fibers in all directions. Using Roark's formulas, we obtain various constants for different dimensions, and subsequently, Equation 7.18 is employed to determine the maximal stress.

$$\sigma_{\max} = \frac{\beta W}{t^2} \tag{7.18}$$

The right plot in Figure 7.12 presents the results for a given web spacing and facing thickness in the two-way floor. It is assumed that the longitudinal and transverse web spacing are the same, resulting in a schematization of rectangular plates with identical edge sizes in both directions. The plot includes the tensile and compressive design strength of the BFRP, which represents the bending stress limit to prevent failure. From the plot, it becomes evident that the two-way floor is less susceptible to local bending failure when compared to the one-way floor. This advantage can be attributed to the plate's ability to distribute the load over a larger area and the restraining effect provided by its edges.

This analytical approximation indicates that the local bending failure becomes critical only for web thicknesses smaller than 12 mm and web spacings larger than 240 mm. However, considering the conservative nature of the analytical approach compared with the numerical approach shown for the one-way floor, it is possible that even smaller thicknesses and larger web spacings could be viable without reaching critical failure conditions. The FEA is not performed for the two-way floor because local bending failure is not a critical factor.
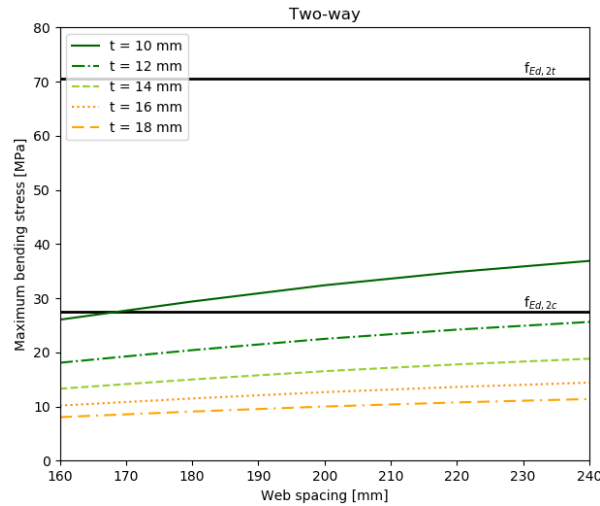
Figure 7.12: Critical bending stresses for two-way floor due to concentrated load between webs for different facing thicknesses and web spacings

On top of web

When a concentrated load is positioned on top of a web, the web is susceptible to buckling. The same approach as for global buckling can be utilized; however, different boundary conditions hold, and an effective width should be considered. The effective width is determined using the stress distribution in Abaqus. Attention should be paid to the fact that the approach in the Eurocode is for long plates and is thus not the most accurate approach in this case. Therefore, an Abaqus buckling analysis has been performed. Several local buckling cases need to be verified for concentrated loads:

One-way:
- Transverse compression at mid-span with SS-SS boundary conditions and an effective width of 150 mm.
- Transverse compression at support with SS-Free boundary conditions and an effective width of 100 mm. *Note*: This check was conservative compared to Abaqus. Therefore, it was also done for SS-SS boundary conditions.
- Shear at support with SS-SS boundary conditions and an effective width of the sum of the support area and the loading area.

Two-way:
- Transverse compression at mid-span with SS-SS boundary conditions and an effective width of 150 mm.
- Transverse compression at support with SS-SS boundary conditions and an effective width of 150 mm.
- Shear at support with SS-SS boundary conditions and an effective width of the web spacing.

The approach to determine the local buckling due to compression has already been discussed. The critical shear stress is calculated using Equation 7.19.

$$f_{\mathrm{xy,cr,k}} = \frac{4}{t \cdot b^2} \cdot \sqrt[4]{D_{11} \cdot D_{22}^3} \cdot (8.13 + 5.05 \cdot K), \text{ if } K \leq 1$$

$$f_{\mathrm{xy,cr,k}} = \frac{4}{t \cdot b^2} \cdot \sqrt{D_{22} \cdot (D_{12} + 2 \cdot D_{66})} \cdot \left(11.7 + \frac{1.46}{K^2}\right), \text{ if } K > 1 \tag{7.19}$$

$$K = \frac{2D_{66} + D_{12}}{\sqrt{D_{11} \cdot D_{22}}} \tag{7.20}$$

7.4.7. ULS: Support
This section elaborates on the strength of the floor at the supports. The local buckling checks have been discussed in subsection 7.4.6.

One-way
The function of the webs is to transfer the loads of the floor to the support. Figure 7.13 shows the reaction force that has to be transmitted through the webs to the support. The load for a single web that has to be transferred can be calculated using Equation 7.21 and 7.22. The procedure discussed for the shear verification is used for the critical shear stress.

$$R_{\text{Ed,w}} = \frac{1}{2} \frac{q_{\text{floor}} L_{\text{floor}} b}{\#_{\text{webs}}} \tag{7.21}$$

$$\tau_{\text{Ed,w}} = \frac{R_{\text{Ed,w}}}{t_{\text{w}} h_{\text{c}}} \tag{7.22}$$
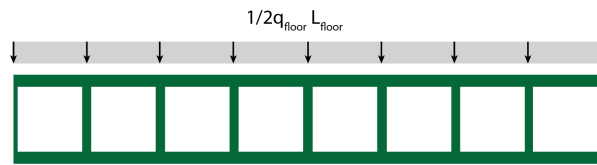
Figure 7.13: Reaction load on the webs

Table 7.3 shows the shear stress at the support. This demonstrates that the web's shear capacity can transfer the reaction forces in any utilized model. The shear capacity of a single web with a QI lay-up is 35.8 MPa. The actual shear stresses will likely fall between the numerical models of simple and rigid support, as the beam's stiffness will influence the stress concentrations at the supports.

Table 7.3: Shear stress of one-way floor at support for different models

	Analytical	Numerical simple support	Numerical rigid support
$\tau_{\text{Ed,w,max}}$ [MPa]	1.4	1.07	2.86

Two-way
The two-way floor is supported by columns, which means higher reaction forces. From the webs, the loads are transferred to the base plate. Figure 7.14 shows the webs on the edge of the base plate that have to transfer the loads. To make an analytical approximation of the floor capacity at the support, for the geometry presented in Figure 7.14, it is assumed that the webs in the middle both transfer 1/3 of the load and the webs at the edges 1/6th. The total design shear capacity at the support can be approximated with Equation 7.23. For a floor with web spacing of 175mm, a web thickness of 8mm, and a core height of 140mm, this results in 70 kN. This is well below the reaction force when it is assumed that 1/4 of the load will be transferred to each column (19.5 kN).

$$V_{\text{support}} = \#_{\text{webs}} \cdot t_{\text{w}} \cdot h_{\text{core}} \cdot f_{\text{v,d}} \tag{7.23}$$
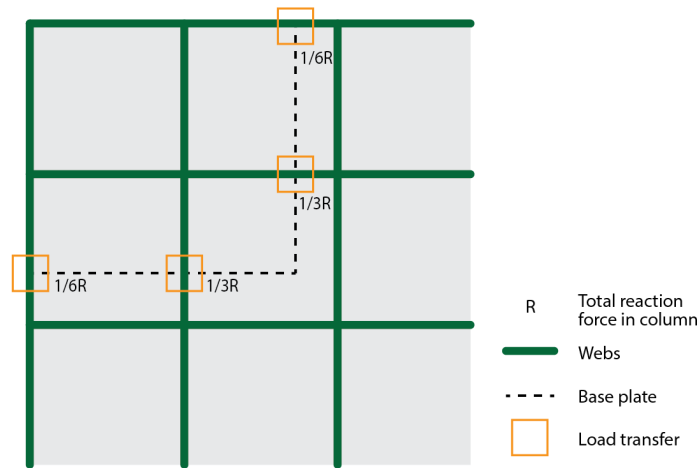
Figure 7.14: Load transfer at column support in two-way floor

7.4.8. ULS: Delamination

Delamination can manifest in the two-way floor at the intersections of the webs, presenting a failure mechanism for which no specific design regulations currently exist. This failure mode is more comprehensively analyzed in chapter 8.

7.4.9. SLS: Deflection

For lightweight floors, deflection is often critical. The final allowed deflection of a floor is L/250, and the maximum additional deflection, due to creep, is 3L/1000. This should be satisfied in the characteristic, frequent, and quasi-permanent action combination. The deflection requirements can be found in Appendix B. C shows the function code utilized to perform the check in the final one- and two-way floors.

The total deflection of the floor results from two main factors: deflection due to bending and deflection due to shear. The proportion of shear-induced deflection in the case of a one-way floor is estimated to be approximately 5%, as elaborated in section 7.9. By employing the fundamental mechanical formula for deflection in a simply supported beam (as shown in Equation 7.24), it is possible to derive an estimate for the required thickness of the facing and height of the core. The values presented in Table 7.4 outline the moment of inertia for various combinations of facing thicknesses and heights, considering only the facing components and excluding the webs. This calculation utilizes a QI lay-up and does not account for long-term effects.

$$w = \frac{5}{384}\frac{ql^4}{EI} \longrightarrow I_{\min} = \frac{5}{384}\frac{ql^4}{Ew_{\min}} = 8.7 \cdot 10^7 \text{ mm}^4 \tag{7.24}$$

When incorporating the influence of creep, which has the potential to double the deflection over 15 years, it becomes evident that a facing thickness of 16mm with a core height of 140mm is the recommended configuration for both one-way and two-way floors. It is worth noting that a facing thickness of 12mm could also be viable for one-way floors, because of the enhanced stiffness and reduced creep effects of a UD-QI lay-up. This particular lay-up aligns more effectively with the load transfer characteristics of a one-way floor.

Table 7.4: Required moment of inertia to meet the deflection criteria without long-term effects

	Moment of inertia [mm^4]	UC	Moment of inertia [mm^4]	UC
	h$_c$ = 120		h$_c$ = 140	
t$_f$ = 10	0.85 ·10^8	1.03	1.13·10^8	0.77
t$_f$ = 12	1.05·10^8	0.83	1.39·10^8	0.63
t$_f$ = 14	1.26·10^8	0.69	1.66·10^8	0.52
t$_f$ = 16	1.49·10^8	0.58	1.95·10^8	0.45

7.4.10. SLS: Local deflection

Concentrated loads positioned between two webs result in localized deflection of the facing. The core material between the webs is considered non-structural, implying that it cannot be relied upon to resist local deformation. Similarly to the local bending check, the local deflection can be estimated by treating the webs as simple supports, see Figure 7.15.

For one-way floor local deflection, the deflection will lie between that induced by a distributed load across the entire area between the webs and that caused by a concentrated load. The magnitude of the distributed load applied over the total area between the webs matches that of the total concentrated load. The E-modulus corresponds to the transverse direction of the UD-QI ply.

In the case of a two-way floor, Roark's formulas can be employed to approximate the deflection [87]. However, it's important to note that Roark's formula is based on a circular loading area. As depicted in Figure 7.15, the concentrated load is distributed over a smaller area, resulting in a slightly more conservative value.

(a) One-way   (b) Two-way
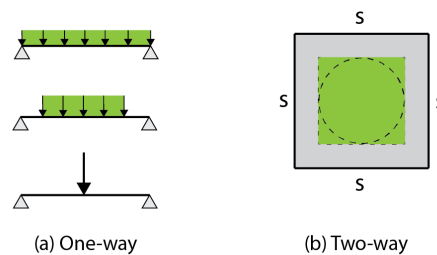
Figure 7.15: Schematization for local deflection calculations

The local deflection adheres to the same criteria as those utilized for the global floor deflection, typically set at L/250, where 'L' denotes the length equivalent to the spacing between the webs. The outcomes across various geometries are presented in Table 7.5, which displays the results of the local deflection evaluation for the one-way floor system. The local deflection restricts the design primarily based on the web spacing and the facing thickness.

Table 7.5: Local deflection of one-way floor between webs for various geometry

	t_f=16mm				t_f = 18mm			
c_s [mm]	w_q [mm]	w_F [mm]	$w_{average}$ [mm]	$UC_{average}$	w_q [mm]	w_F [mm]	$w_{average}$ [mm]	$UC_{average}$
110	0.31	0.45	0.38	0.86	0.22	0.31	0.26	0.60
120	0.43	0.58	0.51	1.06	0.31	0.41	0.36	0.74
130	0.60	0.74	0.67	1.28	0.42	0.52	0.47	0.90
140	0.81	0.92	0.86	1.54	0.57	0.65	0.61	1.08

Table 7.6: Local deflection of two-way floor between webs for various geometry

	t_f=16mm		t_f=18mm	
c_s [mm]	w [mm]	UC	w	UC
150	0.37	0.77	0.26	0.54
175	0.50	0.89	0.35	0.63
200	0.66	1.02	0.46	0.72

The analytical approximation is based on the assumption of simply supported boundaries. However, the webs and adjacent facings may contribute additional stiffness to the system. To validate this, an analytical calculation for a one-way floor configuration with a web spacing of 140 mm, a web thickness of 8 mm, and a facing thickness of 16 mm is compared against the local deflection results derived from the numerical model. The findings are

shown in Figure 7.16 and indicate that the analytical calculations tend to be conservative. This is evident as the numerical model yields deflection values up to four times lower than those predicted by the analytical approach for this specific geometry.
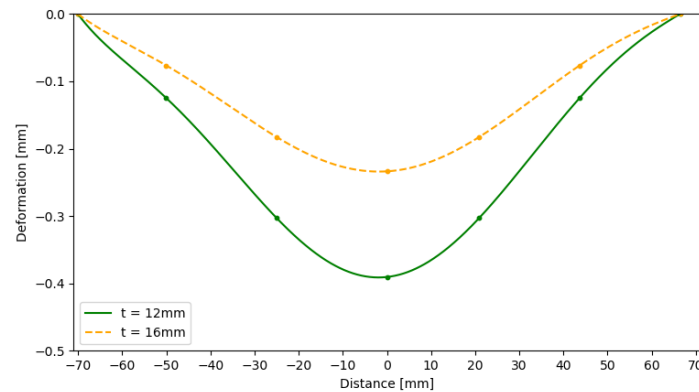
Figure 7.16: Local deflection of the one-way floor for a web spacing of 140 mm from numerical model

For the two-way floor configuration, the results are compiled in Table 7.6. The local deflection is less critical in comparison to the one-way floor arrangement. Consequently, this allows for utilizing larger web spacings without compromising comfort.

7.4.11. SLS: Vibrations

Vibration criteria play a crucial role in the design of lightweight floors. The Eurocode for timber, specifically prEN1995, provides detailed specifications for timber floors, which vary based on their performance class. Refer to Table 7.7 for the levels [24]. In the context of the Natural Pavilion, design considerations lead to the vibration criteria outlined in Table 7.8. The following paragraphs provide a brief overview of each criterion.

Table 7.7: Performance levels according to EN1995

Use category	Quality choice	Base choice	Economy choice
A (residential)	levels I, II, III	level IV	level V
- multi-family block	levels I, II, III, IV	level V	level VI
- single-family house			
B (office)	levels I, II, III	level IV	level V

Table 7.8: Vibration criteria of floors for performance level IV

Response factor R	24
Upper deflection limit	1.0 mm
Stiffness criteria	$w_{1kN} \leq w_{1lim}$ mm
Frequency criteria	$f_1 \geq 4.5$ Hz
Acceleration criteria	$a_{rms} \leq 0.005$ R m/s^2
Velocity criteria	$v_{rms} \leq 0.0001$ R m/s

Stiffness

The stiffness of the floor is assessed by examining the deflection resulting from a vertical static point load of 1 kN placed at the most critical location. This point corresponds to the position with the highest amplitude of the vibration mode.

Fundamental frequency
To verify this aspect, the fundamental frequencies derived from the modal analysis of the numerical model are employed. The boundary conditions of the are simply supported for both floors in this analysis.

Acceleration
Acceleration requirements come into play when the possibility of resonance arises. If the fundamental frequency is less than four times the walking frequency, transient behavior of the floor due to walking can be assumed. Equation 7.25 is applied for calculating the acceleration during potential resonance:

$$a_{\text{rms}} = \frac{k_{\text{res}}\mu F_{\text{dyn}}}{2\sqrt{2}\zeta M^*} \tag{7.25}$$

With the modal mass derived from the numerical modal analysis, the resonant buildup factor set at 0.4, the dynamic load from a walking person of 50 N, the modal damping factor 0.4%, and the resonance factor is computed using Equation 7.26.

$$k_{\text{res}} = \max\left\{0.192\left(\frac{b}{l}\right)\left(\frac{(EI)_L}{(EI)_T}\right)^{0.25}; 1.0\right\} \tag{7.26}$$

Velocity
The root mean square velocity is computed according to the prEN1995 method. The velocity is influenced by the fundamental frequency, walking frequency, and modal mass, which are unique to each floor. The fundamental frequency and modal mass are determined through modal analysis within the numerical model. The walking frequency, as per prEN1995, is 2.5 Hz. The peak velocity is determined using Equation 7.27.

$$v_{1,\text{peak}} = k_{\text{red}}\frac{I_{\text{mod,mean}}}{(M^* + 70\text{ kg})} \tag{7.27}$$

with k_{red} is 0.7 and $I_{\text{mod,mean}}$ calculated using the walking and fundamental frequencies through the equation:

$$I_{\text{mod,mean}} = \frac{42f_{\text{W}}^{1.43}}{f_1^{1.3}} \tag{7.28}$$

To account for the influence of higher vibration modes, beyond just the fundamental mode, the peak velocity response should be multiplied by the factor k_{imp}:

$$k_{\text{imp}} = \max\left\{0,48\left(\frac{b}{l}\right)\left[\frac{(EI)_L}{(EI)_T}\right]^{0,25}; 1,0\right\} \tag{7.29}$$

$$v_{\text{tot,peak}} = k_{\text{imp}}\, v_{1,\text{ peak}} \tag{7.30}$$

The ultimate root mean square velocity to be examined can then be computed using the equation:

$$v_{\text{rms}} = v_{\text{tot,peak}}\,(0,65 - 0,01f_1)\,(1,22 - 11,0\zeta)\eta \tag{7.31}$$

with

$$\eta = \begin{cases} 1,35 - 0,4k_{\text{imp}} & \text{when } 1,0 \leq k_{\text{imp}} \leq 1,9 \text{ else } \eta = 0,59 \text{ (for joisted floors)} \\ 1,35 - 0,4k_{\text{imp}} & \text{when } 1,0 \leq k_{\text{imp}} \leq 1,7 \text{ else } \eta = 0,67 \text{ (for all other floors)} \end{cases} \tag{7.32}$$

7.5. Final Geometry
Considering the verification checks elaborated, a geometry for the floor can be decided upon. The geometry parameters are discussed one by one below to decide upon a geometry for the numerical model.

- **Lay-up**: The choice of flooring type, one-way or two-way, dictates the appropriate lay-up for the facing. QI is better suited for two-way floors due to its more uniform mechanical properties. On the other hand, UD-QI is more suitable for one-way floors because it primarily spans in a single direction, aligning well with the UD lay-up. Due to its superior shear resistance, the web utilizes a QI lay-up in both floor types.

- **Core height**: The core height predominantly influences global deflection. A minimum core height of 140mm for a reasonable facing thickness has been identified.

- **Facing thickness**: This property affects several criteria, with global deflection being the most critical. A minimum facing thickness of 16mm and a 140mm core height provide sufficient bending stiffness. For the one-way floor, a 12mm facing thickness is acceptable due to its enhanced stiffness in the spanning direction facilitated by the UD-QI lay-up. This results in a total height of 168mm and 172mm for one-way and two-way floors, respectively, slightly smaller than the CLT floor in the Natural Pavilion.

- **Web spacing**: The effective width of the facings plays a significant role in determining the optimal web spacing. It becomes inefficient regarding material usage when a substantial portion of the facing remains inactive. While specific guidelines for FRP are not as established as for steel, it is assumed that the web spacing should closely match the core height. This rationale leads to selecting a 140mm web spacing, which does not raise concerns regarding local deflection or bending limits. Since these factors are less critical for the two-way floor and production is easier for a larger web-spacing, a spacing of 175mm is taken for the two-way floor.

- **Web thickness**: The web thickness is 8mm, considering the transversal compressive and shear resistance at the supports.

- **Solid core**: Solid core elements are introduced between the webs at the supports to facilitate the connection detail. These solid cores are not essential for structural requirements.

Table 7.9 summarizes the final geometry for both the one- and two-way floors.

Table 7.9: Final geometry of one- and two-way floor

	One-way	**Two-way**
Lay-up facing	UD-QI	QI
h_c [mm]	140	140
h_{tot}[mm]	168	172
t_f [mm]	12	16
t_w [mm]	8	8
c_w [mm]	140	175

7.6. Interaction and Mesh

Interaction

The model consists of various components, including the webs, facings, core, and supports, all of which must be interconnected and their interactions determined. The support is connected to the facing using a tie constraint, effectively fixing the two parts together. Similarly, the webs are fixed to the facings using tie constraints, as this connection closely mimics the behavior of a single material in real-life scenarios.

To simulate the adhesive layer between the BFRP and solid core in the two-way floor, the Abaqus software employs the 'traction-separation' bilinear cohesive zone model. The interaction properties, such as initial stiffness, were derived from the interface between balsa and FRP, with the core oriented with the grain direction out of the plane. The initial normal, shear, and tension stiffness values are set at 106 N/mm^3 [88].

Mesh

In the case of BFRP plates, which include the webs and facings, S4R shell elements are utilized. The composite lay-up tool in Abaqus is employed to specify the material properties for each ply. The mesh size is close to 2 or 3 times the plate thickness. For the solid core and support, C3D8R elements are employed.

Refinement study

A mesh refinement study is done for the two-way floor to evaluate how different mesh sizes influence the accuracy and reliability of numerical simulations. Optimizing results are obtained by systematically adjusting the mesh density while conserving computational resources. This study facilitates the assessment of mesh convergence, determining whether additional refinement is required to enhance solution accuracy. Both h-refinement (adjusting element size) and p-refinement (changing polynomial order) techniques can be employed to achieve the desired level of accuracy. This iterative process enhances confidence in simulation outcomes.

The results of the mesh sensitivity analysis are presented in Table 7.10. Note that the loading and geometry used for the mesh sensitivity analysis are not according to the design requirements or the final geometry. Regarding h-refinement, the mesh size was reduced by a factor of two. From Figure 7.17, it is evident that the solution remained relatively stable between the second and third refinements after the initial refinement. On the other hand, for p-refinement, it can be observed that the deflection and maximum stress closely approximated the results obtained with linear elements after the first refinement, and the computational time significantly increased between the second and third refinements of the linear elements by nearly a factor of seven. As a result, the mesh size employed in case 3 from Table 7.10 is utilized.

Table 7.10: Mesh sensitivity analysis of two-way floor model

Case	Element type	Element	Nodes	Max deflection [MPa]	Max stress in facing [MPa]	Computational time [s]
1	S4R	7490	9040	5.397	2.67	2320
	C3D8R	416				
2	S8R	7490	26935	4.228	2.29	8403
	C3D20R	416				
3	S4R	13348	15669	4.766	3.32	3107
	C3D8R	712				
4	S8R	13348	46811	4.813	3.39	21278
	C3D20R	712				
5	S4R	53176	61502	4.783	3.21	21273
	C3D8R	4296				
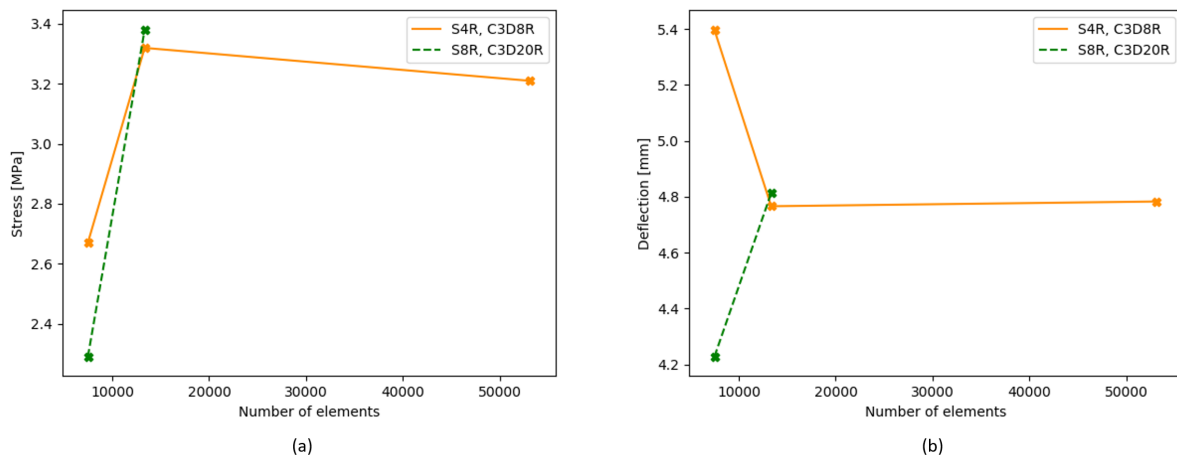
Figure 7.17: Mesh sensitivity analysis for two-way floor; (a) maximum stress in facings, (b) maximum deflection

7.7. Loading and Analysis

Different load combinations and solvers must be included in the numerical model for ULS and SLS. The first model employs a dynamic implicit solver, which runs through the ULS and the SLS load cases. In the loading steps, gravity and loading are applied incrementally. The loading steps are illustrated in Table 7.11. Note that only the critical load combinations are applied to the computational time. The loads are applied with a smooth step lasting 1 second and a time increment set at 0.01 seconds.

Table 7.11: Loading steps for ULS and SLS deflection model

Step	Load	Limit state
1	Gravity	-
2	1 x G	-
3	0.6 x Q	Creep
3	0.4 x Q	SLS
4	0.2 x G	-
5	0.5 x Q	ULS
6	1.5 x $Q_{conc,load}$	ULS

In the second model, multiple solvers were utilized. The initial aim was to determine the fundamental frequency of the floor. This is done using a linear perturbation solver through model analysis. The mass resulting from the permanent load and 10% of the variable load is added as inertia at the top surface. Following this, a steady-state dynamics analysis calculates the accelerations resulting from dynamic loads. Finally, the solver is configured as a dynamic implicit solver to determine the stiffness of the floor by determining the deflection caused by a unit load.

For the modal analysis and steady-state dynamic analysis, the damping ratio needs to be set. The damping that can be applied for GFRP according to prEN19101 is 0.4%. However, BFRP has been shown to have better vibration-damping behavior. According to Prabhakaran et al., the damping in BFRP was over 50% higher than in GFRP [89]. The damping factor for BFRP on a specimen with 3 mm thickness and three plies was 1.4%, whereas it was 0.9% for GFRP on a specimen with 3 mm thickness and six plies. In this research, a damping ratio of 0.4% is considered to be on the conservative side.

7.8. Materials

Table 7.12 and 7.13 show an overview of the material properties and the conversion, partial, and creep factors for BFRP. More details about the material properties and reduction factors can be found in chapter 3 and 4.

Table 7.12: Design values for flax/bio-epoxy composite from Ritsumasyl bridge [35]

Property	UD	[0/90]-ply	QI	1/2 UD + 1/2 QI
E_1 [GPa]	24	14.6	10.8	17.4
E_2 [GPa]	5	14.6	10.8	8.2
G_{12} [GPa]	1.4	1.4	4.0	2.7
ν_{12} [-]	0.3	0.1	0.34	0.33 (ν_{21} = 0.15)
σ_{1t} [MPa]	166	111	92	130
σ_{2t} [MPa]	22	111	92	57
σ_{1c} [MPa]	79.6	48.4	35.8	57.7
σ_{2c} [MPa]	22	48.4	35.8	28
τ_{12} [MPa]	22.1	22.1	35.8	28
τ_{ILSS} [MPa]	22.1	22.1	22.1	22.1
ρ [kg/m^3]			1300	
V_f [%]			50	

Table 7.13: Conversion, creep, and partial factors

Conversion		Creep factor		Partial factor	
$\eta_{ct,fiber}$	0.96	$\phi_{creep,QI,15,deflection}$	2.16	$\gamma_{Rd,laminate}$	1.4
$\eta_{ct,matrix}$	0.87	$\phi_{creep,QI-UD,15,deflection}$	1.93	$\gamma_{Rd,laminate,creep}$	1.5
$\eta_{ct,foam}$	0.92	$\phi_{creep,QI,15,strength}$	2.64	$\gamma_{Rd,core}$	1.5
$\eta_{ct,core}$	0.96	$\phi_{creep,QI-UD,15,strength}$	2.07	$\gamma_{Rd,global\ buckling}$	1.4
$\eta_{cm,perm}$	0.6	$\phi_{creep,QI,50,deflection}$	3.13	$\gamma_{Rd,local\ buckling}$	1.3
$\eta_{cm,var}$	0.8	$\phi_{creep,QI-UD,50,deflection}$	2.79	$\gamma_{Rd,wrinkling}$	1.5
		$\phi_{creep,QI,50,strength}$	3.82	$\gamma_{Rd,indentation}$	1.5
		$\phi_{creep,QI-UD,50,strength}$	3.53	$\gamma_{Rd,punching}$	1.5

For the timber core, the material properties of strength class C24 are utilized. Table 7.14 shows an overview of the properties. These properties are characteristic values, which implies that the partial material factor ($\gamma_M = 1.3$) adapted from the timber Eurocode must be used [24].

Table 7.14: Strength, stiffness and density values for strength class C24 adapted from EN338:2016 [90]

	$f_{m,k}$ [N/mm^2]	$f_{t,0,k}$ [N/mm^2]	$f_{t,90,k}$ [N/mm^2]	$f_{c,0,k}$ [N/mm^2]	$f_{c,90,k}$ [N/mm^2]	$f_{v,k}$ [N/mm^2]	$f_{r,k}$* [N/mm^2]
C24	24.00	14.50	0.40	21.00	2.50	4.00	0.92

	$E_{m,0,mean}$ [N/mm^2]	$E_{m,0,k}$ [N/mm^2]	$E_{m,90,mean}$ [N/mm^2]	G_{mean} [N/mm^2]	ρ_k [kg/m^3]	ρ_{mean} [kg/m^3]
C24	11000	7400	370	690	350	420

*Estimated value

To properly execute the model, the input of the Poisson's ratio is required. The "Wood Handbook: wood as an engineering material" offers Poisson's ratio values for various species at approximately 12% moisture content. Spruce is a commonly used timber species for this model's Poisson ratio values, as shown in Table 7.15. These are average values for the experiments done.

Table 7.15: Average Poisson's ratio's for spruce (Sitka) adapted from [91]

Poisson's ratio	ν_{12}	ν_{13}	ν_{23}
Spruce (Sitka)	0.372	0.467	0.435

7.9. Validation

The numerical model validation is important to ensure the accuracy and reliability of their predictions. This process involves comparing model results with analytical or experimental data critically assessing the model's performance. In this research, no experimental data is available, meaning that analytical calculations validate the model.

Analytical calculation procedures for one-way floors are readily available, but they become more complex when dealing with two-way floors supported by columns. To address this challenge, it has been decided to validate the one-way model in conjunction with an edge-supported two-way model. The two-way model with column support is deemed valid by satisfying these validations. The fundamental frequency will be proven only for the one-way floor since fundamental mechanical equations are not available for the two-way BFRP floor.

For the one-way model, fundamental mechanical equations are used to determine the deflection resulting from bending and shear. Additionally, the fundamental frequency is derived using a simple formula. As for the edge-supported two-way model, the deflection can be determined utilizing Roark's formulas for simply supported homogeneous plates [87]. However, to use this method, deciding on a representative thickness for the BFRP floor. The calculations performed are included in Appendix E. Table 7.16 shows the analytical and numerical comparison results.

Table 7.16: Validation one-way floor for deflection and fundamental frequency

		Analytical	**Numerical**	**Difference**
One-way	**Deflection [mm]**	3.76 (bending) + 0.203 (shear)	3.73	6.0%
	Frequency [Hz]	13.08	12.7	2.7%
Two-way	**Deflection [Hz]**	1.79	1.72	4.2%

7.10. Results

A summary of the conducted verifications discussed in section 7.4 and the outcomes of the numerical model are presented for both the one-way and two-way floor systems. For the one-way floor, the SLS criteria and stresses at mid-span are verified using the model with simple supports. For the two-way floor, the vibration criteria are verified using the simple supports and the deflection criteria and ULS using the rotational supports. Results of concentrated loads are not included here, as the chosen geometry accounts for the limitations associated with concentrated loads.

7.10.1. One-way
Verification
The verification checks discussed before are automatically executed on the numerical model. The results of the checks for the one-way floor can be seen in Table 7.17, 7.18, 7.19, and 7.20. The direction of the stresses corresponds to the coordinate system in Figure 7.18, and direction 3 corresponds to shear stresses.

Table 7.17: ULS checks for one-way

Location	**Check**	**Direction**	**Stress [MPa]**	**UC**
Facing top	Crushing	1	4.43	**0.15**
Facing top	Crushing	2	0.71	0.051
Facing top	Tensile strength	1	0.0078	0.00011
Facing top	Tensile strength	2	0.15	0.0048
Facing bottom	Crushing	1	0.024	0.00085
Facing bottom	Crushing	2	0.11	0.0077
Facing bottom	Tensile strength	1	4.46	0.063
Facing bottom	Tensile strength	2	0.66	0.021
Web	Crushing	1	2.29	0.069
Web	Crushing	2	1.59	0.11
Web	Shear strength	3	1.073	0.070
Web	Tensile strength	1	2.2	0.031
Web	Tensile strength	2	0.010	0.00033

Table 7.18: Local- and global-buckling checks for one-way floor

	Type	BC	b_{eff} [mm]		f_{cr} [MPa]	σ (MPa)	UC	Abaqus α_{cr}	UC
Web	In-plane bending	CL-CL	140	h_w	695.00	-2.29	0.003	-	-
Web	Transverse compression (conc load)	SS-SS	150	Abaqus	61.03	-4.65	0.076	51.1	0.02
Web	Transverse compression (conc load at support)	SS-free	150	Abaqus	6.35	-5.91	0.929	20.5	0.05
		SS-SS	150	Abaqus	61.03	-5.91	0.097		
Web	Shear (conc load at support)	SS-SS	280	Abaqus	106.00	4.24	0.040	34.7	0.03
Facing	Compression	SS-SS	140	c_w	134.67	-4.43	0.033	-	-

Table 7.19: Creep rupture checks for one-way floor

Location	Check	Direction	Stress [MPa]	UC
Facing top	Creep rupture compression	1	1.27	**0.094**
Facing top	Creep rupture compression	2	0.21	0.031
Facing top	Creep rupture tension	1	0.0024	0.00005
Facing top	Creep rupture tension	2	0.046	0.0042
Facing bottom	Creep rupture compression	1	0.0084	0.00062
Facing bottom	Creep rupture compression	2	0.033	0.0051
Facing bottom	Creep rupture tension	1	1.27	0.051
Facing bottom	Creep rupture tension	2	0.19	0.017
Web	Creep rupture compression	1	0.64	0.037
Web	Creep rupture compression	2	0.61	0.072
Web	Creep rupture tension	1	0.61	0.019
Web	Creep rupture tension	2	0.0054	0.00038

Table 7.20: SLS checks for one-way floor

Check	Value	Criteria	UC
Additional deflection	6.27 mm	10.5 mm	**0.60**
Maximum deflection	7.14 mm	14 mm	0.51
Stiffness	0.36 mm	1 mm	0.36
Frequency	13.61 Hz	8 Hz	0.59
Velocity	$1.29 \cdot 10^3$ m/s	$2.4 \cdot 10^3$ m/s	0.54
Acceleration		Transient behaviour	

Output numerical model

Stress distribution

The stress distribution within the one-way floor is straightforward and consistent with expectations for a simply supported beam. As depicted in Figure 7.18, the stress distribution in direction 1 across the facings and webs is shown. As anticipated from the bending moment distribution, the facings experience compression at the top and tension at the bottom. Additionally, minimal activation is observed in the upper and lower portions of the webs.
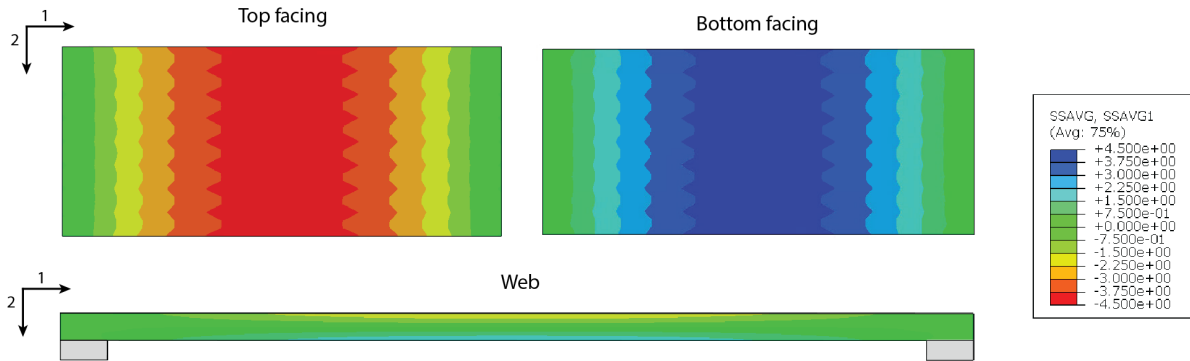
Figure 7.18: Stress distribution in direction 1 of all parts of the one-way floor [MPa]

The webs account for the shear resistance of the floor. In Figure 7.19, the linear shear diagram is recognizable in the web.
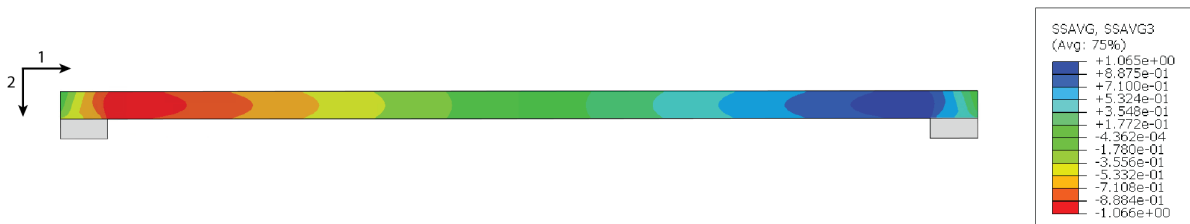
Figure 7.19: Shear stress distribution the web of the one-way floor [MPa]

Deflection

In Figure 7.20, the deflection of the floor is illustrated specifically for the simply supported configuration, as it exhibits the highest deflection levels. Notably, the deflections displayed in the figure do not incorporate partial factors or account for creep effects.
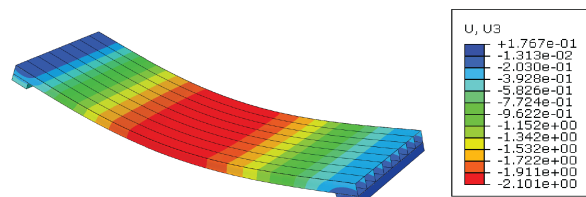
Figure 7.20: Deflection for simple supported one-way floor [mm]

Vibrations

In Figure 7.21, the initial five vibration modes are visually presented along with their corresponding deformations. The first mode corresponds to the fundamental frequency of the system.
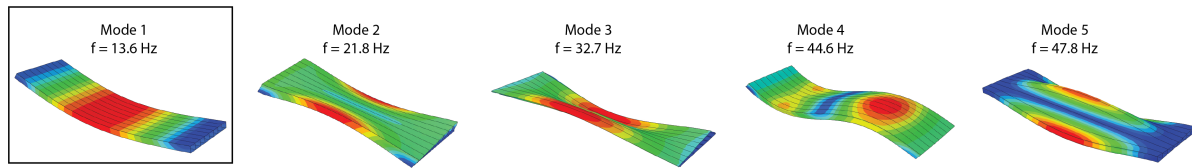
Figure 7.21: Modal analysis results for simply supported one-way floor

7.10.2. Two-way
Verification

The verification checks discussed before are automatically executed on the numerical model. The results of the checks where the solid timber core blocks are not included at the support can be seen in Table 7.21, 7.22, 7.23, and 7.24. A first impression of the two-way floor, where the solid timber core elements are considered structural, is included in Table 7.25. The direction of the stresses corresponds to the coordinate system in Figure 7.24, and direction 3 corresponds to shear stresses. Regarding the web, direction 1 aligns with the web, while direction 2 is oriented out of the floor plane.

Table 7.21: ULS checks for two-way floor

Location	Check	Direction	Stress [MPa]	UC
Facing top	Crushing	1	3.65	0.21
Facing top	Crushing	2	3.15	0.18
Facing top	Tensile strength	1	2.48	0.049
Facing top	Tensile strength	2	4.87	0.096
Facing bottom	Crushing	1	3.06	**0.17**
Facing bottom	Crushing	2	3.65	**0.21**
Facing bottom	Tensile strength	1	3.59	0.071
Facing bottom	Tensile strength	2	2.48	0.049
Web	Crushing	1	5.41	0.30
Web	Crushing	2	11.98	**0.67**
Web	Shear strength	3	6.71	**0.34**
Web	Tensile strength	1	3.37	0.067
Web	Tensile strength	2	4.64	0.092
Intersection	Delamination	1	3.37	**0.53**

Table 7.22: Local- and global-buckling checks for two-way floor

Part	Type	BC	b_{eff} [mm]		f_{cr} [MPa]	σ (MPa)	UC	Abaqus α_{cr}	UC
Web	In-plane bending	CL-CL	140	h_w	695.00	-2.69	0.004	-	-
Web	Transverse compression (conc load)	SS-SS	150	Abaqus	61.03	-3.71	0.06	101.3	0.010
Web	Transverse compression (conc load at support)	SS-SS	150	Abaqus	61.03	-5.01	0.08	88.0	0.011
Web	Shear (conc load at support)	SS-SS	175	c_w	77.88	2.52	0.03	115.3	0.009
Facing	Compression (direction 1)	SS-SS	175	c_w	179.36	-4.52	0.03	-	-
Facing	Compression (direction 2)	SS-SS	175	c_w	179.36	-4.05	0.02	-	-

Table 7.23: Creep rupture checks for two-way floor

Location	Check	Direction	Stress [MPa]	UC
Facing top	Creep rupture compression	1	1.17	0.14
Facing top	Creep rupture compression	2	1.82	0.22
Facing top	Creep rupture tension	1	1.37	0.077
Facing top	Creep rupture tension	2	1.15	0.065
Facing bottom	Creep rupture compression	1	1.40	0.17
Facing bottom	Creep rupture compression	2	1.21	0.14
Facing bottom	Creep rupture tension	1	0.95	0.053
Facing bottom	Creep rupture tension	2	1.86	0.10
Web	Creep rupture compression	1	2.07	0.19
Web	Creep rupture compression	2	4.58	**0.43**
Web	Creep rupture tension	1	1.29	0.057
Web	Creep rupture tension	2	1.78	0.078

Table 7.24: SLS checks for two-way floor

Check	Value	Criteria	UC
Additional deflection	6.86 mm	10.5 mm	**0.66**
Maximum deflection	7.88 mm	14 mm	0.56
Stiffness	0.25 mm	1 mm	0.25
Frequency	12.4 Hz	8 Hz	0.65
Velocity	$7.67 \cdot 10^4$ m/s	$2.4 \cdot 10^3$ m/s	0.32
Acceleration		Transient behaviour	

Timber core

As mentioned, timber elements are included in the support to facilitate the connection to the main structure. These timber core elements also contribute to the load-bearing capacity. They mainly reduce the stresses in the webs at the support. Table 7.25 shows the verification results if a timber core is included. Not the whole floor is verified again, but the checks for wrinkling and the timber core are included. Furthermore, the compressive and shear check on the web at the support is also included to see the difference between with and without core. The rotational boundary conditions are considered.

Table 7.25: Verification checks for two-way floor with timber core elements

Location	Check	Direction	Stress [MPa]	UC
Facing bottom	Wrinkling	1	4.36	0.0021
Facing bottom	Wrinkling	2	3.35	0.0016
Facing top	Wrinkling	1	3.35	0.0016
Facing top	Wrinkling	2	3.0054	0.0015
Web	Crushing	2	2.056	**0.12**
Web	Shear strength	12	4.22	**0.22**
Web support	Wrinkling	1	2.67	0.0041
Web support	Wrinkling	2	2.056	0.0031
Web support	Wrinkling	12	4.22	0.0064
Web support	Wrinkling	12	4.22	0.0064
Timber core	Tensile strength	1	0.68	0.12
Timber core	Tensile strength	1	0.14	**0.88**
Timber core	Tensile strength	3	0.14	**0.88**
Timber core	Compressive strength	1	1.43	0.17
Timber core	Compressive strength	2	0.15	0.15
Timber core	Compressive strength	3	0.17	0.17
Timber core	Shear strength	12	0.39	0.25
Timber core	Shear strength	13	0.046	0.029
Timber core	Shear strength	23	0.029	0.080

Output numerical model

This section presents the raw results obtained from the numerical model, offering insight into the behavior of the floor and providing input for the verification process.

Facings

Figure 7.22 illustrates the stress distribution in direction 1 for both the top and bottom facings. The stresses are highest at the mid-span for the simply supported floor and lowest for the rigidly supported floor. Notably, stress concentrations are observed at the supports for the rigidly supported floor. The rotationally supported floor falls between these two extremes regarding stress distribution.
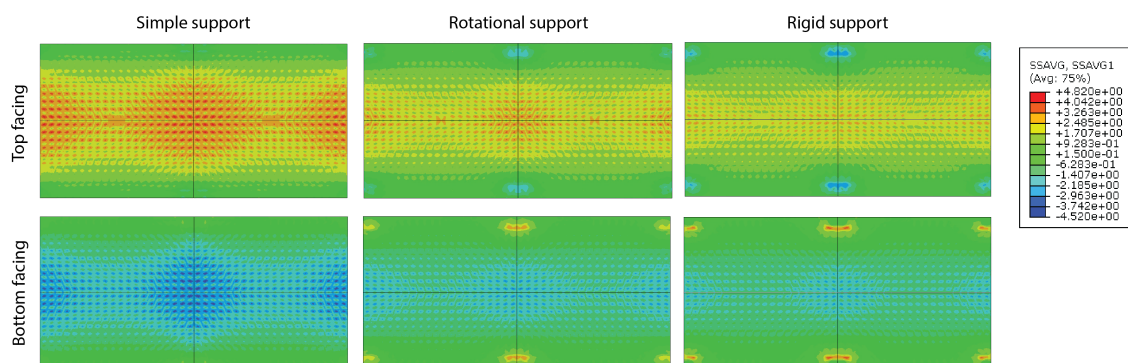
Figure 7.22: Stress distribution in direction 1 of top and bottom facing for all boundary conditions of two-way floor [MPa]

Moving to Figure Figure 7.23, the stress distribution in direction 2 for the top and bottom facings is depicted. In the case of the simply supported floor, it can be observed that the stress at the middle support and the midspan at the edge are higher compared to the other floors. This can be attributed to the fact that this intermediate support essentially functions as the middle support of a continuous beam, resulting in high-hogging bending moments and the edge columns not providing any restraint. In contrast, the rotational and rigid floors exhibit a more evenly distributed stress pattern, with higher stresses in the facings near the outer supports.
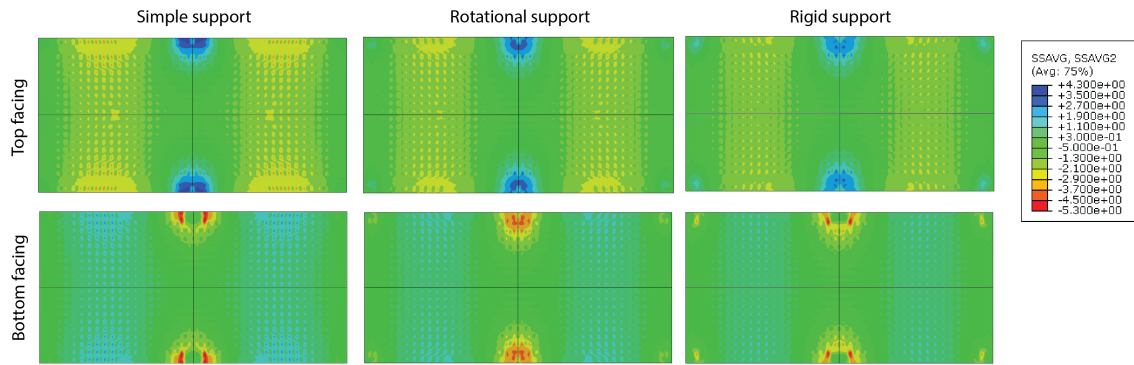
Figure 7.23: Stress distribution in direction 2 of top and bottom facing for all boundary conditions of two-way floor [MPa]

To improve the clarity of the results, a set of plots representing the sections highlighted in Figure 7.24 has been incorporated. These plots illustrate the stress distribution in the facing in direction 1 across sections 1, 2, 3, B, and C. Section A plots the stresses in direction 2 in the facings. Finally, the shear stresses at the midpoint of the web are depicted in section A.
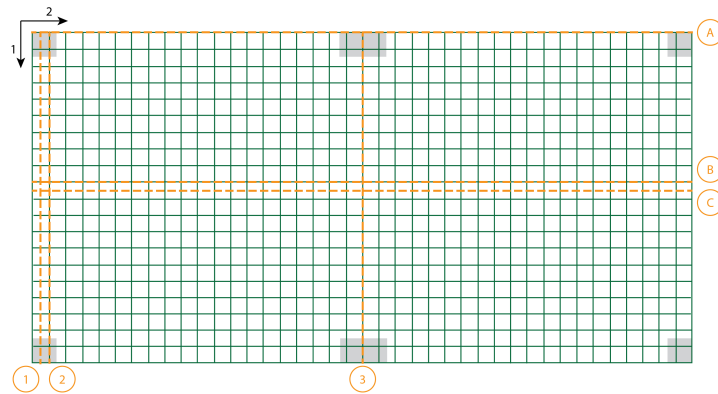
Figure 7.24: Section of stress distribution graphs for two-way floor

Plots for section B and section C at mid-span are provided in Figure 7.25 and 7.26 respectively. Section B shows the stress distribution on top of a web, while section C shows the stresses between webs. Observably, stress fluctuations manifest in both sections. Nonetheless, the amplitude of these fluctuations is larger in section C compared to section B. This distinction can be attributed to the structural behavior resembling a beam between webs and facings, where elevated stresses emerge at mid-span (between webs). This fluctuation in section B, situated on top of the webs, can be attributed to the increased stiffness at the intersection of longitudinal and transverse webs.
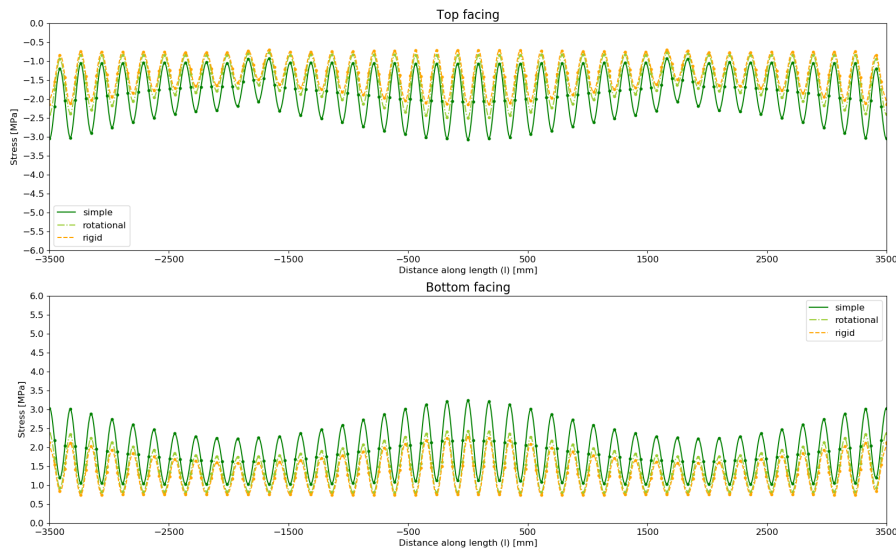
Figure 7.25: Stress distribution in direction 1 in facings at section B [MPa]
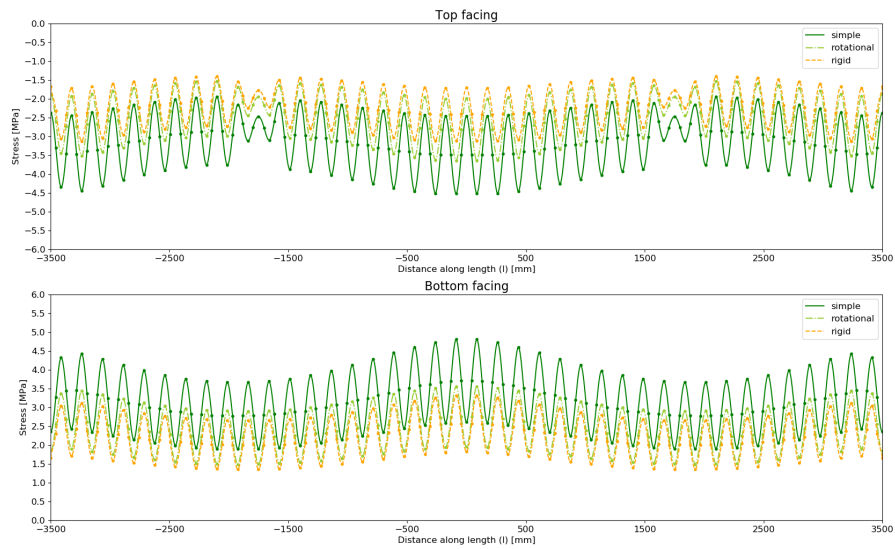
Figure 7.26: Stress distribution in direction 1 in facings at section C [MPa]

Graphs depicting section 1, section 2, and section 3 are shown in Figure 7.27, Figure 7.28, 7.29 respectively. The familiar pattern of stress fluctuations observed in sections B and C also emerges in these sections. In the bottom facing, the maximum stresses at mid-span are more significant for the simply supported floor, whereas stresses increase at the supports for the rigidly supported floor. The stress distribution in the middle of the floor (section 3) is similar to the stress distribution at the edge (section 2).
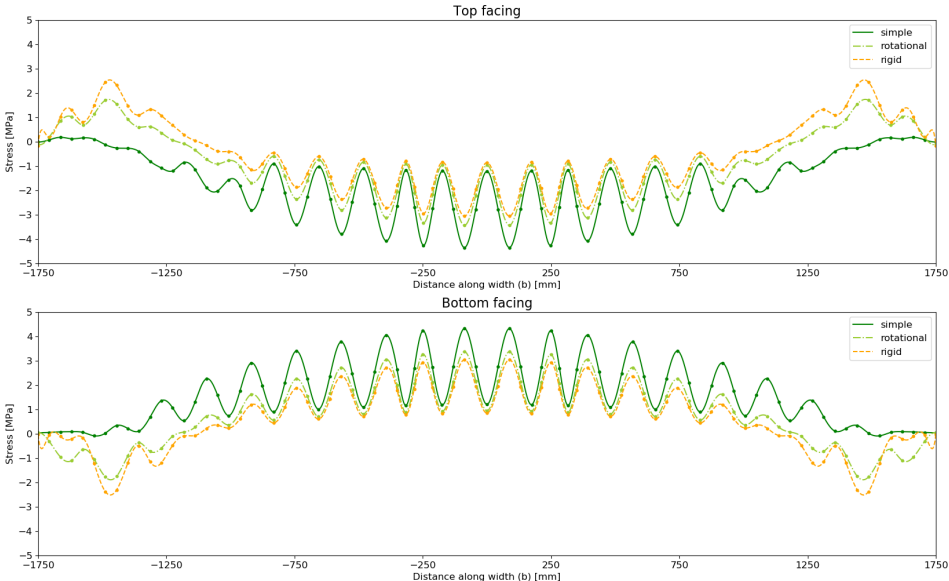
Figure 7.27: Stress distribution in direction 1 in facings at section 1 [MPa]
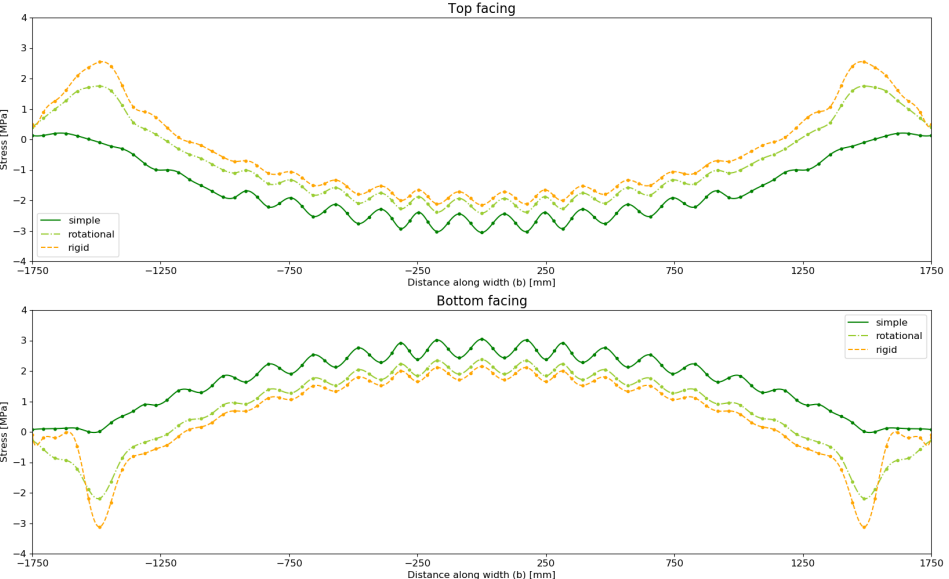
Figure 7.28: Stress distribution in direction 1 in facings at section 2 [MPa]
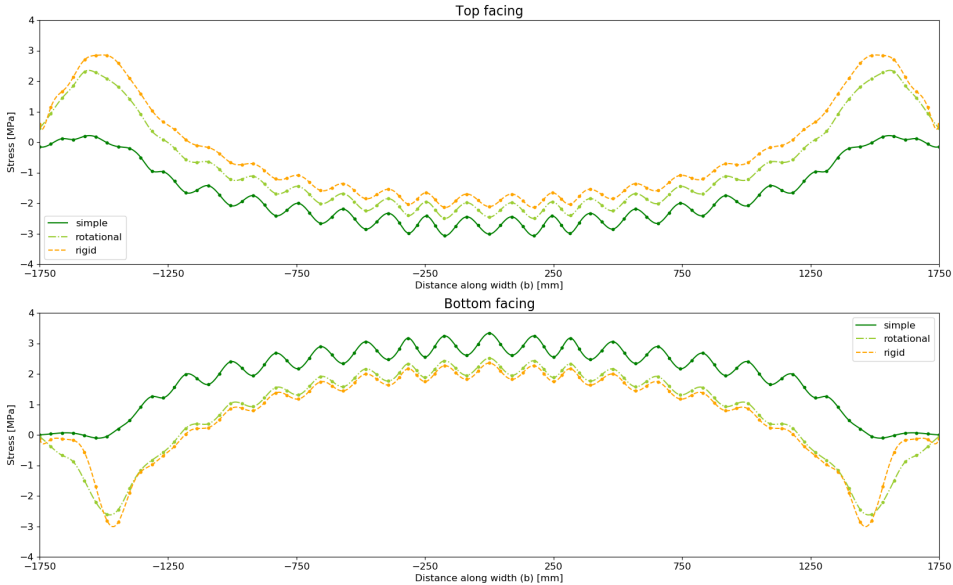
Figure 7.29: Stress distribution in direction 1 in facings at section 3 [MPa]

The stress distribution in direction 2 at section A is illustrated in Figure 7.30. The stress pattern, characteristic of a continuous beam supported by three points, is distinctly evident. Likewise, the variation between the stress distributions of the simply supported and rigidly supported floors, as discussed previously, is observable again.
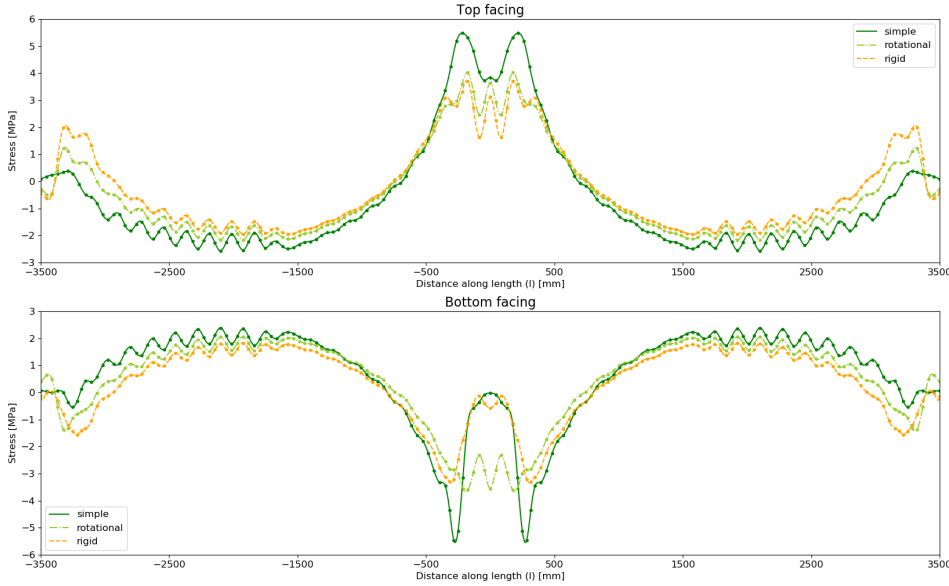
Figure 7.30: Stress distribution in direction 2 in facings at section A [MPa]

Webs

The plot presented in Figure 7.31 depicts the shear stresses in the web at mid-height in section A. It is evident that the shear stress distribution in the case of the simply supported floor closely aligns with a linear shear diagram of a simply supported beam. Conversely, stress peaks are noticeable at the support for both the rotational and rigid floors.
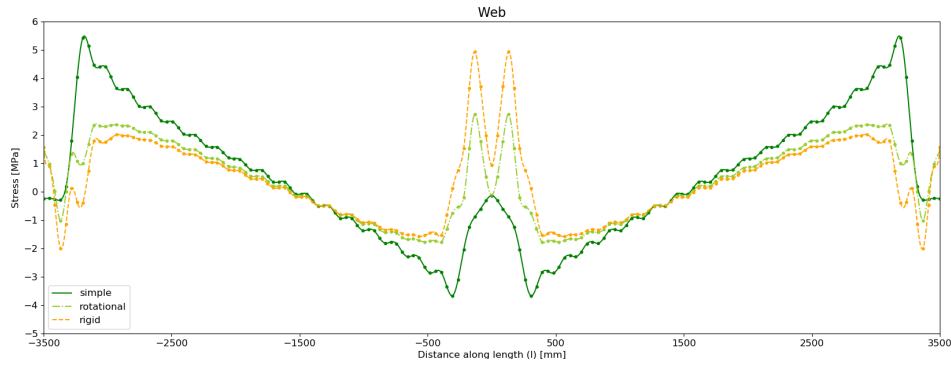
Figure 7.31: Shear stress distribution in at mid-height of the web at section A [MPa]

Figure 7.32, 7.33, and 7.34 visually represent the stress distribution within the web core. The images depict predominantly green regions, indicating relatively low-stress levels. Notably, the stress magnitudes are amplified at the support locations and visually highlighted with the zoomed-in visualization.
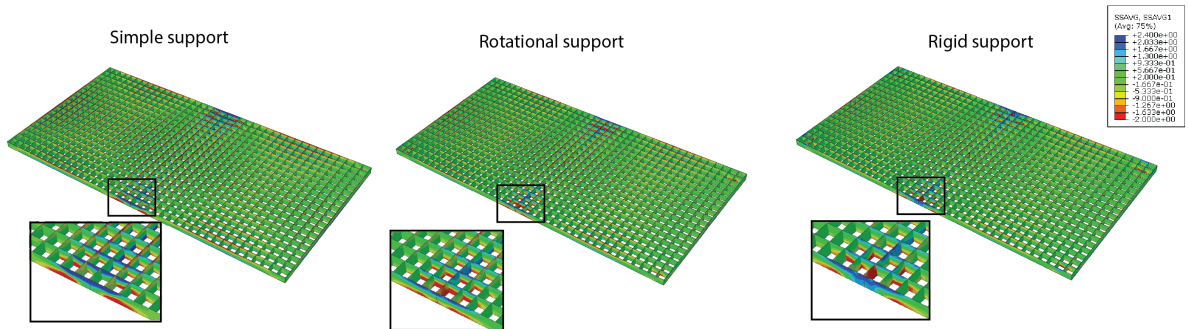
Figure 7.32: Stress distribution in direction 1 of web-core facing for all boundary conditions of two-way floor [MPa]
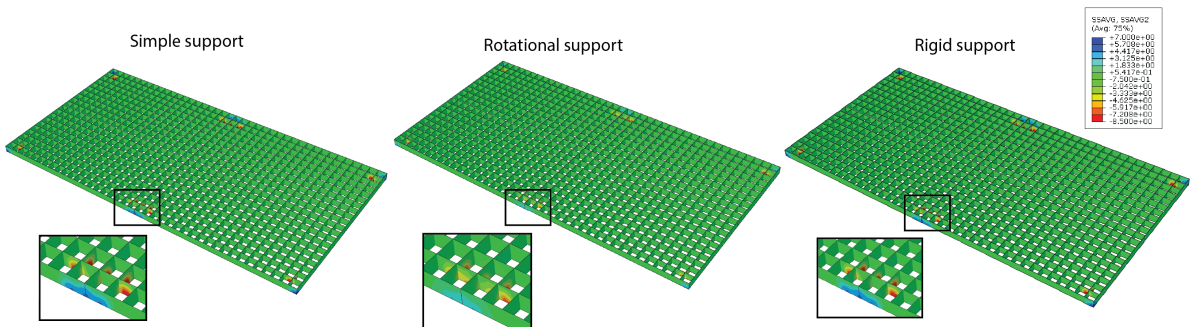
Figure 7.33: Stress distribution in direction 2 of web-core for all boundary conditions of two-way floor [MPa]
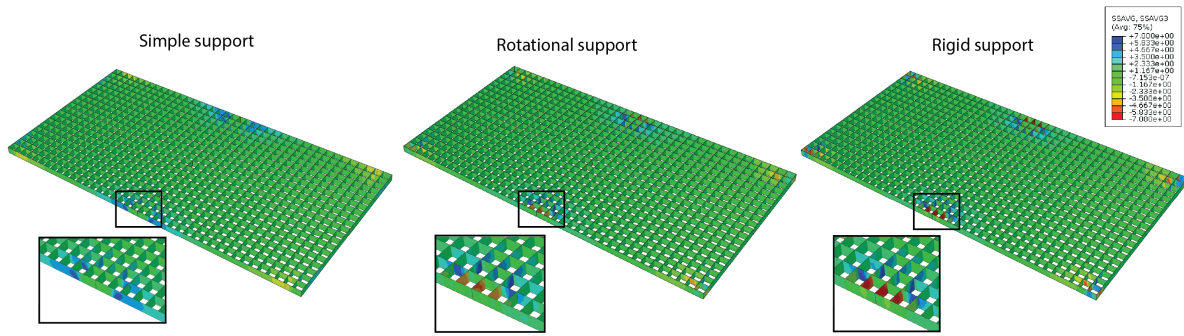
Figure 7.34: Shear stress distribution in direction 12 of web-core for all boundary conditions of two-way floor [MPa]

Deflection

In Figure 7.35, the deflection of the floor is illustrated specifically for the simply supported configuration, as it exhibits the highest deflection levels. Notably, the deflections displayed in the figure do not incorporate partial factors or account for creep effects.
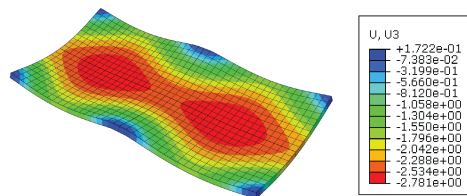
Figure 7.35: Deflection for simply supported two-way floor [mm]

Vibrations

Within Figure 7.35, the initial five vibration modes are visually presented along with their corresponding deformations. The first mode corresponds to the fundamental frequency of the system.
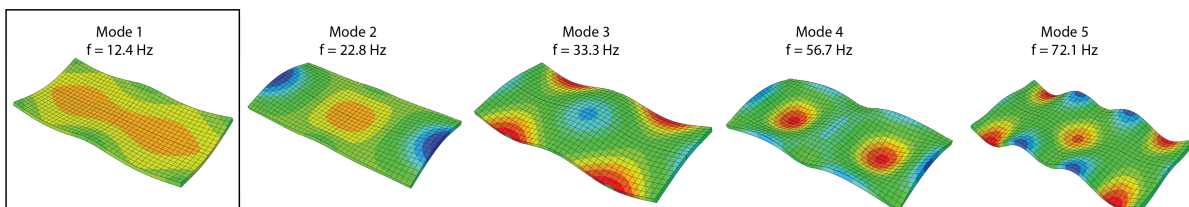
Figure 7.36: Modal analysis results for simple supported two-way floor

7.11. Conclusion

This chapter has finalized the design of the one- and two-way floors. All ULS and SLS checks have been completed, and all criteria are met. The initial ten critical criteria for both floors are shown in Table 7.26, while the floor's geometry is repeated in Table 7.27.

In the case of the one-way floor, the critical aspect is observed to be the local deflection of the facing between the webs. Following this, the SLS criteria become crucial. Specifically, it is essential to consider the deflection and the fundamental frequency. On the other hand, the ULS criteria, in general, do not pose a critical concern for the one-way floor. The most critical factor is the potential crushing of the facing, with only a 15% utilization.

Similar to the one-way floor, rank the SLS criteria for the two-way floor also high. However, the local deflection resulting from concentrated loads is less critical than the one-way floor due to the presence of four-edge supports of the webs. The ULS checks at the supports emerge as a critical concern, particularly regarding potential web crushing. To address this, accounting for the structural contribution of the timber solid core elements in this area can provide a viable solution. It reduces the utilization of crushing of the web at the support from 67% to 12%. Lastly, it is worth noting that, according to the methodology proposed in this research, delamination at the intersections of the webs appears to be of significant importance.

Table 7.26: Ranking of the critical criteria for both the one- and two-way floor

	One-way		Two-way	
	Criteria	**Utilization**	**Criteria**	**Utilization**
1	Local deflection	0.84	Crushing web at support	0.67
2	Additional deflection	0.60	Additional deflection	0.66
3	Frequency	0.59	Frequency	0.65
4	Maximum deflection	0.51	Maximum deflection	0.56
5	Velocity	0.54	Delamination webs	0.53
6	Stiffness	0.36	Creep rupture web at support	0.43
7	Crushing facing at mid-span	0.15	Local deflection between webs	0.39
8	Web crushing due to conc. load	0.11	Velocity	0.32
9	Creep rupture facing at mid-span	0.09	Stiffness	0.25
10	Shear strength web at support	0.07	Crushing facing at support	0.21

Table 7.27: Final geometry of one- and two-way floor

	One-way	**Two-way**
Lay-up facing	UD-QI	QI
h_c [mm]	140	140
h_{tot}[mm]	168	172
t_f [mm]	12	16
t_w [mm]	8	8
c_w [mm]	140	175

8

Local Numerical Model

8.1. Introduction

For a two-way BFRP floor, webs in two directions are employed to ensure efficient load transfer in two directions. The intersection of the longitudinal and transversal webs poses a risk for delamination. In the production of the floor, it is impossible to have continuous fibers at the intersection. Such an intersection is visually represented in Figure 8.1.
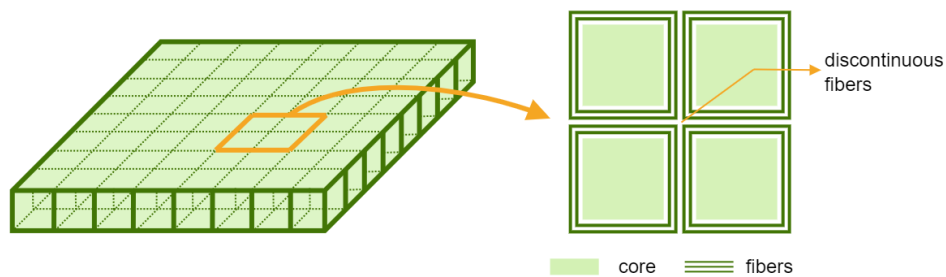
Figure 8.1: Intersection of longitudinal and transversal webs resulting in discontinuous fibers

Upon closer examination of the intersection, a vulnerable area prone to delamination can be identified, as shown in Figure 8.2. This area lacks fiber reinforcement, and the layers will separate if delamination occurs. This leads to decreased floor performance and, ultimately, global failure.
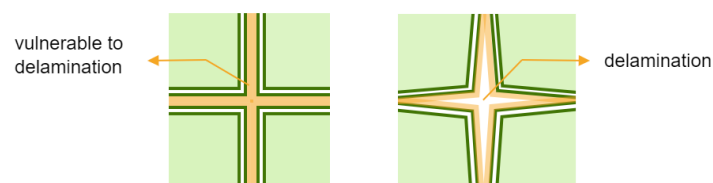
Figure 8.2: Area that is vulnerable to delamination

This chapter aims to determine a stress threshold that avoids delamination. Firstly, the potential failure mode is analyzed, and an appropriate approach to determine the threshold is discussed. Subsequently, the numerical model is explained, and the results are discussed, which are utilized for the global model.

8.2. Failure Modes

To analyze the described failure mode, it is crucial to understand the loading conditions under which delamination occurs. The most apparent loading condition is tension, as it is evident that pulling the webs imposes the highest load on the vulnerable bond. Additionally, shear forces could potentially result in delamination when they need to be transmitted through this susceptible area.

Tension stresses

The floor webs experience tension as a result of bending moments. In the support area, this tension primarily affects the top fibers, while at mid-span, it affects the bottom fibers. Tension in the webs is identified as the primary factor contributing to the risk of delamination in mode I at the intersections. A series of tensile load cases is employed to simulate delamination failure and determine a stress threshold. Figure 8.3 illustrates the local model's investigated cases for mode I delamination. Case (c) in Figure 8.3 involves tension and compression, allowing analysis of the effects when one web is in tension and the other in compression. It should be noted that the facings are not modeled. A conservative approach is taken by not modeling the facings since the facings would provide additional support at the top and bottom.
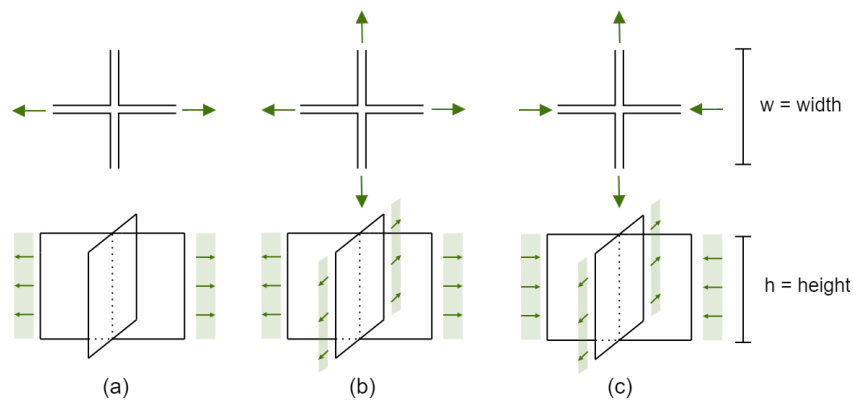
Figure 8.3: Schematic illustration of local model; (a) Tension in 1 direction, (b) Tension in both directions, (c) Tension in 1 direction and compression in 1 direction

Shear stresses

Shear stresses predominantly occur in the support area, and these stresses must be transmitted through the vulnerable interface at the intersection, potentially resulting in delamination. Figure 8.4 illustrates the case investigated in the local model. The objective is to determine whether shear stresses should be considered a potential factor causing delamination.
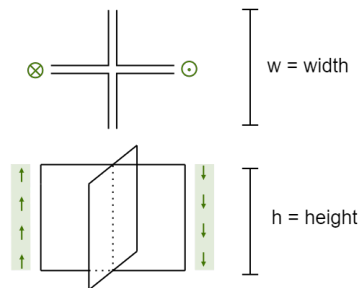
Figure 8.4: Schematic illustration of local model for shear stresses

8.3. Geometry and Boundaries

The geometry of the local model, including its width and height, depends on the global model. For the global model, the expected web spacing falls within the 50 to 200mm range, while the preferred core height ranges from 100 to 200mm. Consequently, a width of 200mm (with w/2 = 100mm) and a height of 100mm are selected as representative geometry. The anticipated web thickness will typically fall between 8mm and 16mm. Therefore, the analysis is conducted for three specific thicknesses: 8mm, 12mm, and 16mm.

The webs have a QI lay-up. It is necessary to model the web using multiple layers called sub-laminates to analyze delamination. The laminate is divided into eight sub-laminates through thickness following the repetitive nature of the stacking sequence. Each sub-laminate with its corresponding fiber direction is represented as an individual section in the model. Each ply is assigned a specific thickness and fiber direction depending on the web thickness. The geometry and dimensions are depicted in Figure 8.5. This approach enables the examination of the vulnerable interface, which is the middle interface between Ply 4 and Ply 4.
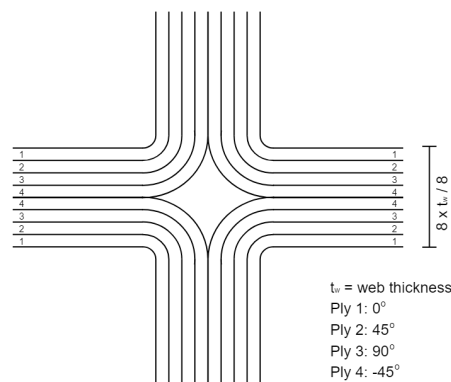
Figure 8.5: Geometry and fiber directions of local model

The boundary conditions vary for each analyzed case. Figure 8.6 depicts the specific boundary conditions for each case. These boundary conditions are applied to the web edge surface. The webs that are not subjected to loading remain free.

8.4. Interaction and Mesh

Interaction

A cohesive interaction property is introduced between the sub-laminates to account for interlaminar damage in the model. To simulate the layer between the BFRP sub-laminates, the Abaqus software employs the 'traction-separation' bilinear cohesive zone model. This is based on a finite-sliding formulation. A general contact property has to be defined as well. The normal behavior was set as hard contact, allowing for separation of the interface under tensile stress while preventing penetration during compression. The tangential behavior is defined as frictionless since the interaction between the laminates relies on cohesive behavior.

Mesh

This model represents all components using eight-noded SC8R continuum shell elements, as they allow for two-sided surface interaction. These elements are equipped with reduced integration and hourglass control. A fine mesh of 2-3 times the sub-laminate thickness is applied to the webs, with an approximate element size of 0.4x0.4mm. As for the curved portion, the element size is smaller due to the curvature of the material. The thickness of the elements in this section is approximately five times smaller than that of the web region. The elements of every sub-laminate align with the sub-laminate next to it.
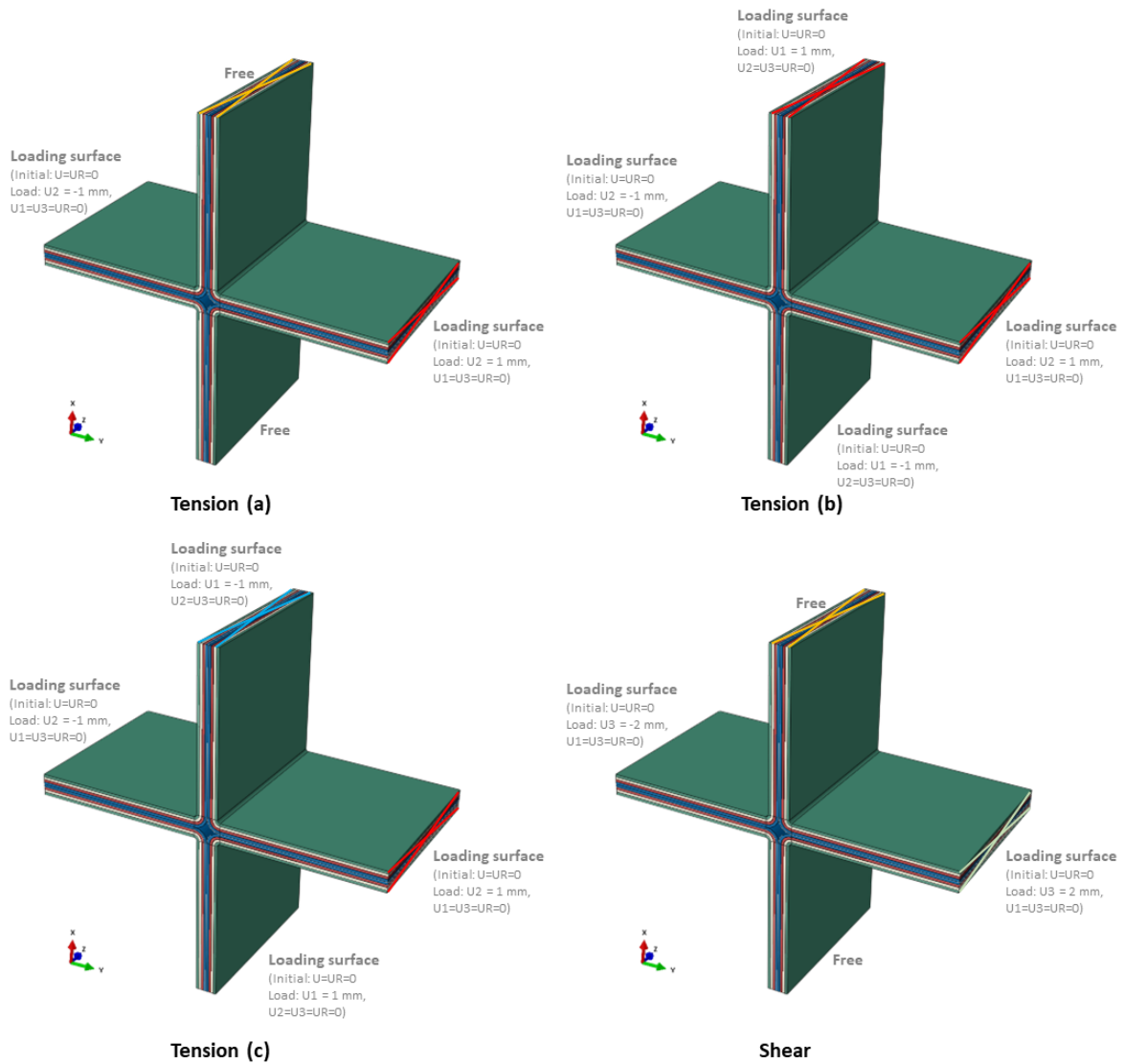
Figure 8.6: Boundary conditions of all cases of the local model

8.5. Loading and Analysis

The loading of the local models is done in 1 step. The loading is applied as a displacement, which makes it possible to read the stresses at delamination. The displacement was applied with a smooth step over the total duration of the time step.

A dynamic explicit solver was used. This provides a more robust contact modeling and is less susceptible to convergence issues. For the loading step, a period of 400s is chosen with a target time increment of 0.005s. Nonuniform semi-automatic mass scaling is applied to the whole model to prevent large computation times.

8.6. Materials

For the local model, both elastic properties and fracture energy properties are required. The elastic properties are the same as for the global model. Since the model is built up per ply, the UD ply properties are applied, listed in Table 7.12.

For the progressive damage, Abaqus uses the Hashin damage model. According to this constitutive model, the material is considered linear elastic until the failure criteria are reached, followed by a linear softening stress-strain curve based on the given value of fracture energy. Fracture tests are not done during the design of the Ritsumasyl bridge, so assumptions on the fracture behavior are made.

There is limited research on flax fibers with an epoxy resin. One research group led by Saadati et al. investigated both translaminar and interlaminar fracture toughness of BFRP with epoxy [92, 93]. Their epoxy was not bio-based, and they utilized hackled fibers instead of yarn fibers, as was used for the Ritsumasyl bridge. Hackled fibers can potentially improve delamination properties due to their less straight and more randomly oriented nature, which enhances the interface. A thermoset Marine 820 Epoxy System, mixed with 18 Wt.% Marine 824 hardener (from ADTECH®Plastic Systems) was used as a resin for both studies. For both studies, a volume fraction of 41% was reached, which is 9% lower than the Ritsumasyl bridge. A higher fiber volume fraction means better delamination resistance.

Table 8.1 shows the design values for the fracture properties utilized. The method described in the FRP Eurocode determines the partial material factor. The coefficient of variation is unknown, meaning that according to Eurocode, the partial material factor is determined based on the sample set size, which is five specimens.

Table 8.1: Damage material properties for representative BFRP with flax fibers

Property	Symbol	Unit	Characteristic value	Design value	γ_M
Longitudinal tensile fracture energy	G_{ft}	N/mm	23.37	18.40	1.27
Longitudinal compressive fracture energy	G_{fc}	N/mm	41.29	33.84	1.22
Transverse tensile fracture energy	G_{mt}	N/mm	-	0.055	-
Transverse compressive fracture energy	G_{mc}	N/mm	-	0.338	-
Viscosity long. tensile	$\eta_{L,t}$	-	-	0.001	-
Viscosity trans. tensile	$\eta_{T,t}$	-	-	0.001	-
Viscosity long. compressive	$\eta_{L,c}$	-	-	0.005	-
Viscosity trans. compressive	$\eta_{T,c}$	-	-	0.005	-
Normal stiffness	K_n	N/mm	-	default	-
Shear stiffness	K_s	N/mm	-	default	-
Tensile stiffness	K_t	N/mm	-	default	-
Normal strength	t_n	MPa	-	22	-
Shear strength	$t_s=t_t$	MPa	-	22.1	-
Normal fracture energy	G_{IC}	N/mm	0.903	0.785	1.15
Shear fracture energy	$G_{II/III}$	N/mm	0.612	0.572	1.07
B-K law to the power factor	η	-	-	0.35	-

8.7. Result

The threshold stress is obtained at the time increment when delamination first occurs. Once delamination initiates, damage begins, and the stress rapidly decreases because the loads on the webs cannot be further increased without damage propagating. As a result, there is a sudden stress drop at the time increment when delamination starts.

Tension loading

Figure 8.7 illustrates the results of the local model, where a tension load is applied to two of the four webs. The stress drop within the web is visible and marked with an "x" marker. After delamination occurs, the stresses fluctuate significantly due to damage propagation. Figure 8.8 depicts the results of the local model with tension applied to all four webs, and Figure 8.9 shows the results when both tension and compression are applied.
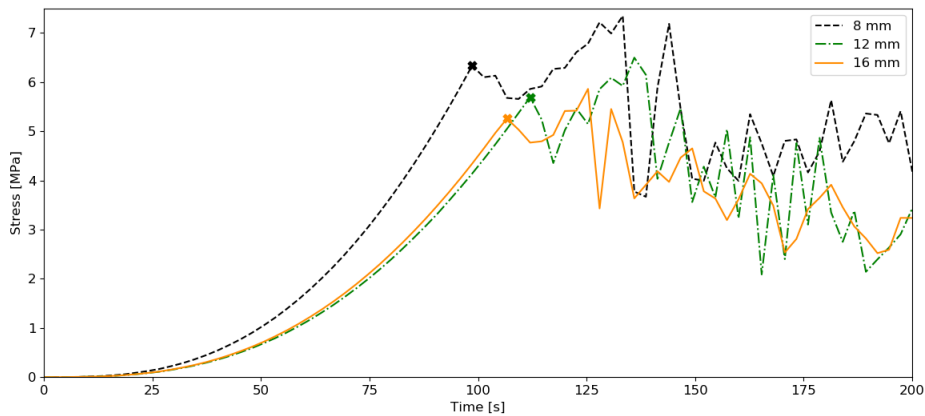
Figure 8.7: Tension loading in 1 direction results in web thickness of 8, 12, and 16 mm
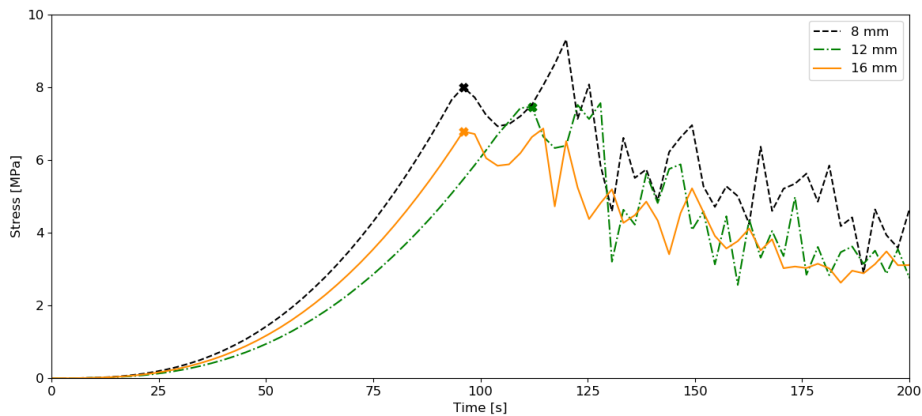
Figure 8.8: Tension loading in 2 directions results in web thickness of 8, 12, and 16 mm

The stress thresholds for each loading case are summarized in Table 8.2. Only the lowest stress threshold is considered for the global model. Based on the results, the threshold derived from the loading scenario involving tension and compression is the lowest. However, this loading condition only occurs in cases of double curvature, resulting in tension and compression at the same height of the intersection in the web. This does not occur in the global model. Therefore, the threshold stress is set for tension loading in one direction. The reason why delamination occurs earlier for pulling two webs can be explained by understanding that when all four webs are subjected to tension, any gaps present in individual webs tend to close.

The threshold for the different web thicknesses is different. The results show that the stresses for a web of 8 mm thickness are higher than for a 16 mm web. It can also be seen that the rate at which it decreases between 8 and 12 mm is similar to that of 12 mm compared to 16 mm. Therefore, a linear interpolation is made for the web thicknesses between the measured thicknesses.
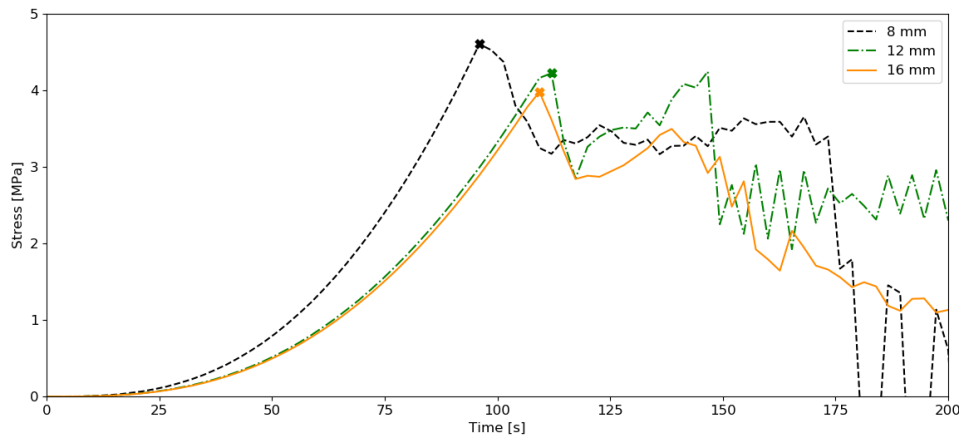
Figure 8.9: Tension loading in 1 direction results in web thickness of 8, 12, and 16 mm

Table 8.2: Stress threshold for all loading cases for web thickness 8, 12, and 16 mm

Web thickness	8 mm	12 mm	16 mm
Tension in 1 direction	6.33	5.69	5.25
Tension in 2 direction	8.00	7.43	6.78
Tension and compression	4.60	4.22	3.98

By employing the thresholds determined through this method, a conservative limit is applied, particularly for the top and bottom sections of the web. The highest stresses occur at the top and bottom of the web due to bending, but this is also where the facings provide extra support. Furthermore, the non-linear behavior of the material has not been considered.

Shear loading

Figure 8.10 illustrates that damage initially occurs at the edges of the web where the load is applied, far away from the intersection susceptible to delamination. To induce delamination at the intersections, the web length is reduced in a new model, bringing the loading closer to the intersection.
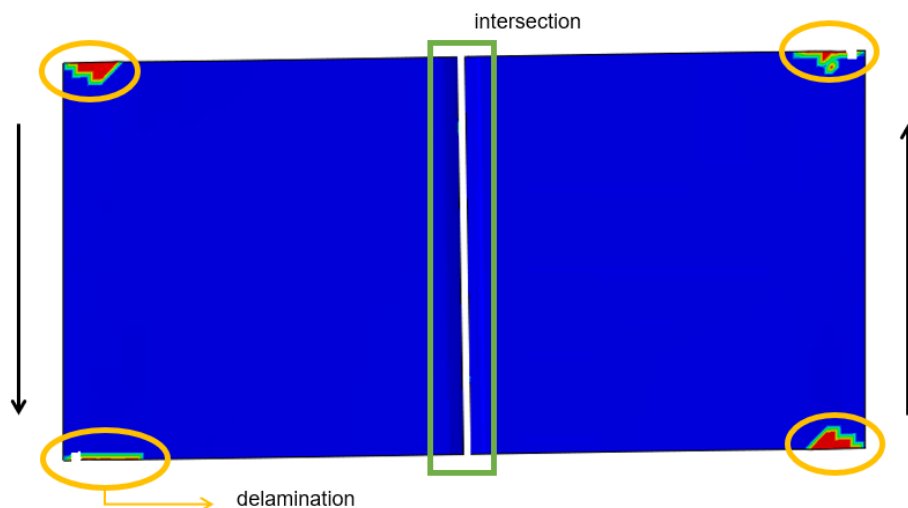
Figure 8.10: Shear loading results for web thickness of 8 mm

Figure 8.11 displays the results of the shear loading case with shorter web lengths. It demonstrates that delamination occurs at the vulnerable interface. However, this corresponds to Mode II delamination, which is unlikely to happen in the actual situation where the top and bottom facings prevent this deformation. Therefore, no threshold for shear loading conditions is included in the global model.
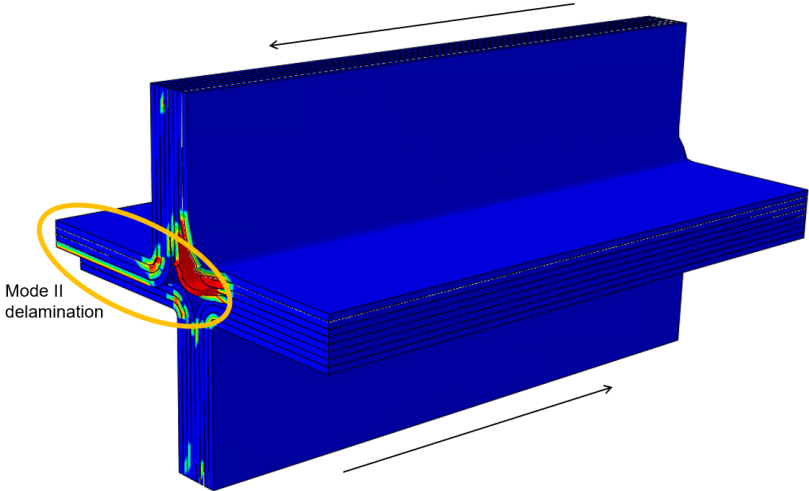
Figure 8.11: Shear loading results for short web thickness of 8 mm

Part III

Research Outcome

9

Comparison

9.1. Introduction

In this chapter, a comparison is made between BFRP and conventional floors. As the research question implies, the evaluation includes structural, environmental, and economic aspects. Initially, the variants that are compared are discussed. Subsequently, a structural comparison involving geometry, weight, and practical factors is conducted. This is followed by an environmental impact assessment using LCA. Finally, an economic comparison is performed.

9.2. Floor Variants

To enable a fair comparison between the BFRP floor developed in this study and the commonly used timber and concrete floors, it is important to ensure that all floors are designed according to the same design requirements. The BFRP floor has been formulated in alignment with the design requirements of the two-way CLT floor used in the Natural Pavilion. Consequently, it becomes necessary for the one-way CLT and concrete floor and the two-way concrete floor to satisfy the same design requirements.

The floor variants, along with the corresponding design methods, are outlined in Table 9.1. The following subsections briefly discuss the design for the CLT one-way floor and the concrete one- and two-way floor. The BFRP and two-way CLT floors are discussed in chapter 6 and 7.

Table 9.1: Floor variants with abbreviation and description

Type	Variant	Abbrev.	Description design method
One-way	BFRP	BFRP1.1	Thesis design of one-way floor with PLA+cork core
One-way	BFRP	BFRP1.2	Thesis design of one-way floor with mycelium core
One-way	BFRP	BFRP1.3	Thesis design of one-way floor with industrial mycelium core
One-way	CLT	CLT1	Product information Derix and Eurocode
One-way	Concrete hollow core slab	HC1	Product information VBI
One-way	Concrete flat slab	FS1	Basic design of two-way floor and Eurocode
Two-way	BFRP	BFRP2.1	Thesis design of BFRP two-way floor with PLA+cork core
Two-way	BFRP	BFRP2.2	Thesis design of BFRP two-way floor with mycelium core
Two-way	BFRP	BFRP2.1	Thesis design of BFRP two-way floor with industrial mycelium core
Two-way	CLT	CLT2	Natural Pavilion design of two-way floor
Two-way	Concrete Flat slab	FS2	Basic design of two-way floor with Eurocode

9.2.1. CLT floor

CLT floors have witnessed increased utilization in construction due to their structural integrity and sustainability. Comprising layers of wood arranged perpendicular to each other and fused through pressure bonding, CLT exhibits a versatile composition tailored to its intended load-bearing direction. This characteristic signifies lay-up optimization for distinct load-bearing scenarios, such as one-way and two-way floors.

In a one-way floor, load transmission occurs solely in a single direction, prompting the utilization of thicker or more layers aligned with the grain in the load-bearing direction. In the Netherlands, Derix stands as a well-known CLT producer. The CLTDesigner software, in conjunction with the product range of Derix, is used to determine the most fitting CLT floor design for this one-way floor [94]. CLTDesigner conducts the checks following the Eurocode for ULS and SLS considerations, including an evaluation for compression perpendicular to the grain resulting from concentrated point loads. Furthermore, a manual assessment using prEN1995 ensures the design's resistance against punching shear failure.

The optimal design for a one-way CLT floor emerges with a 120mm thickness comprising five layers (20-30-20-30-20), specifically Derix's L-120/5s CLT plate. Notably, slimmer than the point-supported CLT floor of the Natural Pavilion, the higher internal shear can explain this, together with the torsion stresses at column support in the two-way variant. The lay-up optimization for the primary load direction in the one-way floor is also better. It is worth noting that fire resistance was not a requirement for the Natural Pavilion design. However, carefully considering structural timber elements with a small cross-section height is vital for structures necessitating robust fire resistance. In real-world applications, a comprehensive fire resistance assessment is essential.
Figure 9.1 shows the cross-section of the CLT plate for the one-way floor. The verification of the floor can be found in Appendix D.
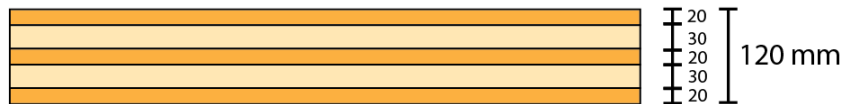
Figure 9.1: Cross-section of CLT one-way floor

9.2.2. Concrete floors

Concrete floors find extensive applications in residential, commercial, and industrial buildings due to their durability, strength, and ease of maintenance. Considering their widespread use, concrete floors serve as a suitable benchmark for evaluating the performance of BFRP floors. Typically, in-situ concrete floors consist of flat slabs spanning one or two directions. However, prefab is also commonly utilized for concrete. Therefore, besides the in-situ floors, a hollow core slab for the one-way floor is included in this comparison.

One-way

The concrete hollow core slab design was obtained using the online calculator provided by VBI, a hollow core slab producer [95]. An additional compression layer of 30 mm is applied to connect the panels and spread concentrated loads. All the designs were assessed under the same loading conditions as those applied in the Natural Pavilion case study. Table 9.2 shows the dimensions and reinforcement for the floor.

The concrete in-situ floor was designed considering practical solutions, and essential verification checks were conducted to ensure bending and shear capacity. For the in-situ floor, main grid reinforcement with a diameter of 8 mm with a spacing of 150 mm is considered minimal for practical reasons during construction. It ensures adequate stiffness for worker access. Furthermore, side formwork is used to serve a crucial role in maintaining structural integrity during the concrete pour, preventing misalignment. For the verification checks, please refer to Table D. Table 9.2 shows the dimensions and reinforcement for the floor. The cross-sections of both floors are illustrated in Figure 9.2.

Table 9.2: Basic information about concrete one-way floor designs

Hollow core slab		In-situ slab	
Concrete	C35/55	Concrete	C30/37
Thickness	200 + 30 mm	Thickness	160 mm
Reinforcement	FeP 1770 / FeP1860	Reinforcement	f_{yd} = 500 MPa
	Ø5 - 150	Top reinforcement	Ø8 - 150 grid
Weight	308 kg/m^2	Bottom reinforcement	Ø8 - 150 grid
		Weight concrete	384 kg/m^2
		Weight reinforcement	5.36 kg/m^2
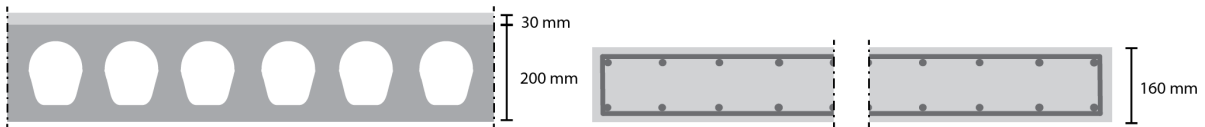
Figure 9.2: Cross-section of concrete one-way floor per meter width

Two-way

The two-way floor exhibits a more complex load and moment distribution than one-way spanning floors. NEN6720 outlines a method for determining bending moments in plates with varying supports. The plate is divided into edge and middle strips in both the x- and y-directions, enabling to determine the maximum sagging and hogging bending moments in each section of the plate. Additional reinforcement is strategically positioned where the main reinforcement is not sufficient. The minimum diameter of the main grid reinforcement is 8 mm, with a spacing of 150 mm, for the same practical motivation as in the case of one-way floors. The main reinforcement is sufficient across the entire floor, except in the x-direction at the mid-support, as depicted in Figure 9.3. The calculation of bending moment distribution is detailed in Appendix D.

When floors are supported by columns, the resistance to punching shear is essential to consider. A comprehensive verification of this part can be found in Appendix D. From this verification, shear reinforcement was found necessary. Figure 9.3 shows the perimeters at which the shear reinforcement is required around the columns. Please refer to Table 9.3 for the fundamental design parameters necessary for comparison.
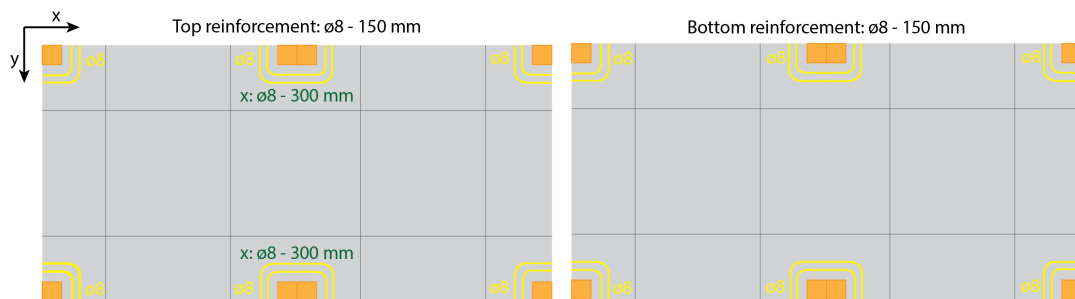
Figure 9.3: Reinforcement for two-way concrete floor. Black = main reinforcement, green = additional reinforcement, yellow = shear reinforcement

9.2.3. Beams

Beams support the one-way floors. The beams are spanning between two columns, and for every one-way floor, timber beams have been designed. The design tables developed by ABT have been used to perform all ULS and SLS checks. Table 9.4 shows the dimensions of the beams. Appendix D shows the results of the verification calculations. It can be seen that the beam designs exceed the height of 180 mm. This means they do not fit the connection detail used for the Natural Pavilion.

Table 9.3: Basic information about concrete two-way flat slab floor design

In-situ two-way slab	
Thickness	200 mm
Concrete	C30/37
Reinforcement	f_{yd} = 500 MPa
Top reinforcement	Ø8 - 150 grid, additional Ø8 - 300 bars at column
Bottom reinforcement	Ø8 - 150 grid
Punching shear reinforcement	Two rows with total of 10xØ8 studs at each column
Weight concrete	432 kg/m^2
Averaged weight reinforcement	5.86 kg/m^2

Table 9.4: Dimensions for the supporting beams for the one-way floors

BFRP1 (C24)		CLT1 (C24)		HC1 (C24)		FS1 (C30)	
b [mm]	h [mm]	b [mm]	h [mm]	b [mm]	h [mm]	b [mm]	h [mm]
180	220	180	220	180	240	180	260

9.3. Structural

Construction height

The height of the floor itself has just a minor difference. The one-way floor has an 8mm smaller thickness. However, beams support the one-way floor, which requires additional construction height. This difference can be seen in Figure 9.4, where the conventional floors are included. It should be noted that it is assumed that the floors are built on top of the beam and are not integrated. This could lead to an overly conservative conclusion, as the beam and floor can be integrated. For instance, a concrete in-situ slab can be poured simultaneously with the beam. Additionally, for the BFRP floor, better solutions might be attainable if integrated with a beam. However, the concrete hollow core slab needs to be stacked.
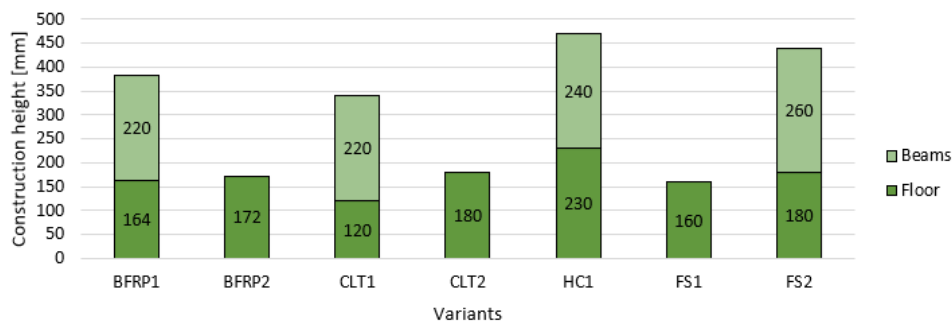
Figure 9.4: Construction height of one- and two-way floors

Weight

The distinction between lightweight and heavy/normal weight floors affects various aspects of a building project. Heavier floors necessitate robust structural design and load-bearing capacity, impacting foundations and support structures. Installation complexity increases with weight, requiring specialized equipment and influencing costs and timelines. Transportation becomes more challenging due to size and mass. In contrast, lighter materials simplify structural demands, foundation design, installation logistics, and transportation requirements.

This underscores the importance of assessing the floors based on their respective weights. The weights and components are comprehensively summarized in Table 9.5 and 9.6. Notably, the BFRP floors emerge as lightweight alternatives comparable to the weight of CLT floors, in stark contrast to the notably heavier concrete floors. Additionally, the variance between the one- and two-way BFRP floors proves to be marginal.

Table 9.5: LCI data for raw materials of two-way variants

Variant	Material	Weight [kg]	Total weight [kg]
BFRP1.1	Flax fibers	606	1781
	40% bio-based epoxy	441	
	PLA	130	
	Cork	138	
	Spruce (beam)	466	
BFRP1.2	Flax fibers	606	1834
	40% bio-based epoxy	441	
	Mycelium	321	
	Spruce (beam)	466	
CLT1	CLT	1433	1899
	Spruce (beam)	466	
HC1	Concrete + reinforcement	7068	7576
	Spruce (beam)	508	
FS1	Concrete	9408	10047
	Reinforcement	131.1	
	Spruce (beam)	526	

Table 9.6: LCI data for raw materials of two-way variants

Variant	Material	Weight [kg]	Total weight [kg]
BFRP2.1	Flax fibers	832	1802
	40% bio-based epoxy	605	
	Spruce (core)	58	
	PLA	65	
	Cork	243	
BFRP2.2	Flax fibers	832	1804
	40% bio-based epoxy	605	
	Spruce (core)	58	
	Mycelium	310	
CLT2	CLT	1985	1985
FS2	Concrete	10584	10727
	Reinforcement	144	

9.4. Environmental

The environmental impact of the BFRP floor and the conventional floor variants are compared in this section. See Table 9.1 for the considered variants. Note that for the BFRP floors, three options for each variant have been included because of the different core options. It is denoted by .1 for industrial mycelium, .2 for regular mycelium, and .3 for PLA and cork. The assumptions of each stage of the LCA are discussed, and the results are presented together with an analysis.

9.4.1. Goal

The main goal is to assess the performance of the BFRP floor compared to the conventional concrete and timber floor. The following sub-goals are defined:

- Generate an overview of the GWP scores for each variant considered.
- Compare the environmental impact scores of all variants.
- Evaluate the effect of captured carbon.
- Conclude the BFRP floor performance.

9.4.2. Scope

For scope definition, the stages included in the LCA should be chosen and kept equal for the compared variants. The stages from sourcing materials to realization of construction are included. These are the same stages that must be considered for the Paris Agreement. This means the use- and end-of-life phases are not included, posing whether the stored carbon in bio-based materials should be included. According to the Dutch Green Building Council, it should not be included as explained in chapter 5. However, examining the amount of carbon captured due to its potential impact on the entire life cycle is noteworthy. In all variants, both cases with and without carbon storage are considered. Carbon emission corresponds to the GWP impact category.

9.4.3. Functional unit

The functional unit for comparing the variants is: **A floor with the dimensions of one module (7x3.5m) that meets the specified design requirements of the Natural pavilion.** This functional unit is applicable for comparing the one-way and two-way floors.

The entire floor system would include a top floor to meet acoustics requirements in the case of the CLT and BFRP floors. The concrete floor would have a finishing floor for aesthetics and water protection. However, only the structural elements without the top floor are considered, as shown in the cross-sections before. The functional unit is highlighted with blue in Figure 9.5. This means that both the beam and the structural floor are included in the one-way floor.

(a) One-way   (b) Two-way
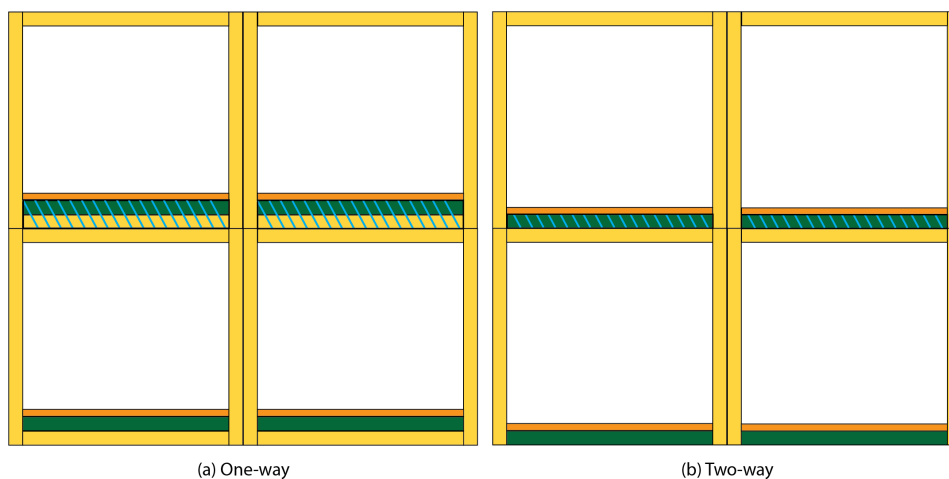
Figure 9.5: Functional unit of floor for LCA

9.4.4. Inventory

The inventory comprises the GWP of stages A1-A5 for all floor variants. The data is sourced from EPDs, public environmental impact databases, or literature. Appendix F shows an overview the LCI. The GWP is determined using the LCI and the amount of materials from Table 9.5 and 9.6. The assumptions concerning materials, production, and captured carbon are outlined as follows:

- **Flax fibers**: Since the EPD is not publicly available, the carbon footprint of Bcomp flax fibers is derived from the LCA study of the Ritsumasyl bridge. The captured carbon is estimated at 1.28 kg CO2 / kg material [96].

- **40% bio-based epoxy**: The EPD for the resin used in the floor design under investigation is not publicly accessible. Instead, a representative 30% bio-based resin from Entropy Resin, with a carbon footprint of 4.08 kg CO2 / kg material, is utilized [97, 98]. With a traditional epoxy, an assumption for 100% bio-based resin has been made to evaluate its potential, see Equation 9.1.

$$0.3 \cdot 100\% \text{ bio-based epoxy} + 0.7 \cdot \text{traditional epoxy} = 30\% \text{ bio-based epoxy} \tag{9.1}$$

- **Resin infusion production**: Data for the resin infusion production of the BFRP floor is retrieved from the EcoCalculator [99].

- **Transportation and assembly BFRP**: Data for the assembly of the BFRP floor is unavailable. Given the similar weight of CLT and BFRP, the same CO_2 equivalent (kg) for stages A4-A5 of the EPD of Derix is applied for both [100].

- **PLA**: BEWI's BioFoam is chosen as one of the core materials [101]. The density ranges from 25-60 kg/m^3, with the higher density considered conservatively.

- **Cork**: To shield against heat during production, determine the PLA foam. The carbon footprint of insulation cork is adapted from the EcoInvent database [99].

- **Mycelium with hemp**: Limited data is accessible on the carbon footprint of mycelium. The research on Fungal-Based Composite bricks by Stelzer et al. is employed to calculate kg CO2 equiv. / kg material from kg CO2 equiv. / kg block [102]. There's potential for a 68% reduction when produced industrially.

- **Solid timber**: Carbon footprint data for solid timber is sourced from GPR Material.

- **CLT**: The CLT used in the study is provided by Derix [100]. An EPD is available that covers all LCA stages (A1-A5). The method outlined by Equation 9.2 is used to determine the captured carbon.

- **Concrete hollow core slab:** The EPD for Concrete hollow core slabs from VBI is utilized, covering all LCA stages (A1-A5) [103].

- **Concrete flat slab**: Inventory data for in-situ concrete is obtained from Quake [104]. The chosen environmental class is XC1, commonly applied on indoor floors. A Dutch average mixture of reinforcement steel information is derived from an EPD of MRPI by Quake.

The amount of captured carbon in timber can be calculated using Equation 9.2 adapted from [105]. This equation relies on timber composition, including cellulose, hemicellulose, lignin, and other components. It has been determined in this analysis that wood predominantly consists of approximately 50% carbon, 44% oxygen, and 6% hydrogen. The calculation method is based on the atomic weights of carbon (12) and oxygen (16). It is worth noting that these percentages may vary slightly depending on the specific type of timber, but they provide a generally applicable estimate of the captured carbon content.

$$\text{Captured carbon} = \frac{V \cdot \rho_{12\%}}{1 + (12/100)} \cdot \frac{3.67}{2} \tag{9.2}$$

with V the timber volume and $\rho_{12\%}$ the density for a moisture content of 12%.

The assumption is that cork and mycelium possess the same carbon content as timber. As a result, a similar approach is employed to calculate the amount of captured carbon in these materials.

9.4.5. Impact assessment

The impact assessment calculates the LCI input data and related amounts of materials and processes into outputs. The impact assessment is done for the GWP A1-A5 according to the defined goal, scope, and functional unit. Figure 9.6 shows an overview of the process.
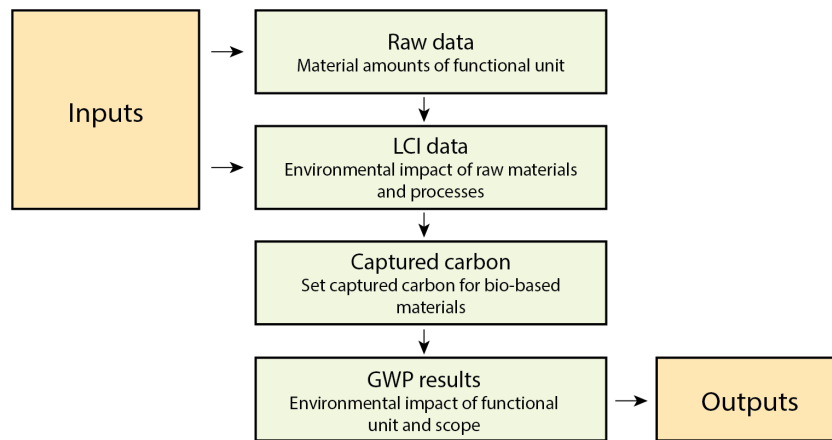
Figure 9.6: Process of performed LCA

9.4.6. Results and discussion

The impact assessment outcomes are merged in Figure 9.7 and 9.8 for both one-way and two-way floors. Each bar in the figures corresponds to a specific variant, with distinct colors denoting various materials and processes. For conventional floors, two distinct categories are formed—including captured carbon and excluding it. In the case of BFRP, four separate groupings are established to differentiate between those with and without captured carbon and to illustrate the potential CO_2 emission reduction achievable with 100% bio-based epoxy resin.

Evidently, the BFRP floors exhibit notably higher environmental impact than concrete and CLT floors. This difference is primarily attributed to the substantial contribution of the resin, both 40% and 100% bio-based, and the utilized production process. However, the BFRP floors demonstrate potential in terms of captured carbon.
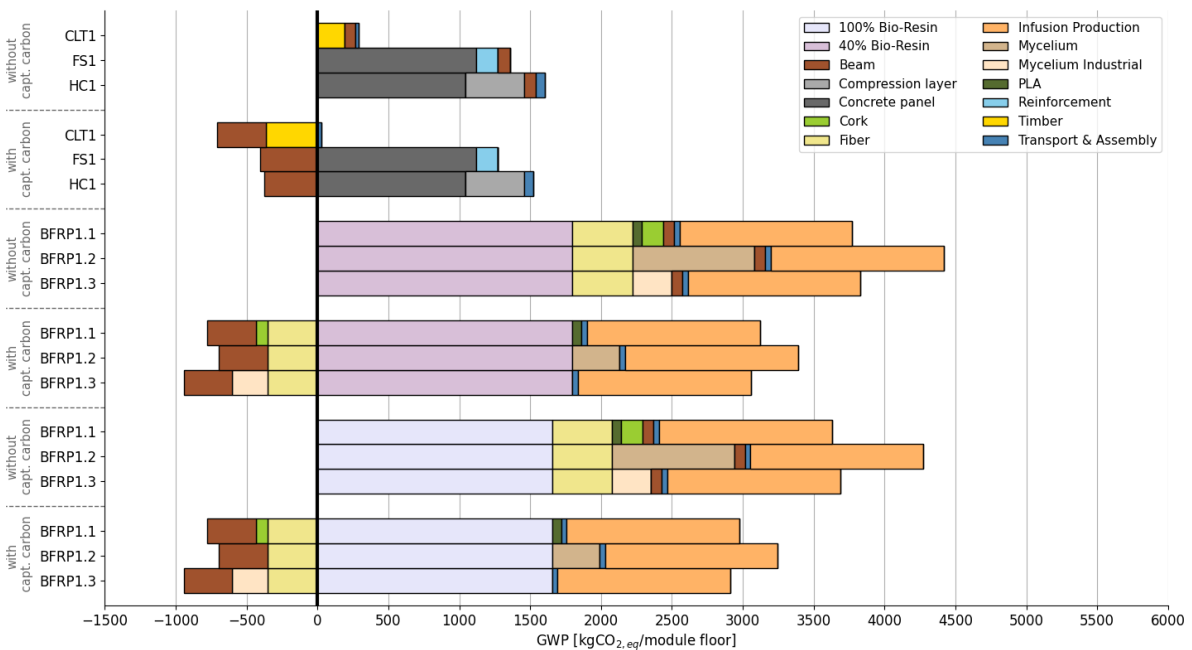
Figure 9.7: Results for all one-way variants of LCA without and with captured carbon
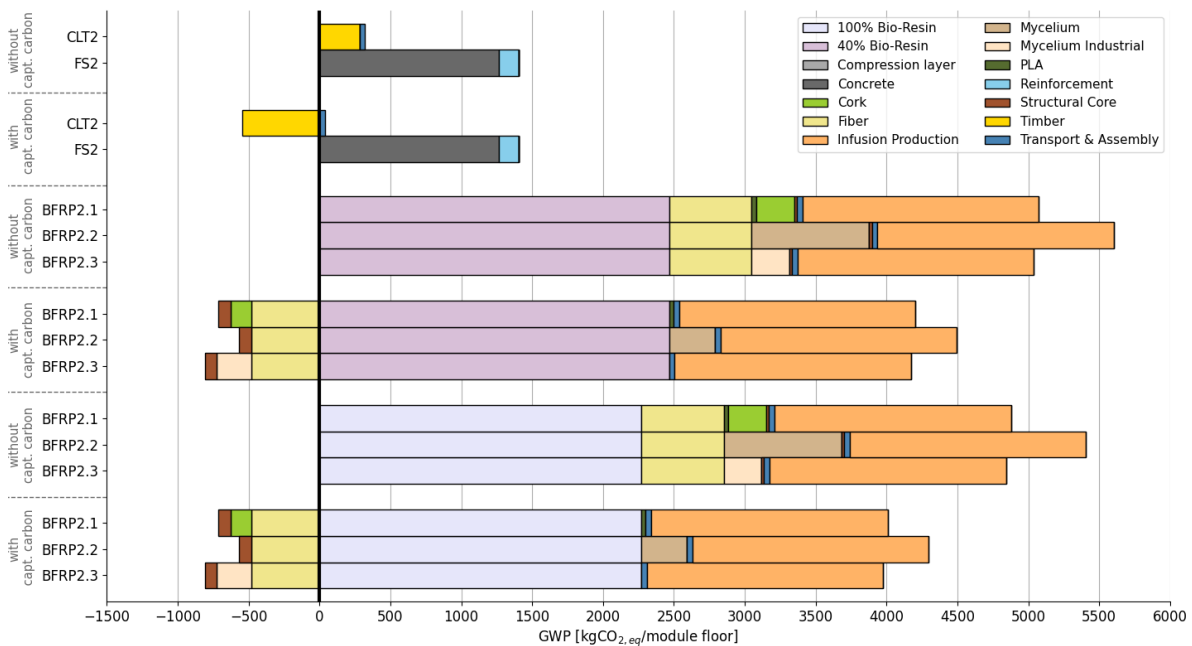
Figure 9.8: Results for all two-way variants of LCA without and with captured carbon

Scope

Given the scope outlined within the LCA, arriving at definitive conclusions concerning the captured carbon potential of the floors presents challenges. A comprehensive LCA encompassing the entire life cycle, including the end-of-life phase, is essential for this assessment. In scenarios involving reuse and high durability, the end-of-life phase becomes instrumental in capturing carbon for an extended duration or reintroducing it into the environment.

LCI data

The availability of LCI data is limited, necessitating numerous assumptions, particularly when considering the bio-based materials. Moreover, the analysis is exclusively conducted for this specific combination of fibers and resin. It is important to recognize that each BFRP laminate could have a different material composition, mandating the creation of a new, detailed LCI dataset. Notably absent from the LCI setup are fillers, additives, and other components typically introduced into resin. These omissions can exert additional influence on the outcomes of the assessment.

Several assumptions were necessary for conducting the LCI for the BFRP floors. As a result, the outcomes are compared against the findings of the LCA for the Ritsumasyl bridge. While the LCA of the Ritsumasyl bridge encompassed stages A to D, this specific LCA was limited to stages A1 to A5. Given this context, it is reasonable to anticipate a higher CO_2 emission for the Ritsumasyl bridge; however, the CO_2 emission for the BFRP, including the production phase, is 1.7 times lower than the emission calculated in this study. If these values are integrated into the LCA of this study, the overall CO_2 emission of the BFRP floors is reduced by approximately 40%.

Processes

The production processes employed for conventional floors are optimized, a necessity driven by the demand for these flooring solutions. Comparatively, applications with (B)FRP have gained traction more recently, but not at the same scale as CLT and concrete floors. Envisioning the future, the potential for up-scaling and automating the production of BFRP floors holds promise in gradually mitigating carbon emissions over time.

Land use

Considering land use for bio-based materials is not a common practice in LCA. Land use has environmental implications, including habitat destruction, soil degradation, and potential impacts on biodiversity. Considering only CO_2 emission, this is not taken into account, and ignoring these factors can lead to an incomplete understanding of the environmental impacts associated with the production of bio-based materials. Furthermore, the

difference in land use and, thus, the growth cycle of the bio-based material can also influence resource depletion of the soil or the captured carbon. For instance, the growth cycle of flax plants is short, as they generally attain maturity and become harvest-ready within a few months post-planting. In contrast, trees undergo a significantly longer growth cycle before reaching maturity and becoming suitable for utilization. These aspects are out of the scope of this research but should be considered in more detailed LCA studies.

9.5. Costs

This research performs a minimal yet insightful cost analysis, comparing the BFRP variants and conventional flooring solutions. The primary scope of consideration is material costs, offering an initial insight into the economic landscape of the variants. It is important to note that certain essential factors have been excluded from this evaluation. These exclusions are essential to recognize as they might introduce some differences in the final costs of the floor.

The following costs are excluded:
- Investing costs
- Engineering costs
- Research costs
- Manufacturing costs
- Transportation costs
- Assembling costs

Table 9.7 shows the material costs considered in the cost analysis. Some remarks have to be made on the assumptions made for the costs:

- **Flax fibers and 40% bio-based epoxy**: The costs for flax fibers and 40% bio-based epoxy resin is based on the LCC analysis conducted for Ritsumasyl and the prices of synthetic fibers and regular epoxy [96, 62]. The costs attributed to synthetic FRP materials are based on Molenaar's comprehensive research conducted at Fiber-Core. Molenaar highlights that these costs encompass both material and labor expenditures. However, it's crucial to recognize that the price values presented are indicative rather than exact. Furthermore, these costs concern regular sandwich structures with webs in one direction. Therefore, it is assumed that additional labor costs have to be considered for the two-way floor since more individual core elements have to be wrapped with fibers. According to the designs in this thesis, there are an additional 750 core elements. It is assumed that wrapping a single core block takes approximately 5 minutes, leading to extra production costs of €3125. The prices from Molenaar are for synthetic materials. Therefore, the costs for BFRP material are determined using the cost differential factor between the BFRP and GFRP variants of the Ritsumasyl bridge. This resulted in the BFRP material being 1.77 times more expensive than the GFRP material.

- **Bio-foam**: The costs of the BioFoam with 0.1 MPa compressive strength of Isobouw has been used [106].

- **Mycelium**: Its utilization within the construction industry remains uncommon. Currently, commercially accessible mycelium products are predominantly finished items like mycelium blocks. The pricing of these blocks serves as a basis for approximating the costs associated with mycelium as a core material [107]. It is essential to recognize that these costs will likely decrease on a larger scale due to implementing more automated processes.

Figure 9.9 shows the results for the material costs of all variants. It can be seen that the costs for BFRP variants are significantly higher than CLT and concrete. They are about twice as expensive as CLT.

While the current analysis provides an introductory glimpse, it cannot be considered an exhaustive representation of the entire picture. However, this research is an initial illustration of how BFRP performs against conventional flooring systems.

Table 9.7: Material costs of all materials used in the BFRP and conventional floors

Type	Material	Per unit	Costs per unit	Source
Timber	CLT	m^3	€ 1250,00	ABT
Timber	Assembly	m^2	€ 15,00	ABT
	Solid timber	m^3	€ 716,24	[108]
Concrete	Concrete C30/35 XC1	m^3	€ 129,00	Bouwkosten.nl
	Reinforcement grid B500 Ø6	kg	€ 1,84	Bouwkosten.nl
	Assembly FS	m^2	€ 76.17	Bouwkosten.nl
	HC-200 with compression layer	m^2	€ 50,10	Bouwkosten.nl
	Assembly HC	m^2	€ 7,76	Bouwkosten.nl
BFRP	Flax fibers	kg	€ 5,32	[96, 62]
	40% Bio-based epoxy resin	kg	€ 6,56	[96, 62]
Core	Bio-foam	kg	€ 10,00	[106]
	Insulation cork	kg	€ 3,33	[109]
	Mycelium	kg	€ 7,97	[107]
	Extra production	# core elements	€ 4.17	Assumption
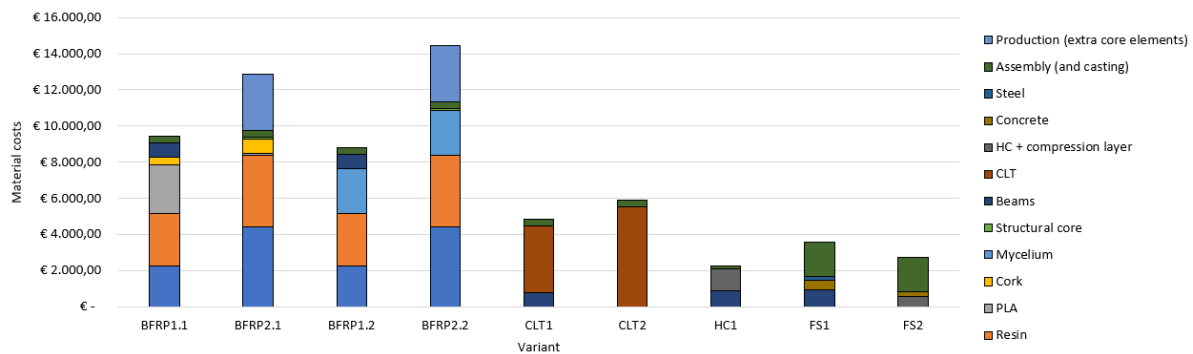
Figure 9.9: Results for material costs of all floor variants

9.6. Conclusion

The conclusions from this chapter are summarized below:

- Structurally, BFRP floors can match the height and weight of conventional floors, sharing similarities with CLT floors' weight for modular construction and transport ease.

- Regarding environmental impact, BFRP floors show higher CO_2 emissions compared to conventional floors due to the resin and infusion production process. Utilizing eco-friendly resin and enhancing energy efficiency in production can improve the environmental profile, with BFRP's CO_2 capturing capacity similar to CLT.

- Cost-wise, BFRP floor materials are notably pricier than conventional and CLT floors. This can be explained by the fact that introducing new design solutions with a sustainability focus often involves higher costs.

10

Discussion

This research covers a broad subject involving a relatively new material not commonly used in real-world applications. Consequently, it is necessary to make certain assumptions and simplifications during the design process. This study has made assumptions while considering the relevant context and research objectives. The subsequent sections discuss the assumptions and their associated limitations and consequences for the research outcome.

10.1. BFRP Material

In this study, a particular BFRP material has been selected to do the floor designs. Using a different material with different fibers, resin, and thus different material properties could mean changes to the floor design. While the same structural typology can still be employed, adjustments to the geometry—either making it more slender or robust—may be necessary to meet the ULS and SLS criteria. It is important to note that when adopting a different BFRP material, thorough testing is important to understand the material properties comprehensively.

Additionally, it is important to consider the effects of temperature, moisture, and creep. In this research, conversion factors for these environmental factors are assumed to be similar to those in the Ritsumasyl bridge. The Ritsumasyl bridge is situated outdoors, whereas the floor is indoors. This distinction is essential because indoor applications experience fewer environmental effects. As a result, there is a possibility of underestimating the performance of the BFRP in question, resulting in over-designing the floor.

To address the delamination issue at the two-way floor's web intersection, a local model was made. It is important to note that the fracture energy properties in this model differ from those applied in the Ritsumasyl bridge. This model incorporates properties for BFRP with hackled fibers combined with an epoxy resin and a 40% fiber volume content. In contrast, the BFRP of the Ritsumasyl bridge utilized yarn fibers with a partially bio-based epoxy resin and a higher fiber volume content. These differences can impact delamination behavior, as yarn fibers tend to exhibit superior properties in this regard. Conversely, the higher fiber content generally enhances resistance against delamination. While the precise effect on the results remains uncertain, the chosen material does provide a valuable indication of the web intersections' capacity, particularly given the conservative approach taken to address this failure mode.

10.2. Floor Design

Decisions have been made throughout the design of the floor. These decisions have implemented certain constraints to the BFRP floors and their applicability. This section discusses the one- and two-way floor potential. Furthermore, fire resistance and acoustic requirements are addressed separately because of their impact on the BFRP floors' application.

10.2.1. Material optimization in one-way floor

The geometry parameters of the initial floor are as follows: floor height = 164 mm, facing thickness = 12 mm, web thickness = 8 mm, and web spacing = 140 mm. The criteria for the one-way floor are ranked in order of importance as follows: local deflection (UC = 0.84), additional global deflection (UC = 0.60), fundamental frequency (UC = 0.59), and maximum global deflection (UC = 0.51). These are all SLS criteria. The ULS criteria, on the other hand, have lower utilization: crushing facing at mid-span (UC = 0.15), crushing of web due to concentrated load (UC = 0.11), creep rupture of facing at mid-span (UC = 0.09), and shear strength of web at support (UC = 0.07).

The local deflection is the most critical factor in the design. However, one could argue that considering local deflection may not be necessary:

1. Deflection limits serve as comfort criteria for people using the floor. Adhering to standard deflection limits yields values less than a millimeter for the utilized web spacing. This may not necessarily lead to a sense of insecurity for the users.

2. Local deflection does not result in excessive deformation that damages other structural elements. However, it's important to note that a small deformation can damage the finishing floor when it cannot follow this deformation.

3. The use of BFRP results in a lightweight floor. Lightweight floors often need a finishing floor for acoustic requirements. The finishing floor leads to a further dispersion of point loads. This results in a more pronounced global deflection response.

4. The current design does not account for the structural contribution of the core material. This will provide resistance from beneath and limit local deflection.

Disregarding local deflection, the web spacing is influenced by local bending failure (UC = 0.21). For the initial geometry, it is possible to increase the web spacing from 140mm to 175mm. This adjustment results in a utilization of approximately 0.90. This is calculated based on the maximum stress in the facing determined with the numerical model, which is then extrapolated using analytical calculations. However, it is better to reduce the web spacing than to increase the facing thickness because the webs make up only 20-25% of the total BFRP material. Therefore, the web spacing is kept at 140 mm, allowing for facing thickness reduction.

Considering global deflection, material use can still be reduced since utilization is only at 0.60. Fundamental mechanical calculations are used to indicate the deflection. Only deflection due to bending by the facings is considered, which contributes to approximately 95% of the total deflection. The facing thickness can be reduced from 12 to 10mm and still meet the deflection criteria (UC ≈ 0.90). This results in a BFRP material reduction of 15%.

The selected case study has a design life of 15 years. Considering a design life of 50 years, which corresponds better to buildings in general, utilization of the global deflection criteria is approximately 1.07 for the initial geometry of the floor. Considering the optimization steps made before (facings thickness of 10 mm), the global deflection utilization is approximately 1.40. To meet the deflection criteria for a design life of 50 years, the floor height is increased from 160mm (140 + 2 · 10) to 200mm (160 + 2 · 10). This increases the BFRP material by approximately 3% with respect to the floor with a facing thickness of 10mm due to the increased height of the webs.

While the strength of the web allows for a reduction in thickness (UC < 0.15), this reduction is constrained by factors such as strength, local buckling, and ply thickness. It is important to note that verification checks have not been conducted for the reduced web thickness. Nonetheless, to offer an estimate of the potential material reduction, consider decreasing the web thickness from 8 to 6 mm. This adjustment could lead to a decrease in BFRP material in the floor by around 7%.

In conclusion, for the one-way floor with a 15-year design life, it is possible to reduce the BFRP material by approximately 21% by reducing the facing and web thickness compared to the initial design. Similarly, for the one-way floor with a 50-year design life, it is possible to reduce the BFRP material by approximately 19% compared to the original design. Extending this reduction to its CO_2 emissions, a reduction of approximately 10% is obtained.

When designing the one-way floor, initial design calculations can be performed using analytical methods in compliance with the specifications outlined in the FRP and timber Eurocode standards. However, it is crucial to consider concentrated loads on top and between webs. For the concentrated loads, utilizing FEA is essential in understanding the structural behavior, especially when factoring in the structural contribution of the core material. Furthermore, the effective width of the facing should be taken into consideration. In cases where the web spacing is too wide, the facing thickness is further reduced, and a non-structural core is considered, there is a potential risk that the facing is not utilized to its maximum capacity.

10.2.2. Material optimization in two-way floor

The geometry parameters of the initial floor are as follows: floor height = 168 mm, facing thickness = 16 mm, web thickness = 8 mm, and web spacing = 175 mm. The criteria for the two-way floor are ranked in order of importance as follows: crushing of web at support (UC = 0.67), additional global deflection (UC = 0.66), fundamental frequency (UC = 0.65), maximum global deflection (UC = 0.56) and delamination of intersecting webs (UC = 0.53).

The critical area is the webs at the supports. However, the timber core elements in the support have conservatively not been considered in this verification. Accounting for the contribution of these core elements, the UC for crushing the web at the support decreases to 0.12. Resulting in global deflection being the most critical.

Considering the global deflection limits (UC = 0.66), improvements can be made in material optimization. Since deflection due to bending contributes to 95% of the total deflection, simplified analytical calculations for a simple supported beam approximate the deflection considering only the facings. Since the analytical calculations are conservative, a correction is made based on the numerical results of the initial floor. Reducing the facing thickness from 16 to 14mm results in an approximate UC of 0.85 and a material reduction of 11%.

The selected case study has a design life of 15 years. Considering a design life of 50 years, which corresponds better to buildings in general, the UC of the global deflection criteria is approximately 1.16 for the initial floor geometry. Considering the optimized floor (facing thickness of 14 mm), the UC worsens and is about 1.48. To meet the deflection criteria for a design life of 50 years, the facing thickness can be increased again; however, since the facing contributes to a more significant portion of the BFRP material, it is better to increase the floor height. For a facing of 14mm, increasing the floor height from 168 (140 + 2 · 14) to 208mm (160 + 2 · 14) will meet the deflection criteria (UC $\approx$ 0.78). This results in a BFRP material increase of 5%.

Since none of the checks are critical for the webs, it is possible to reduce its thickness. However, strength, local buckling, and ply thickness have not been checked. Nonetheless, to offer an estimate of the potential material reduction, consider decreasing the web thickness from 8 to 6 mm. This adjustment could lead to an overall decrease in BFRP material in the floor by around 8%.

The amount of BFRP material can be further optimized by considering the core to have a load-bearing function. If the initially assumed non-structural core contributes, increasing web spacing at mid-span would be possible. The number of webs that can be removed depends on how much the core contributes to load transfer between the facings and to withstand concentrated loads. For example, when the web spacing is increased from 175 to 300 mm at mid-span (with the web spacing at the supports remaining at 175 mm), there is an 8% reduction in BFRP material for the overall floor.

Optimizing the web spacing results in more efficient use of material, leading to the next critical factor in the design: delamination of the intersecting webs (UC = 0.53). The method employed to verify the intersection is conservative, not considering non-linear stress redistribution. This implies that immediate failure is not expected upon initial signs of delamination; instead, stress redistribution will occur, and the facings will act as support. Therefore, it is advised that when delamination becomes the limiting factor in further floor optimization, a more accurate verification procedure of the detail should be investigated.

In conclusion, for the two-way floor with a 15-year design life, it is possible to reduce the BFRP material by approximately 19%, reducing the facing and web thickness compared to the initial design. Similarly, for the two-way floor with a 50-year design life, it is possible to reduce the BFRP material by approximately 15% compared to the original design. The material reduction resulting from increasing the web spacing is not included because of the potential limiting factor of delamination.

When designing the two-way floor, it is advised to use FEA to understand the vibration response, deflection behavior, stress distribution, and delamination at intersections. Furthermore, a more comprehensive analysis should be done for the connection of the floor to the main structure.

10.2.3. Fire resistance

In the case study used in this research, the Natural Pavilion, no fire safety requirements were imposed on the floor because it is a single-compartment structure. Consequently, fire resistance was not taken into account for the BFRP floor. This has consequences for the applicability of the designed floors in this research. They can be utilized in buildings without fire safety requirements. This includes single-compartment buildings and terrace housing, where each house is treated as a separate compartment.

When considering floors in buildings with specific fire safety requirements, it is critical that the floor maintains its load-bearing capacity for the specified duration. This can challenge BFRP with thermoplastic components as the material will meld. On the other hand, BFRP with thermosetting resin holds more promise. This is due to its ability to form a charring layer and protect the material. In this case, the charring rate is a critical factor. The effective thickness of the facings must remain adequate throughout the specified duration. Assuming a charring rate similar to or less to CLT (0.7 mm/min), the facing will be gone within 30 minutes. This means using thicker facings or incorporating protective layers becomes necessary. Moreover, the floor must not worsen the fire's progression. Given the flammability of natural fibers, special attention must be paid to this.

10.2.4. Acoustics

The design of the Natural Pavilion did not have to meet specific acoustic design criteria. As a result, acoustic considerations were not factored into the design of the BFRP floors. If there were mass requirements for sound insulation applied to the BFRP floor, it is assumed to have comparable effects to timber floors. Both types of floors have similar weights, and consequently, they would need similar finishing floors.

10.3. Environment

For the environmental comparison, constraints were set on the functional unit, scope, and environmental impact category. This section discusses the sensitivity of these constraints and reflects on the results obtained. Furthermore, the sensitivity of the LCI on the LCA results is discussed.

Functional unit

The functional unit only includes the structural part of the floor and not the main structure. Lightweight flooring options like BFRP and timber positively impact the primary structure's material use. The main structure needs to be built more robustly for the concrete floor, which increases the environmental impact.

Scope

The scope of the LCA in this research is limited to stages A1-A5. If the entire life cycle were to be considered, the user and end-of-life phase must also be included. During the user phase, maintenance is essential. However, given that the floor is situated in an indoor climate and is not exposed to external environmental conditions, this factor does not significantly influence the comparison between the conventional and BFRP floors.
Looking at the LCA study performed on the Ritsumasyl bridge, maintenance contributed to the favorable outcome of the BFRP bridge. All stages were considered in their LCA, and a repainting interval of every seven years was factored in for the timber bridge. Due to this, the BFRP bridge performed better in terms of CO_2 emission compared to the timber bridge variant. One remark must be made: the repainting interval is a conservative estimate for the maintenance of the timber bridge variant.

When examining the end-of-life phase, differences arise between timber, concrete, and BFRP floors. Timber floors have the advantage of being derived from natural sources, reducing their environmental impact at the end of their lifecycle. In the case of BFRP floors, this primarily depends on the proportion of bio-based material used. It becomes evident that opportunities for higher-value end-of-life applications arise when they can be manufactured using 100% bio-based materials. The material can be utilized to recover energy or residual value through processes such as incineration or composting.

The end-of-life of BFRP also depends on the type of resin used. Recycling the raw materials is more difficult with a thermosetting resin than a thermoplastic. Furthermore, the availability of suitable recycling methods is crucial to facilitate the recycling of raw materials.

In the Ritsumasyl LCA, the end-of-life scenarios for both BFRP and GFRP variants were less favorable than for the concrete, timber, and steel bridges. This is because no options for the recyclability of GFRP and BFRP are provided in the national environmental database. The timber variant came out to perform best for the end-of-life of all variants. The environmental impact of the end-of-life of the concrete bridge was also small. This is because of the high recyclability rate of concrete. However, concrete loses significant value since it is downcycled for aggregate use.

Environmental impact category

In this research, GWP was the only environmental impact category considered. However, the environmental impact differs when more or different categories are considered. For example, in the LCA study of the Ritsumasyl bridge, the BFRP bridge outperformed the concrete, steel, timber, and GFRP variants in terms of CO_2 emissions. However, this did not translate to a better ECI score for the BFRP bridge than the other variants.

Life cycle inventory

The outcome of an LCA highly depends on the LCI. In the BFRP floor, it was seen that the most significant contribution of CO_2 emissions arises from the resin and production process. Changes in the data for these two factors thus largely impact the final results of the LCA. Mainly, the LCI for the production process depends a lot on the data source (different manufacturers) and production scale. If both the resin and production impact are reduced by 65%, as per the data used in this study, the environmental impact for stages A1-A5 would be lower than that of concrete floors.

10.4. Costs

Introducing new design solutions with a sustainability focus often involves higher costs. The novelty of the design and materials means that BFRP floors currently have lower demand than traditional floor systems. This means that economy of scale, which would drive down costs, is much less prevalent. In addition, because of the lower demand, the new production techniques that must be employed for manufacturing BFRP floors have not been optimized for costs yet. Once demand grows, both factors could help improve the competitiveness of BFRP floors. However, the potential effects of higher demand are not considered in the current analysis, skewing the results to favor more traditional materials.

11

Conclusion and Recommendations

This final chapter presents the research conclusions. Based on these conclusions, recommendations for further research are suggested.

11.1. Conclusion

This thesis investigates the feasibility of BFRP floors in modular buildings and compares them to conventional floors, specifically timber and concrete floors. Both a one- and two-way variant of BFRP floors are designed using the second-generation Eurocodes for FRP and timber, analytical calculations, and numerical models. The comparison to conventional floors was done using the structural design results, the LCA, and the cost analysis. The conclusions of this research are presented by answering the sub- and main research questions.

11.1.1. Sub-research questions

The sub-research questions are formulated to answer the main research question. The first two sub-research questions are about the development of the BFRP floor, whereas the last research question dives deeper into the comparison to conventional floors.

1. **Which BFRP can be used in floors, and what are its required physical and mechanical properties?**

This question is discussed in chapter 3 and 4. Any combination of fibers with resin can be used, provided the fibers have favorable properties. This includes adequate cellulose content, a favorable aspect ratio, a microfibril angle close to the fiber direction, and a low lumen porosity. Flax fibers are mostly chosen for construction because they have these desirable physical properties. They have a cellulose content between 64-71%, a microfibril angle between 5-10°, an aspect ratio of 1750 l_f/d_f, and a luminal porosity of only 2-11%. Fibers like hemp or cotton can also be utilized. However, the aspect ratio is substantially lower, 900 and 1000 l_f/d_f respectively, and for cotton, the microfibril angle is much higher at 46%.

While it is preferred to utilize a bio-based resin, the current market lacks options. For example, green-BFRP with a bio-based PLA resin is up to 3 times weaker than a BFRP with epoxy resin. It is important to use a resin with a low curing temperature to avoid the degradation of natural fibers. A thermoset resin is potentially necessary for fire safety but does require more detailed research.

The mechanical properties of the selected BFRP material in this research have appeared to be sufficient to design a floor. The construction height is similar to the timber and concrete floor, and the weight is similar to the timber floor. The tensile design strength of the flax with partially bio-based resin is 166 MPa for a UD ply, and the E-modulus is 24GPa. Material with lower material properties is possible. However, a higher construction height or thicker laminates should be used, which leads to more material used. For example, if the material is two times less stiff, the deflection increases by a factor of two, increasing the floor height by 25%.

2. **What specific design requirements must a BFRP floor satisfy concerning the ultimate and service-ability limit state?**

Designing BFRP floors involves satisfying ULS and SLS requirements aligned with second-generation Eurocodes for FRP and timber. ULS should account for global load-bearing capacity, resistance to concentrated loads, and point supports, with these failure modes outlined in the FRP Eurocode. For the two-way floor, an additional failure mode is considered involving delamination at the location of the intersecting webs. Fire safety is beyond this research scope and is crucial for building applications that are not temporary. SLS concerns the deflection, along with the vibration and acoustic requirements. The SLS requirements are critical because a BFRP floor is lightweight and can be assessed using the second-generation timber Eurocode.

3. **How does the structural, environmental, and economic performance of a BFRP floor compare to that of a conventional floor?**

Structural
Figure 11.1 shows the results of the structural comparison. Regarding BFRP floors, it is possible to design them with similar construction height and weight to conventional floors. CLT and BFRP floors share a similar weight, making them favorable to modular construction, simple assembly, and easy transportation. Concrete floors are 6-8 times heavier than the CLT and BFRP floors.

Examining the height of the floor, both the one- and two-way floors are similar, wherein the one-way variant is a bit thinner. The construction height for the one-way floor increases due to the additional beams. The total construction height presented in Figure 11.1 is conservative because it does not account for beam and floor integration.
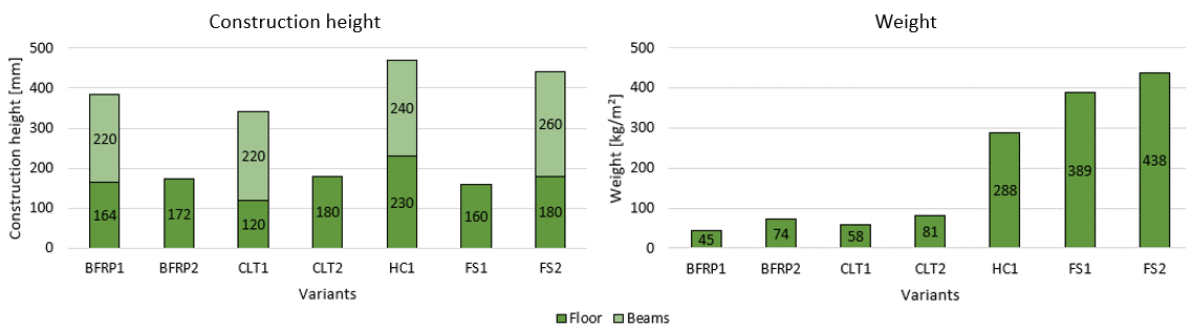
Figure 11.1: Structural comparison results for both the construction height and weight. 1 = one-way floor, 2 = two-way floor, HC = concrete hollow core, FS = concrete flat slab

Environmental
The results of the environmental comparison are illustrated in Figure 11.2. The BFRP floors significantly underperform compared to the conventional floors regarding environmental impact. This is primarily attributed to the resin and infusion production process associated with BFRP floors. Developing a bio-based and more environmentally friendly resin is an important factor for the environmental profile of BFRP. Furthermore, the energy-intensive nature of the infusion production process contributes to a substantial CO_2 emission. It becomes apparent that exploring production processes that enhance energy efficiency for larger-scale applications is crucial. An advantageous aspect of the BFRP floor lies in its comparable capacity to capture CO_2, similar to that of CLT.
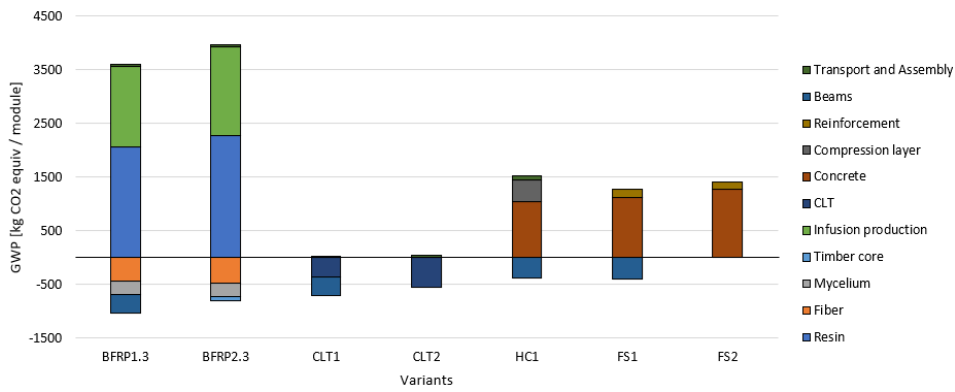
Figure 11.2: LCA comparison results with an indication for captured carbon

Economics

The outcomes of the cost comparison are visualized in Figure 11.3. The materials of the BFRP floors entail notably higher costs than conventional floors. The difference with conventional floors can be explained by the continuous evolution over the years and their extensive usage. Introducing new design solutions with a sustainability focus often involves higher costs, as discussed in chapter 10.
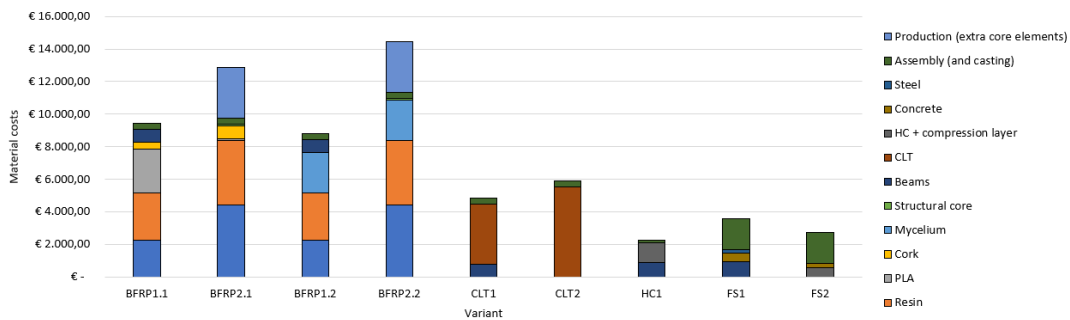
Figure 11.3: Material costs comparison results

11.1.2. Main research question

What is the feasibility and potential of a BFRP floor as a sustainable and cost-effective alternative to conventional floors in modular buildings?

To determine the feasibility and potential of the BFRP floors, two hypotheses have been formulated in the methodology. These hypotheses are used to answer the mean research question. Sub-question one revealed the crucial mechanical properties of the BFRP material for designing a BFRP floor. Sub-question two outlined the design requirements for a floor. Using the conclusions of these questions, the initial hypothesis can be answered. As for sub-question three, the environmental and cost performance of the BFRP floor was researched. These results are used to answer the second hypothesis.

1. **The BFRP floor is feasible for use in modular buildings when thickness and weight are similar or less than the CLT and concrete floors for the same design criteria.**

Both the one- and two-way BFRP floors demonstrate feasibility in terms of construction height and floor weight compared to the conventional floors within the selected case study, the Natural Pavilion. However, certain aspects are important when extrapolating to floors with a design life of 15 to 50 years. Due to creep, the deflection increases over time, and a more robust design is required.

The BFRP floor is feasible for single-compartment buildings or terrace housing when considering the fire safety requirements of the case study. Further research should be done when applying to buildings with strict fire safety requirements, and mitigation measures are necessary.

2. **The BFRP floor has potential in modular buildings when the CO_2 emission and costs are the same or less than the CLT and concrete floors.**

At this moment, the BFRP floor demonstrates unfavorable performance compared to conventional floors in terms of environmental impact and costs. Specifically, its environmental impact is twice that of concrete floors, and its costs are nearly twice as high as those of CLT floors. However, when the environmental impact of the resin and production process is reduced, there could potentially be a future for utilizing BFRP floors with lower CO_2 emissions. Furthermore, when considering the entire life-cycle of the floor and including the end-of-life contribution of a 100% BFRP floor, the CO_2 emissions are even further reduced.

Even though current costs are much higher for BFRP floors than for conventional floors, there is potential for BFRP floors to become more cost-effective and competitive in the future. Because of the novelty of the technology, expenses for the design and production of BFRP floors are relatively high. However, if these floors are used more in the future, prices could drop due to economy of scale and an optimized production process. Moreover, if optimized BFRP floors turn out to be environmentally favorable compared to conventional floors, it can be argued that higher costs are not necessarily a significant obstacle. Other green solutions currently employed in the industry, which are more expensive than traditional methods, are still used because of the reduction in environmental impact. It is difficult to estimate to what extent these economic effects will influence the price of BFRP floors, and therefore, it has not been taken into account in the results. This skews the results in favor of conventional floors.

11.2. Recommendations

11.2.1. Core material

It is recommended that further research be done to explore viable alternatives for the bio-based core. The bio-based core can potentially contribute to the load-bearing capacity of the floor and reduce the BFRP material utilized. The bio-based core materials used in this study have not been thoroughly investigated. Numerous gaps remain in material properties, specifically the shear modulus and resistance, which are essential for their effectiveness as core materials.

11.2.2. Floor design

Regarding floor design in general, it is recommended to prioritize the floor's fire resistance. While the floor design outlined in this research can be applied in single-compartment buildings and terrace housing, it is unsafe for buildings with more strict requirements. Research into the floor's structural integrity during a fire should be done. Additionally, it is recommended to explore how the floor may contribute to the spread of fire when highly flammable natural fibers are exposed to heat.

Furthermore, the BFRP design in this research does not consider a detailed design of the connection of the floor. To build a BFRP floor, it is recommended to further investigate the connection. In the case of the Natural Pavilion, the connection involves a steel shoe and screws located at the sides and bottom. For the BFRP floor, it is crucial to verify whether the combination of timber solid core elements at the support and connection method of the Natural Pavilion is sufficient.

11.2.3. Environmental impact

The highest environmental impact of the BFRP floors comes from the resin and production process. To reduce the environmental impact of the BFRP floor, it is recommended that more research be done into environmentally friendly resins. This reduces the environmental impact of the floor and offers more sustainable end-of-life options, such as incineration and composting when the resin is entirely bio-based.

Furthermore, conducting a more comprehensive environmental impact assessment is recommended. Including different data sources, the entire life-cycle of the floor, and the effect of the floor on the robustness of the main structure. In addition, the LCA does not consider the land use associated with flax fiber. This factor can benefit natural fibers because of the short growth cycle compared to, for example, trees.

Bibliography

[1] J A Ochsendorf. "Sustainable Engineering: The Future of Structural Design". In: (2008). URL: http://www.ascelibrary.org/.

[2] "2018 Global Status Report Towards a zero-emission, efficient and resilient buildings and construction sector". In: *Global Status Report* (2018), pp. 9–11. URL: www.iea.org.

[3] *The Paris Agreement | UNFCCC*. URL: https://unfccc.int/process-and-meetings/the-paris-agreement?gclid=CjwKCAjw-IWkBhBTEiwA2exyO-UI_b9Api2P--5JgvBP6pWDUnub-Rz1G8mPY4_XH3eBhrwZWNk5mhoCr34QAvD_BwE.

[4] *MilieuPrestatie Gebouwen - MPG*. URL: https://www.rvo.nl/onderwerpen/wetten-en-regels-gebouwen/milieuprestatie-gebouwen-mpg.

[5] Norbert Schotte and Yaël Ben-Basat. *Bouwen binnen CO2-budget: benodigde condities en de potentie van Carbon Based Design*. 2023. URL: https://albaconcepts.nl/alba-paper-bouwen-binnen-co2-budget-benodigde-condities-en-de-potentie-van-carbon-based-design/.

[6] Marlies Peschier. "Handvat duurzaam materiaalgebruik voor bouw-en infrabedrijven". In: (Jan. 2021). URL: https://www.bouwendnederland.nl/media/3441/handvat-duurzaam-materiaalgebruik.pdf.

[7] *What are Composites?* URL: https://romeorim.com/what-are-composites/.

[8] F P van der Meer et al. *CIE5128 - FRP Structures Reader*. Course reader. Sept. 2018.

[9] *Bridge decks | Steel and composite | FiberCore Europe*. URL: https://www.fibercore-europe.com/en/products/brugdekken/.

[10] *Full FRP Bridges | Fiberline*. URL: https://fiberline.com/solutions/bridges/full-frp-bridges.

[11] Saptarshi Maiti et al. "Sustainable Fiber-Reinforced Composites: A Review". In: *Advanced Sustainable Systems* 6.11 (Nov. 2022), p. 2200258. ISSN: 2366-7486. DOI: 10.1002/ADSU.202200258. URL: https://onlinelibrary.wiley.com/doi/full/10.1002/adsu.202200258.

[12] *Kennisbank Biobased Bouwen*. URL: https://www.biobasedbouwen.nl/.

[13] de Jonge Hugo. *Beleidsagenda normeren en stimuleren circulair bouwen*. 2022. URL: https://www.rijksoverheid.nl/documenten/kamerstukken/2022/12/23/kamerbrief-over-beleidsagenda-normeren-en-stimuleren-circulair-bouwen.

[14] J. C. Morel et al. "Building houses with local materials: means to drastically reduce the environmental impact of construction". In: *Building and Environment* 36.10 (Dec. 2001), pp. 1119–1126. ISSN: 0360-1323. DOI: 10.1016/S0360-1323(00)00054-8.

[15] Karthik Subramanya, Sharareh Kermanshachi, and Behzad Rouhanizadeh. "Modular Construction vs. Traditional Construction: Advantages and Limitations: A Comparative Study". In: (2020), p. 12. DOI: 10.3311/CCC2020-012. URL: https://doi.org/10.3311/CCC2020-012.

[16] Loizos Loizou et al. "Quantifying Advantages of Modular Construction: Waste Generation". In: *Buildings 2021, Vol. 11, Page 622* 11.12 (Dec. 2021), p. 622. ISSN: 2075-5309. DOI: 10.3390/BUILDINGS11120622. URL: https://www.mdpi.com/2075-5309/11/12/622/htm%20https://www.mdpi.com/2075-5309/11/12/622.

[17] *Flexwoning - Innovative Housing Solutions*. Sept. 2023. URL: https://flexwoning.nl/.

[18] *The Natural Pavilion - ABT Ingenieurs in bouwtechniek*. URL: https://abt.eu/projecten/the-natural-pavilion/.

[19] Ernesto Callegari. *Timber buildings with point-supported flat slabs: is it possible? | LinkedIn*. Oct. 2020. URL: https://www.linkedin.com/pulse/timber-buildings-point-supported-flat-slabs-possible-callegari/.

[20] *Concrete Building Structures CIE3340 / CIE4281*. Course Material. Nov. 2016.

[21] *Eurocodes family | Eurocodes: Building the future*. URL: https://eurocodes.jrc.ec.europa.eu/en-eurocodes/eurocodes-family.

[22] European Committee for Standardization. *FprCEN/TS 19101:2021 Design of fibre-polymer composite structures*. 2021. URL: https://www.cen.eu/work/areas/materials/fibresandcomposites/fibre-polymer/Pages/default.aspx.

[23] *Bouwbesluit 2012*. Ministerie van Binnenlandse Zaken en Koninkrijksrelaties. 2012.

[24] European Committee for Standardization. *Eurocode 5: Design of timber structures - Part 1-1: General - Common rules and rules for buildings*. European Standard. 2004. URL: https://doi.org/10.3403/30389232.

[25] Emil. *One Way Slab and Two Way Slab - The most Important Differences - Tribby3d*. 2022. URL: https://tribby3d.com/blog/one-way-slab-and-two-way-slab/.

[26] *SPC Industries | Product Details - Precast Hollow Core Slab*. URL: https://www.spcind.com/en/product_details/13/Precast%20Hollow%20Core%20Slab.

[27] *Beam & Block Flooring - Treanor Pujol Ltd - Prestressed T Beams*. URL: https://www.treanor-pujol.co.uk/products/beam-and-block/.

[28] *How to design Flat Slab?* URL: https://www.midasstructure.com/blog/en/blog/flat-slab-modeling.

[29] *Types Of Concrete For Metal Decking: Structural Vs. Non-Structural Insulating*. URL: https://blog.metaldeck.com/concrete-for-metal-deck-types.

[30] Tri-Dung Ngo. "Natural Fibers for Sustainable Bio-Composites". In: *Natural and Artificial Fiber-Reinforced Composites as Renewable Sources* (May 2018). DOI: 10.5772/INTECHOPEN.71012. URL: https://www.researchgate.net/publication/324896441_Natural_Fibres_for_Sustainable_Bio-Composites.

[31] Bcomp. *Bcomp: ampliTexTM*. URL: https://www.bcomp.ch/products/amplitex/.

[32] *Biobrug Wildlands - MF Emmen*. URL: https://www.mfemmen.com/en/projecten/bio-bridge-wildlands/.

[33] *Demonstrating biocomposites' properties using Bio-Bridges - AllThings.Bio*. URL: https://www.allthings.bio/demonstrating-biocomposites-properties-using-bio-bridges/.

[34] "Eerste brug van biocomposieten gemaakt in Emmen". In: *RTV Drenthe* (2013). URL: https://www.rtvdrenthe.nl/nieuws/79680/eerste-brug-van-biocomposieten-gemaakt-in-emmen.

[35] Wouter Claassen and Georgios Zarifis. "First Bio-Based Composite Movable Bicycle Bridge". In: 31.2 (2020), pp. 227–232. ISSN: 16830350. DOI: 10.1080/10168664.2020.1840945. URL: https://www.tandfonline.com/doi/abs/10.1080/10168664.2020.1840945.

[36] Willem Souren and Edwin Velds. *Bio-based brug Ritsumasyl*. Tech. rep. 2016036-180125-1431. Witteveen+Bos, June 2019. URL: https://www.drive.frl/biocomposiet/.

[37] *FiberCore Europe*. https://www.fibercore-europe.com/.

[38] Georgios Zarifis. *Application of bio-based FRP on a road traffic bridge*. Delft, Jan. 2018. URL: https://repository.tudelft.nl/islandora/object/uuid%3A311d536e-542d-45b5-97d9-f52b2dd4abf3.

[39] Jongsung Sim, Cheolwoo Park, and Do Young Moon. "Characteristics of basalt fiber as a strengthening material for concrete structures". In: *Composites Part B: Engineering* 36.6-7 (Jan. 2005), pp. 504–512. ISSN: 1359-8368. DOI: 10.1016/J.COMPOSITESB.2005.02.002.

[40] K. L. Pickering, M. G.Aruan Efendy, and T. M. Le. "A review of recent developments in natural fibre composites and their mechanical performance". In: *Composites Part A: Applied Science and Manufacturing* 83 (Apr. 2016), pp. 98–112. ISSN: 1359-835X. DOI: 10.1016/J.COMPOSITESA.2015.08.038.

[41] Yashashree Ingle. *Cultivation of Flax Fiber*. URL: https://www.textilesphere.com/2019/10/cultivation-of-flax-fiber.html.

[42] *Silk Fibre Suppliers 17124878 - Wholesale Manufacturers and Exporters*. URL: https://www.fibre2fashion.com/fibres/silk-fibre-suppliers-17124878.

[43] *Basalt fibre for concrete mix - Beyond Materials Group*. URL: https://beyondmaterialsgroup.com.au/basalt-fibre-for-concrete-mix/.

[44] Darshil U. Shah. "Developing plant fibre composites for structural applications by optimising composite parameters: A critical review". In: *Journal of Materials Science* 48.18 (Sept. 2013), pp. 6083–6107. ISSN: 00222461. DOI: 10.1007/S10853-013-7458-7.

[45] Debes Bhattacharyya, Aruna Subasinghe, and Nam Kyeun Kim. "Natural fibers: Their composites and flammability characterizations". In: *Multifunctionality of Polymer Composites: Challenges and New Solutions* (Jan. 2015), pp. 102–143. DOI: 10.1016/B978-0-323-26434-1.00004-0.

[46] Michael P.M. Dicker et al. "Green composites: A review of material attributes and complementary applications". In: *Composites Part A: Applied Science and Manufacturing* 56 (Jan. 2014), pp. 280–289. ISSN: 1359-835X. DOI: 10.1016/J.COMPOSITESA.2013.10.014.

[47] Malladi Rajinipriya et al. "Importance of Agricultural and Industrial Waste in the Field of Nanocellulose and Recent Industrial Developments of Wood Based Nanocellulose: A Review". In: *ACS Sustainable Chemistry and Engineering* 6.3 (Mar. 2018), pp. 2807–2828. ISSN: 21680485. DOI: 10.1021/ACSSUSCHEMENG.7B03437.

[48] Laura Aliotta and Andrea Lazzeri. "A proposal to modify the Kelly-Tyson equation to calculate the interfacial shear strength (IFSS) of composites with low aspect ratio fibers". In: *Composites Science and Technology* 186 (Jan. 2020), p. 107920. ISSN: 0266-3538. DOI: 10.1016/J.COMPSCITECH.2019.107920.

[49] David B. Dittenber and Hota V.S. Gangarao. "Critical review of recent publications on use of natural composites in infrastructure". In: *Composites Part A: Applied Science and Manufacturing* 43.8 (Aug. 2012), pp. 1419–1429. ISSN: 1359-835X. DOI: 10.1016/J.COMPOSITESA.2011.11.019.

[50] Ming Liu et al. "Effect of pectin and hemicellulose removal from hemp fibres on the mechanical properties of unidirectional hemp/epoxy composites". In: *Composites Part A: Applied Science and Manufacturing* 90 (Nov. 2016), pp. 724–735. ISSN: 1359-835X. DOI: 10.1016/J.COMPOSITESA.2016.08.037.

[51] Amandine Célino et al. "The hygroscopic behavior of plant fibers: A review". In: *Frontiers in Chemistry* 1.JAN (2014). ISSN: 22962646. DOI: 10.3389/FCHEM.2013.00043.

[52] M. Assarar et al. "Influence of water ageing on mechanical properties and damage events of two reinforced composite materials: Flax–fibres and glass–fibres". In: *Materials & Design* 32.2 (Feb. 2011), pp. 788–795. ISSN: 0261-3069. DOI: 10.1016/J.MATDES.2010.07.024.

[53] Gurit. *Composite Materials*. URL: https://www.gurit.com/en/our-business/composite-materials.

[54] L. A. Carlsson and G. A. Kardomateas. "Structural and failure mechanics of sandwich composites". In: *Solid Mechanics and its Applications* 121 (2011), pp. 1–399. ISSN: 09250042. DOI: 10.1007/978-1-4020-3225-7{_}1.

[55] Pablo Resende Oliveira et al. "Bio-based/green sandwich structures: A review". In: *Thin-Walled Structures* 177 (Aug. 2022), p. 109426. ISSN: 0263-8231. DOI: 10.1016/J.TWS.2022.109426.

[56] R. Cristian Neagu et al. "The potential of wood fibers as reinforcement in cellular biopolymers". In: *Journal of Cellular Plastics* 48.1 (Jan. 2012), pp. 71–103. ISSN: 0021955X. DOI: 10.1177/0021955X11431172. URL: https://www.researchgate.net/publication/241644965_The_potential_of_wood_fibers_as_reinforcement_in_cellular_biopolymers.

[57] Elise Elsacker et al. "Mechanical, physical and chemical characterisation of mycelium-based composites with different types of lignocellulosic substrates". In: *PLoS ONE* 14.7 (June 2019). ISSN: 19326203. DOI: 10.1371/JOURNAL.PONE.0213954.

[58] Elise Elsacker et al. "Mechanical, physical and chemical characterisation of mycelium-based composites with different types of lignocellulosic substrates". In: *PLOS ONE* 14.7 (June 2019), e0213954. ISSN: 1932-6203. DOI: `10.1371/JOURNAL.PONE.0213954`. URL: `https://journals.plos.org/plosone/article?id=10.1371/journal.pone.0213954`.

[59] S. Castegnaro et al. "A bio-composite racing sailboat: Materials selection, design, manufacturing and sailing". In: *Ocean Engineering* 133 (Mar. 2017), pp. 142–150. ISSN: 0029-8018. DOI: `10.1016/J.OCEANENG.2017.01.017`.

[60] F. Halimi et al. "Core modifications of sandwich panels fabricated by vacuum-assisted resin transfer molding". In: *Journal of Composite Materials* 47.15 (July 2013), pp. 1853–1863. ISSN: 00219983. DOI: `10.1177/0021998312451763`.

[61] Antoine Le Duigou et al. "PLLA/flax mat/balsa bio-sandwich manufacture and mechanical properties". In: *Applied Composite Materials* 18.5 (Sept. 2011), pp. 421–438. ISSN: 0929189X. DOI: `10.1007/S10443-010-9173-8/FIGURES/18`. URL: `https://link.springer.com/article/10.1007/s10443-010-9173-8`.

[62] Lennart Molenaar. *Design and optimization of FRP traffic decks considering uplift bolt forces: Based on analytical and numerical approaches*. 2022. URL: `https://repository.tudelft.nl/islandora/object/uuid%3Abc215c03-f041-406d-9439-c21f5295ca87`.

[63] Honglei Xie et al. "Flexural property evaluation of web reinforced GFRP-PET foam sandwich panel: Experimental study and numerical simulation". In: *Composites Part B: Engineering* 234 (Apr. 2022), p. 109725. ISSN: 1359-8368. DOI: `10.1016/J.COMPOSITESB.2022.109725`.

[64] Mohamad Tuffaha. *Form-Finding Framework for FRP Shells: A Multi-Step Structural Optimization Tool for Preliminary FRP designs*. Delft, Oct. 2019. URL: `https://repository.tudelft.nl/islandora/object/uuid%3A26451229-0bec-4629-8adf-b13d9d41cbe3`.

[65] F. C. (Flake C.) Campbell. "Structural composite materials". In: (2010), p. 612.

[66] P.K. Gotsis, C.C. Chamis, and L. Minnetyan. *Failure Criteria in Fibre-Reinforced-Polymer Composites*. Elsevier, 2004, pp. 703–725. ISBN: 9780080444758. URL: `http://www.sciencedirect.com:5070/book/9780080444758/failure-criteria-in-fibre-reinforced-polymer-composites`.

[67] Dassault Systèmes. *Abaqus User's Manual*. 2016. URL: `http://130.149.89.49:2080/v6.14/`.

[68] Nederlands Normalisatie-instituut. *NEN-EN 15251*. English. European Standard. The Netherlands, June 2007.

[69] Resoltech. *Resoltech 1800 ECO*. Product datasheet of Hardeners 1804 ECO, 1805 ECO & 1807 ECO. June 2021. URL: `https://www.resoltech.com/en/markets/1800-eco-detail.html`.

[70] A. Thuault et al. "Effects of the hygrothermal environment on the mechanical properties of flax fibres". In: *Journal of Composite Materials* 48.14 (June 2014), pp. 1699–1707. ISSN: 1530793X. DOI: `10.1177/0021998313490217/ASSET/IMAGES/LARGE/10.1177{\_}0021998313490217-FIG8.JPEG`. URL: `https://journals.sagepub.com/doi/10.1177/0021998313490217`.

[71] Michaël Berges et al. "Influence of moisture uptake on the static, cyclic and dynamic behaviour of unidirectional flax fibre-reinforced epoxy laminates". In: *Composites Part A: Applied Science and Manufacturing* 88 (Sept. 2016), pp. 165–177. ISSN: 1359-835X. DOI: `10.1016/J.COMPOSITESA.2016.05.029`.

[72] Hans Joachim Blaß and Carmen Sandhaas. *Timber Engineering: Principles for Design*. KIT Scientific Publishing, Karlsruher Institut für Technologie (KIT), 2017. ISBN: 978-3-7315-0673-7. DOI: `10.5445/KSP/1000069616`.

[73] World Commission on Environmental and Development. *Our Common Future*. Oxford: Oxford University Press, 1987. ISBN: 9780192820808.

[74] Seyed Meysam Khoshnava et al. "Rank of green building material criteria based on the three pillars of sustainability using the hybrid multi criteria decision making method". In: *Journal of Cleaner Production* 173 (Feb. 2018), pp. 82–99. ISSN: 0959-6526. DOI: `10.1016/J.JCLEPRO.2016.10.066`.

[75] Simon Erbe. "Development of a Sustainable Structural Concept for the Maun Science Park". PhD thesis. Konstanz: Hochschule Konstanz, University of Applied Science, Mar. 2021.

[76] *Digital tools for life-cycle assessment – Universität der Künste Berlin*. URL: `https://www.udk-berlin.de/studium/architektur/fachgebiete/konstruktives-entwerfen-und-tragwerksplanung/forschung/a-holistic-and-parametric-approach-for-lca-in-the-early-design-stages/`.

[77] *How to Include Biogenic Carbon in an LCA - WoodWorks | Wood Products Council*. URL: `https://www.woodworks.org/resources/how-to-include-biogenic-carbon-in-an-lca/`.

[78] Endrit Hoxha et al. "Biogenic carbon in buildings: a critical overview of LCA methods". In: *Buildings and Cities* 1.1 (2020), pp. 504–524. ISSN: 26326655. DOI: `10.5334/BC.46`.

[79] M. Spitsbaard and M.L.J. van Leeuwen. *De berekening achter Paris Proof Materiaalgebonden Emissies - Dutch Green Building Council*. Sept. 2022. URL: `https://www.dgbc.nl/publicaties/de-berekening-achter-paris-proof-materialgebonden-emissies-49`.

[80] L. Verstege. *Duurzaamheidsscan biocomposiet fietsbrug Ritsumasyl*. Tech. rep. De Bilt: Sweco Nederland BV and Witteveen+Bos B.V., Jan. 2020. URL: `https://www.drive.frl/wiki/duurzaamheidsscan-biocomposiet-fietsbrug-ritsumasyl/`.

[81] Richard C Hill and Paul A Bowen. "Sustainable construction: principles and a framework for attainment". In: *Construction Management and Economics* 15.3 (1997), pp. 223–239.

[82] Luis Orozco et al. "Arrangement of reinforcement in variable density timber slab systems for multi-story construction". In: *International Journal of Architectural Computing* 20.4 (Dec. 2022), pp. 707–727. ISSN: 20483988. DOI: `10.1177/14780771221135003`.

[83] Zoran Markovic. "Traditional Cultural Elements in Built Environment Design in Botswana Interior Design; Exterior Design; Built Techniques and Technologies Decorations". In: *University of Botswana* ().

[84] *Energiehotel, Ede - Noordereng Groep*. URL: `https://www.noorderenggroep.eu/projectontwikkeling/energiehotelede/`.

[85] ABT. *HoutKern Bouwmethode - ABT Adviseurs in bouwtechniek*. URL: `https://abt.eu/impact/circulair-in-de-toekomst/houtkern-bouwmethode/`.

[86] RDW. *Exceptioneel tranport | RDW*. URL: `https://www.rdw.nl/zakelijk/branches/exceptioneel-transport/ontheffing-aanvragen-voor-exceptioneel-transport/aanvragen-jaarontheffing`.

[87] Kurt Gieck and Reiner Gieck. *Roak's Formulas for Engineers*. 8th edition. New York, NY: McGraw-Hill Education, 2008.

[88] Saman Sayahlatifi, Gholamhossein Rahimi, and Alireza Bokaei. "Experimental and numerical investigation of sandwich structures with balsa core and hybrid corrugated composite/balsa core under three-point bending using digital image correlation". In: *Journal of Sandwich Structures and Materials* 23.1 (Jan. 2021), pp. 94–131. ISSN: 15307972. DOI: `10.1177/1099636218822333/ASSET/IMAGES/LARGE/10.1177{\_}1099636218822333-FIG20.JPEG`. URL: `https://journals.sagepub.com/doi/10.1177/1099636218822333`.

[89] S. Prabhakaran et al. "Sound and Vibration Damping Properties of Flax Fiber Reinforced Composites". In: *Procedia Engineering* 97 (Jan. 2014), pp. 573–581. ISSN: 1877-7058. DOI: `10.1016/J.PROENG.2014.12.285`.

[90] European Committee for Standardization. *Structural timber - Strength classes*. European Standard EN 338:2016. 2016. URL: `https://standards.iteh.ai/catalog/standards/cen/bc7d1689-9b89-4e23-8956-16c267d5b1e5/en-338-2016`.

[91] Robert J Ross and Forest Products Laboratory. USDA Forest Service. *Wood handbook : wood as an engineering material*. Tech. rep. 2010. DOI: `10.2737/fpl-gtr-190`. URL: `https://doi.org/10.2737%2Ffpl-gtr-190`.

[92] Yousef Saadati et al. "A Study of the Interlaminar Fracture Toughness of Unidirectional Flax/Epoxy Composites". In: *Journal of Composites Science 2020, Vol. 4, Page 66* 4.2 (June 2020), p. 66. ISSN: 2504-477X. DOI: `10.3390/JCS4020066`. URL: `https://www.mdpi.com/2504-477X/4/2/66/htm%20https://www.mdpi.com/2504-477X/4/2/66`.

[93] Yousef Saadati et al. "Study of translaminar fracture toughness of unidirectional flax/epoxy composite". In: *Composites Part C: Open Access* 1 (Aug. 2020), p. 100008. ISSN: 2666-6820. DOI: 10.1016/J.JCOMC.2020.100008.

[94] *CLTdesigner - CLTdesigner*. URL: https://www.cltdesigner.at/en/.

[95] *Kanaalplaatvloeren | VBI*. URL: https://www.vbi-techniek.nl/Kanaalplaat.

[96] L Verstege. *Duurzaamheidsscan biocomposiet fietsbrug Ritsumasyl*. Online. De Bilt, Jan. 2020. URL: https://www.drive.frl/wiki/duurzaamheidsscan-biocomposiet-fietsbrug-ritsumasyl/.

[97] Angela Daniela La Rosa et al. "Bio-based versus traditional polymer composites. A life cycle assessment perspective". In: *Journal of Cleaner Production* 74 (July 2014), pp. 135–144. ISSN: 0959-6526. DOI: 10.1016/J.JCLEPRO.2014.03.017.

[98] *High Biobased Laminating Epoxy - Entropy Resins*. URL: https://entropyresins.com/product/one-high-biobased-laminating-epoxy/.

[99] *ecoinvent Database - ecoinvent*. URL: https://ecoinvent.org/the-ecoinvent-database/.

[100] *EPD | X-LAM | Houtbouw | DERIX*. July 2022. URL: https://derix.de/nl/producten/bouwen-met-kruislaaghout/.

[101] *BioFoam® | BEWI*. URL: https://bewi.com/products/biofoam/.

[102] Lisa Stelzer et al. "Life Cycle Assessment of Fungal-Based Composite Bricks". In: *Sustainability 2021, Vol. 13, Page 11573* 13.21 (Oct. 2021), p. 11573. ISSN: 2071-1050. DOI: 10.3390/SU132111573. URL: https://www.mdpi.com/2071-1050/13/21/11573/htm%20https://www.mdpi.com/2071-1050/13/21/11573.

[103] *Environmental Product Declaration (A200) - VBI*. 2020. URL: https://vbi.nl/downloads-2/.

[104] *Quake*. URL: https://quake-innovation.eu/.

[105] *Hout co2 calculator*. URL: https://opslagco2inhout.nl/motivatie.

[106] *Prijslijst & Leveringsprogramma Iso Bouw*. May 2023. URL: https://www.isobouw.nl/media/gqaj5m4r/230001551-isobouw-prijslijst-woningbouw-nl-mei-2023-lr.pdf.

[107] *GROWN bio - Mycelium Block*. URL: https://www.grown.bio/product/mycelium-block/.

[108] *Houthandel Pieter Baks*. URL: https://www.pieterbaks.nl/vurenhout-klasse-c-c24-geschaafd-ronde-hoek-fsc-mix-70-95x195mm.

[109] *Isolatie kurkplaat - Kurk24*. URL: https://www.kurk24.nl/isolatie-kurkplaat-naturel-100-x-50-cm-50-mm.html?utm_campaign=Isolatie+kurkplaat+-+naturel+-+100+x+50+cm+-+50+mm&utm_content=&utm_source=googleshopping&utm_medium=cpc&utm_term=&gclid=CjwKCAjwivemBhBhEiwAJxNWNxSIV2u7eaRBAOV_EtIuoq3NnkhYI3eI6LWaRZHz4Xxyqm70AjaWchoC6pYQAvD_BwE.

[110] Nederlands Normalisatie-instituut. *NEN-EN 1990+A1:2006+A1:2006/C2:2019 Eurocode: Grondslagen van het constructief ontwerp*. Tech. rep. Delft, The Netherlands: Nederlands Normalisatie-instituut, 2019.

[111] Nederlands Normalisatie-instituut. *NEN-EN1991-1-1+C1+C11-NB: National Annex to Eurocode 1: Actions on structures - Part 1-1: General actions - Densities, self-weight, imposed loads for buildings*. Tech. rep. Delft, The Netherlands: Nederlands Normalisatie-instituut, 2019.

[112] "Point support of CLT Analysis sample and theoretical background". In: *Storaenso* (2014). DOI: 10.01.2014.

A
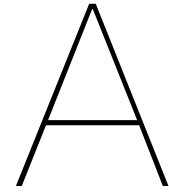
Property Tables

Table A.1: Potential applications of natural FRP adapted from [11]

Sector	Fibers	Applications
Civil construction	Banana	Compressed earth block
	Juce, sisal, ramie, pineapple	Cementitious materials
	Flax, jute, sisal, hemp, coir, palm	Masonry
	Jute	Deck panel
	Kenaf	Ceiling
	Wheat straw, corn husk	Thermal insulation materials
	Wood cellulose, cork	Thermal insulation materials
Furniture and architecture	Lignocellulose, straw	Lounge furniture
	Hemp	Chair furniture
	Hemp. flax	Ignot bio- and Polycal acoustic panel
	Lignocellulose	BioMat research pavilion
Sports and clothes	Hemp. jute, bamboo. sugarcane bagasse, coconut banana	Footwear
	Flax, hemp	Racing bicycle
	Flax	Bicycle frame
	Jute	Winter overcoat
	June. sisal, coconut areca, banana	Helmet shell
	Kenaf	Ballistic armor materials mobile phone casing
	Kenaf, pineapple	Recurve bow
	Palm	Sports utility
Aerospace	Hemp	Electronics racks for helicopter
	Ramie	Aircraft wing boxes
	Kenaf	Aircraft materials
Biomedical and pharmaceutical	Sugarcane	Drugs, antimicrobial, antibiotics
	Flax, ramie	Bone grafting orthopedic implants
	Hemp. sisal, coir	Orthoses materials
	Jute	Enzyme
	Jute, sugarcane, flax, bamboo	Biomedical nanoparticles, antibiotics
	Sisal	Drug delivery
Others	Bamboo	Packaging
	Banana, bamboo, flax, jute, kenaf, palm, sisal	Dielectric materials
	Flax	Electrodes
	Flax, june, coir, sisal	Wind turbine blades
	Flax, seagrass	Marine materials
	June	Solar parabolic trough collector
	June, flax, kenaf, hemp	EMI shielding
	Wood cellulose	Battery

Table A.2: Properties of several natural fibers and commonly used synthetic fibers adapted from [30]

Fiber	Density [g/cm^3]	Elongation [%]	Tensile strength [MPa]	Young's modulus [GPa]
Abaca	1.5	-	980.0	-
Bagasse	1.2	1.1	20.0-290.0	19.7-27.1
Banana	1.3-1.4	2.0-7.0	54.0-789.0	3.4-32.0
Coconut	1.4-3.8	-	120.0-200.0	19.0-26.0
Coir	1.2	15.0-30.0	175.0-220.0	4.0-6.0
Cotton	1.5-1.6	3.0-10.0	287.0-597.0	5.5-12.6
Flax	1.4-1.5	1.2-3.2	345.0-1500.0	27.6-80.0
Hemp	1.4-1.5	1.6	550.0-900.0	70.0
Henequen	1.4	3.0-4.7	430.0-580.0	-
Jute	1.3-1.5	1.5-1.8	393.0-800.0	10.0-30.0
Kenaf	1.2	2.7-6.9	295.0	-
Palf	1.4	3.0	170.0-635.0	6.2-24.6
Pineapple	1.5	2.0-3.8	220.0-938.0	44.0-128.0
Ramie	1.5	2.0-3.8	220.0-938.0	44.0-128.0
Sisal	1.3-1.5	2.0-14.0	400.0-700.0	9.0-38.0
Softwood kraft	1.5	-	1000.0	40.0
Carbon	1.4	1.4-1.8	1500.0-5500.0	230.0-240.0
E-glass	2.5	2.5-3.0	2000.0-3500.0	70.0
S-glass	2.5	2.8	4570.0	86.0
Kevlar	1.4	3.3-3.7	3000.0-3150.0	63.0-67.0

Table A.3: Mechanical properties for BFRP with flax fibers adopted from [40], Bi = bi-axial, Vf = fiber content, ϵ = failure strain, σ_t = tensile strength, E_y = Stiffness/Young's modulus, σ_f = flexural strength, E_f = Flexural modulus (GPa), RTM = resin transfer molding, MAA-PP = maleic acid anhydride modified PP, CM = compression molding

fiber	Matrix	Vf (m%)	ϵ (%)	σ_t (MPa)	E_y (GPa)	σ_f (MPa)	E_f (GPa)	Notes
UD	Epoxy	46/54	0,7-0,9	280/279	35/39			Artic Flax, Enzyme extracted RTM
UD (yarn)	Epoxy	45				311	25	Alkali treatment and pre-impreganation
UD (yarn)	Epoxy	∼31		160	15	190	15	Hand lay-up
UD (yarn)	Epoxy	45		133	28	218	18	Autoclave
UD (yarn)*	Bio-Epoxy	50		166	24			Ritsumasyl Bridge with bio-epoxy of 33% bio-content [35]
UD (sliver)	Epoxy	∼28				182	20	Pultruded
UD (yarn)	VE	∼24	1,5	248	24			RTM
UD (sliver)	UP	∼58		304	30			Soxhlet extracted Vacuum impregnated/CM
UD (yarn)	UP	∼34	1,3	143	14	198	17	RTM
UD (yarn)	PP	72		321	29			Filament wound
UD (yarn)	PP	30		89/70	7/6			Pultruded
UD	PP	50		40	7			Needle punched
UD	PP	39				212	23	Dew retted, boiled, MAA-PP coupled
UD (sliver)	PP	44				146	15	Wrap spun hybrid yarn
UD (hackled)	PLA	∼30	1	53	8,3			Pultruded
UD (hackled)	PLA	∼40	0,9	44	7,3			Pultruded
Bi (sliver)	Epoxy	∼46		200	17	194	13	Weft:warp strength 10:1
Bi (yarn)	Epoxy	∼50		104	10			Sized and dried prior to pre-preg
Bi (yarn)	VE	∼35	1.8	111	10	128	10	RTM

*This data is adapted from the design report of the Ritsumasyl bridge.

The properties are design values instead of test results.

Table A.4: Bio-based sandwich panels with properties

	σ_{skin} [MPa]	τ_{core} [MPa]	$E_{flexural}$ [GPa]	ρ [kg/m^3]
Jute (15%)/PP skins + Balsa core (15mm)	20.0		0.9	
Jute (15%)/PP skins + Balsa core (25mm)	12.9		0.8	
PP laminate skins + Balsa core (15mm)	15.9		0.6	
Flax fiber skins (~0.8mm) + Plywood core (~10mm)	46.8		26.3	488
3-ply wood veneer skin + Sisal reinforced PP -HC core	31.9	1.3		
Piassava skins + Sawdust HC core	73.3	1.4	4.3	
Spruce wood skins + Square Jute -HC core		0.9		
Multiplex skin + Bamboo HC core	9.9			
Flax skins + Bamboo HC (Ø30mm) core	48.4	0.9	4.2	391
Wood /PLA gyroid panel (2.5mm skin/5mm core)	11.8		2.5	658
Flax fiber skins + PLLA /Balsa core	70.5	2.7		617
Paper skin (~0.7mm) + Pulp fibers/PLA core (~8.5mm)	38.1		3.1	439
All - PLA additive manufactured panel	60.7		2.2	649
Flax/PLA skin + PLA - HC core (10mm)	33.1	0.7		362
Flax/PLA skin + PLA - HC core (20mm)	31.4	0.6		279
Flax/PLA skin + PLA - HC core (30mm)	14.7	0.3		164

B

Structural Loads and Limit States

Load Combinations

Eurocodes and national annexes of each country regulate the structural design of European buildings. The limit state design principle is used to evaluate the state of a structure as either satisfactory or unsatisfactory based on whether it meets the limit state design criteria. EN 1990 (Basis of Structural Design) of Eurocode defines two types of limit states that relate to structural safety and usability requirements:

- The Ultimate Limit State (ULS) involves the risk of collapse or other failures that jeopardize personal safety due to instabilities, excessive deformations, or rupture of structural elements.

- The Serviceability Limit State (SLS) refers to deformations that affect a structure's appearance, comfort level, or planned functionality, disrupt its normal use, cause damage, or have long-term effects on its durability.

The structural design process should ensure a sufficiently low probability of failure. Therefore, partial safety factors are used for actions and loads. Table B.1 shows the partial safety factors for ULS considering consequence class 2 for buildings.

Table B.1: Partial safety factors for ULS and SLS

Design	Permanent		Variable	
Load combination	Unfavourable	Favourable	Dominant	Accompanying
ULS (1)	$1.35\ G_{k,j,sup}$	$0.9\ G_{k,j,inf}$	$1.5\ \psi_{0,1}\ Q_{k,1}$	$1.5\ \psi_{0,i}\ Q_{k,1}\ (i{>}1)$
ULS (2)	$1.2\ G_{k,j,sup}$	$0.9\ G_{k,j,inf}$	$1.5\ Q_{k,1}$	$1.5\ \psi_{0,i}\ Q_{k,1}\ (i{>}1)$
SLS	$1.0\ G_{k,j,sup}$	$1.0\ G_{k,j,inf}$	$1.0\ Q_{k,1}\ (i{>}1)$	$1.0\ \psi_{0,i}\ Q_{k,1}\ (i{>}1)$

ψ_0, ψ_1, and ψ_2 are the combination factors applied to variable actions to determine their combination value, as per EN 1990 [110]. The factors for Category C: meeting rooms can be seen in Table B.2.

Table B.2: ψ-factors for buildings according to EN1990 [110]

ψ_0	ψ_1	ψ_2
0.4	0.7	0.6

From NEN-EN1991-1-1 the live load is set and can be seen in Table B.3 [111]. The concentrated force must be applied over an area of 100x100mm.

Table B.3: Live loads according to NEN-EN1991 [111]

	q_k kN/m^2	Q_k kN
Class C - Assembly Rooms	5	3

,ine

Ultimate Limit State

For sandwich panels, the partial factors for the resistance model, γ_{Rd}, as specified in FRP Eurocode should be used [22]. The partial material factor depends on the sample size of the data used and is discussed in section 8.6. For structural timber that is strength graded with rectangular cross-section, the partial material factor is $\gamma_M = 1.3$.

Table B.4: Partial factors for resistance models

Composite material failure	Core material failure	Global buckling	Local buckling	Face sheet/ web wrinkling	Core indentation	Core punching failure
1.40	1.50	1.40	1.30	1.50	1.50	1.50

Serviceability Limit State

Deflection

The maximum allowable deflection of floors is given in Table B.5. Figure B.1 shows a schematic overview of the deflections.

- w_c = sag of not loaded element
- w_1 = initial deflection due to permanent loads determined for the relevant load combination by formulas through using short-term properties
- w_2 = additional deflection due to long-term behavior, equal to the deflection under the quasi-permanent load combination determined using long-term properties, reduced by the deflection under the quasi-permanent load combination determined using short-term properties
- w_3 = additional deflection due to short-term behavior, equal to the deflection resulting from the loads in the relevant load combination determined using short-term properties, reduced by w1
- w_{tot} = total deflection as the sum of w1, w2, and w3
- w_{max} = maximum deflection, taking into account the sag, wtot - wc
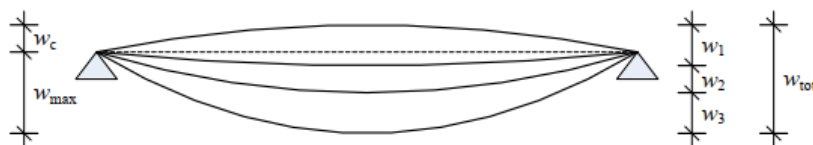
Figure B.1: Allowed vertical deflection [110]

Table B.5: Allowed vertical deflection

Type	Allowed additional deflection ($w_2 + w_3$) [*l_{rep}]	Allowed final deflection (w_{max}) [*l_{rep}]
Floors with people	0.003	0.004
Floors with crack-sensitive partitions	0.002	0.004
Floor partitions at height differences	0.0067	0.0067

As per the Eurocode for FRP, assuming linear relationships between actions and deformations, the deflection of members with components exhibiting the same creep behavior can be calculated for various combinations of actions [22]. Equations B.1, B.2, and B.3 provide the combinations of actions for characteristic, frequent, and quasi-permanent combinations of actions [110].

Characteristic action combination

$$w_2 = \left(w_{G_k} + \sum_j \psi_{2,j} \cdot w_{Q_{k,j}} \right) \cdot \phi(t)$$

$$w_3 = w_{Q_{k,1}} + \sum_{j>1} \psi_{0,j} \cdot w_{Q_{k,j}}$$

(B.1)

Frequent action combination

$$w_2 = \left(w_{G_k} + \sum_j \psi_{2,j} \cdot w_{Q_{k,j}} \right) \cdot \phi(t)$$

$$w_3 = \psi_{1,1} \cdot w_{Q_{k,1}}$$

(B.2)

Quasi-permanent action combination

$$w_1 = w_{G_k}$$

$$w_2 = \left(w_{Gk} + \sum_j \psi_{2,j} \cdot w_{Qk,j} \right) \cdot \phi(t)$$

(B.3)

where $\psi_{i,j}$ are combination factors and $\phi(t)$ the creep conversion factor.

Vibration

The following paragraphs outline the calculations necessary for verification of the vibration criteria. Unless specified differently, all equations and values are adapted from EN1995-1-1 chapter 9 [24].

Frequency criteria

To derive the fundamental frequency of a floor that is approximately rectangular in the plane is a single- or double-span floor and directly rests on rigid supports while primarily subjected to uniform loading, Equation B.4 can be utilized.

$$f_1 = k_{e,1} k_{e,2} \frac{\pi}{2l^2} \sqrt{\frac{(EI)_L}{m}}$$

(B.4)

with

$$k_{e,2} = \sqrt{1 + \frac{\left(\frac{l}{b}\right)^4 (EI)_T}{(EI)_L}}$$

(B.5)

- $k_{e,1}$ = frequency factor (1 for single span and double span with b=l)
- $k_{e,2}$ = frequency factor (1 for single span)
- l = (longer) floor span
- $(EI)_L$ = bending stiffness along floor span per meter width
- $(EI)_T$ = bending stiffness transverse to floor span per meter width
- m = mass per unit area
- b = floor width

Equation B.6 can be employed to calculate the frequency of a single span floor elastically supported on a beam at one or both ends.

$$f_1 = \sqrt{\frac{1}{\frac{1}{f_{1,\text{ rigid}}^2} + \frac{1}{3f_{1,\text{ beam},1}^2} + \frac{1}{3f_{1,\text{ beam},2}^2}}}$$
(B.6)

- $f_{1,\text{ rigid}} = f_1$ when on rigid supports
- $f_{1,\text{ beam, 1}} = f_1$ of supporting beam on side 1
- $f_{1,\text{ beam, 2}} = f_1$ of supporting beam on side 2

Stiffness criteria

The maximum deflection caused by a vertical static point load, F = 1 kN, located in the most unfavorable position where the corresponding vibration mode reaches its maximum amplitude in a single span floor strip with an effective width, must satisfy the criteria specified in Table 7.8. When the point load is positioned in the middle of a simple supported single-span floor, Equation B.7 can be used to determine the deflection.

$$w_{1\text{kN}} = \frac{Fl^3}{48(EI)_L b_{\text{ef}}}$$
(B.7)

- b_{ef} = effective width. The effective width can be determined using Equation B.8 for a uniform transverse bending stiffness.

$$b_{\text{ef}} = \min\left\{0,95l\left(\frac{(EI)_T}{(EI)_L}\right)^{0,25}; B\right\}$$
(B.8)

The same approach may be used for a floor on elastic supports as for the fundamental frequency. The total deflection due to a 1 kN static load is determined by Equation B.9.

$$w_{1\text{kN}} = 0,5w_{\text{beam},1} + 0,5w_{\text{beam},2} + w_{\text{rigid}}$$
(B.9)

- w_{rigid} = deflection of the floor between rigid supports by 1 kN load
- $w_{\text{beam, 1}}$ = deflection of supporting beam 1 by 0.5 kN load
- $w_{\text{beam, 2}}$ = deflection of supporting beam 2 by 0.5 kN load

C
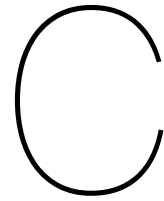
Verification Calculations

Concentrated load between webs

```python
# Maximum bending stress one-way

def conc_load_one_way_max_stress(web_spacing, facing_thickness):
    """Determine maximum bending stress resulting from a concentrated load between two webs.

    Args:
        web_spacing (float): distance between the two webs representing the length of the
    beam in mm
        facing_thickness (float): thickness of the facing in mm

    Returns:
        float: maximum bending stress
    """
    conc_load_area = 100 # mm
    I = 1/12 * conc_load_area * facing_thickness ** 3

    conc_load_kN = 1.5 * 3 # kN with partial factor
    conc_load_N = conc_load_kN * 1000 # N
    conc_load_distributed = conc_load_N / (conc_load_area**2) # N/mm2

    q = conc_load_distributed * conc_load_area #  N/mm
    a = (web_spacing - conc_load_area) / 2 #  mm
    R = (q * conc_load_area) / 2 #  N
    M_max = R * (a + R / (2*q)) #  Nmm
    sigma_max = M_max * (facing_thickness / 2) / I  # N/mm2

    return sigma_max


# Maximum bending stress two-way

def conc_load_two_way_max_stress(web_spacing, facing_thickness):
    """Determine maximum bending stress resulting from a concentrated load between 4 webs in
    a two-way floor. Using Roark approximations for uniform plates.

    Args:
        web_spacing (float): distance between the two webs representing the length of the
    beam in mm
        facing_thickness (float): thickness of the facing in mm

    Returns:
        float: maximum bending stress
    """
    conc_load_kN = 1.5 * 3 # kN with partial factor
    conc_load_N = conc_load_kN * 1000 # N

    a1 = 100 # mm
    b1 = 100 # mm
```

```
46
47      a = web_spacing # mm
48      b = web_spacing # mm
49
50      beta = roak_beta(a1 / b, b1 / b) # Roark's constant
51
52      sigma_max = beta * conc_load_N / (facing_thickness**2)
53
54      return sigma_max
55
56
57  def roak_beta(a1b,b1b):
58      """linear interpolation between Roark's constants to find beta
59
60      Args:
61          a1b (float): a1 / b: selects column to look in
62          b1b (float): b1 / b: selects row to look in
63
64      Returns:
65          float: beta
66      """
67
68      param_lst = np.arange(0,1.01,0.2)
69
70      beta_lst = np.array([[0,1.82,1.38,1.12,0.93,0.76],
71                          [1.82,1.28,1.08,0.90,0.76,0.63],
72                          [1.39,1.07,0.84,0.72,0.62,0.52],
73                          [1.12,0.9,0.72,0.6,0.52,0.43],
74                          [0.92,0.76,0.62,0.51,0.42,0.36],
75                          [0.76,0.63,0.52,0.42,0.35,0.3]])
76
77      for i in range(len(param_lst)-1):
78          if a1b >= param_lst[i] and a1b < param_lst[i+1]:
79              colidx = i
80          if b1b >= param_lst[i] and b1b < param_lst[i+1]:
81              rowidx = i
82
83      beta = beta_lst[rowidx,colidx] + (beta_lst[rowidx+1,colidx]-beta_lst[rowidx,colidx])/0.2
84      * (b1b - param_lst[rowidx]) + (beta_lst[rowidx,colidx+1]-beta_lst[rowidx,colidx])/0.2 * (
85      a1b - param_lst[colidx])
86
87      return beta
```

Listing C.1: Concentrated load between webs

Deflection

```
1   def SLS_deflection_check(deflection_input, design_life:int, span_floor:int = 3500):
2       """Check of deflection according to Eurocode including creep deformation
3
4       Args:
5           deflection_input (DataFrame): Dataframe of the deflections per time step from Abaqus.
6           Note that the time step of 1.5s corresponds to the gravity + permanent load being
       applied
7           and time step 2s corresponds to the gravity + permanent load + variable load being
       applied
8           design_life (int): 15, 50, or 100 years for the creep factors corresponding to QI lay
       -up
9           span_floor (int, optional): _description_. Defaults to 3500 in mm
10
11      Raises:
12          NotImplementedError: design life does not exist
13
14      Returns:
15          _type_: statement about meeting criteria with the criteria and actual deflection
16      """
17
18      step_permanentload = deflection_input['time'] == 2
19      row_index_permanentload = np.where(step_permanentload)[0][0]
```

```
20     deflection_permanentload = abs(deflection_input.iloc[row_index_permanentload]['deflection
       '])
21
22     step_variableload = deflection_input['time'] == 4
23     row_index_variableload = np.where(step_variableload)[0][0]
24     deflection_variableload = abs(deflection_input.iloc[row_index_variableload]['deflection'
       ]) - deflection_permanentload
25
26     if design_life == 15:
27         creep_factor = creep.QI_15_deflection
28     elif design_life == 50:
29         creep_factor = creep.QI_50_deflection
30     elif design_life == 100:
31         creep_factor = creep.QI_100_deflection
32     else:
33         raise NotImplementedError('Design life does not exist')
34
35     w_1 = deflection_permanentload
36     #  Characteristic action combiation
37     w_2_char = (deflection_permanentload + factor.phi_2 * deflection_variableload) *
       creep_factor
38     w_3_char = deflection_variableload
39
40     #  Frequent action combination
41     w_2_freq = (deflection_permanentload + factor.phi_2 * deflection_variableload) *
       creep_factor
42     w_3_freq = factor.phi_1 * deflection_variableload
43
44     #  Quasi-permanent action combination
45     w_2_quasi = (deflection_permanentload + factor.phi_2 * deflection_variableload) *
       creep_factor
46
47     w_additional = max(w_2_char + w_3_char, w_2_freq + w_3_freq, w_2_quasi)
48     w_additional_criteria = 0.003 * span_floor  #  in mm
49
50     w_max = max(w_1 + w_2_char + w_3_char, w_1 + w_2_freq + w_3_freq, w_1 + w_2_quasi)
51     w_max_criteria = 0.004 * span_floor  #  in mm
52
53     criteria_1 = 'meets additional deflection criteria of' if w_additional <
       w_additional_criteria else 'does not meet criteria of'
54     criteria_2 = 'meets maximum deflection criteria of' if w_max < w_max_criteria else 'does
       not meet criteria of'
55
56     overview_deflection_checks = pd.DataFrame([[criteria_1, w_additional_criteria,
       w_additional, criteria_2, w_max_criteria, w_max]], columns=['Additional','Criteria', '
       Additional deflection', 'Maximum', 'Criteria', 'Maximum criteria'])
57
58     return overview_deflection_checks
```

Listing C.2: Global deflection verification

D
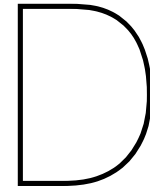
Case Study Designs

CLT

The one-way CLT floor uses CLTDesigner for the basic Eurocode checks and compression checks perpendicular to the grain due to a concentrated load [94]. The punching shear resistance check is done manually using the prEN1995.

As for the applied loads, CLTDesigner includes the self-weight of the floor. The permanent load and variable load are applied manually. This is 0.8 kN/m^2 for the finishing floor 3 kN/m^2, and 3 kN for the variable load. This is the same as for the CLT floor in the Natural Pavilion. The partial safety factors ar γ_G = 1.2 and γ_Q = 1.5. These are the partial factors of the governing loading combination since only that one is considered for the BFRP floors.

Table D.1, D.2, and D.3 provide the material data for the selected CLT floor.

Table D.1: Layer composition of one-way CLT floor

Layer	Thickness	Orientation	Material
# 1	20 mm	0º	C24-DERIX-ETA 2019
# 2	30 mm	90º	C24-DERIX-ETA 2019
# 3	20 mm	0º	C24-DERIX-ETA 2019
# 4	30 mm	90º	C24-DERIX-ETA 2019
# 5	20 mm	0º	C24-DERIX-ETA 2019

Table D.2: Material properties for CLT floor C24-DERIX-ETA 2019 with γ_M = 1.25 and k_{sys} = 1.2

Material properties	C24-DERIX -ETA 2019	Material properties	C24-DERIX -ETA 2019
Bending strength [MPa]	k_{sys}·24	Youngs modulus parallel [MPa]	11000
Tensile strength parallel [MPa]	14.5	5% Youngs modulus parallel [MPa]	9166
Tensile strength perpendicular [MPa]	0.4	Youngs modulus perpendicular [MPa]	370
Compressive strength parallel [MPa]	21.0	Shear modulus [MPa]	690
Compressive strength perpendicular [MPa]	2.5	Rolling shear modulus [MPa]	50
Shear strength [MPa]	2.5	Density [kg/m³]	350
Rolling shear strength [MPa]	1.1	Density mean value [kg/m³]	450

Table D.3: Cross-sectional values for CLT floor C24-DERIX-ETA 2019

Cross-sectional parameters	Values
EA_{eff} [N]	$6.6 \cdot 10^8$
EI_{eff} [Nmm^2]	$1.122 \cdot 10^{12}$
GA_{eff} [N]	$8.308 \cdot 10^6$

General ULS and SLS checks

Figure D.1 provides the results for the ULS checks from CLTDesigner. Table D.4 and D.5 show the results for the SLS checks. All checks correspond to NEN EN 1995-1-1:2005/NB:2013. The results provided summarize the critical values from the full report of CLTDesigner.
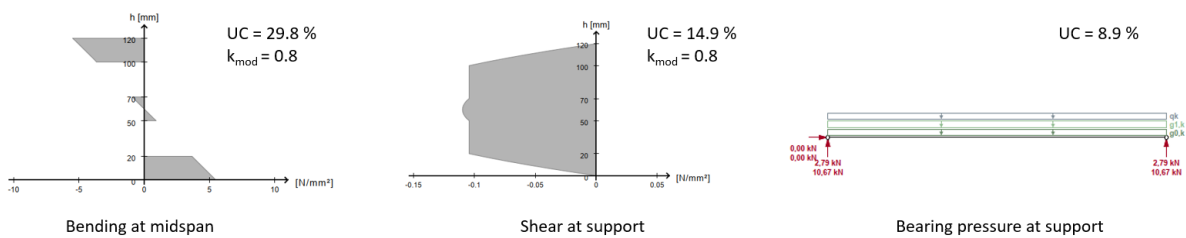
Figure D.1: ULS checks of CLTDesigner for one-way CLT floor

Table D.4: SLS deflection checks of CLTDesigner for one-way CLT floor

Check	Value	Limit	UC
Instantaneous deformation winst t = 0:	8.3 mm	L/300	71.5 %
Final deformation wnet,fin t = inf:	11.8 mm	L/250	84.1%
Final deformation wfin t = inf:	11.8 mm	L/150	50.5 %
Final deformation wnet,fin - winst,G t = inf:	9.2 mm	L/333	87.7 %

Table D.5: SLS vibration checks of CLTDesigner for one-way CLT floor

Check	Value	Limit
Fundamental frequency (f_1)	17.58 Hz	> 8.0 Hz
Stiffness (w_{1kN})	0.901 mm	< 2.00 mm
Velocity/Unit impuls (v)	10.283 mm/s	< 237.92 mm/s
Governing UC	45.5 %	

Concentrated load checks

Even though beams and not columns support the one-way floor, resistance against concentrated loads should be checked. The concentrated load is 3kN with a partial factor of 1.5 over 100x100mm.

Compression perpendicular to grain

Compression perpendicular to the grain is checked using CLTDesigner. The spreading angle is set to 35 degrees conform prEN1995 (8.1.6) [24].
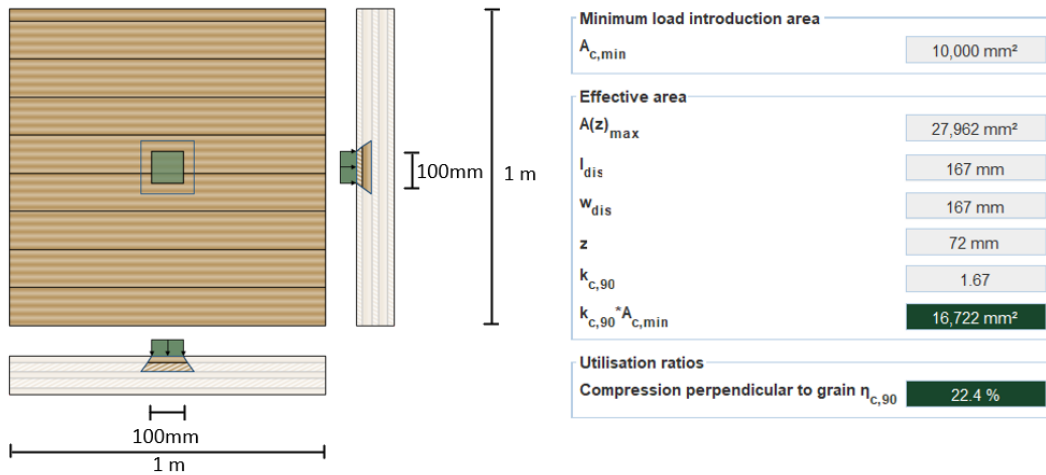
Figure D.2: Compression perpendicular to the grain of CLTDesigner for one-way CLT floor

Punching shear check

Concentrated loads perpendicular to the plane without reinforcement should be checked. Equation D.1 should be satisfied according to prEN1995 appendix G.3.

$$\tau_{\text{rd}} \leq k_{\text{r,pu}} f_{\text{r,d}} \tag{D.1}$$

where $k_{\text{r,pu}}$ is 1.6 for CLT accounting for non-linear behavior and strength combinations.

The rolling shear stress has to be determined at the perimeter representing a 35-degree angle till half the height of the floor, as outlined in prEN1995 Figure G.1. The spreading area and dimensions considered in this verification can be seen in Figure D.3.
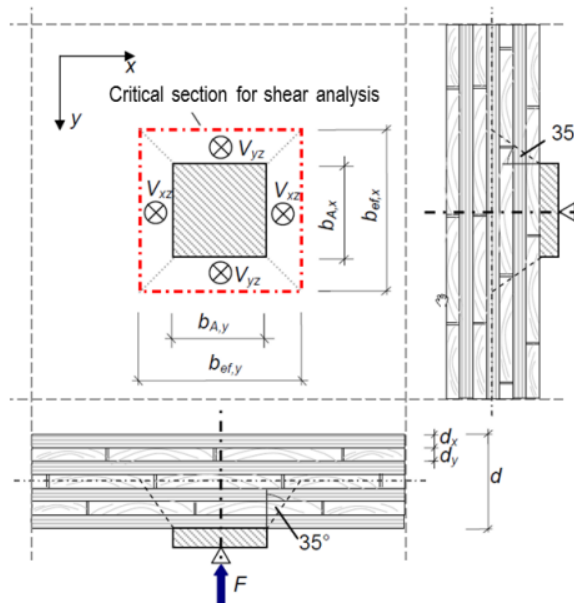
Figure D.3: Spreading area for punching shear analysis adapted from [112]

The equations employed for determining the perimeter, shear force, and design shear stress within the critical cross-section are provided below. These formulas have been adapted from [112]:

$$V_{xz} \approx 0.33 \cdot n^{-0.1} \cdot F \tag{D.2}$$

$$V_{yz} \approx 0.5 \cdot F - V_{xz} \tag{D.3}$$

$$b_{ef,x} = b_{ef,y} = b_{A,x} + d \cdot \tan 35° \tag{D.4}$$

$$\tau_{R,xz} = \frac{V_{xz}/b_{ef,x}}{k_{R,x} \cdot (d_x + d_y)} \tag{D.5}$$

with $k_{R,x}$ is 2 corresponding to 5 layers.

$$\tau_{R,yz} = \frac{V_{yz}/b_{ef,y}}{k_{R,y} \cdot (d_x + d_y)} \tag{D.6}$$

with $k_{R,y}$ is 1 corresponding to 5 layers.

Table D.6 provides the punching shear resistance check results for the one-way CLT floor using prEN1995 appendix 5 and [112]. It can be concluded that the punching shear resistance is not governing.

Table D.6: Punching shear resistance results of CLT floor

Parameter	Value
$b_{eff,x}$	184 mm
$b_{eff,y}$	184 mm
V_{xz}	1264 N
V_{yz}	986 N
$\tau_{r,xz}$	0.07 MPa
$\tau_{r,yz}$	0.20 MPa
f_{rk}	1.1 MPa (Derix) / 0.7 MPa (prEN1995)
UC	**0.11 / 0.18**

Conclusion

To conclude, deflection governs the design of the one-way CLT floor. Secondly, as highlighted in the main report, fire resistance has not been considered in this analysis. Due to the relatively thin nature of the one-way CLT, it becomes essential to assess its fire resistance in real-world applications.

Concrete
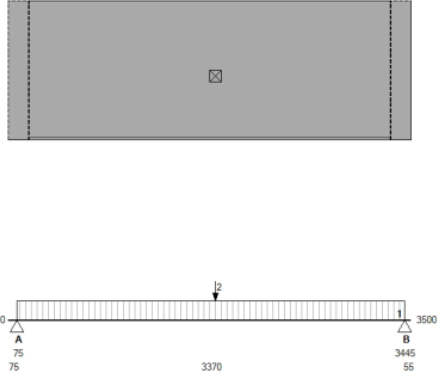
This section pertains to the design verifications conducted for the concrete floors. Specifically, it addresses the design considerations for both one-way floors, involving hollow core slabs and in-situ flat slabs, as well as for two-way concrete slabs.

One-way

Hollow core slab

Choosing and validating the concrete hollow core slab is facilitated by utilizing the VBI hollow core slab calculator [95]. The design methodology draws upon the guidelines stipulated in NEN-EN 1990, NEN-EN 1991-1-1, NEN-EN 1992-1-1, and NEN-EN 1168. Insights regarding this procedure are documented in the VBI calculation sheet that can be seen in Figure D.4. It is noteworthy that the load cases under consideration align with those employed for the analysis of the Natural Pavilion.

ProjectNr.	Element	Elementtyp	Lengte	Breedte	Belastingsfase	Datum Berekend	Wapening
-	Kanaalplaat 1	HL200	3500 mm	1200 mm	Gebruik	31-07-2023	D8-D1

Algemeen

Gevolgklasse	CC1
Ontwerplevensduur	50 jaar
Milieuklasse onder	XC1
XXConstructieklasse	S1
Brandwerendheid	geen
Sterkteklasse	C35/45
Betondekking onderzijde	23 mm

Belastingen

Belastingcategorie	A
Ψ-factoren	Ψ_0: 0.40 Ψ_1: 0.70 Ψ_2: 0.60
Eigen Gewicht	2.83 kN/m²
Druklaag	0.75 kN/m²
Afwerking	0.00 kN/m²
Opgelegd	0.94 kN/m²
Verpl. Scheidingswanden	0.00 kN/m²

Druklaag

Samengestelde doorsnede	constructief
Dikte (L-M-R)	30 - 30 - 30 mm
Kwaliteit	C30/37
Basis wapeningsnet #	Ø5-150 mm
Montagejuk	Geen

Oplegging

	A	B
F_{rep} permanent	7.2	7.2 kN
F_{rep} variabel	9.3	9.4 kN
Niet bedoelde inkl.mom.	nee	nee
Druklaag loopt tot	Wand	Wand
Opleglengte (a)	180	180 mm

Extra Belastingen

Nr	T	S	Grootte	Eenh	Ψ_0	Ψ_1	Ψ_2	Begin	Afm	Eenh
1	Q		3.55	kN/m¹	0.40	0.70	0.60	75	3370	mm
2	Q		3.00	kN	0.40	0.70	0.60	1800		mm

Doorbuiging

	Optr.	Toel.	Eenh.
Veld bijkomend	0	7	mm
Veld totaal	-1	14	mm

Momenten Positief

	Pos.	Optr.	Toel.	Eenh.
Gebruik	1800	18.95	52.12	kNm
Scheurmoment (doorbuiging)	1800	11.59	56.88	kNm
Karakteristiek	1800	15.26	56.88	kNm

Scheurbeheersing

	Pos.	Optr.	Toel.	Eenh.
Toename Staalsp. onder	1800	0	275	N/mm²

Dwarskrachten

	Pos.	Optr.	Toel.	Eenh.
Gebruik	191 (100)	19.16	67.18	kN
Gebruik	3310 (3400)	-19.05	-66.75	kN
Gebruik	1799 (1799)	1.55	71.12	kN
Gebruik	1801 (1801)	-2.52	-70.41	kN
Afschuiving Druklaag	100	0.056	0.406	N/mm²
Afschuiving Druklaag	3400	0.056	0.406	N/mm²

Figure D.4: VBI concrete hollow core slab calculation sheet [95]

In-situ flat slab

For the concrete flat slab spanning in one direction, the determination of both bottom and top reinforcement is necessary. As explained in subsection 9.2.2, the main grid reinforcement is 150Ø8.

The floor has to resist the maximum bending moment at the midpoint of the span of $\frac{1}{8}(q + q_{self})l^2 = \frac{1}{8} \cdot (10.8 + 4.4) \cdot 3.5^2 = 23.3$ kNm/m. Using the formulas below, the required reinforcement is determined for a height of 160 mm. This results in a UC of 0.91.

$$d_x = h_{\text{concrete}} - c_{\text{cover}} - \frac{1}{2}\varnothing_x \tag{D.7}$$

$$d_y = h_{\text{concrete}} - c_{\text{cover}} - \varnothing_x - \frac{1}{2}\varnothing_y \tag{D.8}$$

$$d = (d_x + d_y)/2 \tag{D.9}$$

$$\text{Reinforcement required} = \frac{M}{z \cdot f_{yd}} = 307 \text{ mm}^2/\text{m} \tag{D.10}$$

Table D.7: Geometry concrete one-way flat slab floor design

In-situ two-way slab	
h_{concrete}	160 mm
l	3.5 m
c_{cover}	20 mm

Two-way

The NEN6720 moments distribution method for flat slabs is utilized to determine the required reinforcement. This code addresses moment distribution under varying boundary conditions. However, the boundary conditions of the Natural Pavilion diverge from those covered by NEN6720. Consequently, a scenario where the floor is divided into two sections, each located between four columns, is assumed. Three edges remain free in one of these sections, while the fourth edge is supported, constraining rotational and vertical deformation. Refer to Figure D.5, where the dashed line corresponds to the free edges, and the dashed-dotted line denotes the restrained edge. The circular markers represent the columns. Utilizing the constants provided in NEN6720, the critical bending moment range in every floor zone can be determined. The outcomes are shown in Figure D.5.
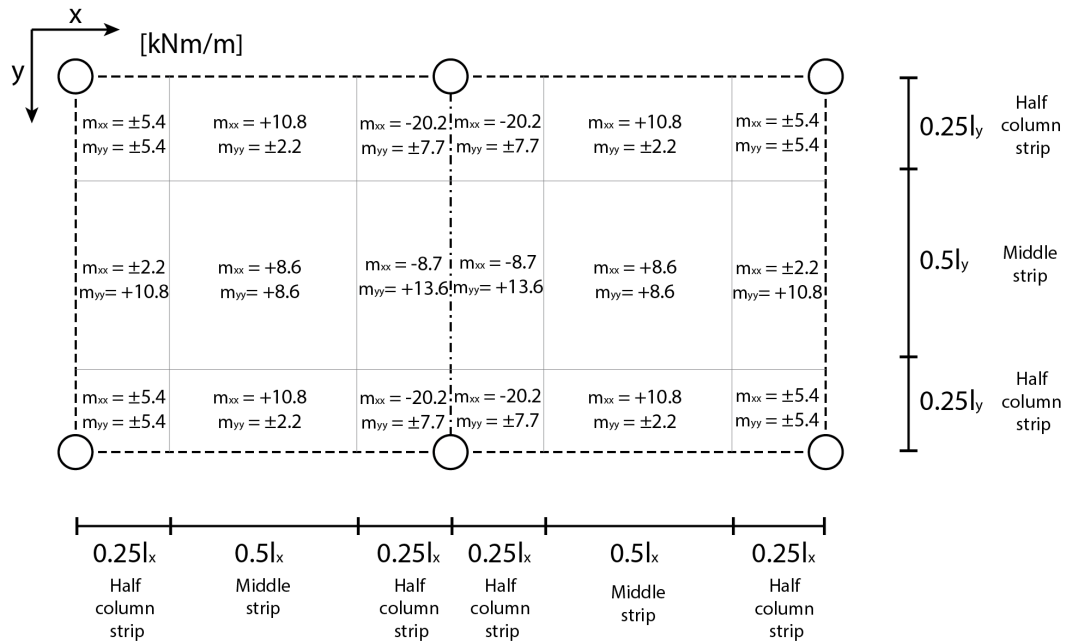
Figure D.5: Moment distribution for two-way concrete flat slab in kNm/m

The moment distribution is used to check whether the ø8 - 150 mm grid is sufficient. This calculation depends on the slab's thickness, determining the moment arm within the cross-section. According to Eurocode, the moment arm is assumed to be $z = 0.9d$. This choice avoids an iterative process to determine the compressive zone. Equation D.11 and the information in Table D.8 are utilized to calculate the moment arm and the required reinforcement area per meter in each specific zone. The primary and additional reinforcement is determined by applying the design concepts discussed in subsection 9.2.2.

$$\text{Reinforcement required} = \frac{m_{\text{xx/yy}}}{z \cdot f_{yd}} \tag{D.11}$$

Table D.8: Geometry concrete two-way flat slab floor design

In-situ two-way slab	
h_{concrete}	180 mm
l_x	3.5 m
l_y	3.5 m
c_{cover}	20 mm

Punching shear

In the context of flat slabs, it is crucial to address punching shear resistance, as elaborated upon in subsection 9.2.2. To verify punching shear resistance, the following three-step process is followed according to Eurocode:

1. **Initial evaluation**: The first step involves verifying whether the maximum shear stress at the column perimeter or the loaded area boundary, as outlined in Equation D.12, remains within acceptable limits.

2. **No shear reinforcement**: If Equation D.13 is satisfied, no shear reinforcement is required.

3. **Shear reinforcement**: In scenarios where shear reinforcement becomes necessary, the criteria defined in Equation D.14 must be met.

$$v_{Ed} \leq v_{Rd,\max} \tag{D.12}$$

$$v_{Ed} \leq v_{Rd,c} \tag{D.13}$$

$$v_{Ed} \leq v_{Rd,cs} \tag{D.14}$$

The design stress for the corner and edge column is determined using Equation D.15 using the perimeters shown in Figure D.6. Table D.9 shows the results and input values for the design stress for both the corner and edge columns. The distributed load is critical load from load combination 2 for the Natural Pavilion together with the self weight of the floor.

$$v_{Ed} = \beta \frac{V_{Ed}}{u_0 d} \tag{D.15}$$

where β is factor obtained from Eurocode, V_{Ed} the reaction force in the columns, u_0 the perimeter and d the effective height.
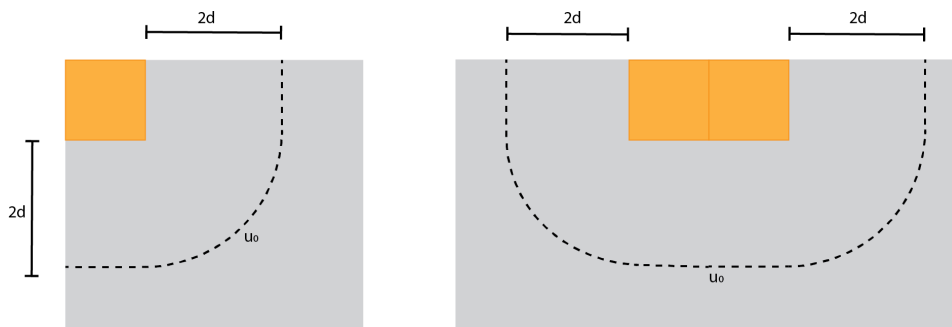
Figure D.6: u_0 perimeter for both corner and edge columns

Table D.9: Results and input for design stress for corner and edge column

	d [mm]	u_0 [mm]	β	V_{Ed} [kN]	v_{Ed} [MPa]
Corner column	152	599	1.5	$\frac{1}{4} \cdot q \cdot l_x \cdot l_y = 46.5$	0.77
Edge column	152	1198	1.4	$\frac{1}{2} \cdot q \cdot l_x \cdot l_y = 93.0$	0.72

Step 1

The maximum shear strength at the perimeter is determined using Equation D.16. This is well above the v_{Ed} of 0.77 and 0.72 MPa.

$$v_{Rd,\max} = \frac{\alpha_{cw} z v_1 f_{cd}}{\cot \theta + \tan \theta} / h_{concrete} = 4.6 \text{ MPa} \tag{D.16}$$

α_{cw} is a factor that accounts for the stress in the compression-loaded edge and is equal to 1 for non-prestressed structures. v_1 is a strength reduction factor for concrete cracked due to shear force and takes a value of 0.6 for concrete compressive strength $f_{cd} < 60$ MPa. Additionally, θ represents the angle between the concrete's compression diagonal and the axis of the beam perpendicular to the shear force, and it is set at 45 degrees.

Step 2

The punching shear resistance without shear reinforcement is determined using Equation D.17.

$$v_{\text{Rd,c}} = C_{\text{Rd,c}} k \left(100\rho_{\text{l}} f_{\text{ck}}\right)^{1/3} \geq v_{\text{min}} \tag{D.17}$$

where f_{ck} is the characteristic strength of concrete and the other parameters as shown in the equations below.

$$k = 1 + \sqrt{\frac{200}{d}} \leq 2,0 \tag{D.18}$$

$$\rho_l = \sqrt{\rho_{\text{ly}} \cdot \rho_{\text{lz}}} \leq 0.02 \tag{D.19}$$

$$C_{\text{Rd,c}} = \frac{0.18}{\gamma_C} = 0.12 \tag{D.20}$$

$$v_{\text{min}} = 0.035 k^{3/2} \cdot f_{\text{ck}}^{1/2} \tag{D.21}$$

Table D.10 shows the results for the punching shear verification. It can be seen that for both the corner and edge columns, additional reinforcement is required.

Table D.10: Results punching shear verification concrete slab

	ρ	**k**	$\mathbf{v}_{min}$ **[MPa]**	$\mathbf{v}_{\text{Rd,c}}$ **[MPa]**	**UC**
Corner column	0.017	2	0.54	0.41	1.41
Edge column	0.017	2	0.54	0.41	1.32

Step 3

Equation D.22 is used to determine the amount of shear reinforcement necessary.

$$v_{\text{Rd,Cs}} = 0,75 v_{\text{Rd,C}} + 1,5 \left(d/s_{\text{r}}\right) A_{\text{sw}} f_{\text{ywd,ef}} \left[1/\left(u_1 d\right)\right] \sin \alpha \leq k_{\text{max}} \cdot v_{\text{Rd,c}} \tag{D.22}$$

where A_{sw} represents the cross-sectional area of the punching reinforcement at a single perimeter around the column, s_r denotes the radial distance between the perimeters of the punching reinforcement, α signifies the angle between the punching reinforcement and the plane of the slab, k_{max} serves as the factor that limits the maximum capacity achievable when employing punching reinforcement, and $f_{ywd,ef}$ as in the equation below.

$$f_{\text{ywd,eff}} 250 + 0,25 d \leq f_{\text{ywd}} \tag{D.23}$$

The shear reinforcement required is limited by the maximum shear resistance that can be obtained according to k_{max}. Around each corner column, 10 studs of 8 mm diameter will be positioned in two perimeters at a radial distance of 100 mm. Around the edge columns, there are 20 studs. Table D.11 shows the input values and the results for the shear reinforcement check. It can be seen that the application of punching shear reinforcement is just enough.

Table D.11: Required shear reinforcement check results

	# studs	$\mathbf{u}_1$ **[mm]**	$\mathbf{s}_r$ **[mm]**	α	$\mathbf{v}_{\text{Rd,cs}}$ **[MPa]**	$\mathbf{k}_{\text{max}}$	$\mathbf{v}_{\text{Rd,cs,lim}}$ **[MPa]**	**UC**
Corner column	10	298	100	90 ^{o}	3.2	1.6	0.87	0.88
Edge column	20	596	100	90 ^{o}	1.8	1.6	0.87	0.82

Beams

Figure D.7, D.8, and D.9 show an overview in Dutch of all the calculations done for the timber beam design using the design tables of ABT. Figure D.10 to D.13 show the beam design verifications for the beams of the BFRP, CLT, concrete hollow core slab, and the concrete flat slab, respectively.

Belastingen

gemiddelde volumieke massa	NEN-EN 1990, art. 4.1.2(5)		ρ_m	kg/m³
blijvende gelijkmatig verdeelde belasting uit eigen gewicht			$G_{k\,(sw)}$	kN/m
blijvende gelijkmatig verdeelde belasting incl. eigen gewicht		$G_{k\,(-sw)} + G_{k\,(sw)}$	G_k	kN/m
belastingduurklasse blijvende belasting	NEN-EN 1995-1-1, tabel 2.1			
belastingduurklasse opgelegde belasting	NEN-EN 1995-1-1, tabel 2.1			
maatgevende belastingduurklasse	NEN-EN 1995-1-1, tabel 2.1			
belastingfactor blijvende belasting, ongunstig, 6.10a	NB_NEN-EN 1990, tabel NB.4		$\gamma_{q,sup,a}$	
belastingfactor blijvende belasting, ongunstig, 6.10b	NB_NEN-EN 1990, tabel NB.4		$\gamma_{q,sup,b}$	
belastingfactor blijvende belasting, gunstig	NB_NEN-EN 1990, tabel NB.4		$\gamma_{q,inf}$	
belastingfactor overheersende veranderlijke belasting	NB_NEN-EN 1990, tabel NB.4		γ_q	
ψ_0-factorwaarde	NB_NEN-EN 1990, tabel NB.2		ψ_0	
ψ_2-factorwaarde	NB_NEN-EN 1990, tabel NB.2		ψ_2	
karakteristieke waarde gelijkmatig verdeelde belasting in z-richting	NEN-EN 1995-1-1, 2.2.3 (2) $\equiv$ NEN-EN 1990, (6.14b)	$G_k + Q_k$	$Q_{k,ar}$	kN/m
quasi blijvende waarde van de gelijkmatig verdeelde belasting in z-richting	NEN-EN 1995-1-1, 2.2.3 (3) $\equiv$ NEN-EN 1990, (6.16b)	$G_k + \psi_2 {}^*Q_k$	$Q_{quasi\,blijvend}$	kN/m
rekenwaarde gelijkmatig verdeelde belasting in z-richting, ongunstig	NEN-EN 1990, art. 6.4.3.2	MAX $(\gamma_{q,sup,a}{}^*G_k + \gamma_q{}^*\psi_0{}^*Q_k \; ; \; \gamma_{q,sup,b}{}^*G_k + \gamma_q{}^*Q_k)$	$Q_{z,d,ong}$	kN/m
rekenwaarde gelijkmatig verdeelde belasting in z-richting, gunstig	NEN-EN 1990, art. 6.4.3.2	MIN $(\gamma_{q,inf}{}^*G_k + \gamma_q{}^*\psi_0{}^*Q_k \; ; \; \gamma_{q,inf}{}^*G_k + \gamma_q{}^*Q_k)$	$Q_{z,d,gun}$	kN/m
rekenwaarde gelijkmatig verdeelde belasting in z-richting	NEN-EN 1990, art. 6.4.3.2, (6.10)	MAX $(Q_{z,d,ong} \; ; \; Q_{z,d,gun})$	$Q_{z,d}$	kN/m
rekenwaarde buigend moment om de y-as		$Q_{z,d} {}^* l^2 / 8$	$M_{y,d}$	kNm
rekenwaarde dwarskracht in z-richting		$Q_{z,d} {}^* l / 2$	$V_{z,d}$	kN

Figure D.7: Overview of load combinations for timber beam design

Doorsnedetoets

materiaal				
materiaalnorm				
modificatiefactor die de invloed van de belastingsduur en het vochtgehalte in rekening brengt_regulier	NEN-EN 1995-1-1, 3.1.3, tabel 3.1		k_{mod}	-
hoogtefactor gezaagd hout	NEN-EN 1995-1-1, vgl. (3.1)	MIN $(150/h)^{0,2} \; ; \; 1,3)$	$k_{h,gezaagd}$	-
hoogtefactor gelamineerd hout	NEN-EN 1995-1-1, vgl. (3.2)	MIN $(600/h)^{0,1} \; ; \; 1,1)$	$k_{h,gelamineerd}$	-
hoogtefactor			k_h	-
partiële factor voor materiaaleigenschap	NEN-EN 1995-1-1, tabel 2.3		γ_M	-

Buiging

karakteristieke buigsterkte			$f_{m,y,k}$	N/mm²
rekenwaarde buigsterkte	NEN-EN 1995-1-1, vgl. (2.14)	$k_{mod}{}^*k_h{}^*f_{m,y,k} / \gamma_M$	$f_{m,y,d}$	N/mm²
weerstandsmoment		$b {}^*h^2/6$	W_y	cm³
rekenwaarde buigspanning		$M_{y,d} / W_y$	$\sigma_{m,y,d}$	N/mm²
unity check buigspanning	NEN-EN 1995-1-1, vgl. (6.11)	$\sigma_{m,y,d} / f_{m,y,d}$	$uc_{m,y,d}$	

Dwarskracht

karakteristieke afschuifsterkte			$f_{v,k}$	N/mm²
rekenwaarde afschuifsterkte	NEN-EN 1995-1-1, vgl. (2.14)	$k_{mod}{}^*k_h{}^*f_{v,k} / \gamma_M$	$f_{v,d}$	N/mm²
rekenwaarde afschuifspanning		$3{}^*V_{z,d} / 2{}^*b{}^*h$	$\tau_{z,d}$	N/mm²
unity check afschuifspanning			$uc_{z,d}$	

Figure D.8: Overview of internal forces check for timber beam design

Doorbuigingstoets

toelaatbare relatieve uiteindelijke vervorming	NB_NEN-EN 1990, art. A.1.4.3(3)		$u_{fin,toel} / l$	/ l
toelaatbare uiteindelijke vervorming		$l {}^* u_{fin,toel} / l$	$u_{fin,toel}$	mm
toelaatbare relatieve bijkomende vervorming	NB_NEN-EN 1990, art. A.1.4.3(3)		$u_{bij,toel} / l$	/ l
toelaatbare bijkomende vervorming		$l {}^* u_{inst,toel} / l$	$u_{bij,toel}$	mm
Gemiddelde elasticiteitsmodulus voor buiging paralel			$E_{m,0,mean}$	N/mm²
vervormingsfactor	NEN-EN 1995-1-1, tabel 3.2		k_{def}	-
oppervlaktetraagheidsmoment		$b {}^*h^3/12$	I_y	cm⁴
ogenblikkelijke vervorming bij belasting G_k	NEN-EN 1995-1-1, art. 2.2.3(5)	$5{}^*G_k{}^*l^4 / 384{}^*E_{m,0,mean}{}^*I_y$	$u_{inst,Gk}$	mm
ogenblikkelijke vervorming bij belasting Q_k	NEN-EN 1995-1-1, art. 2.2.3(5)	$5{}^*Q_k{}^*l^4 / 384{}^*E_{m,0,mean}{}^*I_y$	$u_{inst,Qk}$	mm
ogenblikkelijke vervorming		$u_{inst,Gk} + u_{inst,Qk}$	u_{inst}	mm
uiteindelijke vervorming bij belasting G_k	NEN-EN 1995-1-1, vgl. (2.3)	$u_{inst,Gk}{}^*(1+k_{def})$	$u_{fin,Gk}$	mm
uiteindelijke vervorming bij belasting Q_k	NEN-EN 1995-1-1, vgl. (2.4)	$u_{inst,Qk}{}^*(1+\psi_2{}^*k_{def})$	$u_{fin,Qk}$	mm
uiteindelijke vervorming		$u_{fin,Gk} + u_{inst,Qk}$	u_{fin}	mm
bijkomende vervorming		$u_{fin} - u_{inst,Gk}$	u_{bij}	mm
unity check uiteindelijke vervorming			uc_{fin}	
unity check bijkomende vervorming			uc_{bij}	

Figure D.9: Overview of deflection check for timber beam design

Invoer

type vloer of dak			overige vloeren en daken die intensief door personen worden gebruikt
uiterlijk			het uiterlijk van de constructie is van belang
gevolgklasse			CC2
belastingcategorie			Categorie C: bijenkomstruimtes_algemeen
klimaatklasse			1
materiaal			gezaagd_naaldhout
sterkteklasse			C24
breedte	b	mm	180
hoogte	h	mm	220
overspanning	l	m	3,50

Belastingen

					vgl. 6.10a		vgl. 6.10b	
blijvende gelijkmatig verdeelde belasting excl. eigen gewicht	$G_{k\,(-sw)}$	kN/m	2,7					
opgelegde gelijkmatig verdeelde belasting	Q_k	kN/m	5,3	* 1,5 * 0,4 =	3,2		* 1,5 =	7,9
blijvende gelijkmatig verdeelde belasting incl. eigen gewicht	G_k	kN/m	2,9	* 1,35 =	3,9		* 1,2 =	3,4
kar. waarde gelijkmatig verdeelde belasting in z-richting	Q_{kar}	kN/m	8,1					
rekenwaarde gelijkmatig verdeelde belasting in z-richting	$Q_{z,d}$	kN/m	11,3		7,0			11,3

Buiging

buiging	$M_{y,d}$	kNm	17,3	<=	21,4	uc:	0,81
dwarskracht	$V_{z,d}$	kN	19,8	<=	65,0	uc:	0,30
uiteindelijke doorbuiging	u_{fin}	mm	13,1	<=	14,0	uc:	0,93
bijkomende doorbuiging	u_{bij}	mm	9,9	<=	10,5	uc:	0,94

BFRP

Weight	0,937	kN/m2
Finishing	0,61	kN/m2
Total	2,707	kN/m

Figure D.10: Beam design for BFRP floor

Invoer

type vloer of dak			overige vloeren en daken die intensief door personen worden gebruikt
uiterlijk			het uiterlijk van de constructie is van belang
gevolgklasse			CC2
belastingcategorie			Categorie C: bijenkomstruimtes_algemeen
klimaatklasse			1
materiaal			gezaagd_naaldhout
sterkteklasse			C24
breedte	b	mm	180
hoogte	h	mm	220
overspanning	l	m	3,50

Belastingen

					vgl. 6.10a		vgl. 6.10b	
blijvende gelijkmatig verdeelde belasting excl. eigen gewicht	$G_{k\,(-sw)}$	kN/m	2,0					
opgelegde gelijkmatig verdeelde belasting	Q_k	kN/m	5,3	* 1,5 * 0,4 =	3,2		* 1,5 =	7,9
blijvende gelijkmatig verdeelde belasting incl. eigen gewicht	G_k	kN/m	2,2	* 1,35 =	2,9		* 1,2 =	2,6
kar. waarde gelijkmatig verdeelde belasting in z-richting	Q_{kar}	kN/m	7,4					
rekenwaarde gelijkmatig verdeelde belasting in z-richting	$Q_{z,d}$	kN/m	10,5		6,1			10,5

Buiging

buiging	$M_{y,d}$	kNm	16,0	<=	21,4	uc:	0,75
dwarskracht	$V_{z,d}$	kN	18,3	<=	65,0	uc:	0,28
uiteindelijke doorbuiging	u_{fin}	mm	11,8	<=	14,0	uc:	0,84
bijkomende doorbuiging	u_{bij}	mm	9,4	<=	10,5	uc:	0,89

CLT one-way floor

Dikte	130	mm
	0,13	mm
Density	420	kg/m3
	4,12	kN/m3
Weight	0,536	kN/m2
Finishing	0,61	kN/m2
Beam load	2,005	kN/m

Figure D.11: Beam design for CLT floor

Invoer

type vloer of dak		overige vloeren en daken die intensief door personen worden gebruikt
uiterlijk		het uiterlijk van de constructie is van belang
gevolgklasse		CC2
belastingcategorie		Categorie C: bijenkomstruimtes_algemeen
klimaatklasse		1
materiaal		gezaagd_naaldhout
sterkteklasse		C24
breedte	b mm	180
hoogte	h mm	240
overspanning	l m	3,50

Belastingen

			vgl. 6.10a			vgl. 6.10b	
blijvende gelijkmatig verdeelde belasting excl. eigen gewicht	$G_{k\,(-sw)}$ kN/m	5,0					
opgelegde gelijkmatig verdeelde belasting	Q_k kN/m	5,3	* 1,5 * 0,4 =	3,2		* 1,5 =	7,9
blijvende gelijkmatig verdeelde belasting incl. eigen gewicht	G_k kN/m	5,1	* 1,35 =	6,9		* 1,2 =	6,2
kar. waarde gelijkmatig verdeelde belasting in z-richting	Q_{kar} kN/m	10,4					
rekenwaarde gelijkmatig verdeelde belasting in z-richting	$Q_{z,d}$ kN/m	14,0			10,1		14,0

Buiging

buiging	$M_{y,d}$ kNm	21,5	<=	25,5	uc:	0,84
dwarskracht	$V_{z,d}$ kN	24,6	<=	70,9	uc:	0,35
uiteindelijke doorbuiging	u_{fin} mm	13,2	<=	14,0	uc:	0,94
bijkomende doorbuiging	u_{bij} mm	8,8	<=	10,5	uc:	0,83

Hollow core slab

Weight	2,83	kN/m2
Beam load	4,953	kN/m

Figure D.12: Beam design for concrete hollow core floor

Invoer

type vloer of dak		overige vloeren en daken die intensief door personen worden gebruikt
uiterlijk		het uiterlijk van de constructie is van belang
gevolgklasse		CC2
belastingcategorie		Categorie C: bijenkomstruimtes_algemeen
klimaatklasse		1
materiaal		gezaagd_naaldhout
sterkteklasse		C30
breedte	b mm	180
hoogte	h mm	260
overspanning	l m	3,50

Belastingen

			vgl. 6.10a			vgl. 6.10b	
blijvende gelijkmatig verdeelde belasting excl. eigen gewicht	$G_{k\,(-sw)}$ kN/m	8,7					
opgelegde gelijkmatig verdeelde belasting	Q_k kN/m	5,3	* 1,5 * 0,4 =	3,2		* 1,5 =	7,9
blijvende gelijkmatig verdeelde belasting incl. eigen gewicht	G_k kN/m	8,9	* 1,35 =	12,0		* 1,2 =	10,7
kar. waarde gelijkmatig verdeelde belasting in z-richting	Q_{kar} kN/m	14,1					
rekenwaarde gelijkmatig verdeelde belasting in z-richting	$Q_{z,d}$ kN/m	18,6			15,2		18,6

Buiging

buiging	$M_{y,d}$ kNm	28,4	<=	37,4	uc:	0,76
dwarskracht	$V_{z,d}$ kN	32,5	<=	76,8	uc:	0,42
uiteindelijke doorbuiging	u_{fin} mm	13,2	<=	14,0	uc:	0,94
bijkomende doorbuiging	u_{bij} mm	7,7	<=	10,5	uc:	0,73

Flat slab

Weight concrete	500 kg/m2
Weight steel	5,84 kg/m2
Weight total	505,8 kg/m2
Floor load	4,962 kN/m2
Beam load	8,684 kN/m

Figure D.13: Beam design for concrete flat slab floor

E

Validation Numerical Model

One-way

The validation has been done with the geometry presented in Table E.1. Even though a UD-QI is more appropriate for a one-way floor, a QI lay-up has been considered in this validation. The loading considered is the permanent and variable load discussed in chapter 6. Creep effects are not taken into account.

The bending stiffness and shear stiffness are determined with the equations below:

$$EI = E_{QI} \cdot 2 \cdot (\frac{1}{12}bt_f^3 + b \cdot (h_c/2 + t_f/2)^2) = \tag{E.1}$$

$$10800 \cdot 2 \cdot (\frac{1}{12} \cdot 1120 \cdot 16^3 + 1120 \cdot (140/2 + 16/2)^2) = 2.23 \cdot 10^{12} \text{ N/mm}^4$$

$$G_{total} = \frac{\#_{webs} \cdot t_w}{b} \cdot G_{QI} = \tag{E.2}$$

$$\frac{8 \cdot 8}{1120} \cdot 4000 = 257 \text{ N/mm}^4$$

Where the E is 10800 MPa and G is 4000 as discussed in chapter 3.

Table E.1: Geometry of one-way floor used for validation

Parameter	Value	Unit
L	3.5	m
b	1.12	m
t_f	8	mm
t_w	16	mm
h_c	140	mm
h_t	172	mm
c_w	140	mm

Deflection

Both bending and shear deflection contribute to the overall deformation. They can be easily determined using fundamental mechanical equations.

$$w_{\text{bending}} = \frac{5}{384} \frac{qL^4}{EI} = \frac{5}{384} \frac{5.29 \cdot (3500 - 180)^4}{2.23 \cdot 10^{12}} = 3.76 \text{ mm} \tag{E.3}$$

$$w_{\text{shear}} = \frac{1}{8} \frac{qL^2}{Gh_c} = \frac{1}{8} \frac{5.29 \cdot (3500 - 180)^2}{257 \cdot 140} = 0.203 \text{ mm} \tag{E.4}$$

Fundamental frequency

The fundamental frequency is determined using the approach provided by prEN1995; see Appendix B [24]. The mass determining the fundamental frequency is the permanent load, including 10% of the variable load. This results in a mass of 264 kg/m² for this case.

$$f_1 = k_{e,1} k_{e,2} \frac{\pi}{2l^2} \sqrt{\frac{(EI)_L}{m}} = 1 \cdot 1 \cdot \frac{\pi}{2 \cdot (3500 - 180)^2} \sqrt{\frac{2.23 \cdot 10^{12}}{264}} = 13.08 \text{ Hz} \tag{E.5}$$

Two-way

Determining the deflection of a two-way floor supported on columns analytically can be challenging. Changes to the boundary conditions were made to validate the deflection calculations of the two-way floor. A square floor, supported on its edges, was modeled in Abaqus, and Roak's formulas were utilized to determine the deflection analytically [87].

The Abaqus model incorporates edge support on all sides, with a symmetry axis positioned in the center. To avoid excessive constraint on the floor, the edges are only restrained in the vertical (z) direction, while the symmetry axis prevents movement in the horizontal (x) direction. Additionally, one edge is constrained in the lateral (y) direction. Figure E.1 illustrates the boundary conditions employed for validation. The constraints are positioned along the midline of the edge beams, which have a width of 250 mm. This width is derived from the support area used in the connection for the Natural Pavilion. The Abaqus analysis yields a deflection of 1.72 mm.
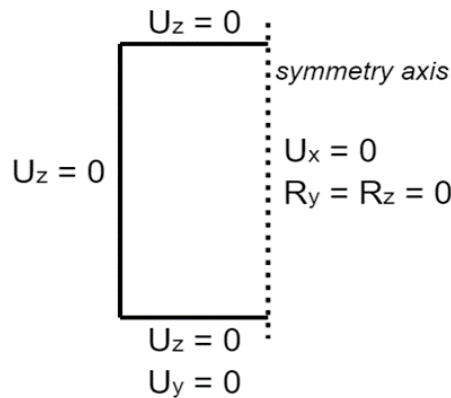

Figure E.1: Boundary conditions for edge supported floor in Abaqus

Using the following equation, the deflection of a homogeneous plate with a uniform load can be determined:

$$w = \frac{-\alpha q b^4}{E t^3} = \frac{-0.0444 \cdot 0.00531 \cdot (3500 - 250)^4}{10800 \cdot 110^3} = 1.79 \tag{E.6}$$

Here, α represents 0.0444 for a plate where the length equals the width. Since this equation is used for homogeneous plates, a representative thickness for a solid laminate with the same EI has been determined, resulting in a thickness of 110 mm.

The deflection obtained from the analytical approach differs from the numerical model by 4.2%.

F

Life Cycle Inventory

The LCI data for the in-situ concrete floors is integrated into the Quake tool of ABT and depends on several factors, such as the concrete class and type of mixture [104]. The data for reinforcement is adapted from MRPI, and the concrete ingredients are from ontwerptoolgroenbeton.nl but are not included in this overview.

Table F.1: Life Cycle Inventory

Material	Unit	CO2 equiv / unit	Source
Timber			
CLT Derix with carbon storage	m^3	-680.55	Derix EPD
CLT Derix without carbon storage	m^3	73.11	Derix EPD
Solid timber C24	kg	0.30	Nationale Milieu database 3.0
Solid timber C30	kg	0.33	Nationale Milieu database 3.0
Concrete			
Concrete VBI (Kanaalplaatvloer 200)	m^2	51.70	VBI EPD
BFRP			
PLA Biofoam (>85% bio-content)	kg	0.50	IsoBouw EPD
Cork as insulation	kg	1.10	EcoInvent
Mycelium with hemp shives	kg	2.68	[102]
Resin Infusion	kg	1.16	EcoInvent
Bcomp ApliTex fibers	kg	0.70	EcoInvent
SuperSap Entropy resin	kg	4.08	[98]